







Università degli Studi di Napoli Federico II

Dottorato di Ricerca in Ingegneria Strutturale, Geotecnica e Rischio Sismico XXXVII Cycle

THESIS FOR THE DEGREE OF DOCTOR OF PHILOSOPHY

Multi-scale structural assessment and sustainable technologies for seismic risk mitigation of historical masonry buildings

by

VALENTINA BUONOCUNTO

Advisors: Prof. Fulvio Parisi

Prof. Giorgio Serino

2025



SCUOLA POLITECNICA E DELLE SCIENZE DI BASE

DIPARTIMENTO D STRUTTURE PER L'INGEGNERIA E L'ARCHITETTURA









La borsa di dottorato è stata cofinanziata con risorse del Programma Operativo Nazionale Ricerca e Innovazione 2014-2020, risorse FSE REACT-EU

Azione IV.4 "Dottorati e contratti di ricerca su tematiche dell'innovazione" e Azione IV.5 "Dottorati su tematiche Green"









Multi-scale structural assessment and sustainable technologies for seismic risk mitigation of historical masonry buildings

Ph.D. Thesis presented

for the fulfillment of the Degree of Doctor of Philosophy in Ingegneria Strutturale, Geotecnica e Rischio Sismico

by

VALENTINA BUONOCUNTO



Approved as to style and content by

Prof. Fulvio Parisi, Advisor

Prof. Giorgio Serino, Advisor

Università degli Studi di Napoli Federico II

Ph.D. Program in Ingegneria Strutturale, Geotecnica e Rischio Sismico

XXXVII cycle - Chairman: Prof. Iunio Iervolino











Candidate's declaration

I hereby declare that this thesis submitted to obtain the academic degree of Philosophiæ Doctor (Ph.D.) in Ingegneria Strutturale, Geotecnica e Rischio Sismico is my own unaided work, that I have not used other than the sources indicated, and that all direct and indirect sources are acknowledged as references.

Parts of this dissertation have been published in international journals and/or conference articles.

Naples, 07 February 2025

Valentina Buonocunto

To my mother Elvira and my father Vincenzo, with love and gratitude.



Abstract

Masonry buildings constitute a significant component of Italy's built heritage, encompassing both monumental structures protected under Law 1089/39 and buildings of historical and architectural interest. These structures, still in use after centuries, stand as material evidence of the nation's historical and cultural identity. Unlike modern structures, the design and construction rules of these buildings did not meet principles of structural mechanics nor engineering design methods but were rooted in traditional craftsmanship methods and empirical rules, based on performance observed on previous similar buildings and equilibrium of rigid bodies. In earthquake-prone areas, empirical rules led to some specific construction techniques to mitigate damage to structures.

The decline of masonry construction due to reinforced concrete and seismic events has shifted in recent years, with renewed interest in traditional methods. With 63% of Italian buildings being masonry, 36% pre-1919, tailored seismic vulnerability assessments are crucial due to the diversity of historical structures. This thesis proposes a multi-scale analysis methodology for assessing seismic vulnerability and strengthening historical masonry buildings, tailoring intervention strategies to the specific characteristics of local contexts.

The research integrates global and local modeling approaches to perform a comprehensive multi-scale seismic vulnerability analysis. Global analysis evaluates the overall structural behavior, while local analysis focuses on specific elements, such as masonry panels and vaults. Using nonlinear static analyses, fragility curves were generated for both in-plane and out-of-plane failure mechanisms. These were subsequently combined to provide a comprehensive framework for understanding and mitigating seismic risks. The buildings were then analyzed in their strengthened configurations, applying both traditional and innovative reinforcement techniques. The associated losses were calculated, highlighting the importance of structural strengthening for ensuring the safety and preservation of these structures.

The developed methodology was applied to a real case study of a historic masonry building located in Portici, Naples. Analyses conducted using an equivalent frame model facilitated the assessment of the building performance under seismic loads. The results demonstrated the effectiveness of targeted

interventions in enhancing structural resilience, as measured through capacity curves, ductility ratios, and reduction of damage indices, while preserving the architectural value of the heritage asset.

Keywords: Historical masonry buildings, Multi-scale methodology, Risk mitigation, Strengthening

Sintesi in lingua italiana

Gli edifici in muratura rappresentano una componente fondamentale del patrimonio edilizio italiano, includendo sia strutture monumentali tutelate dalla Legge 1089/39 sia edifici di rilevanza storica e architettonica. Queste costruzioni, ancora oggi in uso dopo secoli, costituiscono una testimonianza tangibile dell'identità storica e culturale della nazione. A differenza delle strutture moderne, i criteri di progettazione e costruzione di questi edifici non si basavano sui principi della meccanica strutturale o sui metodi dell'ingegneria, ma su tecniche artigianali tradizionali e regole empiriche, derivate dall'osservazione del comportamento di edifici simili preesistenti e dall'equilibrio di corpi rigidi. Nelle aree a rischio sismico, queste regole empiriche portarono allo sviluppo di specifiche tecniche costruttive volte a mitigare i danni strutturali.

Il declino della costruzione in muratura, avviato con l'introduzione del calcestruzzo armato e aggravato dagli eventi sismici, ha registrato un'inversione di tendenza negli ultimi anni, grazie a un rinnovato interesse verso i metodi costruttivi tradizionali. Considerando che il 63% degli edifici in Italia è in muratura e che il 36% risale a prima del 1919, diventa cruciale sviluppare valutazioni specifiche della vulnerabilità sismica, tenendo conto della diversità tipologica di questi edifici storici. Questa tesi propone una metodologia di analisi multi-scala per la valutazione della vulnerabilità sismica e il consolidamento degli edifici storici in muratura, adattando le strategie di intervento alle peculiarità locali.

La ricerca si articola nell'integrazione di approcci di modellazione globale e locale per l'analisi multi-scala della vulnerabilità sismica. L'analisi globale valuta il comportamento strutturale complessivo, mentre quella locale si concentra su elementi specifici, come pannelli murari e volte. Attraverso analisi statiche non lineari, sono state ottenute curve di fragilità per i meccanismi di collasso nel piano e fuori dal piano, successivamente combinate per fornire un quadro completo dei rischi sismici. Gli edifici sono stati quindi sottoposti a interventi di consolidamento, sia con tecniche tradizionali sia con soluzioni innovative, e sono state calcolate le perdite associate, dimostrando l'importanza del rinforzo strutturale per garantire la sicurezza e la conservazione di queste strutture.

La metodologia sviluppata è stata applicata a un caso studio reale, rappresentato da un edificio storico in muratura situato a Portici, Napoli. Le analisi condotte, basate su un modello a telaio equivalente, hanno consentito di valutare le prestazioni dell'edificio sotto l'azione di carichi sismici. I risultati ottenuti evidenziano l'efficacia degli interventi mirati nel migliorare la resilienza strutturale, misurata attraverso curve di capacità, rapporti di duttilità e riduzione degli indici di danno, preservando al contempo il valore architettonico del bene storico.

Parole chiave: Edifici storici in muratura, Metodologia multi-scala, Mitigazione del rischio, Consolidamento.

ACKNOWLEDGEMENTS

This PhD journey has been an intense and rewarding experience, and I am deeply grateful to those who have supported me along the way.

First and foremost, I would like to express my deepest gratitude to my tutors, Prof. Fulvio Parisi and Prof. Giorgio Serino, for their invaluable guidance, feedback, and support throughout the course of my research. Their profound expertise, meticulous attention to detail, and constant encouragement have been instrumental in shaping this work, allowing me to refine my ideas and navigate the complexities of my study. Beyond their academic mentorship, I am especially grateful for their patience, availability, and ability to inspire critical thinking, which have significantly contributed to my growth as a researcher.

I am also sincerely grateful to Prof. Iunio Iervolino, Coordinator of the Doctoral Program in Structural and Geotechnical Engineering and Seismic Risk, for his leadership and for fostering a stimulating research environment.

Furthermore, I wish to acknowledge the financial support of my PhD scholarship, which was co-funded by resources from the National Operational Program for Research and Innovation 2014-2020, through FSE REACT-EU resources, under Action IV.4 "Doctorates and research contracts on innovation topics" and Action IV.5 "Doctorates on Green topics".

I extend my sincere gratitude to the thesis reviewers, Prof. Luigi Sorrentino and Dr. Pietro Meriggi, for their insightful comments and valuable suggestions, which have helped refine this work.

Finally, my deepest and most heartfelt thanks go to Eng. Elia Acconcia, who has supported and guided me. His constant support, valuable advice, and help in every situation have been invaluable. This work is also dedicated to you, as it would not have been possible without your help.

To all those who have contributed to this journey, whether through guidance, support, or inspiration—thank you.

CONTENTS

ABSTR	ACT	VII
SINTES	I IN LINGUA ITALIANA	IX
ACKNO	WLEDGEMENTS	XI
CONTE	NTS	XII
LIST O	F FIGURES	XV
LIST O	F TABLES	XX
СНАРТ	ER 1 – INTRODUCTION	22
1.1. M	IOTIVATIONS AND OBJECTIVES OF THE STUDY	22
1.2. O	UTLINE OF THE THESIS	23
СНАРТ	ER 2 – STATE-OF-THE-ART	25
2.1	CHARACTERISTICS OF HISTORICAL MASONRY CONSTRUCTIONS	25
2.1.	1. Types of Damage in Masonry Structures	30
2.2	MULTI-LEVEL CONCEPT IN VULNERABILITY ASSESSMENT	35
2.3	APPROACHES FOR RISK MITIGATION IN HISTORICAL BUILDINGS	39
	ER 3 – PROPOSAL OF A METHODOLOGY FOR VULNERA MENT OF HISTORICAL MASONRY BUILDINGS	
	DATA COLLECTION AND STATISTICAL ANALYSIS ON THE EXISTING NATIONAL	
3.2. M	IULTI-SCALE STRUCTURAL MODELLING	55
3.2.	1. STRUCTURAL SYSTEM	61
3.2.	2. STRUCTURAL SUB-SYSTEM	71
3.2.	3. SINGLE ELEMENT	77
3.3. IN	N-PLANE AND OUT-OF-PLANE STRUCTURAL PERFORMANCE ANALYSIS	95
3.4. F	RAGILITY ASSESSMENT	99
СНАРТ	ER 4 – VULNERABILITY ASSESSMENT AND RISK MITIGATION	102

4.1	VULNERABILITY ASSESSMENT OF CAMPANIA REGION	102
	. COMPREHENSIVE ASSESSMENT OF MASONRY STRUCTURES: GLOBAL BEHAVIOR IE DAMAGE, AND OUT-OF-PLANE RESPONSE	
4.1.2	. FRAGILITY MODELS FOR IN-PLANE AND OUT-OF-PLANE FAILURES	112
4.1.3	. STRENGTHENED INTERVENTION AND IMPACT ON FRAGILITY	124
4.2. RIS	K ASSESSMENT	131
4.2.1	RISK EVALUATION	133
4.2.2	2. EVALUATION OF THE INFLUENCE OF SOIL TYPE ON SEISMIC RISK	136
4.2.3	3. RISK ASSESSMENT FOR IN-PLANE AND OUT-OF-PLANE FAILURE	139
4.2.4	4. IMPACT OF SUSTAINABLE TECHNOLOGY FOR RISK MITIGATION	144
	R 5 – APPLICATION TO A REPRESENTATIVE CASE-STUDY BUILDING (PROVINCE OF NAPLES)	
5.1	SELECTION OF THE CASE STUDY	150
5.2	GEOMETRICAL AND MECHANICAL PROPERTIES OF THE BUILDING	151
5.3	STRUCTURAL ANALYSIS AND APPLICATION OF THE PROPOSED METHODOLOGY	157
СНАРТЕ	R 6 – CONCLUSION AND POTENTIAL FUTURE DEVELOPMENTS	178
BIBLIOG	RAPHY	182
AUTHOR	2'S PUBLICATIONS	190
APPEND	IX A	192
A PPEND	IX R	195

LIST OF FIGURES

Figure 2.1 – National exposure of existing buildings (ISTAT 2011)	26
Figure 2.2 – Percentage of masonry buildings for different ages of construction	27
Figure 2.3 – Percentage of masonry type for historical buildings <1919	28
Figure 2.4 – Diffusion of masonry types over time (ISTAT 2011)	29
Figure 2.5 - Failure mechanisms of masonry walls: (a) in plane of the wall; (b) out of plane wall	
Figure 2.6 - Mechanisms of wall panel failure: (a) flexural or overturning; (b) sliding shear; diagonal shear	
Figure 2.7 - Mechanisms for computation of limit lateral capacity of masonry façades. (D'Ay. & Speranza, 2003)	
Figure 2.8 – Type of intervention: (a) as-built; (b) reinforced plaster; (c) FRCM	39
Figure 3.1 – Methodology flowchart.	44
Figure 3.2 – Distribution of Masonry Types by Demographics	50
Figure 3.3 – Distribution of Masonry Types by Altitude	51
Figure 3.4 – Percentage of buildings by number of storeys	52
Figure 3.5 – Percentage of buildings by type of vaults	52
Figure 3.6 – Percentage of buildings by type of floors	53
Figure 3.7 – Distribution of floors and vaults in historical buildings	54
Figure 3.8 – Structural system	56
Figure 3.9 – Vertical structural sub-systems and single elements	58
Figure 3.10 – Horizontal structural sub-systems and single elements	60
Figure 3.11 – Example of equivalent frame schematisation	63
Figure 3.12 – Fiber discretization of the macroelement	64
Figure 3.13 – Set-up of compression and shear tests	65

Figure 3.14 – Uniaxial constitutive model	57
Figure 3.15 – Comparison of numerical and experimental shear curves	57
Figure 3.16 - Experimental setup of the full-scale unreinforced masonry wall with opening und lateral load	
Figure 3.17 - Equivalent wall frame6	59
Figure 3.18 – Comparison of numerical and experimental capacity curves	59
Figure 3.19 – Schematisation of the <i>i-th</i> building using the EFM.	⁷ 0
Figure 3.20 – Benchmark wall	1
Figure 3.21 – EFM model of the benchmark wall	13
Figure 3.22 – Capacity curves for the benchmark wall obtained using MATLAB, TREMURI, ar ABAQUS models	
Figure 3.23 – Identification of Panel M3 in the Benchmark Wall	14
Figure 3.24 – Resistance domains of panel M3	15
Figure 3.25 – Zoom on resistance domains of panel M3	15
Figure 3.26 – Floor plans of Archetype 1: a) Ground floor; b) Typical floor	19
Figure 3.27 - Position of the centre of pressure for the i-th section	30
Figure 3.28 – Identification of Vaults in Archetype 1	31
Figure 3.29 - Geometry of Arch 1	32
Figure 3.30 – Geometry of Arch 2	32
Figure 3.31 – Graphical Results of Arch 1	34
Figure 3.32 – Graphical Results of Arch 2	34
Figure 3.33 – Identification of displacement values set the t/R _m value (background plot from I Carlo and Coccia 2020)	
Figure 3.34 – Correlation between collapse displacement and b/a ratio	37
Figure 3.35 - Vault crisis on the Y+ capacity curve with mass-proportional distribution	38
Figure 3.36 – Comparison of vault capacities and limit states of Archetype 1 (Dist. Ma proportional, Dir. Y+)	
Figure 3.37 – Distribution of percentage errors in drift calculation for flexural failure)2

Figure 3.38 – Distribution of percentage errors in drift calculation for shear failure93
Figure 3.39 – Flowchart of the methodology for in-plane and out-of-plane actions95
Figure 3.40 – Mechanisms for computation of limit lateral capacity of masonry façades through FaMIVE
Figure 4.1 - Type of masonry in Campania region
Figure 4.2 - Percentage of buildings by number of storeys
Figure 4.3 – Distribution of floor types for different masonry categories
Figure 4.4 – Global capacity curves of buildings for X direction and proportional to 1 st mode of vibration: (a) 1 storey; (b) 2 storeys; (c) 3 storeys; (d) 4+ storeys
Figure 4.5 – Definition of damage states on global capacity curve
Figure 4.6 - Definition of damage states on out-of-plane capacity curves
Figure 4.7 – Capacity curves for out-of-plane response: (a) 1 storey; (b) 2 storeys; (c) 3 storeys; (d) ≥4storeys
Figure 4.8 – Pseudo-acceleration response spectra of 22 ground motions components from FEMA P695
Figure 4.9 – Intensity of selected ground motion records in terms of PGA: (a) PGA versus moment magnitude; (b) PGA versus epicentral distance
Figure 4.10 – Fragility curves for in-plane failure: (a) 1 storey; (b) 2 storeys; (c) 3 storeys; (d) 4+ storeys.
Figure 4.11 – Fragility curves for out-of-plane failure: (a) 1 storey; (b) 2 storeys; (c) 3 storeys; (d) 4+ storeys.
Figure 4.12 – Combined fragility curves: (a) 1 storey; (b) 2 storeys; (c) 3 storeys; (d) 4+ storeys.
Figure 4.13 – Distribution of types of seismic intervention in buildings in Campania
Figure 4.14 – Capacity curves in the X-direction: (a) as-built \propto masses; (b) as-built \propto 1 st mode; (c) RP \propto masses; (d) RP \propto 1 st mode; (e) FRCM \propto masses; (f) FRCM \propto 1 st mode127
Figure 4.15 – Capacity curves in the Y-direction: (a) as-built \propto masses; (b) as-built \propto 1 st mode; (c) RP \propto masses; (d) RP \propto 1 st mode; (e) FRCM \propto masses; (f) FRCM \propto 1 st mode
Figure 4.16 – Fragility curves: (a) as-built vs. RP; (b) as-built vs. FRCM
Figure 4.17 – Flowchart on the risk calculation steps through IRMA

Figure 4.18 – Damage maps at DS4 as the soil type differs: (a) Soil type A; (b) Soil type B; (c) Soil type C; (d) Soil type D
Figure 4.19 – Damage maps by percentage of buildings at collapsed: (a) in-plane failure; (b) out of-plane failure; (c) combination in-plane and out-of-plane failure
Figure 4.20 – Percentage of damaged buildings for different damage states for different failure modes
Figure 4.21 – Number of human losses (fatalities and injured) for different failure modes 141
Figure 4.22 – Number of buildings' usability for different failure modes
Figure 4.23 – Economic losses for different failure modes
Figure 4.24 – Damage maps by percentage of buildings at collapsed: (a) as-built; (b) RP; (c) FRCM
Figure 4.25 – Percentage of damaged buildings for different damage states for different retrofit technologies
Figure 4.26 – Number of human losses (fatalities and injured) for different retrofit technologies
Figure 4.27 – Number of buildings' usability for different retrofit technologies
Figure 4.28 – Economic losses for different retrofit technologies
Figure 4.29 – Economic losses and cost of retrofit for different retrofit technologies
Figure 5.1 – Ground floor plan of the case study
Figure 5.2 – First floor plan of the case study
Figure 5.3 – Second floor plan of the case study
Figure 5.4 - Identification of the walls along x and y direction of the case study154
Figure 5.5 – Structural system of case study building: equivalent frame view
Figure 5.6 – Structural system of case study building: solid view
Figure 5.7 – First mode of vibration
Figure 5.8 – Second mode of vibration
Figure 5.9 – Third mode of vibration
Figure 5.10 – Capacity curves for Y direction
Figure 5.11 – Capacity curves for X direction

Figure 5.12 – Global capacity curves of buildings for Y direction and proportional to 1st mode of vibration and masses
Figure 5.13 – Global capacity curves of buildings for X direction and proportional to 1st mode of vibration and masses
Figure 5.14 – MDOF, SDOF and bilinear curve for proportional analysis of the first mode of vibration
Figure 5.15 – MDOF, SDOF and bilinear curve for mass-proportional analysis
Figure 5.16 – Response spectrum of the site under examination
Figure 5.17 – Comparison of capacity / demand ratios for the X-direction, force profile proportional to the first mode and masses
Figure 5.18 – Comparison of capacity and demand ratios for the Y-direction, force profile proportional to the first mode and masses
Figure 5. 19 – Comparison of ζ_E values with the application of strengthening
Figure B.1 – Beam elementary displacement
Figure B.2 – Moment and curvature profiles under increasing drift ratio (Parisi and Acconcia 2020)
Figure B.3 – Fibres discretisation of the macroelement
Figure B.4 – Drift-shear curve of a flexure-dominated wall, highlighting the individual contributions of flexural, shear, and rocking components. (Parisi and Acconcia 2020)203
Figure B.5 – Shear-drift response of a flexure-dominated URM wall, showing the contribution of flexural, shear, and rocking components to the overall behavior. (Parisi and Acconcia 2020) 206

LIST OF TABLES

$Table \ 3.1-Correspondence \ between \ `CARTIS' \ and \ Commentary \ No. \ 7/2019 \ masonry \ types \ 4800000000000000000000000000000000000$
Table 3.2 – Spread of masonry types on a regional scale
Table 3.3 – Geometric and load characteristics of the panels. L:length (horizontal dimension); H:height (vertical dimension); T: thickness; H/L=aspect ratio; N/Nu=normalized axial load66
$Table \ 3.4-Mechanical \ properties \ of \ tuff \ masonry: \ f_t \ Tensile \ strength \ of \ masonry, \ f_m \ Compressive \ strength \ of \ masonry, \ E \ Young's \ modulus, \ G \ Shear \ modulus$
Table 3.5 – Mechanical properties of masonry: f_m : compressive strength; τ_{0d} :shear strength; ν : Poisson's ratio; E:Young's modulus; G:Shear modulus; w:unit wight(density)
Table 3.6 – Assumed slab loads per level for benchmark wall
Table 3.7 – Goal seek τ_k values for different softwares
Table 3.8 – Geometric characteristics of the vaults
Table 3.9 – The stiffness values of the vaults
Table 3.10 – Geometrical characteristics of barrel vaults
Table 3.11 – Displacement values of supports determining the collapse condition in vaults 88
Table 3.12 – Percentage difference between global displacement for different limit states and the limit state of the vaults
Table 3.13 – Summary statistics (mean, standard deviation, minimum, maximum) for parameters of 180,000 masonry panels.
Table 4.1 – Uncertainty modelling of material properties
Table 4.2 – Minimum thicknesses for masonry walls proposed by Milani (1920)106
Table 4.3 – Definition of damage states for in-plane failure
Table 4.4 – Definition of damage states for out-of-plane failure
Table 4.5 - Characteristics of selected ground motion records
Table 4.6 - Parameters of fragility curves for in-plane failure
Table 4.7- Parameters of fragility curves for out-of-plane failure

Table 4.8 – Parameters of combined fragility curves
Table 4.9 – Coefficients to be assigned to parameters for FRCM
Table 4.10 - Difference in peak displacement, peak shear and initial stiffness between strengthened and as-built buildings
Table 4.11 – Matrix 1 building usability impact (Borzi et al. 2018, 2020)
Table 4.12 – Matrix 2 percentages used for computation of economic losses (Borzi et al. 2018, 2020)
Table 4.13 – Matrix 3 relationship among damage level, fatalities and injuried (Borzi et al. 2018, 2020)
Table 4.14 – Number of buildings damaged (DS4) and percentage error for each soil type compared to the aggregation proposed by Forte et al. (2019)
Table 5.1 – Mechanical properties
Table 5.2 – Parameters obtained from the case study analysis
Table 5.3 – Difference in peak displacement and peak shear between strengthened and as-built buildings for Y direction
Table 5.4 – Difference in peak displacement and peak shear between strengthened and as-built buildings for X direction
Table 5.5 – Relationships between capacity and demand in terms of displacement for the X direction
Table 5.6 – Relationships between capacity and demand in terms of displacement for the Y direction
Table 5.7 – Values of ζ_E for the X direction and Y direction
Table A.1 – Numerical Report of Arch 1
Table A.2 – Numerical Report of Arch 2

CHAPTER 1 – INTRODUCTION

1.1. Motivations and objectives of the study

Historical masonry buildings constitute the majority of the built heritage in Italy, representing a tangible testimony to the nation's history and architectural evolution. This invaluable architectural heritage showcases the construction skills and structural techniques employed by past civilizations, revealing a profound understanding of materials and sophisticated engineering artistry. Understanding the characteristics of historic masonry is fundamental for preserving these structures and ensuring that they continue to tell their story over time.

This dissertation aims to explore in detail the main characteristics of historical buildings in Campania, drawing on extensive and authoritative literature to provide a comprehensive understanding of their composition, structural elements, and risk mitigation strategies. Historical buildings display various compositions and construction techniques influenced by geographical, cultural, and temporal factors. Common materials include natural stone, fired clay brick, and mortar, each with specific properties that affect the durability, aesthetics, and structural response of the building (Huerta, 2008). The use of locally sourced materials was a common practice, thus contributing to the diversity and richness of masonry constructions across different regions, imparting each structure with a unique and context-rooted character.

The structural integrity of historical buildings is founded on a series of well-defined architectural elements. These include vertical structures such as load-bearing walls, horizontal structures such as floors, and curved structures (arches and vaults), which are essential components of the structural system (Lourenco, 2002). These latter elements, in particular, exemplify the ingenuity of past master masons, capable of efficiently distributing loads, ensuring stability, and simultaneously adding architectural elegance. The use of such structures

demonstrates the complexity and sophistication of construction techniques that

The preservation of historical buildings presents a range of complex challenges related to environmental factors, natural aging, and often inadequate maintenance. The effects of freezing, humidity ingress, and environmental contamination are just some of the causes that contribute to the progressive deterioration of masonry structures. Effective conservation strategies require a delicate balance between respecting historical authenticity and implementing interventions aimed at ensuring structural stability and building safety. Therefore, a combined approach is essential, encompassing the assessment of both in-plane and out-of-plane response mechanisms of the walls.

To ensure the longevity of these buildings, it is necessary to adopt conservation methodologies informed by a deep understanding of their overall structural behavior and construction details. Drawing inspiration from existing literature, strengthening interventions can be designed to reduce expected losses in the event of seismic or other stresses, employing techniques that minimize environmental impact while preserving the authenticity and original aesthetics of the structures as much as possible. The ultimate goal is to safeguard and enhance this heritage, ensuring that it continues to serve as a source of cultural and historical identity for future generations.

1.2. Outline of the Thesis

combine functionality with aesthetic appeal.

The thesis is organized into seven chapters. Chapter 1 summarizes the motivations that led to study and address historical masonry buildings and outlines the main contents of this research. Chapter 2 provides an overview of the state of the art, including an in-depth literature review on the seismic behavior of historical masonry buildings and assessment methodologies. It explores traditional construction techniques, empirical vulnerability models, and analytical and numerical approaches for structural analysis. Furthermore, it discusses past seismic events and their impact on masonry structures, highlighting key lessons learned. The chapter also establishes the connections between these concepts, providing a solid foundation for the methodologies and analyses developed in this research.

Chapter 3 focuses on presenting a new methodology developed for historical masonry buildings. Starting from the study of available data and the construction

of a database for building generation, a vulnerability analysis was conducted on multiple scales, starting from the structural system down to individual elements. The analysis considered not only the global behavior of the structure but also local behaviors, including out-of-plane actions on the walls. The process then continued with the strengthening of these structures to understand the impact on their behavior. Both traditional and innovative techniques were employed to maximize structural performance while minimizing costs.

Chapter 4 analyzes the structural behavior and illustrates the fragility analysis conducted on these structures. Additionally, the influence of different parameters on their earthquake performance was investigated, allowing for the assessment of risk and the evaluation of mitigation strategies. The main issues to which masonry buildings are most susceptible were analyzed, investigating their causes, consequences, and solutions. A real case study is examined in Chapter 5. This building is located in the Campania region, specifically in the municipality of Portici, Naples. The developed methodology was applied to the selected case study. This building was modeled using an equivalent frame approach and analyzed with a MATLAB (2023) code, with its structural performance evaluated through nonlinear static analysis.

Chapter 6 outlines the main outcomes of the PhD thesis, providing a basis for potential future developments that could lead to a better understanding of historical masonry buildings and their intervention techniques.

CHAPTER 2 – STATE-OF-THE-ART

2.1 Characteristics of Historical Masonry Constructions

Masonry buildings constitute a substantial part of Italy's residential and monumental heritage. This group includes not only monumental structures identified and protected under Law 1089/39 but also buildings of significant interest, whether for their uniqueness or for the historical and architectural unity of the surrounding context to which they contribute.

These buildings, which have been passed down to us and are still in use after centuries, serve as a material testament to the historical and cultural identity of our nation. The principles guiding their construction did not follow the classical rules of material mechanics and structural design but were instead based on the traditional craftsmanship methods of the time. These methods, primarily founded on the principles of equilibrium in rigid bodies, provided guidelines for geometric proportioning and construction practices.

Although these structures were not originally designed to resist seismic forces, in areas with high seismic risk, specific construction techniques can already be identified in their original designs, indicating that the frequent occurrence of earthquakes led builders to anticipate such actions. Moreover, the mere fact that these buildings still stand is evidence of their structural integrity and the effective application of traditional techniques. (Di Pasquale 1996 and Como et al. 2019) For builders, constructing according to traditional craftsmanship standards was akin to adhering to modern regulations. Additionally, these craftsmanship methods varied depending on the geographical region, mainly because building materials differed from one area to another (for instance, it is evident that the geometric proportioning of a wall cannot follow the same rules when transitioning from brick masonry to rough-hewn stone masonry (Rondelet 1827, Beymann and Adolf 1926)).

The advent of reinforced concrete towards the end of the 19th century marked the close of a millennia-long era during which masonry structures dominated (Figure 2.1). However, the situation in Italy significantly worsened in the 1950s. After World War II, widespread damage to existing buildings, which at the time were almost entirely masonry, led to their gradual abandonment in favor of

reinforced concrete, which was rapidly gaining popularity. Another reason for moving away from masonry construction came from the damage suffered by historical buildings due to seismic events that affected large parts of the country over the past fifty years, such as in Friuli, Irpinia, Umbria, Molise (Riuscetti et al. 1997, Braga et al 1982, Dolce et al. 2018) up to more recent events like the 2016 Central Italy earthquake. (Sorrentino et al. 2019)

The decline in interest in masonry buildings and the preference for reinforced concrete, mistakenly considered universally safer, resulted in the loss of an immense wealth of technical and construction knowledge refined over millennia of masonry tradition, in just over a century.

In the past fifteen years, however, there has been a significant reversal of this trend, with a strong reassessment of the entire masonry building heritage. This includes both monumental buildings, recognized for their undeniable artistic and architectural value, and traditional structures, now seen as expressions of the historical memory of local cultures.

This change has placed professionals in the position of intervening on buildings often centuries old, under both static and seismic conditions. After a period of considerable difficulty, significant strides have been made in recent years, enabling the recovery of knowledge related to masonry construction and its reorganization into a more scientific rather than empirical framework.

Therefore, understanding the structural behavior and seismic strengthening of such buildings represents a complex challenge, as defining verification procedures for their safety, similar to those for ordinary buildings, is problematic. Their typological diversity prevents the adoption of a single, reliable modeling and analysis strategy.

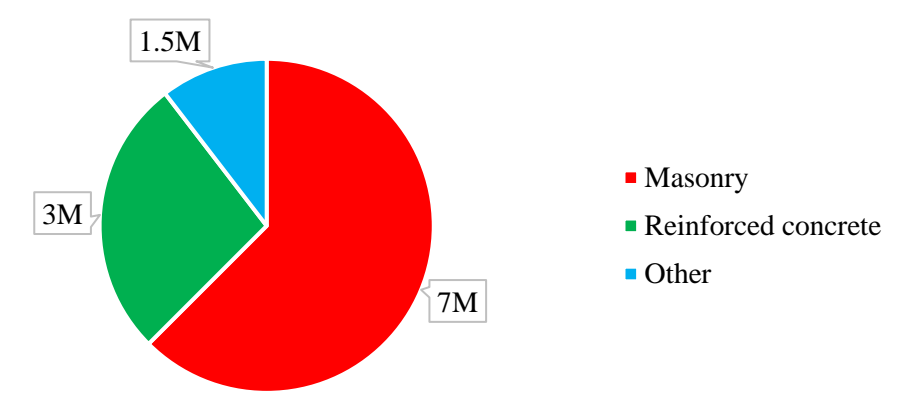


Figure 2.1 – National exposure of existing buildings (ISTAT 2011)

Masonry buildings represent approximately 63% of the national building stock, and of this percentage, 36% consists of buildings constructed before 1919, which are therefore considered "historic" buildings. As previously mentioned, with the advent of reinforced concrete, a progressively lower percentage of masonry buildings can be observed, decreasing from 36% to around 3% for buildings constructed after 1976 (Figure 2.4).

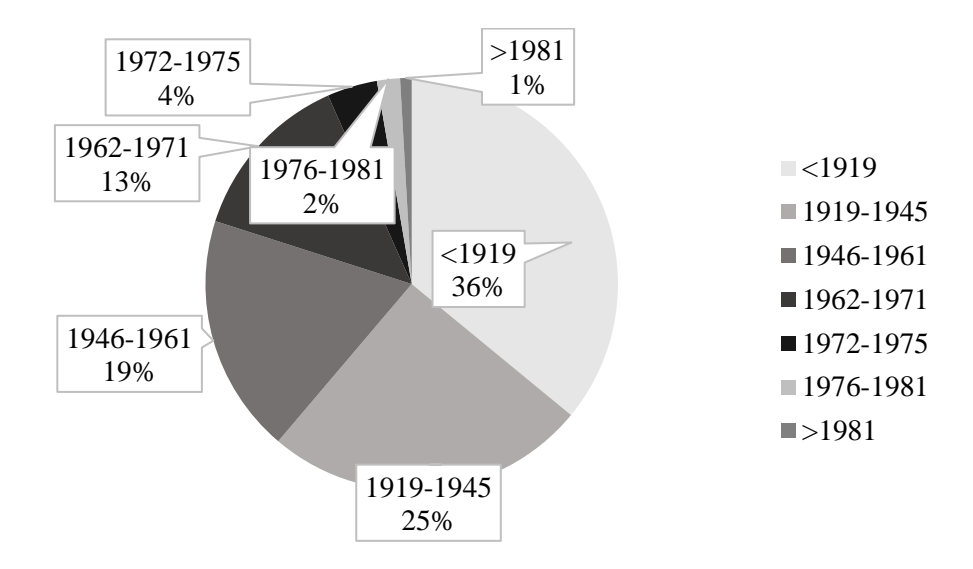


Figure 2.2 – Percentage of masonry buildings for different ages of construction

After selecting the class of buildings (<1919), the distribution of masonry types present throughout the national territory was studied. It can be seen from Figure 2.3 that the most common type of masonry in the country is "A," or irregular stone masonry, found in 59% of cases; "C2," or solid fined clay bricks, in 26% of cases; and "C1," or ashlar masonry with regular squared blocks and mortar joints, in 10% of cases. The structural characterization data of the masonry was integrated with data regarding the age of the first construction to observe how the use of different types changed over time.

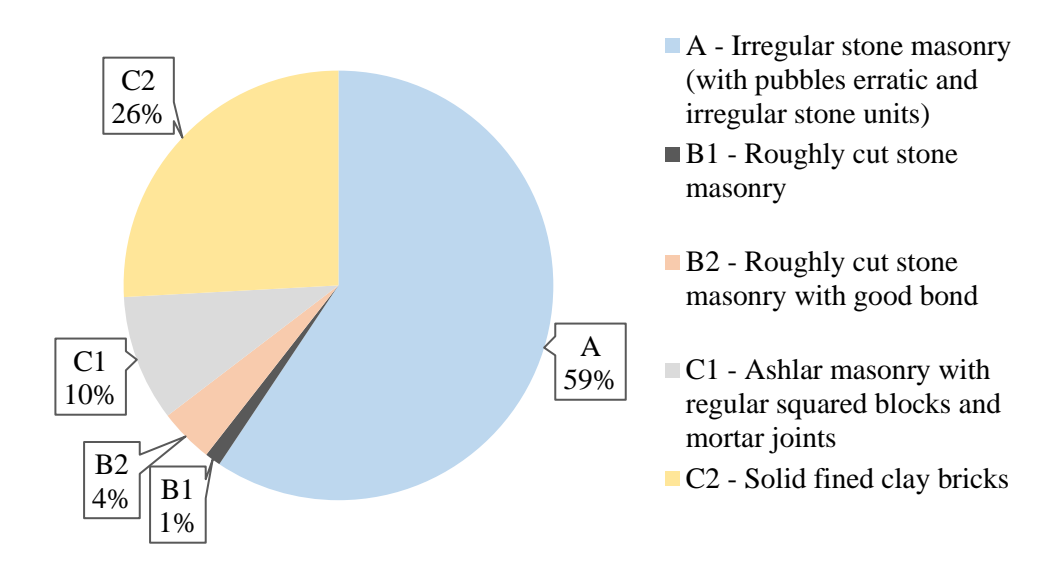
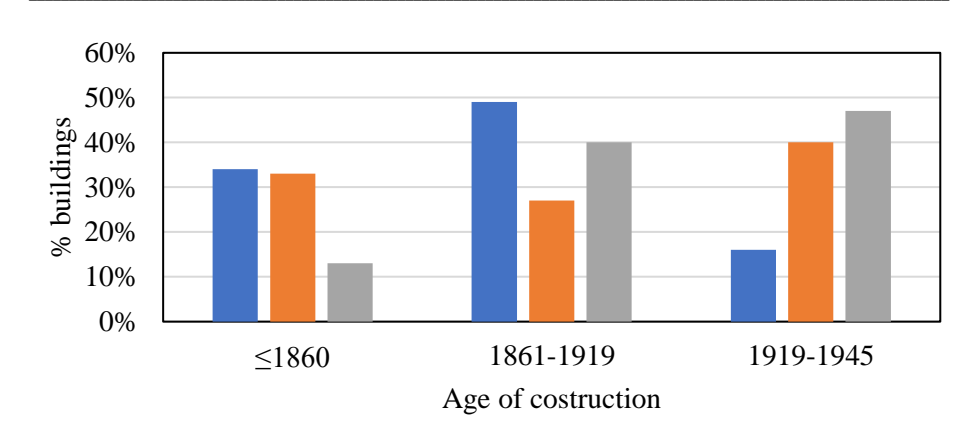


Figure 2.3 – Percentage of masonry type for historical buildings <1919

Specifically, irregular masonry with rough stone, while remaining the most widespread, shows a decreasing trend in use over time. Regular masonry, on the other hand, becomes increasingly adopted as the years progress (Figure 2.4). After completing an initial general assessment of the entire Italian territory, regional and local considerations were made. Firstly, the spread of different masonry types for each region was observed.

From this, it emerges that the A2 type, irregular masonry with rough stone, is most widespread in central and southern Italy, while C2, regular brick masonry, is more representative of central and northern Italy. This information aligns with expectations, as historically, the quarries from which stone was extracted were predominantly located in central and southern Italy, explaining the greater prevalence of rough stone in those areas.



- Irregular stone masonry (with pubbles erratic and irregular stone units)
- Roughly cut stone masonry with good bond
- Ashlar masonry with regular squared blocks and mortar joints

Figure 2.4 – Diffusion of masonry types over time (ISTAT 2011)

Conversely, the sites where stone was quarried and cut were mainly found in the north, which accounts for the frequent use of regular masonry there. Southern Italy, and in particular the Campania region, is characterized by C1 masonry, regular masonry with soft stone (tuff), consistent with expectations since tuff is the most commonly used material for masonry buildings in this region.

2.1.1. Types of Damage in Masonry Structures

The damage mechanisms observed in masonry buildings can essentially be grouped into two categories (Giuffrè, 1999), depending on the type of response of the walls and their mutual degree of connection:(Sorrentino et al. 2019)

- > first mode mechanisms:
- > second mode mechanisms.

The first category (Figure 2.5b) includes mechanisms related to the out-of-plane response of masonry walls, where the stress is primarily flexural, and the collapse occurs due to overturning.



Figure 2.5 - Failure mechanisms of masonry walls: (a) in plane of the wall; (b) out of plane of wall

Second mode mechanisms (Figure 2.5a), on the other hand, are related to the in-plane response of walls to forces, with damage typically occurring due to shear and bending. The activation of these collapse modes is closely dependent on the overall behavior of the structure, which in turn is a function of the building's typological, technological, and construction characteristics. From this perspective, identifying the structures that resist external forces and their mutual interaction is of fundamental importance in investigating their influence on overall behavior.

A masonry panel can resist lateral forces acting within its plane due to the combined effects of its flexural stiffness, shear stiffness, and the panel's inertia when considered as a rigid body. The distribution of the force between these three resistance components depends on the panel's geometric and mechanical

properties, the loading conditions, and the boundary conditions. Generally speaking, for squat panels, the primary contribution to lateral displacement comes from shear deformation, while for slender panels, it is primarily due to flexural deformation, and for very slender panels, the rigid body behavior dominates.

The main in-plane failure mechanisms are three (Figure 2.6):

- the failure mechanism by flexural or overturning mechanisms.
- the sliding shear failure mechanism;
- the diagonal shear failure mechanism;

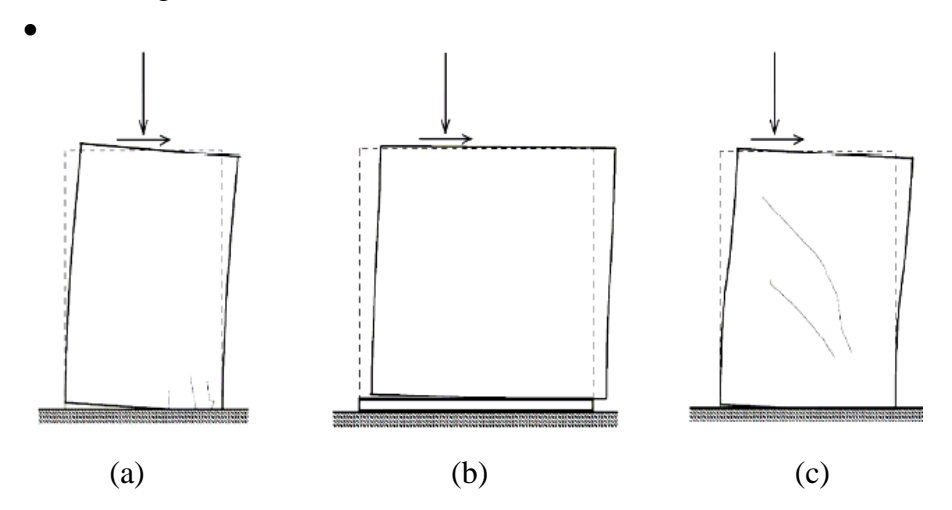


Figure 2.6 - Mechanisms of wall panel failure: (a) flexural or overturning; (b) sliding shear; (c) diagonal shear

Shear failure mechanisms usually include cracking mechanisms of a different nature, attributable to the effect of tangential stresses originating from the horizontal actions in combination with normal stress components. The type of damage, even in the presence of the same collapse mode, is strongly influenced by the type of construction and the characteristics of the masonry.

Out-of-plane collapse mechanisms play a key role in determining the mechanical behavior of masonry panels and their interaction with the overall structure. The earliest attempt to describe and analyze these mechanisms was likely made by Rondelet in 1827; he proposed three basic mechanisms, where the collapse load is calculated based on the wall's boundary conditions and geometry.

In recent years, several researchers (Giuffrè, 1989 - Hobbs, Ting, and Gilbert, 1994 - Casapulla, 1999 - De Felice, 1999) have further explored out-of-plane

collapse mechanisms, while also working on mathematical models to predict their initiation. In 2003, D'Ayala and Speranza, during a study on the seismic vulnerability of historical buildings, compiled a thorough collection of all out-of-plane collapse mechanisms. Figure 2.7 illustrates the mechanisms they identified. Below is a brief overview of the most common out-of-plane collapse mechanisms found in masonry buildings. These can be categorized into four groups:

- simple overturning mechanisms;
- vertical flexural mechanisms;
- horizontal flexural mechanisms:
- compound overturning mechanisms.

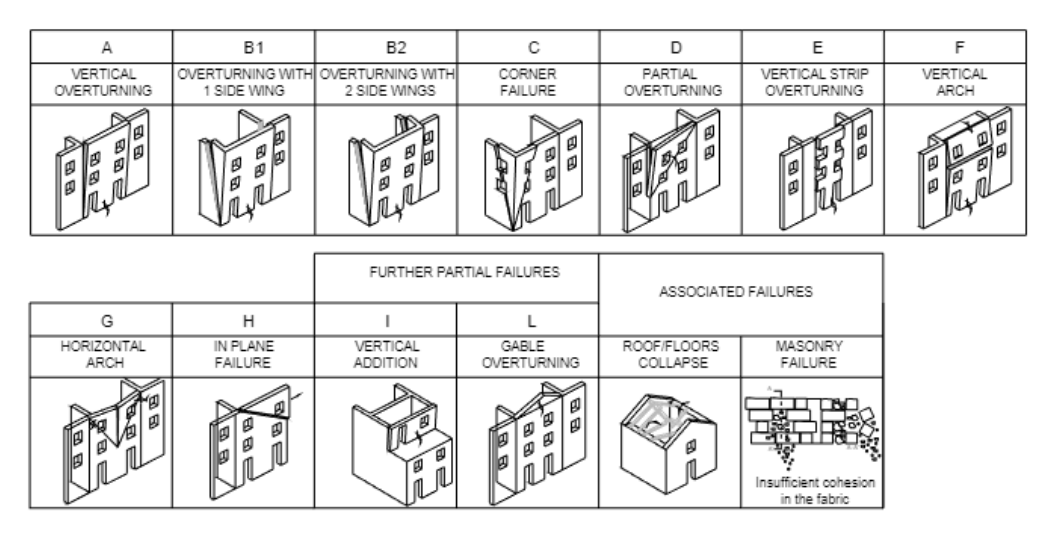


Figure 2.7 - Mechanisms for computation of limit lateral capacity of masonry façades. (D'Ayala & Speranza, 2003)

Among these, the simple overturning of a building's external walls is the most frequently encountered and the most hazardous.

This mechanism can be compared to a rigid body rotating around a cylindrical hinge formed at the base of the wall, triggered by seismic forces acting perpendicular to the wall's plane. A lack of connection between the wall subjected to the seismic action and the floor seismic thrust (due to the absence of a tie beam or tie rod) and poor connections at the corners with perpendicular walls facilitate the activation of this mechanism, which can affect multiple floors of the building. The geometric shape in which this failure occurs can vary depending on the crack pattern or the presence of openings in the wall, both of which influence its progression. Vertical bending mechanisms occur when a wall spans

two consecutive floors, has a tie beam at the top, but lacks a connection between the intermediate floor and the panel. In this scenario, the top tie beam prevents the entire wall from overturning outwards, but collapse can still occur due to vertical instability. This type of collapse is more likely to occur in low-quality masonry (such as rubble masonry), which makes the wall vulnerable to horizontal forces acting perpendicular to its plane, often caused by thrusting elements like arches or vaults, or by unsupported floors. However, it has also been observed in good-quality brickwork when the height-to-thickness ratio is large, as noted by Bisol et al. (2023). . This mechanism, which presents as an outward leaning of the wall, can affect several floors of the building. Horizontal bending mechanisms arise when masonry panels are firmly bonded to orthogonal walls, but the top of the wall lacks a connection to the floor. In this case, a horizontal arching mechanism forms within the wall, driven by forces acting perpendicular to its plane. These forces are transferred to the orthogonal walls and can be broken down into two components: T, acting perpendicular to the wall, and H, acting parallel to its plane. Compound overturning, which can be viewed as a variation of the simple overturning mechanism, is heavily influenced by the type of masonry and the presence of openings in the bracing walls, which determine the size and shape of the detachment wedge. This mechanism typically occurs in masonry with monolithic behavior and can only develop in walls of good quality and craftsmanship.

In addition to evaluating the overall response of the building, it is essential to assess the local collapse mechanisms. If there are weaknesses in the connections between orthogonal walls or between walls and floors, even in small sections of the building, the structure will be unable to develop a cohesive global response during an earthquake. This would normally allow the walls to work together to distribute the induced forces. Instead, each wall would respond independently, increasing the likelihood of local collapse mechanisms, characterized by out-of-plane behavior of the affected walls. The assessment of out-of-plane mechanisms is generally based on a local structural model, where the wall located between two consecutive floors is subjected to a distributed load proportional to its mass and acting perpendicular to its plane.

When floors are rigid within their plane and properly connected to both the wall in question and the orthogonal bracing walls, they act as a restraint against out-of-plane bending. In such cases, out-of-plane deflections of the walls are significantly minimized, encouraging a "box-behavior" and enhancing the overall

redundancy of the building. Conversely, if the floors are not rigid within their plane (as is the case in older buildings), or if they are not properly connected to load-bearing walls, the issue becomes significantly more complicated. In this scenario, the floors no longer provide restraint but instead introduce dynamic forces perpendicular to the wall they rest on. In buildings with timber floors that lack effective anchorage to the masonry and without ties, for instance, the walls tend to detach along the vertical intersections, leading to the formation of noticeable cracks.

In these conditions, the walls are prone to collapse due to the forces acting perpendicular to their plane. The risk of out-of-plane collapse or overturning is further increased by the presence of thrusting elements, such as vaults, arches, or roofs. In these situations, the simplified approach used by Italian seismic regulations (NTC 2018) assumes concentrated horizontal forces proportional to the vertical load transmitted by the floors to the wall in question.

In this study, both in-plane and out-of-plane failure mechanisms of walls are carefully considered, as, as previously discussed, it is essential to account for both actions in historical masonry structures. The vulnerability of these buildings cannot be adequately understood without a combined analysis: in-plane stresses directly affect the walls' ability to withstand lateral loads, while out-of-plane stresses are a critical factor for wall overturning, especially in the presence of insufficient connections between walls and floors, and sometimes thrusting elements.

The primary innovation of this approach lies in achieving an integrated vulnerability assessment that accounts for the structural complexity of historical buildings by developing fragility curves representing a combination of both failure mechanisms. This methodology allows for a more accurate estimation of the likelihood of wall collapse or damage under different seismic scenarios, thus overcoming the limitations of traditional analyses, which often focus on only one type of structural response.

2.2 Multi-level concept in vulnerability assessment

The seismic vulnerability of a structure refers to its susceptibility to damage in the event of an earthquake. This evaluation is critical for seismic risk analysis and for estimating damage scenarios across a range of earthquake intensities. By assessing vulnerability, I can design targeted interventions—both global and local—to extend the lifespan and safety of these structures. Furthermore, large-scale prevention policies and risk analyses (Calvi et al. 2006) are feasible when vulnerability is evaluated across widespread structural typologies within a given territory.

My doctoral research focuses on the seismic vulnerability of historical masonry buildings, addressing vulnerability on two levels: regional and site-specific. At the regional scale, I begin by quantifying exposure and developing fragility models for both in-plane and out-of-plane mechanisms. This analysis then leads to a seismic risk assessment and the proposal of sustainable strengthening strategies to mitigate this risk. However, I place particular emphasis on regional vulnerability, as national-level studies—especially following the 2009 L'Aquila earthquake (De Martino et al. 2018)—have produced comprehensive vulnerability maps and fragility curves that serve as foundational tools for large-scale analyses.

Regional vulnerability, however, requires a more localized approach that accounts for the unique characteristics of a specific area, such as the type of masonry and local construction techniques. In this context, my thesis aims to provide a more precise understanding of seismic vulnerability at the regional level, grounded in the specific features of local masonry typologies and traditional building practices.

At the site-specific scale, the research advances to multi-scale structural modeling, addressing the behavior of the overall structural system, sub-systems, and individual elements. This multi-scale approach allows for a detailed evaluation of site-specific vulnerability and leads to the selection of optimal reinforcement measures. These measures are chosen from a "dataset" of regional reinforcement solutions developed during the regional vulnerability analysis, ensuring that the proposed interventions are both effective and tailored to the particular structural and cultural needs of the area in question.

In summary, the goal of this research is to bridge the gap between regional and site-specific seismic vulnerability assessments, thereby enabling the development of reinforcement strategies that are not only effective at reducing vulnerability but also sustainable and responsive to local structural characteristics. This two-fold approach, from regional analysis to site-specific intervention, offers a comprehensive framework for enhancing the resilience of historical masonry buildings.

To achieve this goal, the Eucentre Foundation, commissioned by the Italian Civil Protection Department (DPC), developed the web platform Italian Risk Maps (IRMA) (Borzi et al. 2018, 2020), a shared tool among researchers to predict loss scenarios calculated using a series of fragility curves. Once the exposure is assessed and fragility curves for various building classes—based on their vulnerability and different damage levels—are inputted, damage can be calculated. The platform is accessible to researchers and scholars who can upload their own data to enrich the database or download available curves.

For exposure calculation, the Characterization of Structural Types (CARTIS) form (Basaglia et al. 2021, Brando et al 2021), developed by the Plinius Study Center (Tocchi et al. 2021) under the DPC's mandate, was used. This form is utilized to gather data on the geometric and structural characteristics of residential buildings through interviews with local technicians. Additionally, for certain Italian seismic events, post-earthquake damage data are collected and made available on the Observed Damage Database (DaDO.) web-GIS platform by the DPC (Dolce et al. 2017, 2019), allowing an in-depth analysis of the vulnerability of Italian residential buildings while also providing the event's ShakeMap (Faenza et al. 2021).

Many authors have addressed this problem using various approaches. The most common methods for assessing building vulnerability at different scales aim to define a Damage Probability Matrix (DPM) or fragility curves (Biglari et al. 2020). The first DPM proposal was made by Whitman (1973) after the San Fernando earthquake, based on a statistical sample of 1,600 buildings, and was later developed for Italy by Braga et al. (1982) following the 1980 Irpinia earthquake on a sample of 38,000 buildings. Fragility curves can be derived through different approaches in the literature, categorized into four main groups: (i) expert-based method, (ii) empirical method (EM), (iii) hybrid method (HM), and (iv) analytical method (AM).

In the first case, damage distribution for a building under different seismic intensities is estimated by experts in earthquake engineering (ATC 1985). The second method (EM) is the most widespread and is based on visual inspection of buildings during the post-emergency phase and damage data from observed past earthquakes (Del Gaudio et al. 2017, Rosti et al. 2019, 2020b). This method uses typological building classes or vulnerability indices, and may be related to material types or specific building characteristics (Zucconi et al. 2018). However, its validity is limited to specific geographic areas and seismicity (D'Ayala 2013). The third case (HM) combines empirical and analytical methods, where postearthquake loss data is combined with analytical methods for a particular building type (Dolce et al. 2006, Kappos et al. 2006, Lagomarsino et al. 2021). Here, visual inspection data reduces computational efforts in analytical methods but requires large data sets due to the combination of empirical and analytical methods. The final method (AM) involves detailed vulnerability assessment algorithms that account for the physical and mechanical properties of buildings, which can be calibrated for specific building stock characteristics (Donà et al. 2020). Deriving fragility curves through analytical methods is time-consuming and computationally intensive, making it challenging to develop curves for different regions or countries with distinct building features. Most studies, after deriving fragility curves, validate them against the 2009 L'Aquila earthquake scenario.

In the study by Rota et al. 2010, the analytical method was used to derive fragility curves through the TREMURI software, considering a representative Italian prototype building. Other authors, such as Zucconi and Sorrentino (2022), derived empirical fragility curves from observed damage in the 2009 L'Aquila earthquake, considering six building classes (three construction period categories and two repair status categories available from census data). They concluded that older buildings are more vulnerable, with repair status being a significant factor in fragility.

The innovation of this study lies in considering the actual distribution and characteristics of buildings in the Campania region to estimate vulnerability assessment. A new advanced methodology is proposed to obtain analytical fragility curves for building classes in Campania, starting with data analysis in the CARTIS database and considering both in-plane and out-of-plane mechanisms. Historical masonry buildings are generated through a Monte Carlo simulation based on exposure statistics at the regional level. For in-plane

mechanisms, an equivalent frame method (EFM) approach is employed with fiber-based macroelement through a fully implemented MATLAB procedure (Acconcia and Parisi 2020); the same walls are then modeled using a rigid-body approach and analyzed with the Failure Mechanism Identification and Vulnerability Evaluation (FaMIVE) procedure (D'Ayala and Speranza 2003) to obtain out-of-plane mechanisms. The resulting sets of fragility curves are then combined to generate unique fragility curves that encompass both out-of-plane and in-plane mechanisms. These final curves will then be used for regional-scale risk assessment and subsequent consequence calculations.

2.3 Approaches for Risk Mitigation in Historical Buildings

The approach to risk mitigation in historical buildings requires a combination of traditional and modern techniques that respect the architectural and cultural integrity of the structures while enhancing their safety. This type of approach must necessarily balance the preservation of historical and artistic value with the need for protection and safety, maintaining an equilibrium between invasive and non-invasive interventions. One of the crucial initial phases of any mitigation strategy is the in-depth assessment of the seismic and static vulnerability of the building, which can be conducted using multi-scale analysis as previously described. This methodology enables the identification of critical issues at both a global level, encompassing the overall structural behavior of the building, and at a local level, focusing particularly on weaknesses in the connections between vertical walls and horizontal structures. Identifying these weak points is essential for developing intervention plans aimed at preventing potentially catastrophic collapse mechanisms, such as out-of-plane failures of load-bearing walls. Intervention techniques (Figure 2.8) can range from traditional solutions, such as the use of reinforced plaster (RP), to more innovative methods involving the application of advanced composite materials like Fibre Reinforced Cementitious Matrix (FRCM). Both reinforced plaster and FRCM contribute to increasing the shear strength and ductility of structures while ensuring compatibility with historical materials and minimize visual impact. Ductility is a crucial aspect for promoting a "box-like" behavior in the building, which allows for the distribution of seismic forces and reduces the likelihood of out-of-plane collapse mechanisms.

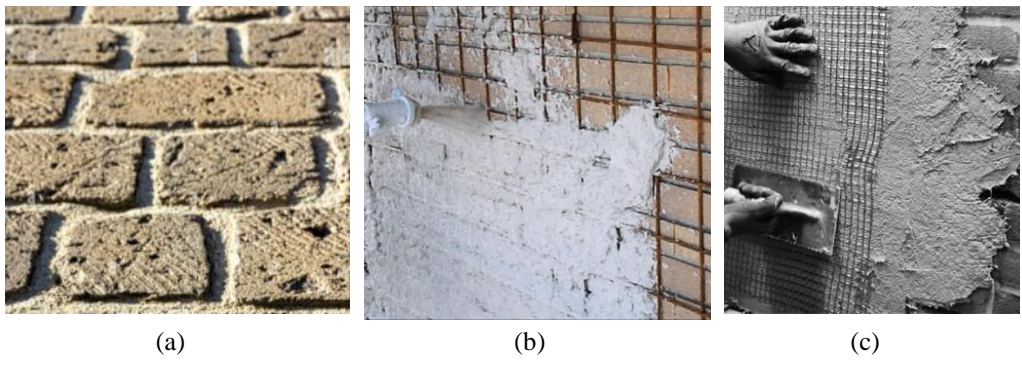


Figure 2.8 - Type of intervention: (a) as-built; (b) reinforced plaster; (c) FRCM

The adoption of structural models to simulate behavior under seismic loads is a fundamental pillar for planning interventions. These models enable engineers to predict the building's response and to virtually test different reinforcement solutions, thereby optimizing the effectiveness of the intervention and reducing overall costs. The use of advanced analysis tools, such as those implemented in the IRMA platform, has allowed this research to obtain accurate estimates of damage and expected losses in case of a seismic event.

The analysis results have shown a significant reduction in losses, both in terms of human lives and economic damage, in reinforced buildings compared to non-reinforced ones. In particular, the use of innovative techniques, such as the application of FRCM, proved highly effective. These interventions not only demonstrated a significant improvement in the structural response of the building but also offered additional advantages: such as potentially lower environmental impact compared to cementitious and carbon-steel-reinforced plaster. However, the reduced mortar thickness in FRCM may require a higher-strength matrix, which could affect compatibility with historical masonry.

In summary, the combination of detailed multi-scale analysis, the use of advanced computational models, and the adoption of innovative reinforcement techniques represent a comprehensive and sustainable approach to risk mitigation in historical buildings. This approach allows for the preservation of cultural heritage while simultaneously ensuring the safety of occupants and reducing economic losses in the event of seismic events.

CHAPTER 3 – PROPOSAL OF A METHODOLOGY FOR VULNERABILITY ASSESSMENT OF HISTORICAL MASONRY BUILDINGS

The flowchart in Figure 3.1 illustrates the methodology adopted in this study for the seismic vulnerability assessment of historical masonry structures and probabilistic seismic risk calculation.

The innovation of this methodology lies in two fundamental aspects that characterize its unique approach. The first aspect concerns the multi-scale modeling of the structural system, a process that allows for the analysis of the building as a whole while simultaneously breaking down the system into smaller sub-elements to better understand both global and local behavior. This type of modeling captures the intrinsic complexities of masonry buildings, providing a detailed view of the strengths and vulnerabilities that may emerge under various loading conditions.

The second innovative aspect of the methodology is the analysis of two distinct failure mechanisms in masonry walls: in-plane and out-of-plane mechanisms. In-plane mechanisms relate to the structural response of walls under horizontal actions acting within the plane, such as parallel seismic forces. On the other hand, out-of-plane mechanisms refer to the behavior of walls under perpendicular loads, which can lead to collapse due to overturning or transverse bending.

Initially, these mechanisms were analyzed separately to isolate the specific characteristics and critical issues of each. This approach allowed for a clear understanding of the factors contributing to structural vulnerability both in-plane and out-of-plane. Subsequently, the results of the two analyses were integrated and combined to achieve an overall estimate of the vulnerability of the selected class of buildings. This combination is essential for providing a more accurate

and representative assessment of the building's behavior under complex and

and representative assessment of the building's behavior under complex and multidirectional seismic forces.

The proposed methodology offers a detailed framework that integrates multiscale modeling and the assessment of failure mechanisms, thus providing a powerful tool for planning more effective and targeted reinforcement and preservation interventions.

The following is a point-by-point explanation based on the described methodology:

- Data collection on historical masonry structures: The initial phase involves the detailed collection of data on historical masonry structures, including geometric information, materials, and conservation conditions.
- Statistical data processing and uncertainty modeling: The collected data is then statistically processed to identify common characteristics and significant variables. Uncertainty modeling is performed to account for intrinsic variations in the data.
- Definition of representative building archetypes of historical buildings:
 Using the processed data, models of buildings and masonry walls are automatically generated. This phase is crucial for creating accurate representations of real structures.
- *Multi-scale structural modeling*: In this phase, modeling is performed not only on the structural system as a building archetype but also on the individual parts that compose it, such as sub-structural systems and individual elements.
- Structural performance assessment against different failure modes:
 - In-plane analysis (IP): An EFM is used, implemented through MATLAB code, which employs fiber-based macro-elements to represent the behavior of masonry walls.
 - Out-of-plane analysis (OOP): Rigid body modeling is used to analyze the failure mechanisms of out-of-plane walls, implemented through the FAMIVE software.
- Capacity curves and definition of damage states: The analyses conducted produce capacity curves representing structural resistance as a function of displacements. Damage states (DS) and collapse thresholds (DT) are defined.

$\hbox{Chapter $3-$ Proposal of a methodology for structural assessment of historical masonry buildings}$

- *Fragility modelling*: Fragility curves are developed, representing the probability of reaching or exceeding specific damage states as a function of seismic intensity.
- *Probabilistic risk assessment*: Risk is calculated in terms of economic losses and loss of human lives.

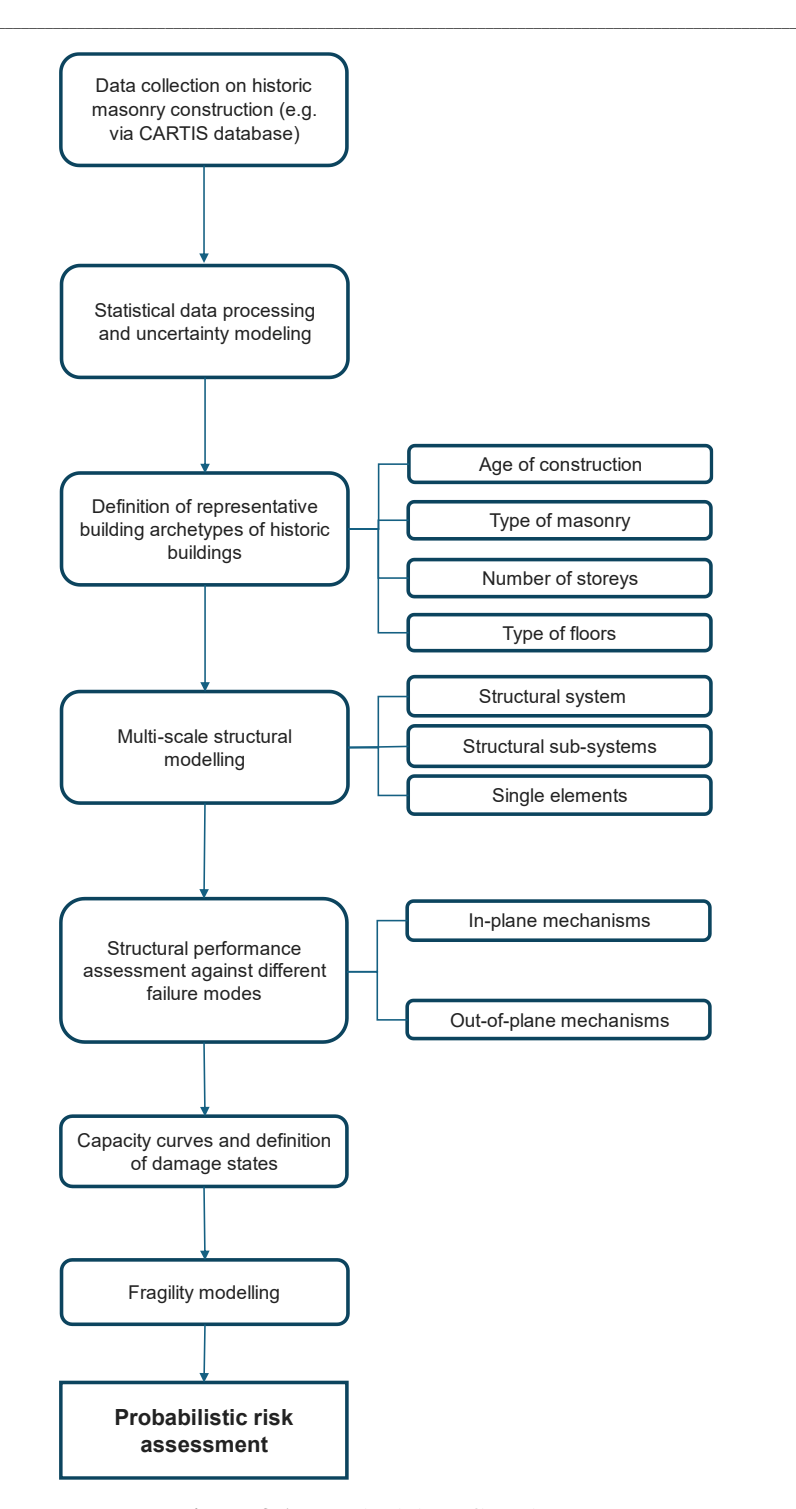


Figure 3.1 – Methodology flowchart.

3.1. Data collection and statistical analysis on the existing national built stock

The first step in calculating risk is exposure. The CARTIS database (Zuccaro et al. 2015, Brando et al. 2021, Basaglia et al. 2021) was used to construct a solid database containing the information necessary for the generation of archetypes.

The CARTIS form can be divided into first and second level CARTIS, the first of which consists of a survey of building types within municipal or sub-municipal areas, known as compartments. The compartments are areas comprising homogeneous building types, in terms of age of construction and construction and structural techniques. The buildings are ordinary, predominantly multi-storey dwellings or services consisting of a masonry or reinforced concrete structure with wall or diaphragms and have moderate storey heights and spacing between columns.

The CARTIS form was studied and designed as part of the three-year Network of University Laboratories in Earthquake Engineering (ReLUIS) 2014-2016 project, with the contribution of the DPC and under the line 'Development of a systematic methodology for the assessment of exposure at territorial scale based on typological/structural characteristics of buildings'. Knowledge and experience gained in the previous work on typological characterisation on the Italian territory carried out by the research unit Naples, now called PLINIVS/LUPT Study Centre, with the current Seismic and Volcanic Risk Office of the DPC were exploited to develop the form. The study acknowledges that the generation of the CARTIS form began as a study of local building characteristics, investigating the national building scene and examining the structural characteristics of ordinary buildings.

Over the centuries building techniques in Italy have changed, due to local cultures and influences. This has led to a variety of constructions and structural characteristics, which have played a fundamental role in the different seismic response of buildings differing in these respects. The compilation of CARTIS forms is fundamental for the assessment of the seismic vulnerability of buildings in our country. The compilation of the forms requires the collaboration of an expert from the relevant ReLUIS research unit, with the help of a municipal

practitioner or a practitioner belonging to other public bodies such as the region, province, mountain community or civil engineering department, or a freelance practitioner. The information obtained for the purposes of compilation must be critical and follow a path where information can be obtained through interviews with various local technicians who have a strong knowledge of the buildings in the area under consideration. It is essential that the compiler carries out several visits, if possible, accompanied by the interviewee.

The compilation of the CARTIS card follows three different sections:

- Section 0 is divided into Part A and Part B. It allows the identification of the municipality under examination and the compartments within it by the ReLUIS Unit expert and the interviewed technician.
- Section 1 identifies each of the prevailing typologies in a general way and must be completed for every typology of each subdivision of the municipality under review.
- Section 2 contains a brief description of the building type under consideration, providing various information such as: number of floors, average floor height, average floor area, age of construction and prevalent use.
- Section 3 is divided into 3.1A and 3.1B, the former to be filled in if the buildings in question are of masonry or mixed construction, the latter if of reinforced concrete. Section 3.2 must be completed in all cases.

To be able to search for data in a database, the information it contains is structured and linked together according to a particular logical model, such as the relational, hierarchical, reticular or object model, chosen by the database designer. With the objective of creating, manipulating and consulting a database, appropriate query languages are used, through programs commonly known as Data Base Management System (DBMS, such as Access, or MySQL, PgAdmin). In this case, the PgAdmin program was used to search and group the data of interest. For the selection of the case studies, research was carried out into the typological-structural information regarding the existing buildings in the areas under study, in order to generate a sample of prototype buildings that could represent the residential buildings actually present in the examined areas. To collect and process the data in CARTIS, the data was organised in terms of type of masonry, number of storeys, construction period and type of floor.

The definition of a historical building is purely based on the age of construction; therefore, initially, any building constructed until 1919 was considered as such. Focusing the analysis exclusively on masonry buildings, it is necessary to consider the time period in which this construction type was most widespread.

Based on this premise, by accessing the "Cartis" database, it was possible to filter and extract data according to the structural type and construction period of the buildings. The age of construction considered are:

- ≤ 1860 ;
- 1861 1919:

Once the relevant information was selected, the first data obtained was the number of historical buildings surveyed, which currently amounts to 203,128 units. This data was initially compared with the number of masonry dwellings constructed before 1945 surveyed by census (ISTAT 2011), which totals 2,854,768 units. The comparison highlights a first limitation of the analysis conducted, as only 7% of the total historical buildings present on the national territory have been recorded.

Given the availability of information for only a small percentage of the total, non-negligible uncertainties must be considered in the results of the statistical evaluations, as relevant data on the distribution of certain types of masonry or specific geometric and structural characteristics may be missing.

Following these preliminary investigations, it was possible to further filter the information from the database based on the types of masonry found in the surveys. The CARTIS database forms include six different categories of masonry:

- Type A1 Irregular stone masonry (with pubbles erratic and irregular stone units);
- Type A2 Irregular stone masonry (with pubbles erratic and irregular stone units);
- Type B1 Roughly cut stone masonry;
- Type B2 Roughly cut stone masonry with good bond;
- Type C1 Ashlar masonry with regular squared blocks and mortar joints;
- Type C2 Solid fined clay bricks.

It is noted that the listed masonry types do not correspond to those found in the 2019 Commentary to the Italian Building Code (Commentary n. 7/2019). In order to obtain, for each of these types, the mechanical parameters required for a subsequent phase of modeling and analysis, it was necessary to establish a correspondence between the code and the "CARTIS" project by comparing the images and descriptions of the masonry types found in the manual for completing the forms with the description in the commentary.

Table 3.1 – Correspondence between 'CARTIS' and Commentary No. 7/2019 masonry types

Type of masonry (CARTIS database)	Type of masonry (Commentary n.7/2019)		
A1 – Irregular stone masonry (with pubbles erratic and irregular stone units)	Irregular stone masonry		
A2 – Irregular stone masonry (with pubbles erratic and irregular stone units)	Roughly cut stone masonry with non-homogeneous thickness		
B1 – Roughly cut stone masonry	Irregular stone masonry with soft stone		
B2 – Roughly cut stone masonry with good bond	Roughly cut stone masonry with good bonding		
C1 – Ashlar masonry with regular squared blocks and mortar joints	Ashlar masonry with regular squared blocks (Tuff masonry)		
C2 – Solid fined clay bricks	Solid/Semi-solid fined clay bircks		

From the statistical analysis conducted on the extracted data, it emerges that the most common masonry types nationwide for historical buildings are A2, which is found in 53% of cases, C2, identified in 26%, and finally, C1, present in 10% of cases.

The data on the structural characterization of masonry was integrated with that regarding the period of initial construction to observe how the use of different types has changed over time. Specifically, irregular masonry with rough stone, while remaining by far the most widespread, has been increasingly less used over time. In contrast, regular masonry types have begun to be used more frequently as the years progress.

After completing an initial general assessment of the entire Italian territory, regional and subsequently local considerations were made. Firstly, the distribution of the different masonry types in each region was observed.

Table 3.2 – Spread of masonry types on a regional scale

Region / Type of masonry	A1	A2	B 1	B2	C1	C2
Abruzzo	15%	40%	3%	0.0%	11%	30%
Basilicata	17%	75%	2%	6%	0%	0%
Calabria	16%	45%	6%	4%	14%	15%
Campania	5%	23%	4%	15%	53%	0%
Emilia-Romagna	0%	2%	0%	0%	0%	97%
Friuli	0%	49%	0%	0%	0%	51%
Lazio	0%	84%	0%	0%	16%	0%
Liguria	34%	66%	0%	0%	0%	0%
Lombardia	18%	26%	0%	0%	0%	56%
Marche	3%	13%	0%	3%	0%	81%
Molise	30%	34%	2%	33%	0%	2%
Piemonte	9%	83%	0%	0%	0%	8%
Puglia	0%	8%	0%	0%	92%	0%
Sicilia	1%	75%	0%	7%	17%	0%
Toscana	7%	86%	1%	1%	0%	4%
Trentino Alto Adige	30%	66%	0%	4%	0%	0%
Umbria	11%	86%	0%	1%	0%	2%
Veneto	7%	65%	0%	0%	0%	28%

It appears that the A2 masonry type, irregular masonry with rough stone, is more widespread in central and southern Italy, while C2, regular brick masonry, is representative of central and northern Italy. This information aligns with expectations, as historically, the quarries from which stone was extracted were primarily located in central and southern Italy, explaining the greater prevalence of rough stone in those areas. In contrast, the facilities where stone was processed were mainly located in the north, which accounts for the frequent use of regular masonry in that region.

On a local level, the distribution of masonry types was analyzed based on the size and altitude of the surveyed municipalities (Figure 3.2). In the first case, the municipalities were categorized by population size as follows:

• Large municipalities – population over 50,000 inhabitants;

- Medium-large municipalities population between 10,000 and 50,000 inhabitants;
- Medium-small municipalities population between 2,000 and 10,000 inhabitants;
- Small municipalities population under 2,000 inhabitants.

The result of this analysis shows that regular masonry is most commonly found in large municipalities. It is important to note that, so far, surveys have been conducted primarily in smaller municipalities, resulting in a lack of information for more populous and significant cities.

In the second case, municipalities were categorized based on altitude as follows (Figure 3.3):

- Mountain municipalities altitude above 600 m above s.l.
- Hill municipalities altitude between 300 and 600 m above s.l.
- Plain municipalities altitude below 300 m above s.l.

In this case, there is a limited distribution of masonry types in mountain municipalities. Due to the limited number of surveys conducted in these areas, there is uncertainty regarding the statistical representativeness of the data.

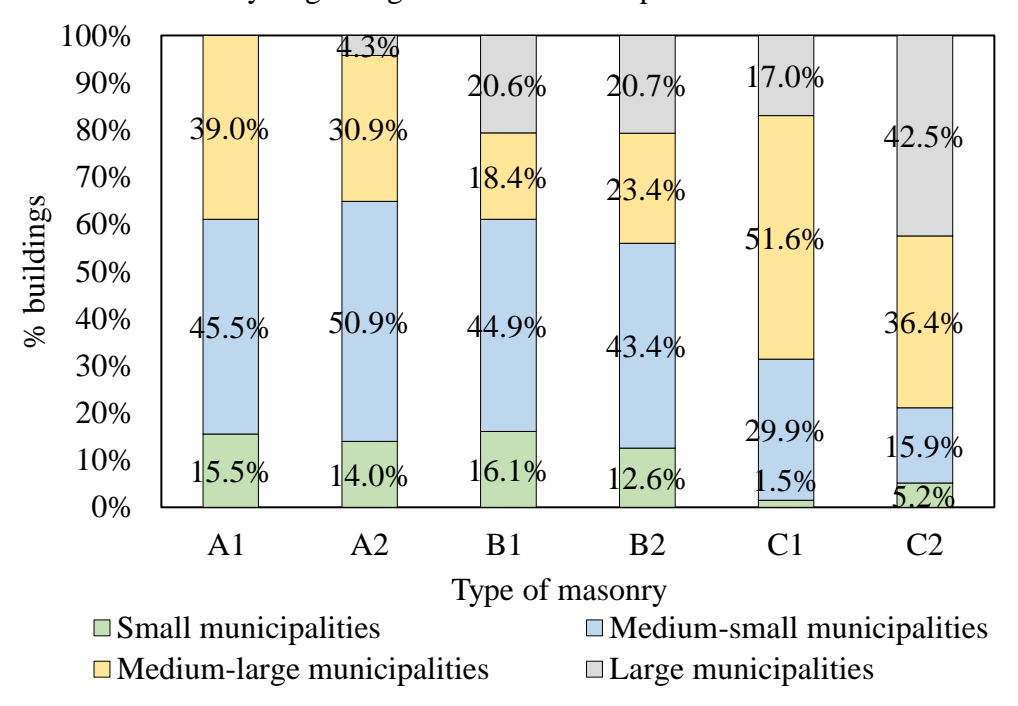


Figure 3.2 – Distribution of Masonry Types by Demographics

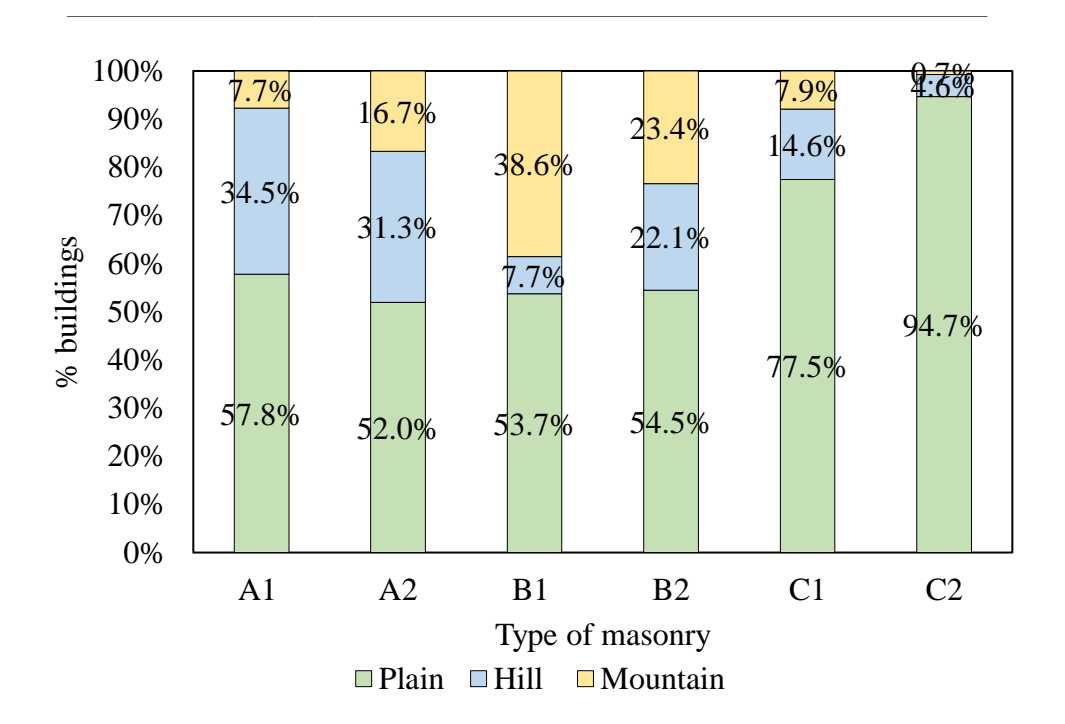


Figure 3.3 – Distribution of Masonry Types by Altitude

After analyzing the distribution of masonry types at national, regional, and local levels, the next step involves disaggregating the data to individually identify the structural and geometric characteristics of historical buildings and examining how these vary over time. This process will be repeated for each masonry type to obtain results that will be useful for the future phase of building and modeling structural archetypes.

The first data examined is the number of storeys (Figure 3.4). Statistics show that the majority of historical structures have three levels.

In interpreting these data, it is important to note that taller buildings are typically found in larger and more significant municipalities. However, the surveys have predominantly involved smaller urban centers, resulting in a concentration of the graph around three and four floors.

Further investigation was conducted on the presence and variety of vaults within historical structures (Figure 3.5). It was observed that only 7% of the surveyed buildings have vaults, with barrel vaults being the most predominant type.

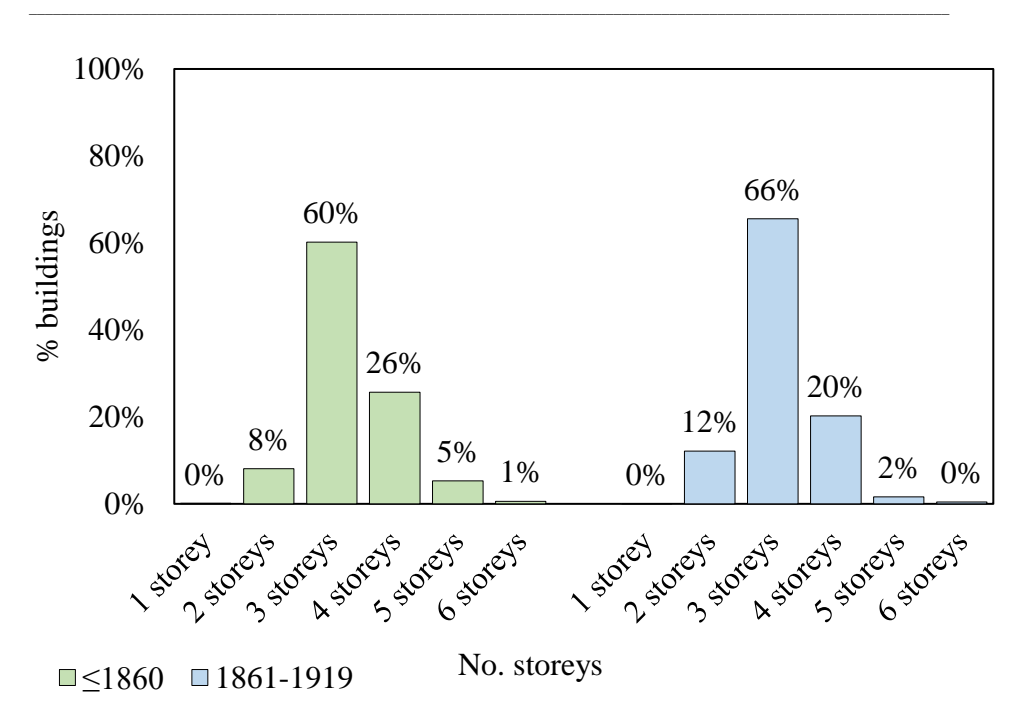


Figure 3.4 – Percentage of buildings by number of storeys

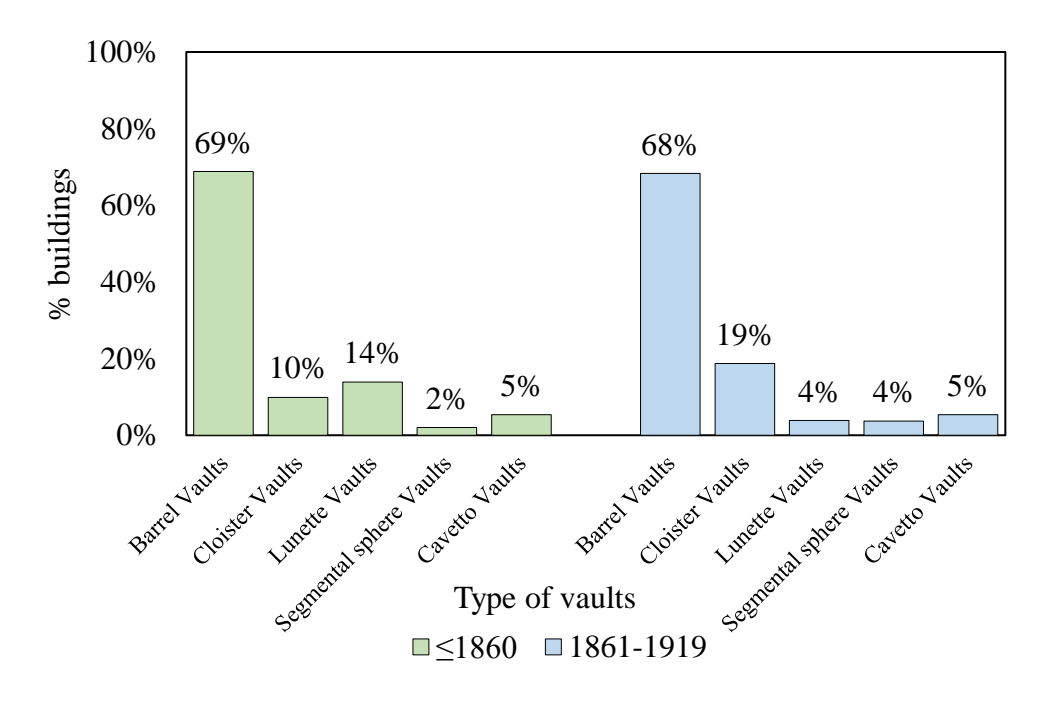


Figure 3.5 – Percentage of buildings by type of vaults

For certain data to be complete and truly representative from a statistical standpoint, it is essential for surveyors to access the dwellings and conduct specific and thorough inspections. This, however, is often difficult, and in many cases, data are either collected based on what is observable from outside the building or are not recorded at all.

For the study of floor types characterizing historic structures, a similar approach to that used for vaults should be applied. For horizontal structures, an in-depth on-site investigation is essential, yet it is rarely conducted, compromising the reliability of the information extracted from the database (Figure 3.6). Despite this limitation, the most commonly found floor type is deformable, typically consisting of wooden beam structures. Semi-rigid floors, such as those made of steel beams with hollow clay tiles (*ferro e tavelloni*), and rigid floors, primarily reinforced concrete slabs, began to be used on a broader scale starting from 1945.

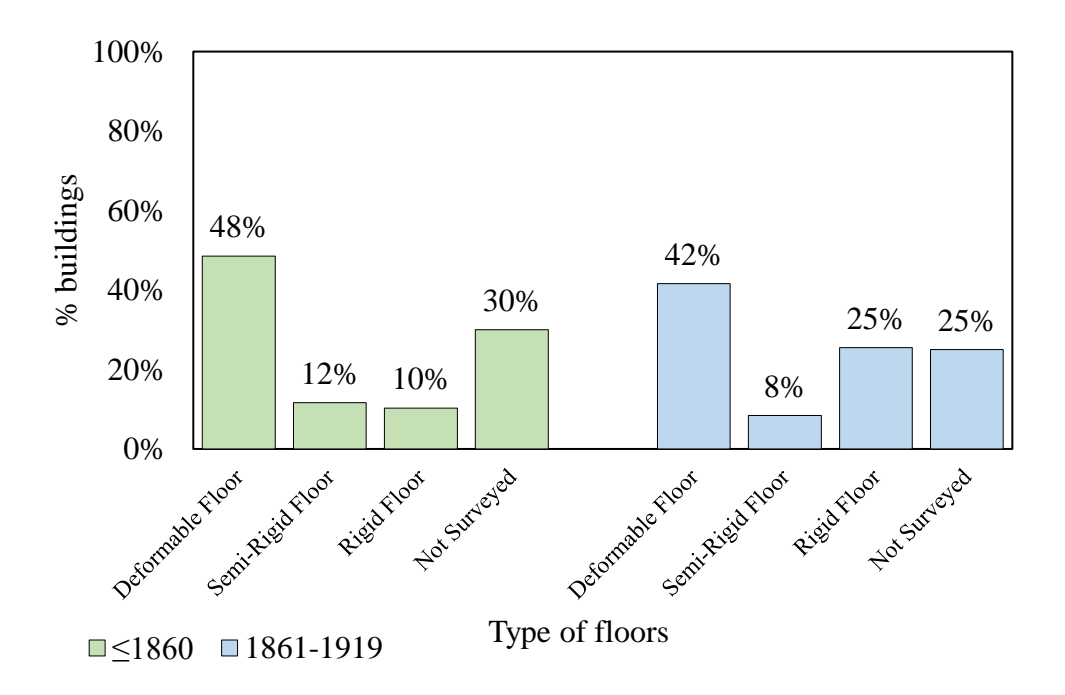


Figure 3.6 – Percentage of buildings by type of floors

The integration of information regarding vaults and that pertaining to floors offers the opportunity to verify an additional property of historical structures. It is common to find vaults at the ground floor of a building and floors at the upper levels. In the absence of data on vaults in the database, only the presence of floors

was assumed, and vice versa; however, in cases where there was information on both vaults and floors, it was hypothesized that a vault is present on the ground floor and floors on the upper levels.

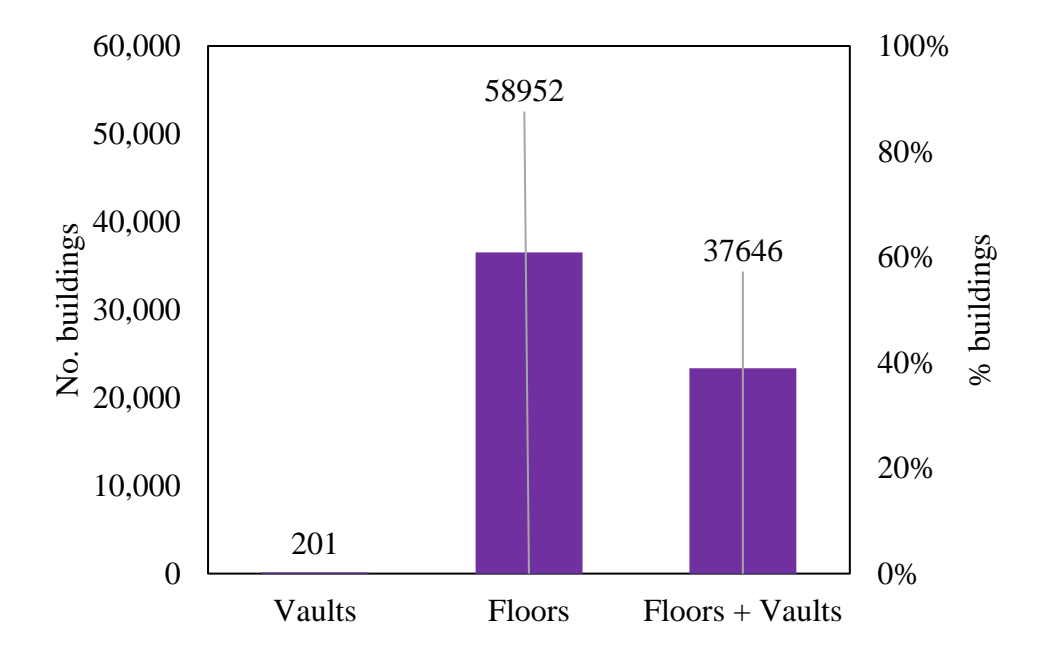


Figure 3.7 – Distribution of floors and vaults in historical buildings

This initial phase of statistical analysis has allowed for the identification of the general characteristics of historical structures by examining the most common masonry types in Italy.

In the next chapter, specifically Chapter 4, and with the aim of reducing the uncertainties highlighted during the presentation of results, the statistics will be broken down for the selected building class, verifying their compatibility with the "rules of the art" in use during the period under examination.

This integration will facilitate the development of building archetypes, representing realistic structures that can be modeled and analyzed.

3.2. Multi-scale structural modelling

To study and deeply understand masonry structures, it is essential to introduce the concept of multi-scale analysis. This methodological approach allows for the examination of the complexity of masonry buildings from various perspectives and levels of detail, starting from the overall structural system down to the individual constituent elements. The main objective of this work is to analyze not only the entire building as a representative archetype but also to break down the investigation into sub-structural systems and, ultimately, individual components to obtain a comprehensive and integrated view of the building's behavior. This type of analysis enables the identification and focus on specific vulnerabilities that can critically impact the overall response of the structure.

Given that a detailed database of representative masonry archetypes has been developed, analyzing these structures with advanced modeling techniques (such as finite element method, FEM, or discrete element method) would require a high computational burden. This complexity arises from the need to adapt models based on the specific geometric and mechanical characteristics of each archetype. Therefore, a single modeling approach would be ineffective for accurately capturing the typological diversity of historical masonry buildings.

To address these challenges, a multi-scale methodology has been adopted, which optimizes the balance between result accuracy and computational efficiency. In this approach, buildings are initially considered as complete structural systems and are modeled with an EFM approach using MATLAB-based code. This EFM modeling allows for the examination of a large number of buildings with a low computational load, providing reliable results for preliminary and comparative assessments.

At the scale of structural subsystems and individual elements (such as load-bearing walls, floors, arches, and vaults), more detailed modeling can be conducted. At this level, models capture the local behavior of structural elements and their interactions, providing deeper insights into the mechanical and geometric characteristics of each component. This multi-scale strategy not only enables the assessment of differences between various models and structural responses but also allows for a more accurate and comprehensive view of the behavior of historical masonry buildings under both static and dynamic conditions.

In summary, this multi-scale approach offers a flexible and comprehensive methodology, integrating global analysis with local insights, to effectively address the complexity and diversity of historical masonry structures while optimizing computational resources. This strategy ensures a holistic view of the structure, providing critical insights necessary for preserving and enhancing the resilience of historical masonry buildings.

A masonry building can be described as a structural system (Figure 3.8Figure 3.8) composed of vertical elements, such as load-bearing walls, which ensure the capacity to support gravitational loads and transfer lateral forces to the ground, and horizontal elements, such as floors, which connect the walls, stabilize the structure, and influence its behavior. These elements interact in a complex manner, contributing to the overall functioning of the building and determining its ability to withstand both static and seismic stresses.

The multi-scale approach adopted in this study allows for structural analysis with a systematic and holistic perspective. Starting from the evaluation of the building as a whole, the focus then shifts to sub-systems to identify how these interactions influence global behavior. Finally, the study of individual elements, such as masonry panels, arches, and vaults, enables an understanding of local issues that may represent weak points for the structure.

This methodology ensures a detailed comprehension of structural behavior, essential for designing effective reinforcement and conservation interventions, and provides a solid foundation for a more in-depth analysis of vulnerabilities and potential strategies for improving structural safety.

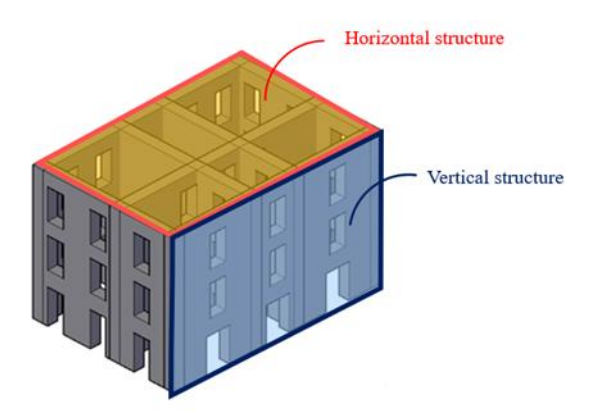


Figure 3.8 – Structural system

Vertical structures (Figure 3.9), specifically load-bearing walls, play a crucial role in defining the overall stability and load-bearing capacity of masonry buildings. These walls can be classified as either regular or irregular based on their construction characteristics and material composition. Regular walls typically exhibit uniform construction, such as consistent geometry. This uniformity generally leads to predictable structural behavior, facilitating modeling and analysis under both static and seismic loads.

Conversely, irregular walls are often found in historical masonry structures. These walls are characterized by non-uniform construction, which may involve a combination of different materials or a variable distribution of openings. Irregular walls frequently result from traditional construction methods, where locally sourced materials and construction practices were influenced by resource availability and the craftsmanship of the time. Such walls present unique challenges for structural analysis due to their inherent heterogeneity and complex behavior under various loading conditions.

The focus on irregular load-bearing walls is particularly significant for understanding the seismic vulnerability of historical buildings. Unlike regular walls, which can be assessed using relatively straightforward modeling techniques, irregular walls require advanced analyses to capture their detailed response to stress. The irregular arrangement of openings can lead to stress concentrations and local weaknesses, which may manifest as points of failure during seismic events. Additionally, these walls exhibit anisotropic properties, meaning that their mechanical response can vary depending on the direction of the applied loads.

By focusing on the analysis of both regular and irregular load-bearing walls, this research aims to deepen the understanding of their mechanical properties and response under various loading scenarios. These structures were analyzed using different software tools to discern the differences and identify the most effective structural modeling approach to capture various failure modes.

From the sub-structural systems (Figure 3.9), individual elements such as masonry panels can be isolated, which represent fundamental components for a detailed analysis of masonry structures. Studying masonry panels allows for the identification of local vulnerabilities that, if overlooked, could compromise the safety and stability of the entire building. The analysis of these elements is crucial for understanding how stresses are distributed and concentrated, providing valuable insights into the structure's response to different types of loads. In this

work, the behavior of masonry panels was examined under various boundary conditions to identify how these conditions influence their performance. Panels were studied in their original (as-built) configuration as well as reinforced panels, using both traditional interventions, such as the application of RP, and innovative techniques, such as the use of composite materials. The goal was to capture and compare differences in terms of displacement (drift), shear resistance, and failure modes. This analysis allowed for the evaluation not only of the residual load-bearing capacity of the masonry panels but also for a better understanding of how reinforcement interventions can modify structural behavior, improving ductility and reducing potential weaknesses. Regarding horizontal structures (Figure 3.10), or floor systems, these can be either flat (floors) or curved (vaults). In historical masonry buildings, it is common to find vaulted horizontal structures on the ground floor, while the upper floors are often characterized by flat structures.

These differences stem from traditional construction practices and the functional requirements typical of the era in which the buildings were constructed, influenced also by the availability of materials and local construction techniques.

Structural sub-systems

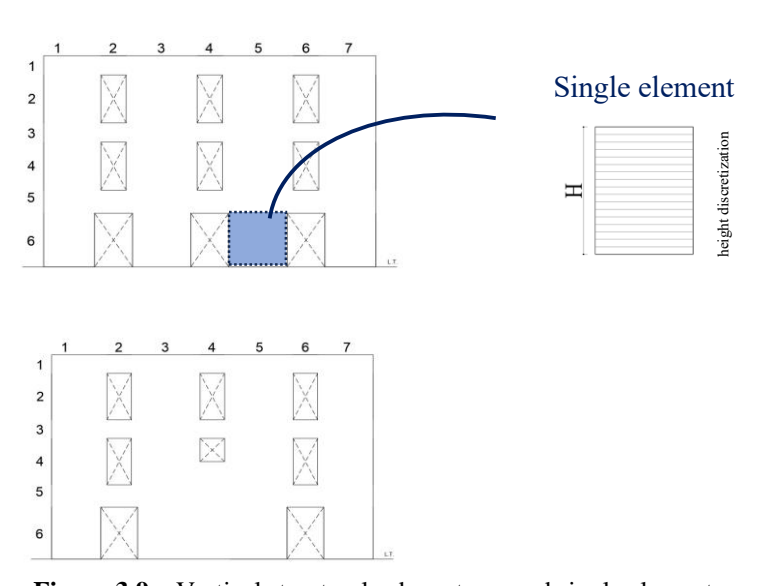


Figure 3.9 – Vertical structural sub-systems and single elements

Among the vaulted structures, barrel vaults are particularly common in residential masonry buildings due to their ability to efficiently distribute loads, ensuring a good load-bearing capacity even in very old buildings. In studying vaulted structures, these were analyzed as individual elements by simplifying their complex three-dimensional geometry into two-dimensional structures represented by arches. This simplification allowed a focus on the abutment reactions, i.e., the forces transmitted at the ends of the arch, which are useful for a better understanding of the vaults' behavior and for implementation in global structural models of buildings.

The analysis of arches as simplified representations of vaults provided valuable data on load transmission modes and potential critical issues, such as failure mechanisms that individual vaults may introduce to the overall structural behavior, particularly under seismic actions. The reactions were calculated using the *Arco* software developed by Professor Gelfi and subsequently implemented at the corresponding nodes in the EFM of the building. A more detailed discussion of the modeling approach is provided in Section 3.3.3 This methodology allows for the calculated reactions to be integrated into more complex computational models, contributing to a more realistic simulation of the building's overall structural behavior.

This detailed attention to the simplified modeling of vaults, combined with the analysis of their structural reactions, is a crucial step for assessing the interaction between horizontal and vertical structures and for ensuring a comprehensive understanding of the dynamic behavior of historical masonry constructions.

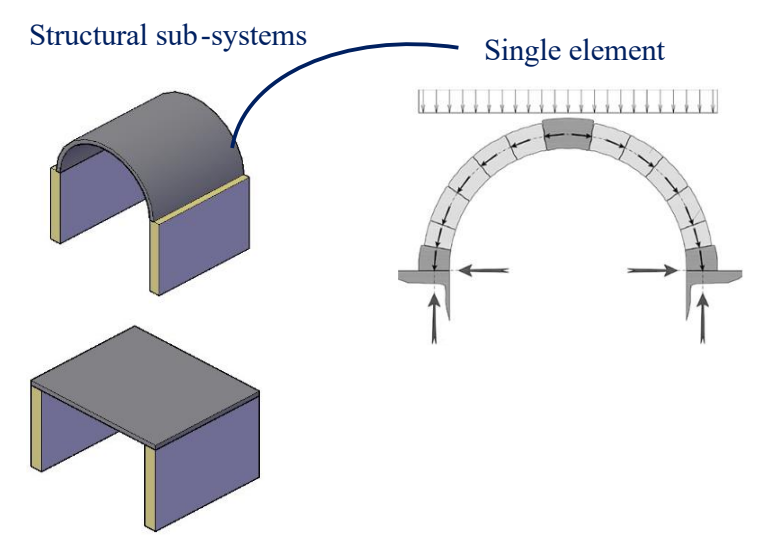


Figure 3.10 – Horizontal structural sub-systems and single elements

3.2.1. Structural system

The seismic vulnerability of existing unreinforced masonry buildings is a significant concern, particularly in light of historical earthquakes and recent seismic events. These structures are widespread across various regions, often situated in high seismic hazard zones. Beyond ensuring occupant safety, preserving these buildings for their historical and artistic value is also crucial.

Analyzing earthquake-induced damage highlights how structural behavior varies based on construction characteristics. Two primary categories of damage mechanisms are observed: first-mode and second-mode. First-mode mechanisms describe the out-of-plane behavior of masonry walls, while second-mode mechanisms relate to in-plane damage, including shear and bending effects.

The structural response of a building under horizontal actions can be modeled by considering masonry walls as an assembly of interconnected panels. Seismic damage observations and experimental tests show that specific wall sections, such as piers adjacent to openings, spandrels, and lintels, are especially vulnerable to concentrated damage.

Conversely, intersections between piers and spandrels - known as "nodes" - typically remain unaffected. This understanding has led to structural models that use deformable elements to represent various wall sections, along with rigid zones for the nodes.

Several modeling approaches have been developed to address the unique behaviors of masonry structures, and they can primarily be classified into four categories: block-based models, continuum models, geometry-based models, and macroelement models (D'Altri et al. 2020):

- 1. *Block-Based Model (BBM)s*: These models (Angelillo et al. 2018, Portioli et al. 2017) treat masonry structures as discrete elements or blocks connected by interfaces, with each block acting as a rigid body. They are effective in capturing localized phenomena, such as cracking or block movements, and are often used for analyzing historical masonry structures or detailed structural components.
- 2. Continuum Models(CHM): These models (Valluzzi 2007) represent masonry as a homogeneous, continuous material, accounting for its nonlinearity and heterogeneous mechanical properties. Using methods

such as FEM, continuum models can accurately simulate complex structural responses, including global deformations and interactions

within the structure.

3. *Geometry-Based Models(GBM)*: These models (Chiozzi et al. 2017,2018; Block et al. 2006; Marmo and Rosati 2017) explicitly represent masonry structures based on the geometry and arrangement of individual units, allowing analysis of bond patterns, joint thickness, and geometric irregularities. Useful for examining structural response at the microscale, they offer insights into the effects of geometry on overall stability.

4. *Macroelement(EFM)s*: For my research, I utilized the macroelement modeling approach, which offers a simplified yet effective means of representing essential behaviors of masonry structures. Macroelements use one-dimensional or two-dimensional elements to approximate the main structural components, such as walls or arches. This approach effectively incorporates nonlinear masonry characteristics, including compression, tension, and shear resistance. Macroelements are particularly beneficial for seismic analysis, providing a balance between computational efficiency and accuracy (Penna et al. 2014, Lagomarsino et al. 2013).

The utility of macroelement models in seismic analysis has been well-documented in existing studies. They facilitate the assessment of dynamic responses, contribute to understanding structural behavior under seismic loads, and inform the development of retrofitting techniques.

This dissertation builds upon these foundational studies, employing macroelement modeling to further evaluate seismic performance, aiming to enhance both the understanding of masonry behavior and practical methodologies for preserving these historically significant structures.

In the equivalent frame approach for modeling masonry structures, piers and spandrels are typically represented by vertical and horizontal frame elements, respectively. This methodology enables a simulation of the mechanical behavior of masonry walls, capturing their influence on the overall structural performance. In this framework, piers function as column-like elements, with properties such as cross-sectional area, length, depth, material characteristics, and connection specifications tailored to match those of the actual masonry walls.

Accurate representation of piers and spandrels in equivalent frame modeling

requires attention to the following key factors: (i) interface conditions: Properly defining the connections among piers, spandrels, and other frame elements is essential to simulate the mechanisms of load transfer. These connections may be modeled as rigid or semi-rigid interfaces, depending on the response of mortar joints, reinforcement, or other elements that provide continuity within the masonry assembly; (ii) boundary conditions: Supports and boundary conditions for piers and spandrels must reflect the real constraints they experience. For example, base piers may be fully or partially restrained, while spandrels are often supported by adjacent piers or beams, affecting load distribution; (iii) material properties: Mechanical properties of piers and spandrels, such as compressive strength, elastic modulus, and Poisson's ratio, should be specified to reflect the masonry materials used in construction.

It should be noted that equivalent frame modeling is inherently a simplified approach, with the model's reliability contingent upon the assumptions made and the considered level of detail. More advanced analysis methods, such as FEM, can yield highly accurate representations of the behavior of piers, spandrels, and other masonry elements; however, they also require a significantly higher level of computational resources and technical expertise.

In this thesis work, an equivalent frame approach was used (Figure _).

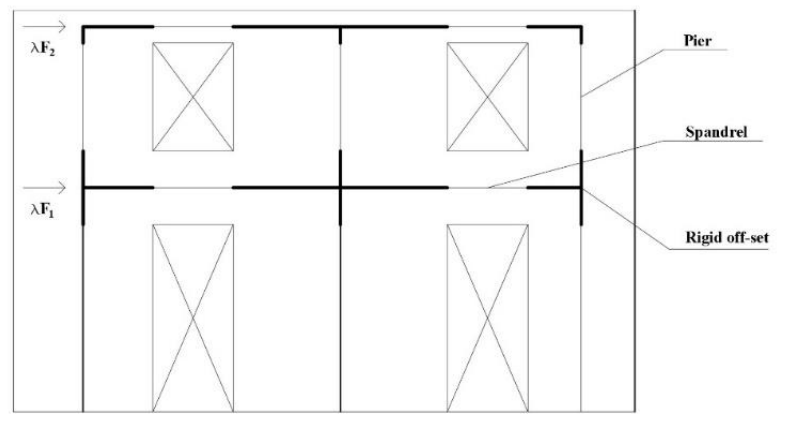


Figure 3.11 – Example of equivalent frame schematisation

The macro-elements were discretized into fibers (Acconcia and Parisi. 2020), considering flexural, shear behavior, and the influence of in-plane rocking.

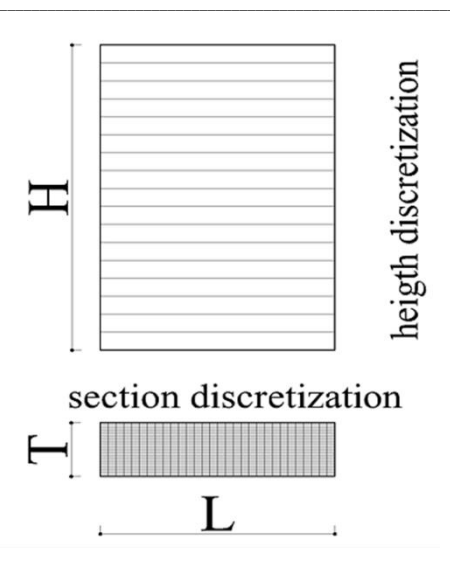


Figure 3.12 – Fiber discretization of the macroelement

The flexural behavior is simulated through numerical integration of moment-curvature diagrams along the height. The rocking contribution is accounted for by adding an additional displacement due to a pseudo-rigid rotation of the wall caused by progressive crushing at the base. The lateral resistance force corresponding to shear strength is predicted using local strength criteria. Shear stiffness is updated at each phase of the analysis to account for flexural cracking in the cross-sections and the gradual reduction of the secant shear modulus as the secant Young's modulus decreases under increasing inelastic stresses.

In Appendix B, the three behaviors are described along with their formulations. By integrating the flexural, shear, and rocking components, the outlined procedure enables the calculation of displacements and stresses throughout the entire element, with particular focus on the end sections, using the axial load and curvatures at these ends (which are initially unknown).

$$\delta = \delta_F + \delta_S + \delta_r \tag{1}$$

where and δ_F , δ_S , δ_r are the flexural, shear and rocking contributions to the displacement that are calculated in the Appendix B.

Combining these three components shows that it is unnecessary to separately know the individual contributions to the end-node displacement to determine the displacement at the opposite end. Likewise, the rotation can be determined. (see

Appendix B)

This approach provides the foundation for the iterative algorithm designed to establish the curvature at the ends of the macroelement, summarized as follows: (i) initial curvature values are assigned at the beam ends and (ii) using these values, the end-node displacements are calculated.

If the computed values align with the known ones within the accepted tolerance, the initial curvature values are accurate. Otherwise, the initial curvatures are adjusted, and the displacements recalculated. This iterative procedure is repeated until the curvatures that produce the required displacements are obtained.

Upon completing this iterative process, the stress characteristics relative to the element and the imposed displacements are determined, enabling the derivation of the element's fundamental stiffness matrix corresponding to the specified displacements.

Subsequently, the macroelement was validated through laboratory tests. Four tuff masonry wall specimens were tested under constant axial load and cyclically increasing lateral displacement in their plane.

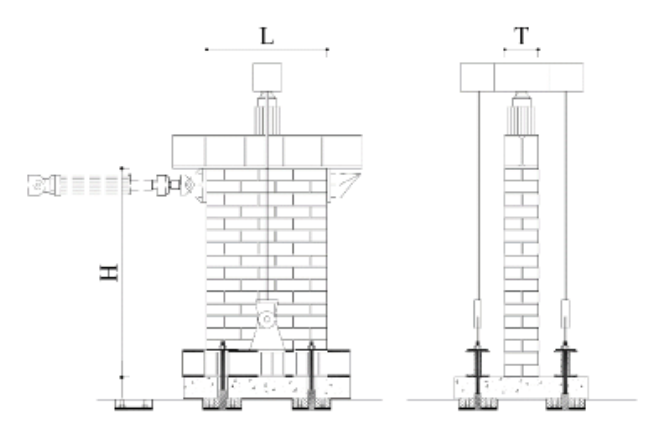


Figure 3.13 – Set-up of compression and shear tests

The following table 3.3 shows the dimensions of the panels, the ratio of the height to the width and thus the panel aspect ratio and the dimensionless normal stress.

In order to validate the analytical capacity model, each experimental test was simulated numerically.

Table 3.3 – Geometric and load characteristics of the panels. L:length (horizontal dimension)	;
History Histor	

				N/Nu
1.08	1.88	0.31	1.74	0.1
1.08	1.88	0.31	1.74	0.3
1.50	1.88	0.31	1.25	0.1
1.50	1.88	0.31	1.25	0.3
	1.08 1.50	1.08 1.88 1.50 1.88	1.08 1.88 0.31 1.50 1.88 0.31	1.08 1.88 0.31 1.74 1.50 1.88 0.31 1.25

In line with fiber modeling, the proposed approach enables the use of a uniaxial material model that varies for each fiber. The constitutive behavior is represented by a data set that specifies stress as a function of strain. This model can be simplified by linearizing the constitutive relationship, or alternatively, it can be discretized to incorporate (i) tensile strength, (ii) nonlinear behavior in the elastic phase, and (iii) post-peak behavior, which may exhibit softening or hardening characteristics.

In the applications presented, compressive behavior is modeled using the stress-strain relationships suggested by Augenti and Parisi (2010) in the direction perpendicular to mortar joints. In contrast, the tensile behavior of the masonry is treated as linear elastic up to the tensile strength, following an exponential softening curve to zero stress based on specified fracture energy.

For simplicity, it was assumed that the self-weight of the masonry was negligible compared to the assigned axial load and remained constant along the height of the panels. This assumption can also be removed, leading to increased computational costs. The constitutive model adopted for masonry under compression is Figure 3.14, discretized into 60 points. The peak compressive strength and corresponding strain were set at 3.96 MPa and 2.44x10⁻³, respectively. The ratio of peak tensile strength to peak compressive strength was set to $f_t/f_m = 0.05$, while the tensile fracture energy was set to $G_{ft} = 0.015 \, \text{N/mm}$. The diagonal tension shear strength at zero axial stress f_{v0} and the sliding shear strength at zero axial stress τ_0 were set to 0.0225 f_m . The displacement ductility factors $\mu_{v,max}$ and μ_v were set to 2.25 and 3.38, respectively. The residual shear force was considered a:

$$V_r = 0.3 V_{max}. \tag{2}$$

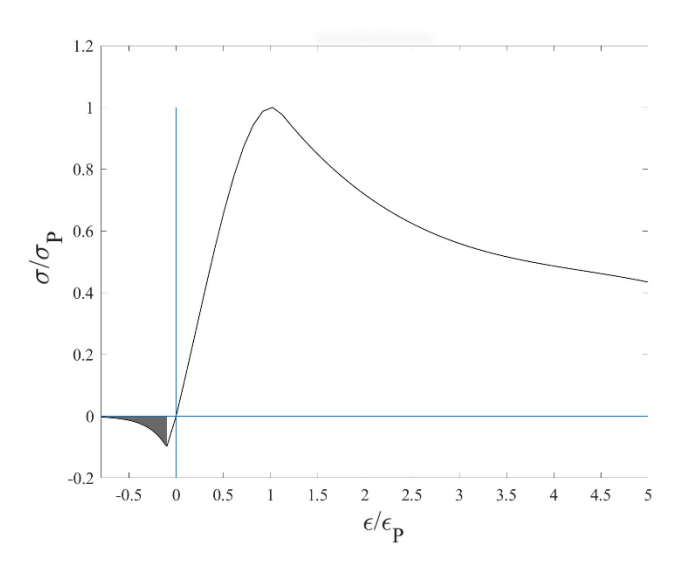


Figure 3.14 – Uniaxial constitutive model

Figure 3.15 shows both numerical and experimental shear diagrams for the four samples tested, which behaved differently from each other.

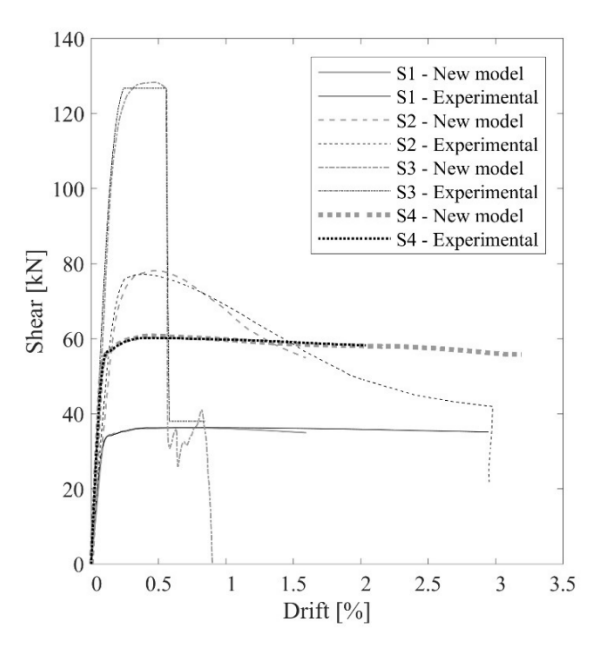


Figure 3.15 – Comparison of numerical and experimental shear curves

Having validated the code at the element scale, the equal-frame idealisation was validated by means of a laboratory test on a perforated wall (Parisi et al. 2011).

The wall was made of tuff masonry with stretcher bond and 10 mm mortar joints.

Overall dimensions: 5.10 m long, 3.62 m tall, and 310 mm thick. The piers were 1.70 m long, while the spandrel was 1 m high. The specimen was subjected to vertical loads of 200 kN on the piers, followed by horizontal displacement-controlled force applied at approximately 3.00 m from the piers' base.

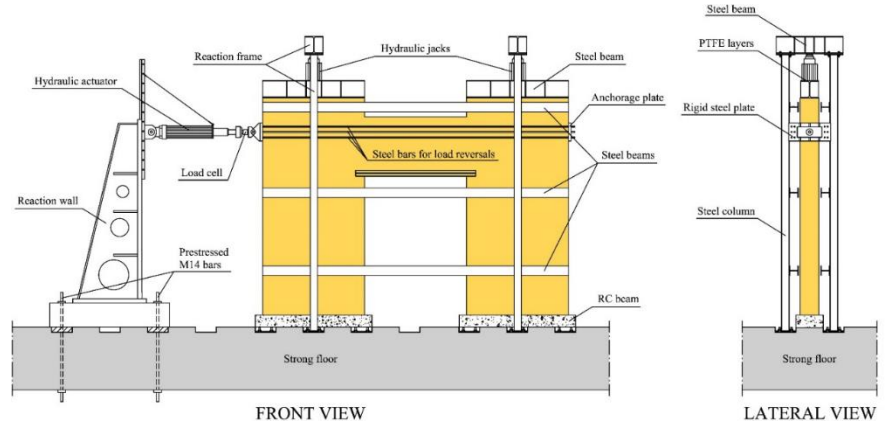


Figure 3.16 - Experimental setup of the full-scale unreinforced masonry wall with opening under lateral load

Our wall therefore consists of two pier panels, one spandrel panel and two node panels and has the following mechanical characteristics:

Table 3.4 – Mechanical properties of tuff masonry: f_t Tensile strength of masonry, f_m Compressive strength of masonry, E Young's modulus, G Shear modulus

Material	f_t	f_m	Е	G	
	[MPa]	[MPa]	[GPa]	[GPa]	
Tuff masonry (spandrel)	0.192	3.85	2.07	0.86	
Tuff masonry (piers)	0.198	3.96	2.22	0.92	

For load determination, two vertical forces of 200 kN were applied to the node panels to account for an upper storey, as done during the experimental test using hydraulic jacks that applied this force.

Once the equivalent frame was constructed (Figure 3.19) and a linear static analysis was performed using the developed calculation code, a nonlinear static

analysis of the structure was conducted to calculate the internal forces within the wall. This allowed for deriving the capacity curve, which could then be compared with the curve obtained from laboratory tests.

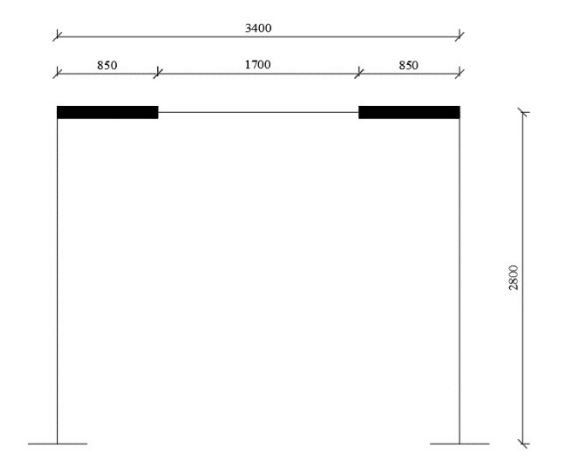


Figure 3.17 - Equivalent wall frame

Figure 3.18 show the numerical-experimental comparison in terms of base shear versus top displacement curves. The numerical procedure delivers satisfactory reproduction of the initial stiffness, peak base shear (experimental value of 184.31 kN vs. numerical value of 182.96 kN) and maximum lateral displacement.

The damage observed on the wall specimen at the end of the test was also well simulated, indicating flexural failure of both columns and diagonal shear cracking in the spandrel.

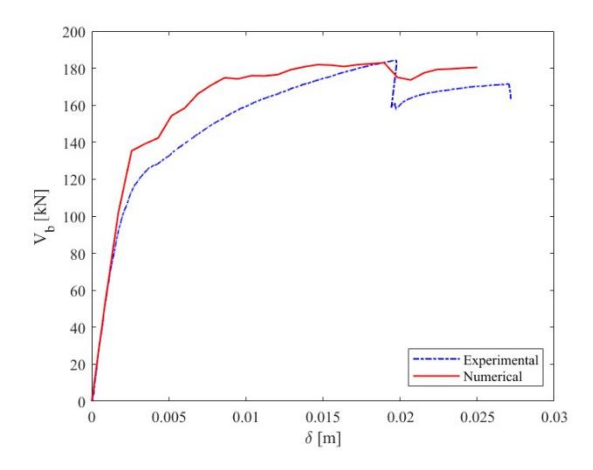


Figure 3.18 – Comparison of numerical and experimental capacity curves

For the analysis of the global behavior, the building was simulated through an

EFM, where macro-elements were modeled as beam elements connected by rigid offsets. These offsets were sized appropriately to account for variations in the deformability of the nodes. This approach produced a structure similar to the one depicted in the Figure 3.19. In this work, among four characteristic floor plans (courtyard, L-shaped, U-shaped and rectangular) the rectangular plan was chosen in order to obtain regularity in plan and height and to be able to carry out the analysis with less computational effort.

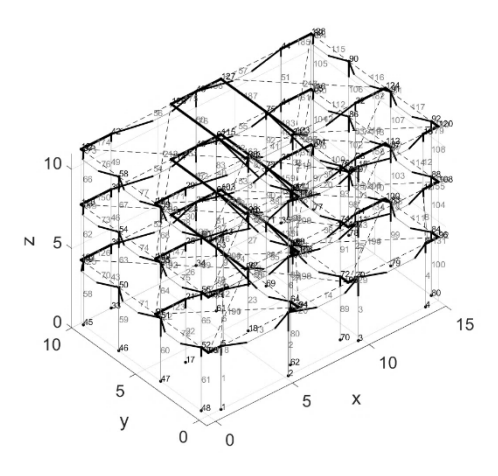


Figure 3.19 – Schematisation of the *i-th* building using the EFM.

The automatic generation of 1000 buildings for each selected sub-typology was carried out using a procedure entirely implemented in MATLAB, based on a Monte Carlo sampling algorithm of random variables and multi-parametric design, according to the percentage obtained from the CARTIS data for that sub-typology considered. The next step was the automatic generation of the building using a procedure developed in MATLAB. It was then assumed that each wall had a single opening in the space delimited by the intersection with two consecutive orthogonal walls, setting the height of the opening at 2.10 m and a pier length obtained by considering the percentage of opening provided by CARTIS.

The floors were modelled using equivalent diagonal rods to which, according to the type of floor (deformable, semi-rigid, rigid), an appropriate stiffness was attributed. A timber floor (deformable), a mixed floor made of steel beams and clay blocks (semi-rigid) and a slab of clay block and reinforced concrete (rigid) were considered. The permanent loads were determined separately for the three types of floors, one-way slab configuration in a single direction for the rigid

floors and an alternating one-way slab arrangement (with orthogonal orientations) for the deformable and semi-rigid floors.. Once the i-th building had been generated from these properties, the non-linear static analysis was carried out.

3.2.2. Structural sub-system

For the modeling of structural subsystems within the seismic vulnerability assessment of historical masonry buildings, a benchmark wall from the ReLUIS-DPC 2022-2024 project, specifically in WP10, task 10.3, was used. This wall was chosen for its representativeness of both internal walls and external facades typical of masonry buildings, providing a reference element for vulnerability and structural modeling studies.

The benchmark wall (Figure 3.20) is inspired by a spine wall of the P. Capuzzi school in Visso (Macerata), identified as "Wall d" in the ReLUIS guidelines and later renamed "Wall XX" in the document's version 2.0. With significant dimensions (21.7 m in length, 8.77 m in height, and 0.55 m in thickness), this two-story wall has a geometric ratio of 0.4, a configuration that allows for realistic simulation of the behavior of masonry walls in historical buildings.

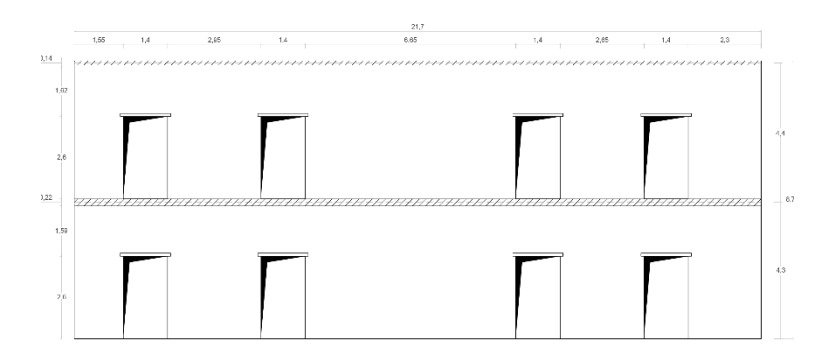


Figure 3.20 - Benchmark wall

The whole wall is made of the same masonry. Each spandrel is supported by a lintel made of prefabricated reinforced concrete and clay block beams, anchored at the ends for 10 cm. At the floor level, a reinforced concrete ring beam ensures the connection between the masonry panels and floors. This ring beam has a thickness of 0.55 m, with a height of 0.22 m on the first floor and 0.14 m on the

second floor. Its reinforcement includes four longitudinal bars with a diameter of 12 mm and 8 mm stirrups with a 100 mm spacing, meeting the requirements for strength and stability.

The floors acting on the benchmark wall are of two types: a reinforced concrete floor on the first level and a mixed steel beam-clay block floor on the second level, in addition to a saddle roof that generates an equivalent distributed load. The masonry can be assumed as equivalent to the "Roughly cut stone with good bond masonry" type in the Commentary n.7/2019. The mechanical properties of the masonry were selected with an intermediate knowledge level (LC2), applying a confidence factor of 1.2 to reduce the strengths.

The modulus of elasticity (E) and shear modulus (G) of the masonry do not account for degradation effects due to cracking, while the concrete characteristics are similar to those of class C12/15 in the Italian building code(NTC18). The longitudinal bars and stirrups have a tensile strength of 412 MPa and a yield strength of 294 MPa, with a maximum deformation of 20%, also reduced by the confidence factor.

Table 3.5 – Mechanical properties of masonry: f_m : compressive strength; τ_{od} :shear strength; ν : Poisson's ratio; E:Young's modulus; G:Shear modulus; w:unit wight(density)

f_m	$ au_{0d}$	v	E	G	w
[MPa]	[MPa]	[-]	[MPa]	[MPa]	$[kN/m^3]$
2.67	0.054	0.50	1740	580	21

For load modeling, the permanent structural and accidental load of the floors and the combined seismic load are those reported in the Table 3.6. (g: dead load; q: live load; w_s : design load for the quasi-permanent combination)

The influence length is assumed to be 5 m, considering that the spine wall supports the floors on both sides. In conclusion, this benchmark wall, fixed at the base and with no internal constraints at the floor level, was used as a structural subsystem for analyzing and modeling structural behaviors in the context of seismic vulnerability.

It provides a reliable foundation for calibrating numerical models and simulating the seismic response of historical masonry buildings.

Level	Floor type	g	q	w_s
		$[kN/m^2]$	$[kN/m^2]$	$[kN/m^2]$
1st	one-way lightweight reinforced concrete ribbed slab	4.85	3.00	6.65
2nd	steel-clay slab	1.92	-	2.42
	roof	1.50	-	3.42

The benchmark wall was modeled using an equivalent frame approach through the code described in Section 3.3 (Figure 3.21). The resulting capacity curve was then compared with capacity curves obtained from other softwares, specifically ABAQUS (a FEM software) and TREMURI (an EFM software).

These comparisons allow for a comprehensive validation of the modeling approach, highlighting the reliability and accuracy of the EFM used in the analysis.

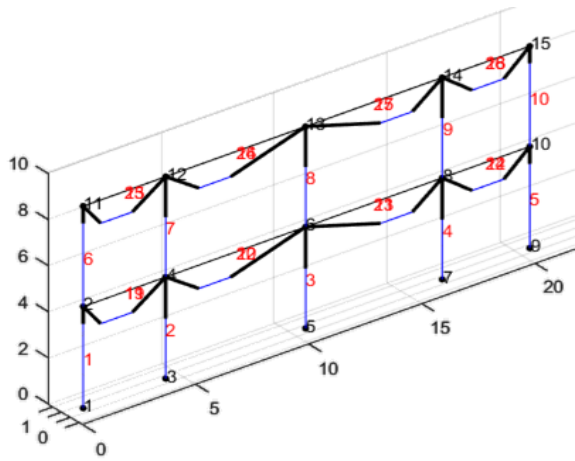


Figure 3.21 – EFM model of the benchmark wall

Figure 3.22 presents the capacity curves of the benchmark wall obtained through three different models: MATLAB, TREMURI, and ABAQUS.

Observing the ABAQUS model (gray line), we see a higher peak shear strength compared to the other two, followed by a decrease due to stress redistribution and material plasticization. Similarly, the TREMURI software (orange line), reaches a higher maximum shear than the MATLAB model (blue line), which exhibits a more consistent trend with a lower peak shear.

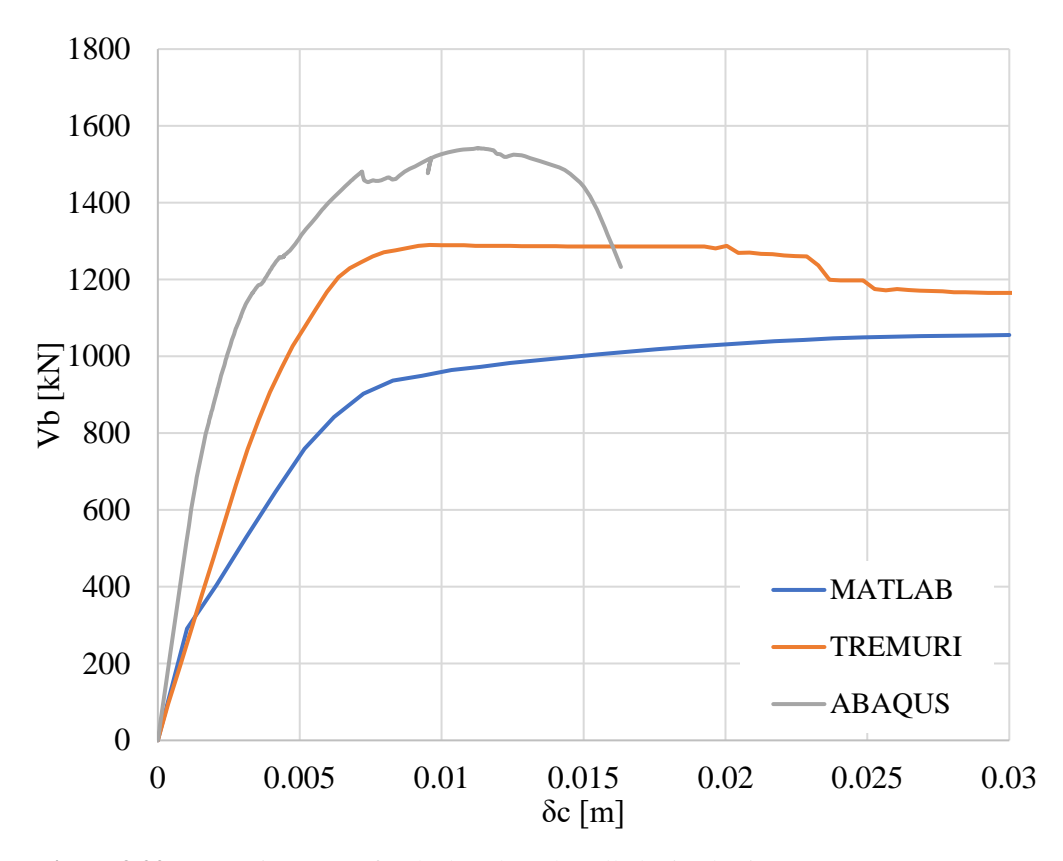


Figure 3.22 – Capacity curves for the benchmark wall obtained using MATLAB, TREMURI, and ABAQUS models

The discrepancy in the peak shear values among the models can be attributed to the behavior of the wall panel M3 (Figure 3.23), a central, squat element that is influenced by shear resistance criteria.

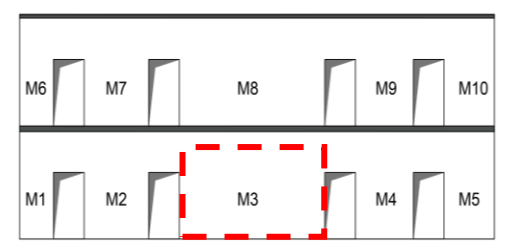


Figure 3.23 – Identification of Panel M3 in the Benchmark Wall

In the ABAQUS and TREMURI models, the shear-tension failure criterion (V_t) , which limits the shear capacity of the panel, is not considered. As a result, these

models display higher shear capacities since they continue to support greater shear forces. In contrast, the MATLAB model includes the V_t criterion, causing panel M3 to reach failure upon exceeding the specified shear stress limit.

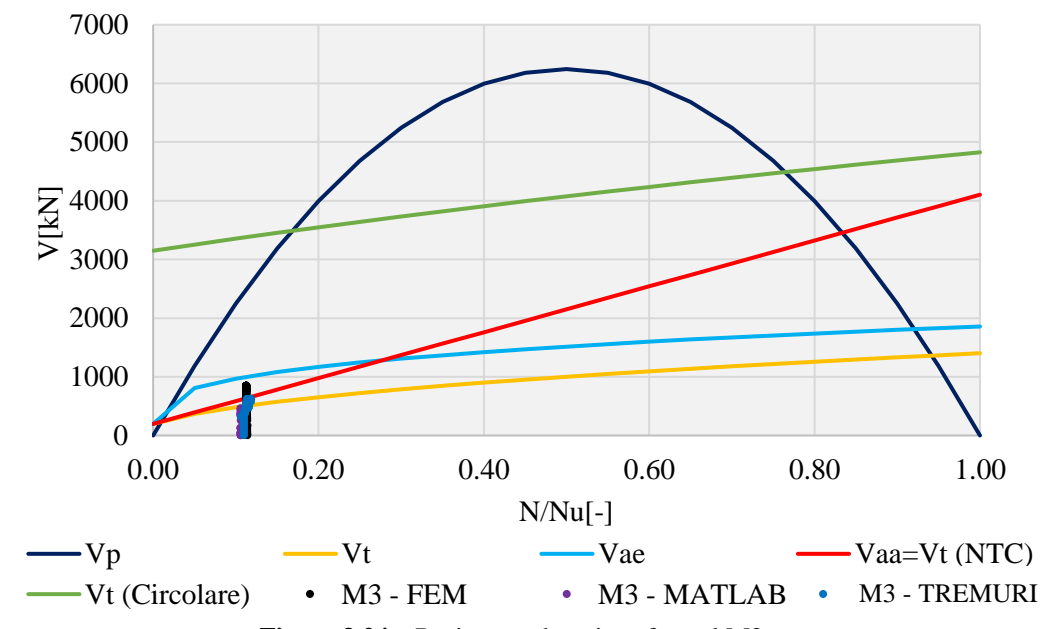


Figure 3.24 – Resistance domains of panel M3

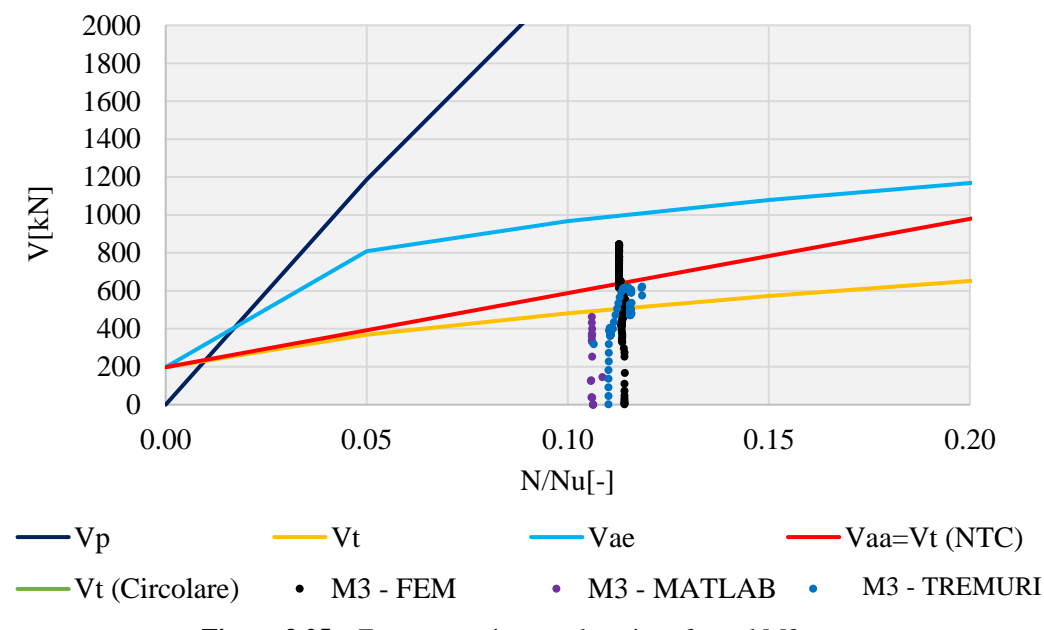


Figure 3.25 – Zoom on resistance domains of panel M3

To quantify this difference in shear capacity, an analysis on the τ_0 value (Table 3.7) was conducted. It was found that, to achieve the peak shear of the 3MURI and ABAQUS models, τ_k values of 0.074 and 1.124, respectively, would be required, compared to the reference value of 0.054 specified in Commentary No. 7/2019 for the masonry type under study.

In conclusion, while the FEM modeling in ABAQUS provides a more detailed and accurate analysis compared to the EFM approach, it necessitates a more rigorous calibration of both the model and material properties to yield realistic results. On the other hand, the EFM approach, especially as implemented in the MATLAB model, offers an efficient balance between computational effort and simulation reliability, achieving a realistic representation of structural behavior while adhering to failure criteria without excessive computational complexity.

The table 3.7 presents the values of V_t obtained for the panel under analysis. However, it is unrealistic to reach these values in TREMURI and ABAQUS, as achieving them would require an equally high τ_k value. Such a value is not feasible for the selected masonry type and exceeds the limits provided by Commentary n.7/2019 for this masonry category.

Regarding the reviewer's concern, V_t is not a predefined code strength but rather the maximum shear force reached in the analysis for the given τ_k . The variation in V_t across different software results from differences in modeling approaches, assumptions, and how each program handles material behavior and failure criteria.

Table 3.7 – Goal seek τ_k values for different softwares

Software	$\mathbf{V}_{\mathbf{T}}$	V _T /N _u	$ au_{ m k}$
Software	[kN]	[-]	[MPa]
TREMURI	611.8	0.06265	0.074
MATLAB	461.3	0.04723	0.054
ABAQUS	840.2	0.08604	1.124

3.2.3. Single element

The horizontal structures (vaults, floors, roofs), in addition to transferring gravitational loads to the vertical load-bearing elements, serve as stiffening structures capable of distributing horizontal actions. Their stiffness influences the overall response of the building; for instance, in the case of rigid floors, actions are distributed among the walls. Conversely, with infinitely flexible floors, no redistribution occurs when the ultimate conditions of a wall are reached. For these reasons, in historical buildings where vaults are commonly present, assessing the flexibility of the horizontal structures becomes crucial.

The evolution of construction methods and techniques over time has enabled the creation of various types of vaulted structures, each exhibiting distinct structural behavior based on: geometry, stiffness, mass distribution, past interventions, masonry pattern, boundary conditions.

When the horizontal structures consist of vaults, modeling becomes more complex, as it requires schematizing and quantifying the vault's response.

In order to study these specificities, one of the building archetypes obtained by automatic generation was examined, which will be referred to below as 'Archetype 1'.

Archetype 1 features irregular masonry with rough stone (A2). It can be modeled as a rectangular parallelepiped with a total area of 150 m² and an overall height of 11 m. The structure extends over two levels, in addition to an accessible roof reachable through an internal staircase covered by a tower with a total height of 2.40 m. The ground floor has a height of 4mand is occupied by two units designated for non-residential use, symmetrically arranged around the staircase. The upper levels are each 3.50mhigh and contain one residential unit per floor. The building includes a common entrance leading to a vestibule providing access to the staircase, while access to the ground-floor spaces is allowed through external doors. Each residential unit primarily consists of spacious, shared areas.

The building's vertical load-bearing structures consist of four perimeter walls and three internal walls. These walls are built of masonry with a thickness of 0.75 m and an average spacing of 5 m. On the first floor, two masonry barrel vaults are present, having spans of 3.40 and 5.10 m, respectively. On the second and third levels, the floors are made of timber, with beams oriented in a single

direction, composed of 20 cm-thick oak beams set into the masonry walls, supporting a 3 cm-thick chestnut plank decking.

Cantilevered elements consist of masonry beams embedded directly into the walls, supporting marble slabs. As previously mentioned, the floors are connected by a staircase with cantilevered stone steps directly embedded into the masonry walls. Access to each floor is provided by two flights of stairs separated by a landing.

Figure 3.26 shows the ground floor plan and a typical floor plan of Archetype 1.

In Archetype 1, the subject of this analysis, barrel vaults (present on the first level) were examined using the ARCO program (Gelfi 2002), to determine the forces transferred to the masonry piers. Subsequently, for modeling in the equivalent frame, the methodology proposed by Cattari et al. (2008) was adopted.

In this approach, vaults are modeled as diaphragms in membrane state using finite elements with isotropic or orthotropic behavior and equivalent stiffness.

The analysis of the statics of masonry arches and vaults began in the late 17th century, with later fundamental contributions by Coulomb about collapse mechanisms, and Méry about the concept of the thrust line.. It was only in the 1960s, thanks to studies conducted by Heyman 1982, that the foundations for analyzing masonry arches using limit analysis theory were established.

The use of the static and kinematic theorems is due to the computational difficulties arising from uncertainties related to constitutive laws, cracking, and load history.

The static theorem of limit analysis can be stated as follows: "If a thrust line can be found, for the complete arch, which is in equilibrium with the external loading (including self-weight), and which lies everywhere within the masonry of the arch ring, then the arch is safe.".

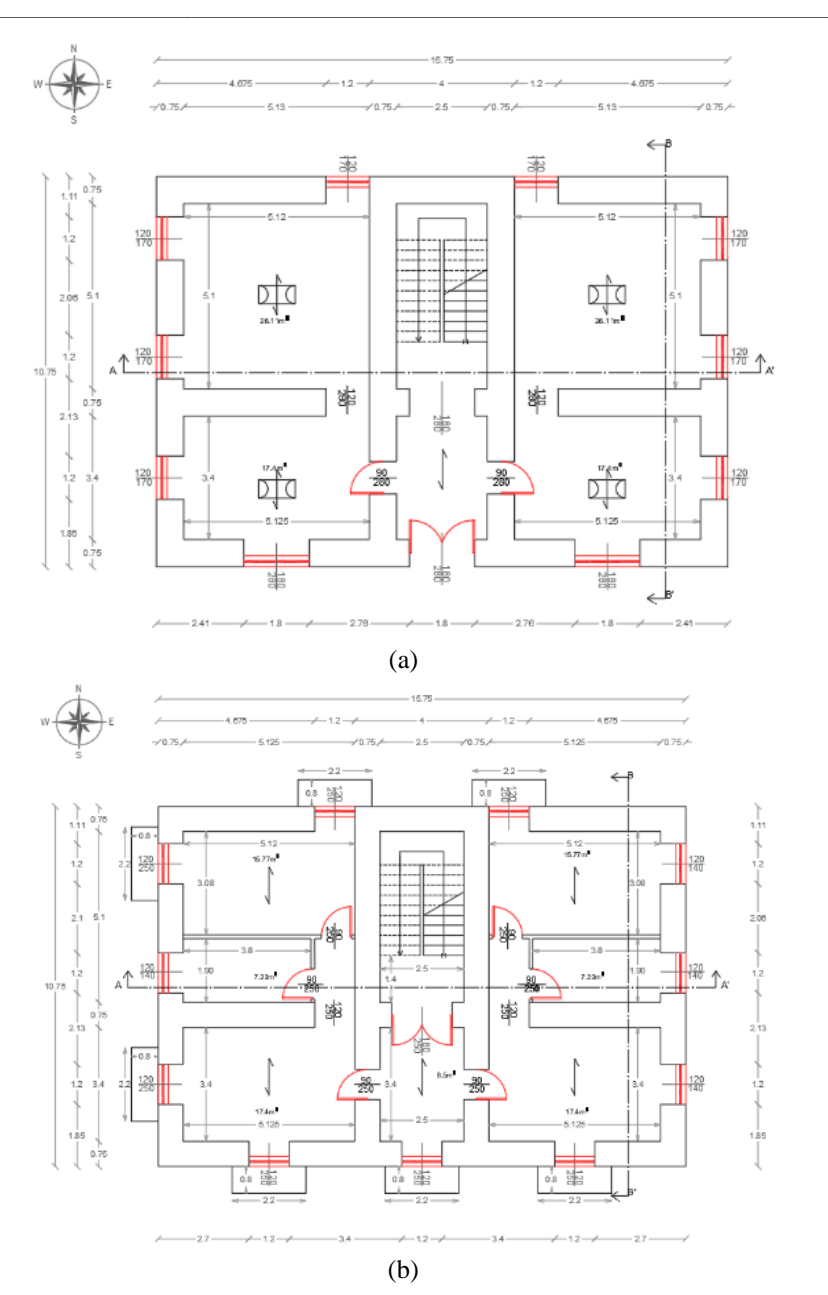


Figure 3.26 – Floor plans of Archetype 1: a) Ground floor; b) Typical floor

This theorem justifies Méry's method, which seeks the thrust line within the arch. Specifically, the arch structure, which is three times statically indeterminate, is made statically determinate by introducing three hinges at locations where moments are assumed to be zero. The positions of these hinges

are varied to find an admissible stress state. If the thrust line remains within the

kern in every section, the arch will be uncracked.

From a numerical perspective, it is possible to derive the center of pressure (e_i) of an i-th section by first calculating the support reactions H, V_s and V_d of the arch, and subsequently determining the internal forces M_i , N_i and T_i in the section under consideration. With reference to Figure 3.27, the following relationships can be obtained:

$$H_i = H \tag{3}$$

$$V_i = R_q + R_r + R_a - V_s \tag{4}$$

$$M_i = V_S \cdot b_{VS} - H \cdot b_h - R_q \cdot b_{Rq} - R_r \cdot b_{Rr} - R_a \cdot b_{Ra}$$

$$\tag{5}$$

$$N_i = H_i \cdot \cos \alpha i - V_i \cdot \sin \alpha_i \tag{6}$$

$$T_i = -H_i \cdot \sin \alpha i - V_i \cdot \cos \alpha_i \tag{7}$$

$$e_i = M_i / N_i \tag{8}$$

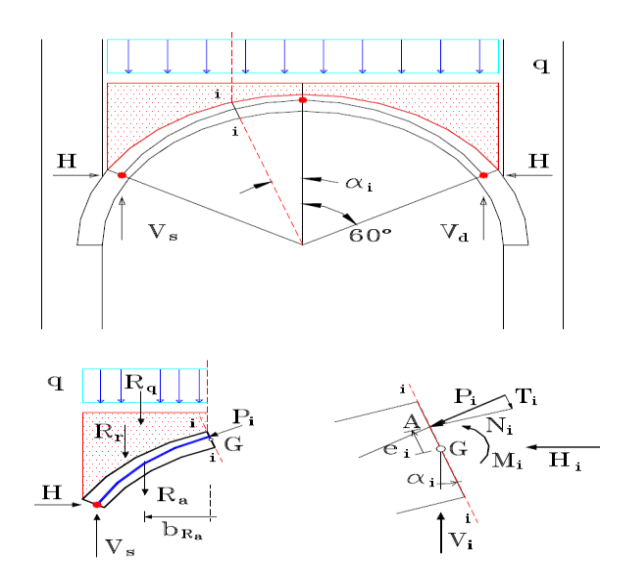


Figure 3.27 - Position of the centre of pressure for the i-th section

Considering the barrel vaults in the case study as a succession of arches, it was possible to analyze them using the ARCO software, which is based on the concepts just outlined. By relying on the static theorem of limit analysis, this program allows for the calculation of the reactions exerted by the arch at its supports and its pressure line (line passing through the centers of pressure) as a function of geometry, mechanical parameters, and applied loads. After defining

the intrados of the arch, the program requires the input of the following geometric data and material mechanical parameters: L (Span); h (Rise); t (Thickness); n (Number of voussoirs); h_1 (Thickness of the filling at the crown);); γ_m (Specific weight of the arch); γ_1 (Specific weight of the filling); γ_2 (Specific weight of the finishing layer).

Once the geometry of the arch is defined, load application follows. In applying the limit state verification method, partial safety factors for actions and resistances are employed. The selection of these factors must account for both the effect of the self-weight, which tends to center the pressure line, and uncertainties related to the geometry of the arch as well as the applied loads.

In Archetype 1, there are two different barrel vaults, each of which spans two floor bays.

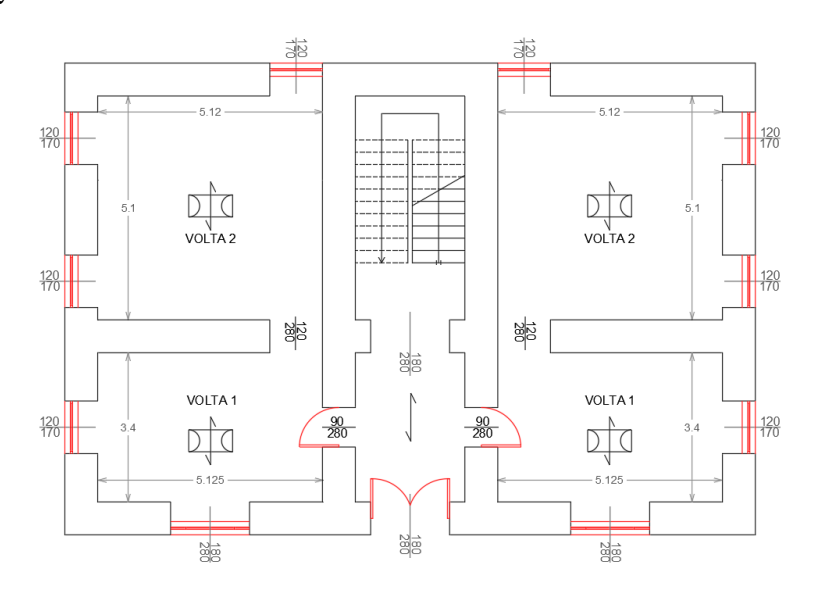


Figure 3.28 – Identification of Vaults in Archetype 1

The arch used to schematize Vault 1 has a span of 3.40 meters, a rise of 0.66 meters, and a crown filling of 0.2 meters. The thickness of the arch is 0.24m (voussoir height) at both the springing and the crown. The design density values for the materials, considering a partial safety factor of 0.9, are 18 kN/m³ for the masonry, 15 kN/m³ for the filling, and 16 kN/m³ for the vault cover. Finally, the design value for the live load is 12.18 kN/m², using a partial safety factor of 2.

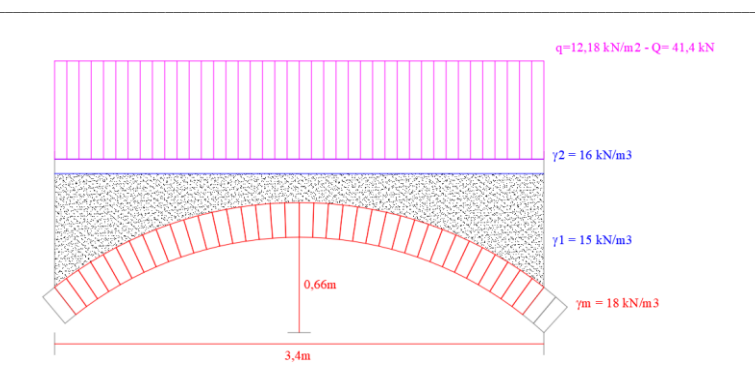


Figure 3.29 - Geometry of Arch 1

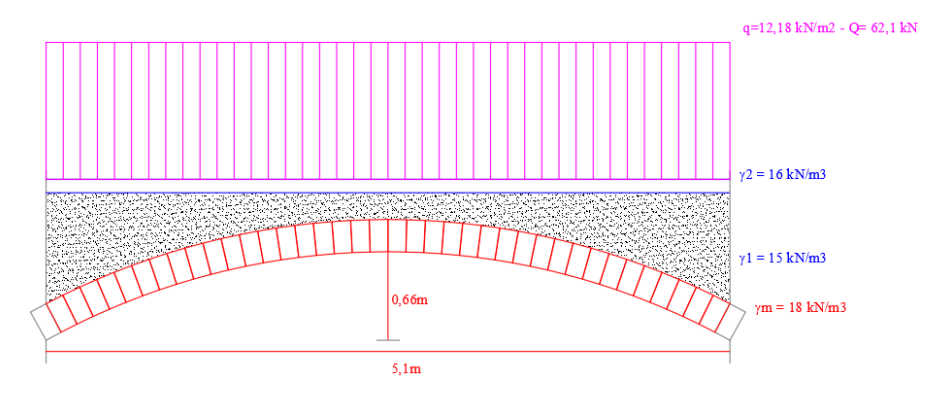


Figure 3.30 – Geometry of Arch 2

The arch used to schematize Vault 2 is equal to that of Vault 1 but has a span of 5.10 m.

Once the arch is implemented in the program, it is possible to set the calculation options. At this stage, users can choose to optimize the pressure line and consider passive pressures. Optimizing the pressure line allows for an improved solution by defining the number of segments into which the arch thickness is divided, to vary the hinge positions during analysis. Initially, the optimal hinge positions are equal to the arch thickness divided by the number of steps; subsequently, if the pressure line is not fully contained within the arch, it is updated by the program.

Considering passive pressures allows for accounting for the effect of horizontal actions that can be mobilized when the arch pushes against the backfill. In particular, under asymmetric loading conditions, the arch tends to deform toward the backfill material, which reacts with its passive resistance. For safety, the program considers the backfill as an additional load without accounting for passive thrusts. However, in some cases, to satisfy verification requirements, it

is necessary to consider horizontal pressures, as they help recenter the pressure line. In this regard, the passive pressure calculation option allows users to input a thrust coefficient, typically between 0.5 and 2, and the number of voussoirs subject to these actions.

In the present case, pressure line optimization was considered, setting the default number of steps to 10, which offers a good balance between accuracy and computational time. Passive pressures were not included, as a uniformly distributed load is applied across the entire span. With the geometric and mechanical characteristics of the arch defined and the calculation options set, the analysis proceeds. The ARCO software graphically displays the position of the pressure line and the maximum stress diagrams in each section at the extrados and intrados. The stress values are calculated according to the elastic theory for materials that do not resist tension.

$$\sigma_{max} = \frac{2N}{3u} \tag{9}$$

In the (9) σ_{max} is the maximum stresses at the extrados and intrados of each section, computed using classical elastic theory under the assumption of nontensile-resistant materials N is the axial compressive force per unit width of the arch; u is the distance of the pressure line from the compressed edge.

If the pressure line lies outside the section, equilibrium cannot be achieved without tension; therefore, stresses are calculated by considering the entire section as reactive:

$$\sigma_{max} = \frac{N}{t} + \frac{6Ne}{t^2} \tag{10}$$

These values are included in a numerical report, which also lists the percentage of the compressed section, the values of the horizontal and vertical components of the reactions at the supports, the tension in any tie rod assumed to be positioned at the supports, and the values of horizontal forces and bending moments due to passive pressures (if considered). Below are the results of the analyses conducted on the arches used to schematize the vaults in Archetype 1:

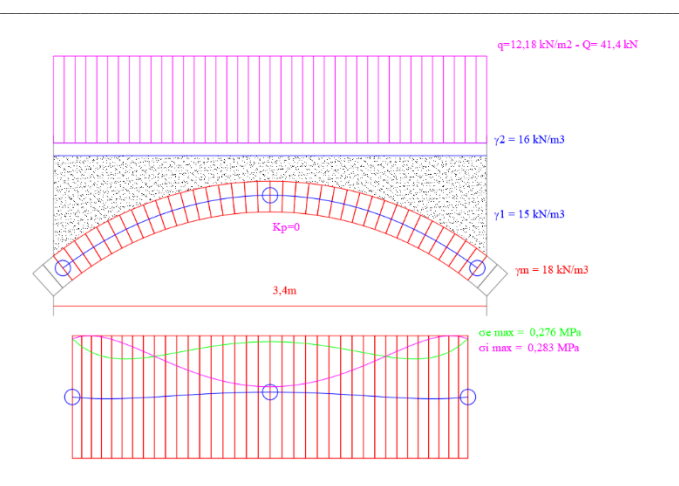


Figure 3.31 – Graphical Results of Arch 1

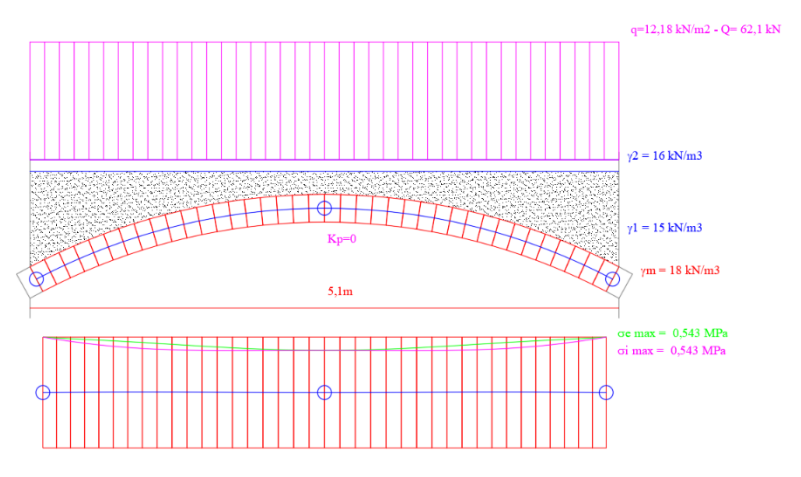


Figure 3.32 – Graphical Results of Arch 2

In Appendix A, the results of the analyses conducted on the arches used to schematize the vaults of the archetype are presented.

Modeling vaults within the EFM approach is essential for both studying the global response of the building and estimating how vaulted elements influence structural behavior. In this regard, Cattari et al. (2008) propose correlating the axial and shear stiffness of vaults with that of an equivalent plate characterized by the same plane dimensions and thickness. Here is a summary of the main steps based on the approach by Cattari et al. (2008):

- 1. Modeling as an equivalent plate: vaults are modeled as an equivalent plate with the same plane dimensions and thickness to determine elastic parameters in the x, y directions, and the shear modulus.
- 2. Axial and shear behavior analysis: displacements and self-equilibrated forces are applied to one side of the plate (with constraints on the opposite side) to calculate the equivalent Young's modulus for axial stiffness and the shear modulus.
- 3. Parametric analysis: thickness-to-span and rise-to-span ratios, along with boundary conditions, are varied to explore the influence of geometry and support conditions.
- 4. Analytical models: analytical expressions for axial (E_V/E) and shear (G_V/G) stiffness ratios are derived based on numerical results, with distinctions made for different vault types.

These steps provide the equivalent stiffness values of vaults, which are then incorporated into the building's EFM to assess the global response. It then proceeded with the calculation of the ratios E_V/E and G_V/G for the vaulted structures in Archetype 1 (Table 3.9), given their geometric characteristics (rise, span, and thickness – Table 3.8)

Table 3.8 – Geometric characteristics of the vaults

Vault	Rise (f)	Span (L)	Thickness (s)	f/L	s/L
vaun	[m]	[m]	[m]	[-]	[-]
1	0.66	3.40	0.24	0.19	0.07
2	0.66	5.10	0.24	0.13	0.05

By considering the average values of the mechanical properties, the elastic moduli of the material composing the vault (rough-cut ashlar masonry with unevenly thick facings) are determined. By multiplying these values by the stiffness ratios obtained from the formulas, the moduli Ev/E and Gv/G are defined for use in modeling the vaulted structures within the equivalent frame.

Table 3.9 – The stiffness values of the vaults

Ev/E	Gv/G [-]	E [MPa]	G [MPa]	Ev [MPa]	Gv [MPa]
6.18E-04	0.7963	1230	410	0.76	326.48
3.20E-04	0.8988	1230	410	0.39	368.52

Defined the modeling of the vaults within MATLAB using the equivalent frame approach, the deformational capacity of the vaults was analyzed to identify their limit state within the capacity curves of Archetype 1.

Specifically, with the displacements of all structure nodes available for each analysis step, the collapse condition of the vaults was determined based on the displacement of the supports.

In this context, given that barrel vaults are generated by the translation of an arch, the methodology proposed by Di Carlo and Coccia (2020) was applied.

The authors examine the failure condition of elliptical masonry arches under permanent loads and finite support displacements, utilizing the kinematic approach of limit analysis and modeling the deformed structure as a system of rigid blocks in frictional contact. Additionally, the authors conduct a parametric analysis using graphical tables to evaluate the influence of geometric characteristics on the horizontal collapse displacement of the supports and the associated thrust. This methodology, which enables the assessment of internal hinge positions within the arch as support displacement increases up to collapse, is based on Heyman's assumptions.

Using the parametric study results, the behavior of Archetype 1 vaults was analyzed in terms of the support displacement leading to collapse. Specifically, by varying the thickness t, the semi-axes a and b, and the mean radius R_m of an equivalent circular arch of the same thickness, it is possible to reference a chart providing the dimensionless collapse displacement.

In particular, the chart displays the trend of collapse displacement, dimensionless with respect to the arch thickness, as the ratio between thickness and mean radius (t/R_m) varies for different geometries (ratios between semiaxes of the ellipse, b/a, with a=(L+t)/2 and b=f+t/2). Archetype 1 features, on its first level, four vaults with the following geometric parameters:

Table 3.10 – Geometrical characteristics of barrel vaults

Vaults	t	a	b	b/a	$\mathbf{R}_{\mathbf{m}}$	t/R_m
vauns	[m]	[m]	[m]	[-]	[m]	[-]
1 and 3	0.24	1.82	0.78	0.4	1.25	0.2
2 and 4	0.24	2.67	0.78	0.3	1.73	0.15

Since the curves corresponding to the calculated b/a ratios for the vaults in question were not available in the chart, a trend line was determined to derive the

collapse displacement. By using the computed $t/R_{\rm m}$ ratio on the graph, the corresponding ordinate values were identified for all represented geometries (see Figure 3.33).

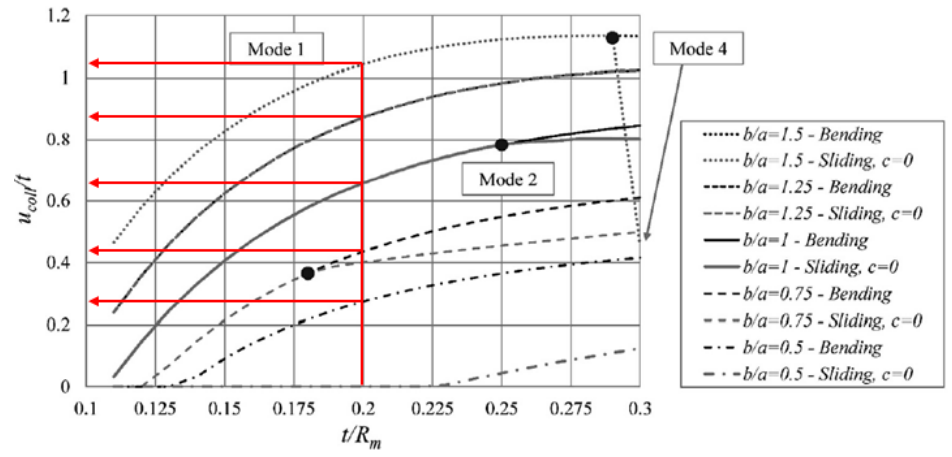


Figure 3.33 – Identification of displacement values set the t/R_m value (background plot from Di Carlo and Coccia 2020)

Each value was then plotted on a Cartesian plane with the elevation-to-span ratio (b/a) on the x-axis and the dimensionless collapse displacement (u_{col}/t) on the y-axis. Setting the y-intercept to zero for the condition where b/a=0, in which the arch resembles a beam, a trend line was established that best represents the data pattern. Specifically, in both cases, a fourth-degree polynomial function with an R^2 parameter close to one was identified.

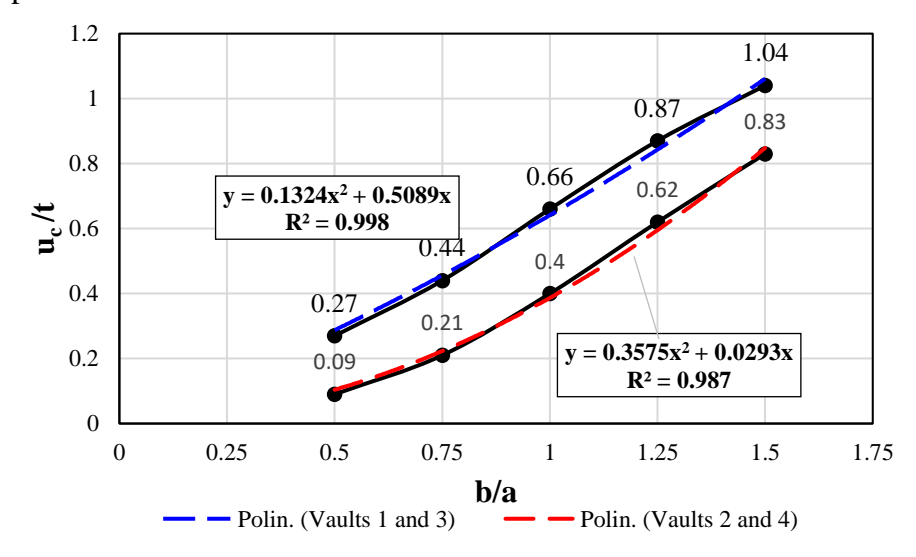


Figure 3.34 – Correlation between collapse displacement and b/a ratio

By inputting the b/a ratios of the arches representing the vaults in the studied building archetype into the derived functions, the support displacements that lead to collapse conditions were determined.

Table 3.11 – Displacement values of supports determining the collapse condition in vaults

Vaults	t/R _m	b/a	uc/t	u c
vauns	[-]	[-]	[-]	[m]
1 and 3	0.2	0.4	0.21	0.050
2 and 4	0.15	0.3	0.04	0.009

Once these values were obtained, it was essential to compare them with the displacements of the vault supports from the nonlinear static analysis. This enabled the identification of the specific point on the capacity curves where the vault collapse occurs. As an example, the following Figure 3.35 presents the capacity curve in the positive Y direction for a mass-proportional distribution.

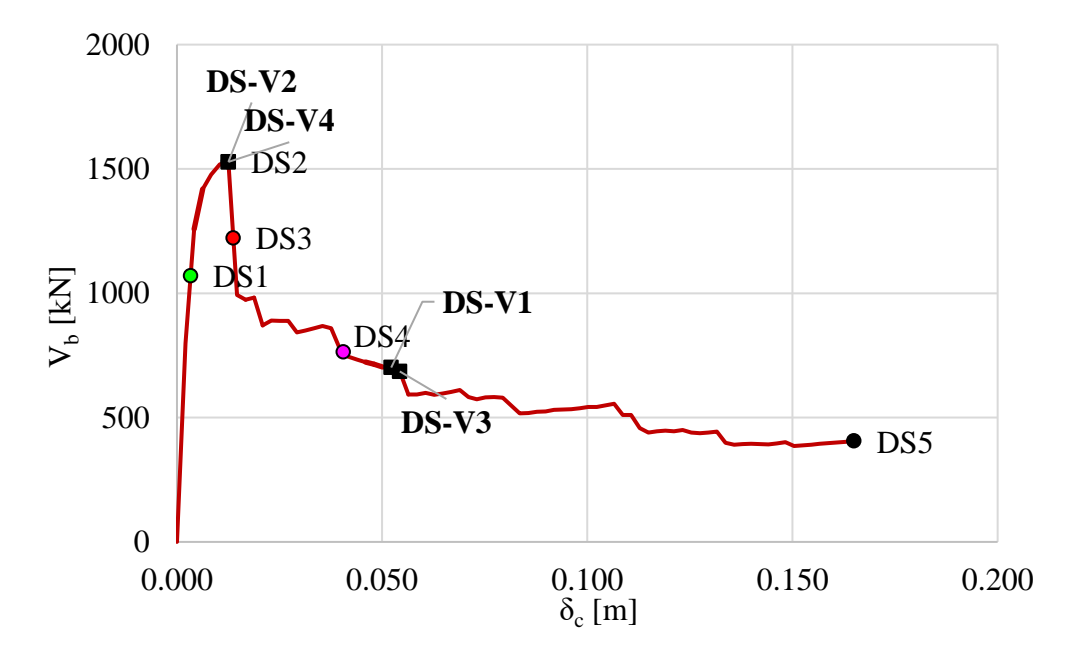


Figure 3.35 - Vault crisis on the Y+ capacity curve with mass-proportional distribution

On all pushover capacity curves, five damage states were identified as:

- DS1 at 70% of the maximum base shear (V_{b,max}) on the increasing branch of the capacity curves.
- DS2 at V_{b,max}.

- DS3 at 20% degradation of V_{b,max}.
- DS4 at 50% degradation of $V_{b,max}$.
- DS5 when the ultimate displacement is reached.

Finally, it was considered appropriate to assess the influence of the vault collapse condition on the overall damage of the building. This analysis was conducted by comparing the displacement capacity of the building at the point where the first vaulted structure of the archetype reaches failure (DS-V) with the points representing the attainment of limit states for the entire structure (DS1, DS2, DS3, DS4, DS5) (Figure 3.36 and Table 3.12).

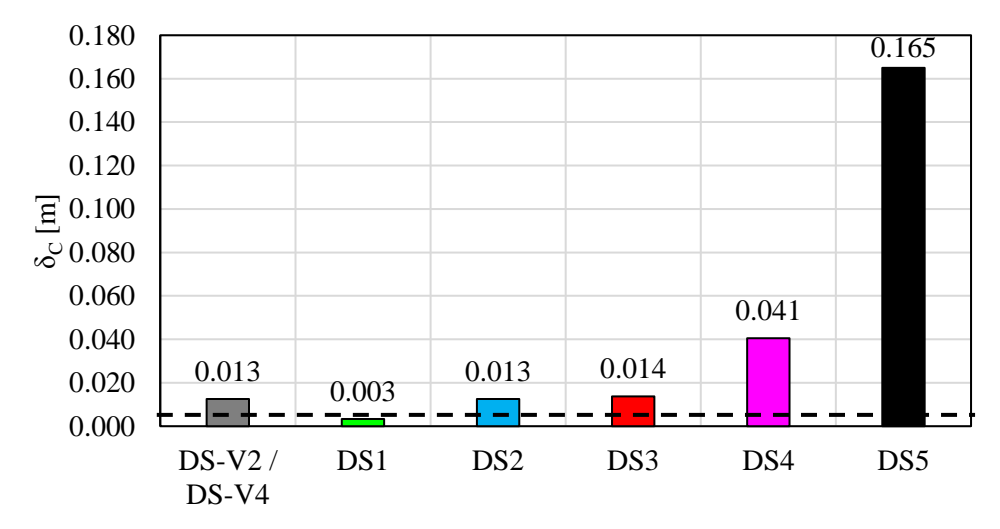


Figure 3.36 – Comparison of vault capacities and limit states of Archetype 1 (Dist. Mass proportional, Dir. Y+)

It can be observed that the collapse of vaults 2 and 4 occurs at the attainment of the maximum base shear that the structure can withstand. Theoretically, with the collapse of these ground-floor vaults, the capacity curve should terminate at that displacement value. This highlights the significant influence of the vaults on the overall structural behavior, especially when they are located on the ground floor of historical masonry buildings, where their damage or collapse could compromise the stability of the entire system.

This underscores the importance of studying individual elements that introduce specific vulnerabilities but ultimately impact the total vulnerability of the structure.

Table 3.12 – Percentage difference between global displacement for different limit states and the limit state of the vaults

5			
	DS	δc	Δδς
	[-]	[m]	[%]
	DS-V2 / DS-V4	0.013	-
	DS1	0.003	-73.5%
	DS2	0.013	+0.0%
	DS3	0.014	+9.5%
	DS4	0.041	+223.2%
	DS5	0.165	+1216.7%

To gain a comprehensive understanding of the structural behavior of masonry buildings, it was essential to focus on individual elements within the walls, such as masonry panels. This study specifically targeted the most influential parameters governing failure behavior in masonry panels. Leveraging artificial intelligence models and using the Python programming language, analytical expressions were formulated for calculating panel drift, distinguishing between flexural and shear failures. This approach allowed results to be obtained that accurately reflect the influence of each parameter without relying directly on complex numerical models.

A robust database comprising approximately 180,000 panels with varying geometric characteristics was first constructed. Using a shear span equal to 1, the analysis concentrated on damage state 5 (collapse prevention), aiming to develop formulations aligned with the provisions of the Italian Building Code (NTC) 2018.

A critical aspect of this approach was the use of symbolic regression. Unlike traditional regression methods, symbolic regression does not assume a predefined functional form but instead searches for a mathematical relationship that best describes the provided data. It combines optimization and machine learning techniques to identify algebraic structures that correlate input and output variables. Symbolic regression was chosen over other methods because, in addition to providing accurate predictions, it yields interpretable expressions that facilitate understanding of the physical behavior of masonry panels. This is especially valuable for correlating panel drift with geometric and mechanical parameters in a way that remains faithful to structural reality and regulatory standards.

Several mathematical models were developed, and the most representative model with the lowest mean square error was selected. The derived formulations were then compared with numerically obtained drift values using a fiber-based macroelement model (discussed in the previous section), enabling an estimation of error and standard deviation relative to numerical models to validate and calibrate the proposed approach.

Table 3.13 – Summary statistics (mean, standard deviation, minimum, maximum) for parameters of 180,000 masonry panels.

Statistics	Н	T	f _m	τ0	fv ₀
Statistics	[m]	[m]	[MPa]	[MPa]	[MPa]
mean	3.630	0.702	2.566	0.060	0.144
std	0.727	0.131	0.329	0.009	0.022
min	2.500	0.350	2.000	0.040	0.100
max	5.000	0.950	3.199	0.080	0.190

The drift formulation for flexural-compression failure, derived from the mathematical model, is as follows:

$$\theta_{PF} = 0.0591 * a + 0.00475 \tag{11}$$

In the equation (11) the parameters a is:

$$a = e^{-0.915*(0.0349H-1)^2 - 79.3\left(0.0114H + \frac{N}{Nu} - 0.0402\lambda - 0.0336\right)^2}$$
 (12)

In particular, in equation (12), λ is the slenderness ratio of the panel, N/N_u represents the normalized axial load ratio, where N is the applied axial force and N_u is the ultimate axial capacity of the panel and H represents the height of the panel [m].

This model achieved an R² of 0.9661, indicating high reliability as the R² value is close to one. The mean error and standard deviation in percentage were also calculated to quantify data dispersion and the reliability of results.

For flexural-compression failure, these values are as follows:

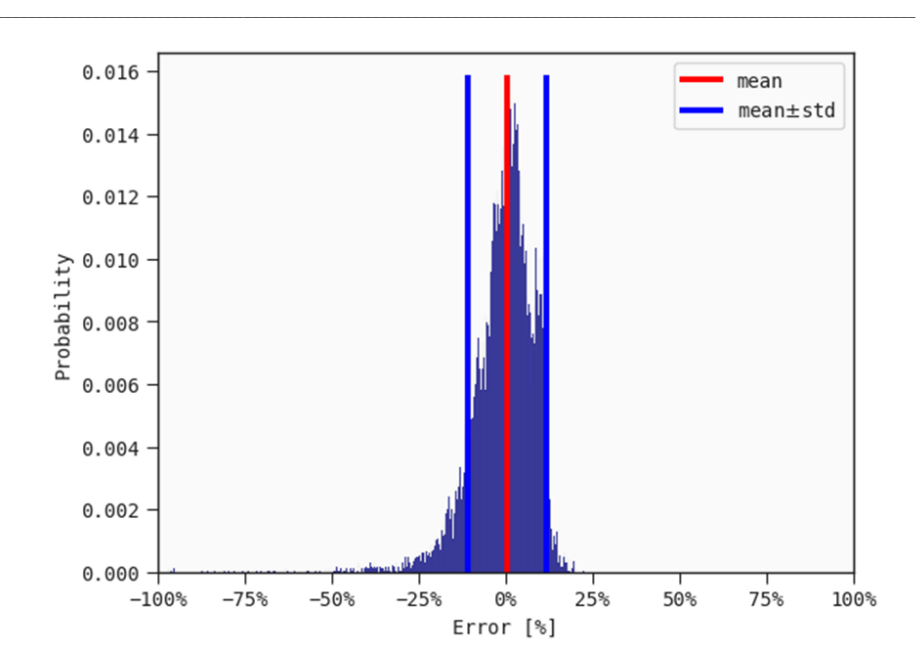


Figure 3.37 – Distribution of percentage errors in drift calculation for flexural failure

This histogram illustrates the distribution of percentage errors in the drift calculation for flexural-compression failure. The red line represents the mean error, which is located close to zero, indicating that, on average, the model does not systematically overestimate or underestimate the drift values. The two blue lines mark the range of one standard deviation (mean \pm std=11%), highlighting the spread of error values around the mean.

The concentration of data around the mean suggests a high level of accuracy in the model predictions. Most errors fall within a small range around zero, confirming the model's reliability for estimating drift under flexural-compression failure conditions. The tails in the distribution indicate fewer occurrences of larger error magnitudes, showing limited cases of significant underestimation or overestimation. This overall distribution supports the validity of the model in predicting drift with minimal deviation.

The drift formula for shear failure, developed through the mathematical model, is as follows:

$$\theta_V = -0.0137 * (-0.0427H - 1.54\lambda + 1.68) * b + 0.00228$$
 (13)

In the equation (13) the parameters b is:

$$b = e^{-6820* \left(\frac{N}{N_u} - 0.145\right)^2 e^{-32.1(0.425\lambda - 1)^2 - 7.24(\tau_0 - 0.0192)^2}}$$
(14)

For shear failure, this formula yields an R²=0.43. Although the R² value is not particularly close to unity, the root mean square error (RMSE) is very close to zero, indicating that the results are still reliable.

Similarly, the mean of the errors and the standard deviation, expressed as percentages, have been calculated to quantify data dispersion and assess the reliability of the results.

For shear failure, these values are as follows:

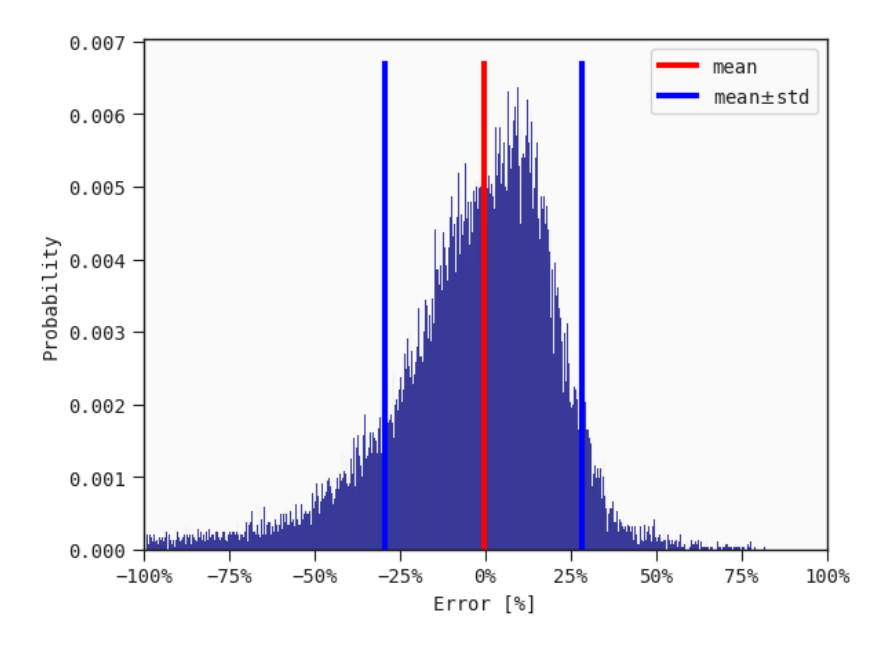


Figure 3.38 – Distribution of percentage errors in drift calculation for shear failure

This histogram illustrates the distribution of errors (%) in the drift calculation for shear failure. The red line represents the mean error, which is located around zero, indicating that, on average, the mathematical model does not introduce systematic bias. The blue lines mark the mean \pm one standard deviation, which in this case is $\pm 27\%$. This relatively wide spread indicates a notable degree of variability in the error distribution, but the concentration of values around zero still suggests a generally accurate prediction of the mean from the model.

$\label{eq:chapter-3-Proposal} Chapter \, 3 - Proposal \, \text{of a methodology for structural assessment of historical masonry buildings}$

The error distribution's shape also highlights that the majority of errors fall within the $\pm 27\%$ range, although there are some outliers extending further away from the mean.

3.3. In-plane and out-of-plane structural performance analysis

The flowchart in Figure 3.39 shows the methodology used to assess the seismic fragility of historical masonry structures, considering both in-plane (IP) and out-of-plane (OOP) actions.

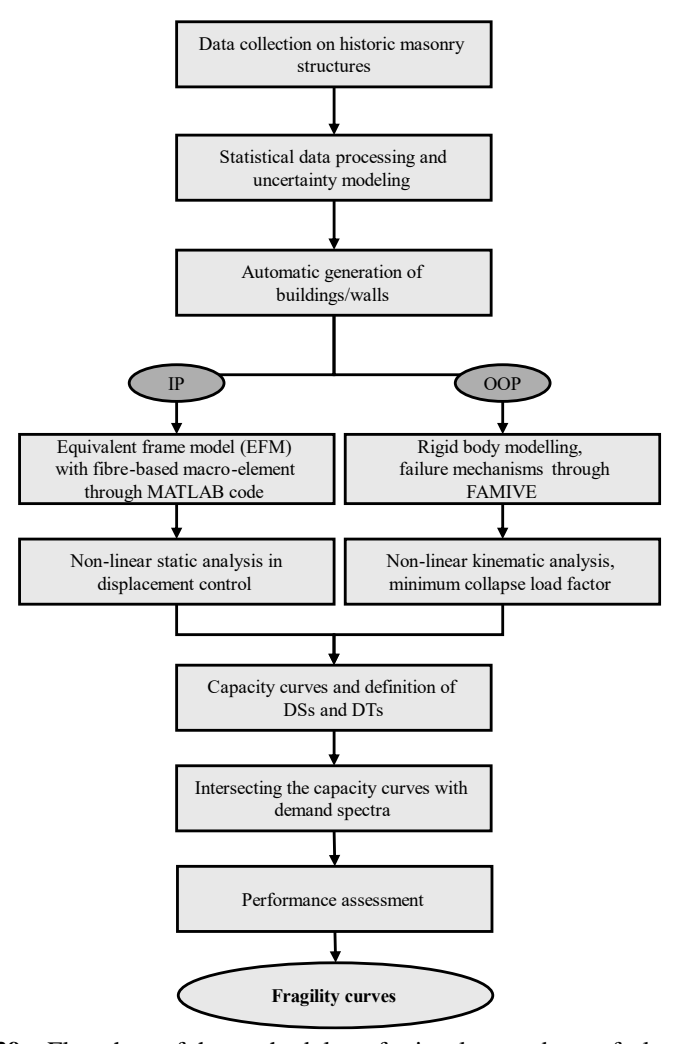


Figure 3.39 - Flowchart of the methodology for in-plane and out-of-plane actions

This flowchart integrates with the one shown in Figure 3.1, advancing the process once the exposure data has been acquired and the archetypes for analysis have been created. The study then proceeds with the evaluation of the behavior of masonry walls for both IP and OOP actions, which is essential for understanding the response of these structures during seismic events.

The IP analysis is conducted through the automatic generation of buildings using a MATLAB code, allowing the simulation of a variety of structural responses by leveraging the modeling described in Section 3.3.1. In parallel, the OOP behavior is evaluated using the FaMIVE procedure, a tool specifically developed to study collapse mechanisms occurring perpendicular to the wall plane.

For the OOP analysis within this study, each perimeter wall in the automatically generated building models was implemented within the FaMIVE software framework. The tool allowed for a detailed assessment of each wall's structural response by calculating collapse multipliers specific to each wall configuration, identifying the most probable collapse mechanism based on geometry and load, and evaluating the wall's nonlinear behavior under seismic accelerations.

The FaMIVE-generated collapse mechanisms are illustrated in Figure 3.23, highlighting the possible modes of failure that can occur in masonry walls under seismic action.

FaMIVE		SEISMIC VUL FAILURE M			UCL
A TO THE	VERTICAL OVERTURNING	E)	VERTICAL STRIP OVERTURNING	H2 1	IN PLANE SPANDREL FAILURE
B1 1 V TEE	OVERTURNING WITH 1 SIDE WING	FF	VERTICAL ARCH		IN PLANE SPANDREL FAILURE
B2 1 1 1 1 1 1 1 1 1 1 1 1 1 1 1 1 1 1 1	OVERTURNING WITH 2 SIDE WINGS	G1	HORIZONTAL ARCH	M1	SHEAR
c the first	CORNER FAILURE	G2 1	HORIZONTAL ARCH DUE TO BUTTRESS	M2	SHEAR
DITTER	PARTIAL OVERTURNING	H NIX	IN PLANE PIER FAILURE	N	BUTTRESS DETACHMENT

Figure 3.40 – Mechanisms for computation of limit lateral capacity of masonry façades through FaMIVE

The FaMIVE, developed at University College London (UCL), is a specialized analytical tool designed to assess the seismic vulnerability of masonry structures,

particularly with respect to OOP wall collapse mechanisms (D'Ayala, 1999, 2005, 2013; D'Ayala and Speranza, 2003). This tool plays a critical role in evaluating the structural integrity of walls under seismic loading, providing a framework for identifying potential collapse behaviors, calculating critical seismic loads.

FaMIVE supports a robust assessment process with three primary analytical capabilities: (i) identification of collapse mechanisms: the tool examines each wall in the model to determine potential OOP collapse mechanisms. Typical collapse types include overturning, sliding, and bending, which are determined based on the geometry, boundary conditions, and material characteristics of the masonry wall. This stage is essential for understanding each wall's likely behavior in response to seismic events, highlighting areas prone to OOP collapse; (ii) calculation of collapse multipliers: using a kinematic approach, FaMIVE calculates the collapse multipliers for each identified failure mechanism, effectively quantifying the seismic vulnerability of the wall. These multipliers represent the critical level of horizontal seismic acceleration (as a fraction of gravity) required to initiate collapse. This is achieved through a nonlinear kinematic analysis, where FaMIVE iteratively optimizes the collapse multiplier using a lower-bound approach to identify the minimum load factor that could trigger the mechanism under consideration. (iii) generation of capacity curves: FaMIVE further generates capacity curves that illustrate the relationship between applied lateral force and the resulting displacement of the wall. These curves are instrumental in evaluating the nonlinear response of masonry walls under seismic loads, providing insights into the deformation and energy dissipation characteristics of the structure prior to failure.

The modeling approach employed by FaMIVE leverages a rigid-body assumption for masonry walls, which simplifies each wall unit into discrete, non-deforming blocks or macro-elements. This assumption is well-suited for the brittle nature of masonry, where failure typically occurs due to relative displacements between rigid units rather than extensive material deformation. Each macro-element is represented as a rigid block connected by frictional or cohesive interfaces, allowing for analysis of both sliding and rocking mechanisms as well as mixed-mode responses.

The material behavior of masonry in FaMIVE is characterized by two key assumptions:

• Infinite Compressive Strength: The masonry is assumed to have an

infinite compressive strength, reflecting the real-world common condition of compressive stress being small compared to compressive strength. This assumption simplifies the model by allowing FaMIVE to focus on tensile and shear failure modes which are more critical for OOP collapse.

• Shear Resistance According to Mohr-Coulomb Criterion: For shear behavior, FaMIVE applies the Mohr-Coulomb criterion, which governs the onset of sliding between masonry units. According to this criterion, shear failure occurs if the shear stress on an interface exceeds the sum of the material cohesion and the product of normal stress and friction coefficient. This model accurately captures the sliding and detachment behavior that often occurs in unreinforced masonry under seismic loads.

Subsequently, the study performs a nonlinear static analysis to evaluate both the global behavior of the entire building and the local behavior of individual walls. These analyses help to understand how the structure and its components respond to seismic forces.

Based on the results from the nonlinear static analyses, damage states (DSs) are defined on the capacity curves of the structures. These DSs, ranging from minor damage to complete collapse, represent a spectrum of potential outcomes depending on seismic intensity, as discussed in Section 4.1.1.

The next step involves intersecting the capacity curves with the demand spectra, identifying the performance points—points where the seismic capacity of the structure meets the expected seismic demand. Finally, the process concludes itself with the derivation of the fragility curves corresponding to the performance points. The fragility curves are a key element of the process, representing the probability of reaching or exceeding specific DSs at various seismic intensities. The fragility curves derived individually for the two failure mechanisms are ultimately combined using the maximum likelihood method, generating a unique set of curves that encompass both mechanisms, as described in Section 4.2.2.

3.4. Fragility assessment

The fragility assessment of structures, particularly those subjected to seismic actions, is a crucial component in evaluating their vulnerability and estimating potential damage levels. Fragility curves are graphical representations that show the probability of a structure reaching or exceeding specific DSs as a function of seismic intensity, typically measured through parameters like peak ground acceleration (PGA).

The development of fragility curves typically involves several steps:

- 1. Definition of DSs: DSs are predefined levels of structural damage, ranging from minor damage (e.g., cosmetic cracks) to complete collapse. These states are critical in determining the structure's performance under various seismic intensities.
- 2. Identification of seismic demand and capacity: This involves determining the relationship between the seismic intensity (demand) and the structure's ability to withstand these demands (capacity). In seismic analyses, demand is often represented by spectral displacement or acceleration, while capacity is associated with the structure's maximum tolerable displacement or force before reaching each DS.
- 3. Performing nonlinear analysis: Nonlinear analysis is used to simulate the response of structures under increasing seismic demands. The N2 method (Fajfar 1996, 2000), which is a performance-based seismic assessment procedure, combines nonlinear static (pushover) analysis with response spectrum analysis. This approach allows for a simplified, yet effective, estimation of structural demands under earthquake loading conditions.

The N2 method is a widely accepted in Europe approach for seismic performance assessment and has been incorporated into Eurocode 8(EN-1998). It is particularly suitable for low to medium-rise buildings and is well-suited for the fragility assessment of historical masonry structures.

The N2 method involves the following steps:

1. Pushover analysis: A nonlinear static pushover analysis is performed on a structure to determine its capacity curve, which represents the relationship between base shear and a control point displacement (frequently located at the roof centroid). This curve provides insight into the building's behavior from initial linear response to yielding and eventual collapse.

- 2. Transformation to an equivalent single-degree-of-freedom (SDOF) system: The capacity curve obtained from the pushover analysis is transformed into an equivalent SDOF system. This transformation simplifies the analysis by reducing the multi-degree-of-freedom (MDOF) structure into a SDOF system characterized by equivalent mass, stiffness, and damping.
- 3. Intersection with demand spectrum: The demand spectrum, which represents the expected seismic demand at various intensity levels, is then plotted on the same axes as the SDOF capacity curve. The point at which the capacity curve intersects the demand spectrum is known as the performance point. This point represents the expected displacement demand on the structure for a given level of seismic intensity.
- 4. Definition of DSs on the capacity curve: Based on predefined damage thresholds, specific points on the capacity curve are selected to represent different DSs. For example, a minor DS may correspond to initial yielding, while collapse may correspond to a large displacement nearing the ultimate capacity.
- 5. Probability of exceedance for each DS: For each intensity level, the probability of exceeding a DS is calculated by comparing the demand displacement at that intensity with the capacity at each damage threshold. This is often done using a lognormal distribution, which describes the probability of exceeding each DS as a function of seismic intensity.

Using the N2 method, fragility curves can be constructed by plotting the probability of exceedance for each DS against the seismic intensity measure. For each DS, a fragility curve is created, usually with the following steps: (i) *Statistical fitting*: the results of the nonlinear analysis (performance points) are fitted to a statistical model (lognormal cumulative distribution function). This function describes the probability of exceeding a DS for varying levels of seismic intensity; (ii) *Parameters estimation:* the parameters of the lognormal distribution (mean and standard deviation) are estimated from the performance points. These parameters define the shape of each fragility curve; (iii) *Generation of curves:* with the distribution parameters established, the fragility curves are

CHAPTER 3 – PROPOSAL OF A METHODOLOGY FOR STRUCTURAL ASSESSMENT OF HISTORICAL MASONRY BUILDINGS

generated, illustrating the likelihood of exceeding specific damage levels as seismic intensity increases.

The N2 method is advantageous for fragility assessment due to its balance of simplicity and accuracy. By reducing a complex multi-degree-of-freedom system to an equivalent SDOF system, it significantly simplifies calculations without sacrificing much accuracy. This makes it particularly useful in assessing the seismic vulnerability of historical masonry structures, which often require a computationally intensive approach due to their complex material behavior and geometry.

The N2 method also enables a direct visual representation of structural performance through capacity curves and fragility curves, providing a clear and understandable assessment of seismic risk. By coupling demand and capacity in a straightforward way, the N2 method facilitates the development of fragility curves that can inform retrofitting decisions, prioritize interventions, and guide risk mitigation strategies for vulnerable structures.

CHAPTER 4 – VULNERABILITY ASSESSMENT AND RISK MITIGATION

4.1 Vulnerability assessment of Campania region

After an initial general assessment of the entire Italian territory and the development of the methodology to be applied for risk evaluation on a regional scale, the Campania region was selected as a case study to test the effectiveness of the analytical process. This approach required disaggregating statistical data from the CARTIS database, which provides a detailed characterization of the historical masonry building stock at the national level.

Specifically, the focus was placed on buildings constructed before 1919, filtering and analyzing the data exclusively for the Campania region. This selection allowed the extraction of specific and representative statistics for the area of interest, which were essential for defining the building archetypes to be analyzed in subsequent stages.

The regional data elaboration highlighted (Figure 4.1) a clear predominance of C1 masonry typology (ashlar masonry with regular squared blocks and mortar joints), accounting for 59% of masonry buildings in the region. This is followed by the B2 category (roughly cut stone masonry with good bond) with 22%, and the A2 category (irregular stone masonry with pubbles erratic and irregular stone units) with 19%. This framework provides a clear understanding of the predominant typological characteristics of the historical building stock in Campania, establishing a robust foundation for subsequent seismic vulnerability assessment and associated risk evaluation.

Having chosen the age of construction (<1919) and the type of masonry (C1 - Regular soft stone masonry), the data were disaggregated. The third parameter investigated was the number of storeys. Figure 4.2 shows that in Campania there

are more low masonry buildings with 2 or 3 storeys than tall buildings with more than 4 storeys.

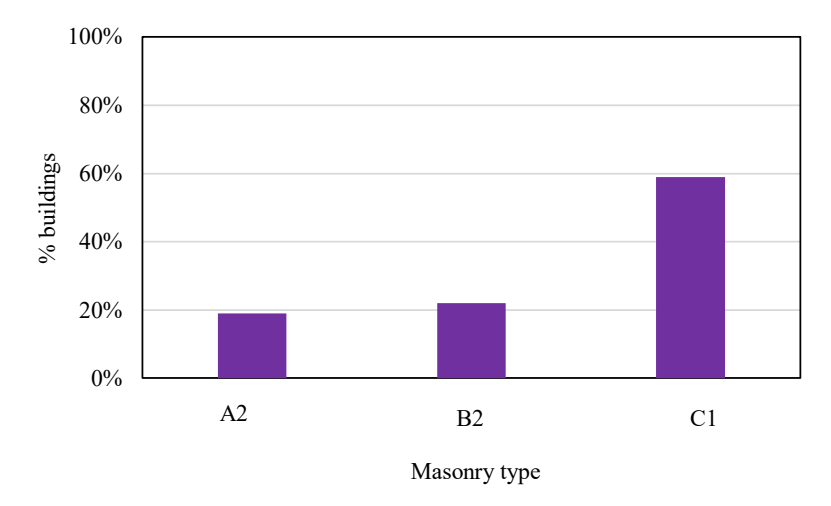


Figure 4.1 - Type of masonry in Campania region

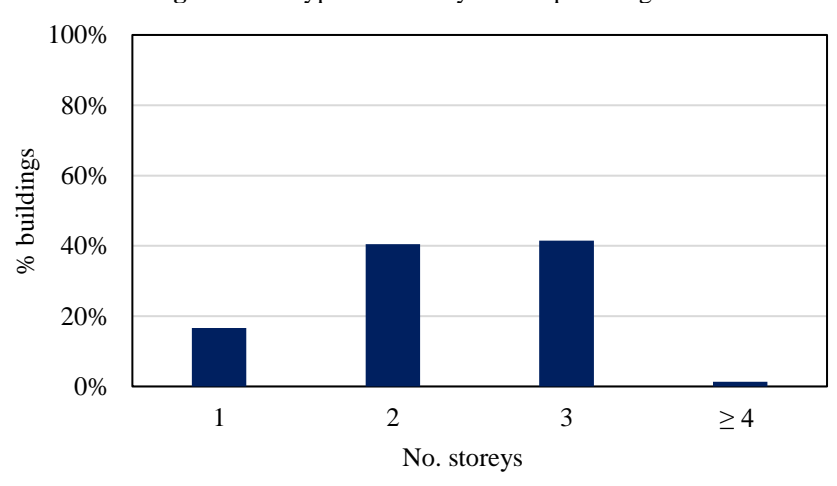


Figure 4.2 - Percentage of buildings by number of storeys

For the mechanical properties, the maximum and minimum values of each parameter indicated in Commentary 7/2019 (IMIT, 2019) were considered for which the probability distributions indicated in the CNR-DT 212/2013 Instructions (CNR, 2014) were considered. The calculation model used requires the selection of a constitutive model for the masonry subjected to uniaxial compression. The constitutive model of Augenti and Parisi (2010) was adopted for the masonry type.

All the adopted constitutive models require that the maximum compressive strength and the corresponding extensional strain are known and can be defined in a way that is consistent with the assigned normal modulus of elasticity. In this way, it is possible to model the whole non-linear behaviour of the masonry, also considering the progressive resistance degradation until the achievement of a final deformation defined by amplifying the extensional deformation corresponding to the maximum resistance. For uniaxial tensile behaviour, it is necessary to know or assign the maximum tensile strength and the tensile fracture energy, having assumed that the modulus of elasticity in tension is equal to that in compression.

Regarding the compressive behaviour, the peak normal stress in compression was assumed equal to the compressive strength (f_m), while the peak extensional strain in compression was assumed so that the secant modulus of elasticity at 30% of the peak value was equal to the modulus of elasticity (E) provided by Commentary 7/2019 (MIT, 2019) and the ultimate extensional strain was assumed deterministically equal to 0.5%. For the tensile behaviour, the peak normal stress in tension was assumed to be 5% of the peak normal stress in compression and the tensile fracture energy was deterministically assumed to be 0.025 N/mm.

Table 4.1 – Uncertainty modelling of material properties

Category Item		Variable Unit of		Value		Distribution	μ	β
gy			measurement	min	max		[MPa]	[MPa]
		f_m	MPa	2.00	3.20	Lognormal	2.60	0.24
	Ashlar	$ au_0$	MPa	0.04	0.08	Lognormal	0.06	0.35
	masonry stone	f_{v0}	MPa	0.10	0.19	Lognormal	0.14	0.32
Material	with regular squared blocks	E	MPa	1200	1620	Lognormal	1410	0.15
		G	MPa	0.33*E		-	-	-
	(C1)	f_t	MPa	0.05	5*f _m	-	-	-
		$G_{\!\scriptscriptstyle ft}$	N/mm	0.025		-	-	-
Geometry	Walls	t	m	Acco to the	rule	-	-	-

Uncertainties about property values were modelled by assuming a lognormal probability distribution, the dispersion of which was defined as follows:

$$\beta = \frac{X_{max} - X_{min}}{2} \tag{15}$$

where *X* is the logarithm of the value of the property considered.

Each of the sub-types of buildings has been assigned a value of the mechanical properties thus obtained.

The results of the statistical analyses conducted on data extracted from the "CARTIS" database are necessary but not sufficient to define an archetype on which to base an overall assessment. In the study of the existing building stock, it is also crucial to understand the development of construction techniques that characterized masonry works, as construction methods and material properties are among the many factors influencing the mechanical behavior of structures. The investigation into the design criteria of historical masonry, in addition to verifying the plausibility of the obtained results, is also useful for assessing the vulnerability of existing buildings and for planning repair, strengthening, or retrofitting interventions.

Design principles and construction details have never been uniform but have always varied over historical periods and across different regions, influenced by various factors, including the availability of materials. The construction of buildings relied on techniques and processes deemed valid based on empirical testing. These principles, known as the "rules of art," led to the construction of structures that, despite not conceived according to a structural engineering design, have survived to this day. A significant step toward a general theory of masonry construction, linking empirical rules with experimental assessments and mathematical calculation criteria, was made in the 19th century. This development is often associated with the work of the French architect Jean-Baptiste Rondelet (Lyon 1743 – Paris 1829), particularly his treatise Traité théorique et pratique de l'art de bâtir (1827). However, the evolution of masonry theory was a complex process involving multiple contributions over time (see, e.g., Huerta 2004). In this treatise, Rondelet sought to define a general methodology for the design of masonry structures based on experimental studies of material mechanical properties and the analysis of existing structures. Highlighting a significant difference between the results of theoretical formulas

and the dimensions of buildings of the time, he concluded that the only reliable formulas for the proportioning of masonry works were those derived from the observation of real cases. Regarding wall thickness, s, he provided formulas based on the observation of existing buildings:

$$s = \frac{T + H}{48} \tag{16}$$

for external walls of multi-story buildings with two bays.

$$s = \frac{T + H}{36} \tag{17}$$

for internal walls, where in equations (16) and (17) T is the depth of the building; H is the height of the building.

Although the design rules proposed by Rondelet were primarily empirical, they represented a fundamental starting point for other scholars who worked on masonry construction in subsequent years.

In 1920, the book "L'ossatura murale" by Giovanni Battista Milani (Rome 1876) was published. In this work, the author presents formulas proposed by various researchers for calculating the thickness s of masonry walls as a function of H and T (16). Among these is the formula by Rondelet, accompanied by an explanatory diagram.

The author also provides a table specifying the minimum thicknesses required for load-bearing walls of buildings with up to five stories. The indicated values vary depending on the material used for masonry units (brick or stone)

Table 4.2 – Minimum thicknesses for masonry walls proposed by Milani (1920)

Floors	Brick	Stone
4 th floor	0.45 m	0.45 m
3 rd floor	0.45 m	0.45 m
2 nd floor	0.60 m	0.60 m
1 st floor	0.60 m	0.75 m
Ground floor	0.75 m	0.90 m

These contributions provided a significant foundation for understanding and designing masonry structures.

Building upon the traditional "rules of art", the wall thicknesses for the architectural archetypes to be generated were carefully determined to align with

the construction practices and guidelines prevalent at the time when the buildings under examination were constructed. This approach ensures that the defined archetypes faithfully represent the structural characteristics and dimensional criteria historically adopted, reflecting the empirical knowledge and design principles that shaped the built environment of the period. By adhering to these historically contextualized parameters, the analysis captures not only the mechanical behavior of the masonry structures but also their cultural and technical authenticity.

The data was further disaggregated to consider the floor type associated with the three categories of masonry (A2, B2, C1) present in the Campania region. As shown in the Figure 4.3, the most common floor type at the time was flexible, followed by semi-rigid and rigid floors, with progressively lower percentages.

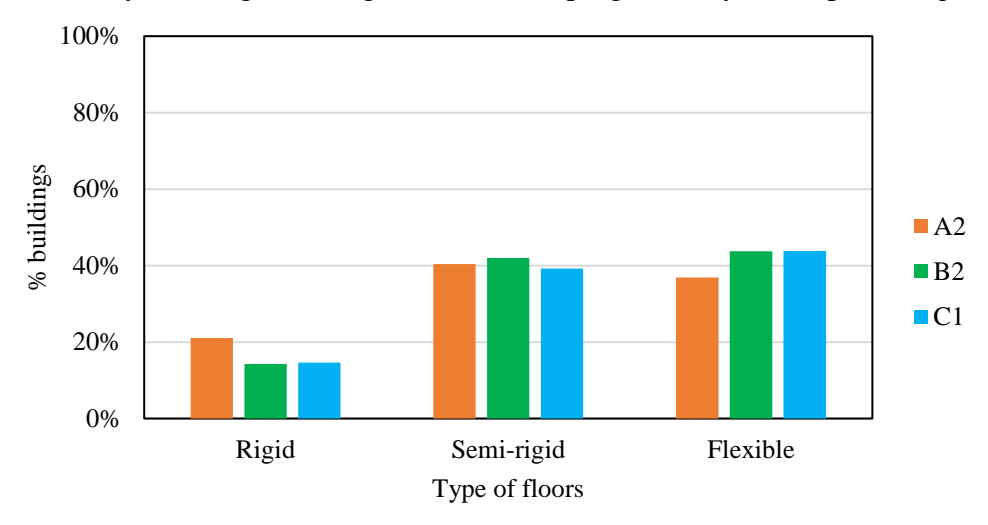


Figure 4.3 – Distribution of floor types for different masonry categories

This trend consistently reflects the construction characteristics of the period in which the buildings under study were built, where the use of flexible floors was more widespread. The gradual reduction in the prevalence of semi-rigid and rigid floors aligns with the construction techniques and materials available in the past. Additionally, the distribution across the different floor types also reflects the diversity of building practices and the socio-economic conditions that influenced the design and construction of historical buildings. In this study, the building class will be constructed with masonry type C1, considering the floor type percentages derived from data analysis.

4.1.1. Comprehensive Assessment of Masonry Structures: Global Behavior, In-Plane Damage, and Out-of-Plane Response

Once the database for building generation and the percentage of buildings by floor type were obtained, which allowed determining the number of buildings to analyze for each type, the modeling of archetypes was initiated.

The archetypes were analyzed using an EFM (Section 3.3) and employing a Monte Carlo extraction for the random generation of buildings with varying properties.

Each building was modeled for IP actions, using MATLAB, and for OOP actions, using the FAMIVE tool.

For each building, and for each of the above-mentioned actions, nonlinear static (push-over) analyses were performed for both directions and for two force combinations (Figure 4.4 and Figure 4.7). Subsequently, the displacement demand was evaluated using the N2 method for a variable PGA ranging from 0 to 1 g, as explained in the following section.

Once the push-over analysis determined the capacity curves in terms of base shear and displacement, it was necessary to define the damage states in terms of a mechanical parameter directly obtainable from the analysis.

Specifically, four damage states were identified on each capacity curve (Table 4.3), as follows:

- DS1: at 70% of the maximum base shear (Vb,max) on the ascending branch of the capacity curve;
- DS2: at Vb,max;
- DS3: at a 20% degradation of Vb,max;
- DS4: at a 50% degradation of Vb,max.

The damage states on global capacity curve considered are illustrated in Figure 4.5, where they are shown on a representative global pushover curve of a building.

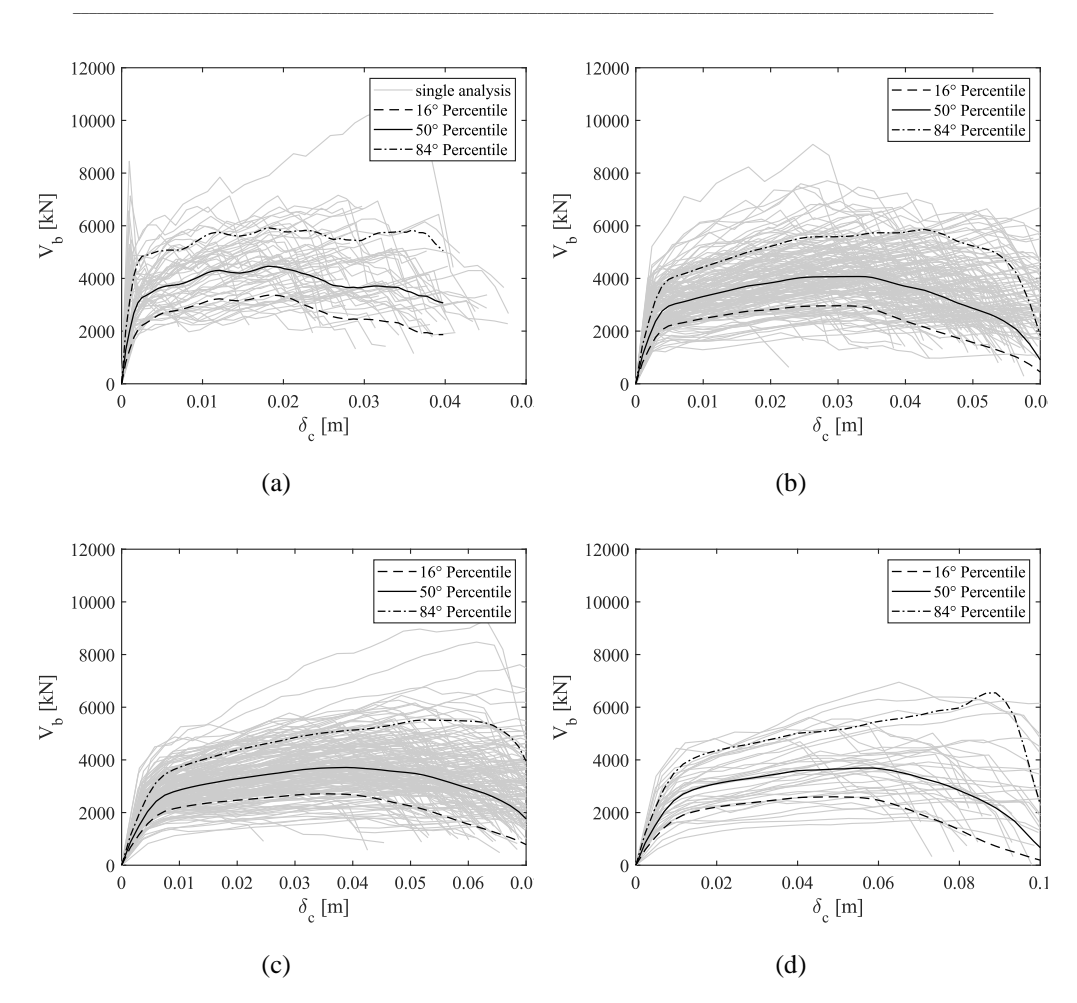


Figure 4.4 – Global capacity curves of buildings for X direction and proportional to 1st mode of vibration: (a) 1 storey; (b) 2 storeys; (c) 3 storeys; (d) 4+ storeys

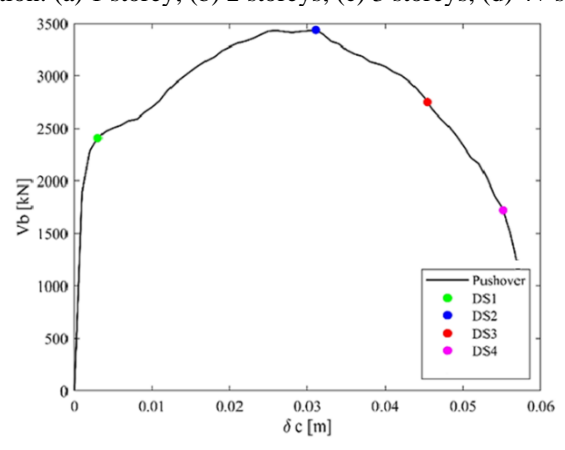


Figure 4.5 - Definition of damage states on global capacity curve

Table 4.3 – Definition of damage states for in-plane failure	
---	--

DS	Damage level	Limit
DS1	operational	70% of the maximum base shear $(V_{b,max})$ on the rising branch of the capacity curve
DS2	immediate occupancy	$V_{b,max}$;
DS3	life safety	20% base shear drop (i.e. $0.8V_{b,max}$)
DS4	collapse prevention	50% base shear drop (i.e. $0.5V_{b,max}$)

The table 4.4 describes the damage states and their corresponding thresholds on capacity curves for out-of-plane actions. Here's the explanation:

- DS1 (Operational): the first change in the slope of the capacity curve, representing the initial cracking of the structural element;
- DS2 (Immediate Occupancy): the first displacement value at which the maximum shear force is reached, corresponding to the peak of the curve;
- DS3 (Life Safety): the midpoint of the plateau where the shear force remains constant after reaching its maximum;
- DS4 (Collapse Prevention): the displacement at which the shear force has decreased by 20% from its maximum value in the descending branch of the curve.

The damage states on capacity curve considered are illustrated in Figure 4.6.

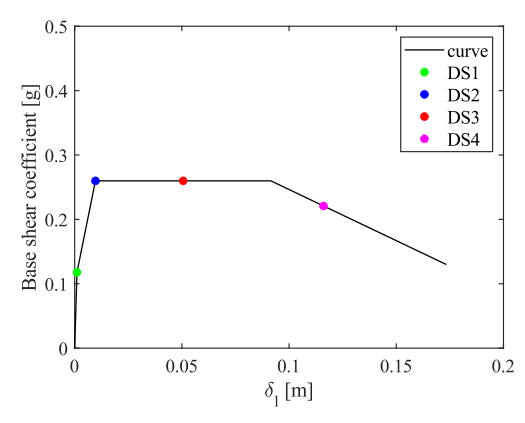


Figure 4.6 - Definition of damage states on out-of-plane capacity curves

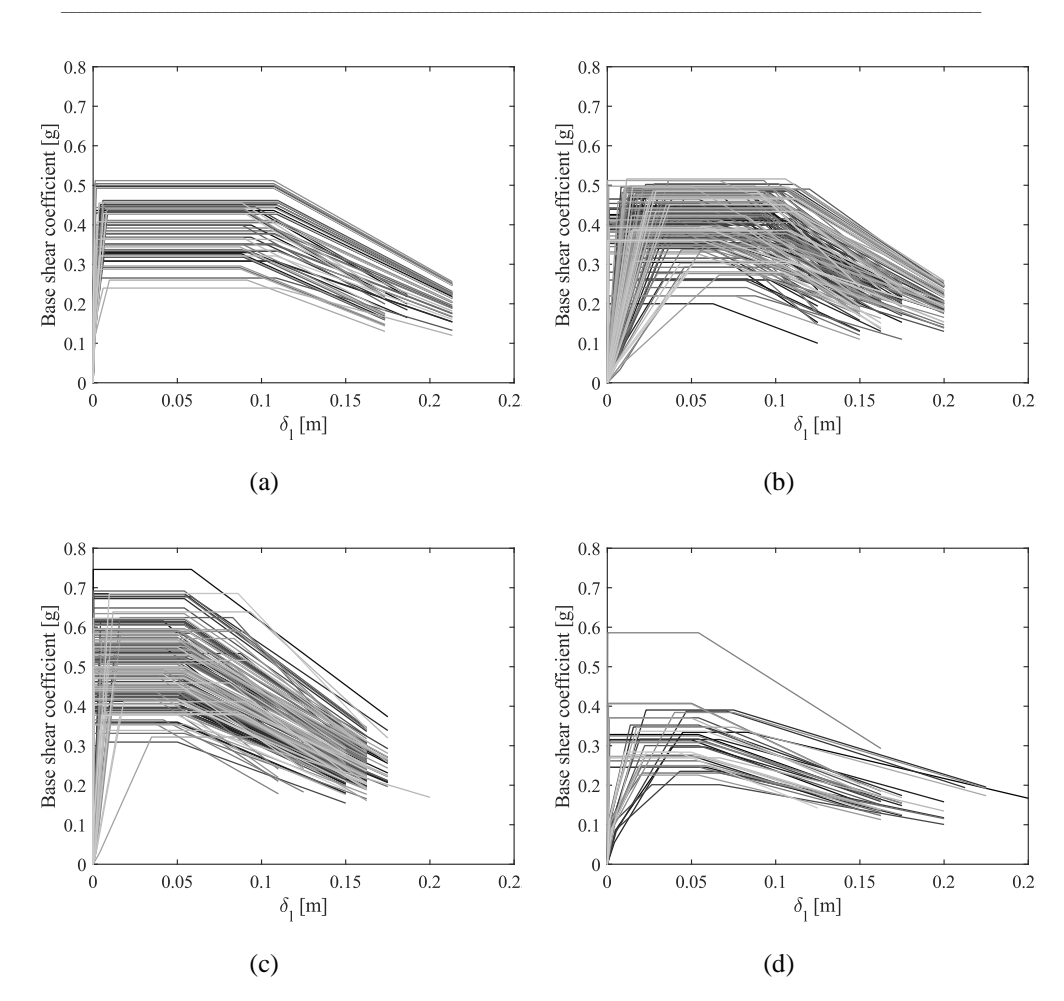


Figure 4.7 – Capacity curves for out-of-plane response: (a) 1 storey; (b) 2 storeys; (c) 3 storeys; (d) ≥4storeys.

Table 4.4 – Definition of damage states for out-of-plane failure

DS	Damage level	Limit
DS1	operational	First change in the slope of the capacity curve (initial cracking)
DS2	immediate occupancy	$\delta_{ m Vb,max}$
DS3	life safety	Midpoint of the plateau with $V=V_{b,max}$
DS4	collapse prevention	20% base shear drop (i.e. $0.8V_{b,max}$)

4.1.2. Fragility models for in-plane and out-of-plane failures

Ground motion variability often introduces more uncertainty into fragility curves than capacity and modeling methods. In this study, uncertainties related to seismic demand are addressed by utilizing a selected set of ground motion records. A collection of 22 ground motions, as recommended by FEMA P695 (FEMA 2009), is used to capture the inherent variability within seismic records.

This selection encompasses a wide range of characteristics, including shaking duration and PGA. It is important to highlight that the FEMA P695 ground motion suite, consisting of 44 components from multiple stations, provides a comprehensive dataset for our analysis. From each pair in this set, we select the more intense component for our investigation.

The acceleration spectra of these chosen components are graphically illustrated, while details of each event—such as name,, magnitude—are documented in Table 4.5.

The selected ground motions exhibit a PGA range between 0.2 and 0.8 g, with notable variability in spectral accelerations at shorter periods. This dispersion is essential to our assessment, enabling a detailed examination of how record-to-record differences impact the derived fragility functions. Such an approach is critical to build a thorough understanding of the effects of seismic variability on the structural performance of the buildings under study.

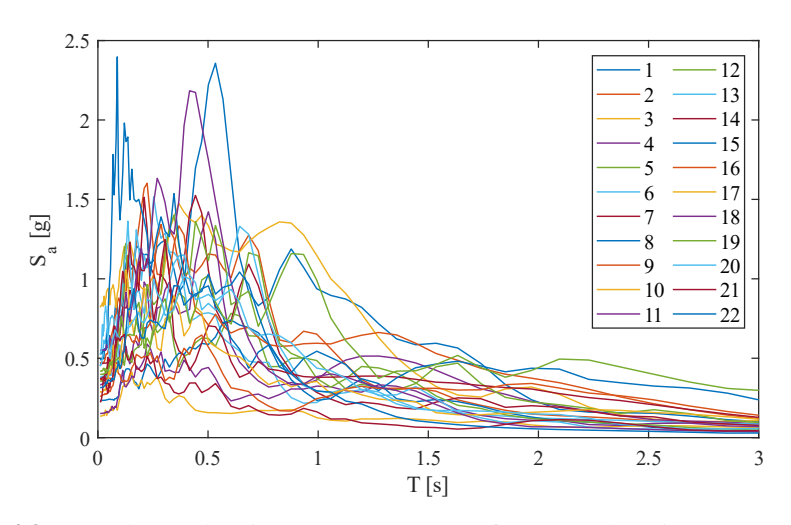


Figure 4.8 – Pseudo-acceleration **r**esponse spectra of 22 ground motions components from FEMA P695

Table 4.5 - Characteristics of selected ground motion records

ID	Event name	$M_{\rm w}$	PGA _{max} [g]	Distance epicentral [km]
1	Northridge	6.7	0.52	13.3
2	Northridge	6.7	0.48	26.5
3	Duzce, Turkey	7.1	0.82	41.3
4	Hector Mine	7.1	0.34	26.5
5	Imperial Valley	6.5	0.35	33.7
6	Imperial Valley	6.5	0.38	29.4
7	Kobe, Japan	6.9	0.51	8.7
8	Kobe, Japan	6.9	0.24	46
9	Kocaeli, Turkey	7.5	0.36	98.2
10	Kocaeli, Turkey	7.5	0.22	53.7
11	Landers	7.3	0.24	86
12	Landers	7.3	0.42	82.1
13	Loma Prieta	6.9	0.53	9.8
14	Loma Prieta	6.9	0.56	31.4
15	Manjil, Iran	7.4	0.51	40.4
16	Superstition Hills	6.5	0.36	35.8
17	Superstition Hills	6.5	0.45	11.2
18	Cape Mendocino	7	0.55	22.7
19	Chi-Chi, Taiwan	7.6	0.44	32
20	Chi-Chi, Taiwan	7.6	0.51	77.5
21	San Fernando	6.6	0.21	39.5
22	Friuli, Italy	6.5	0.35	20.2

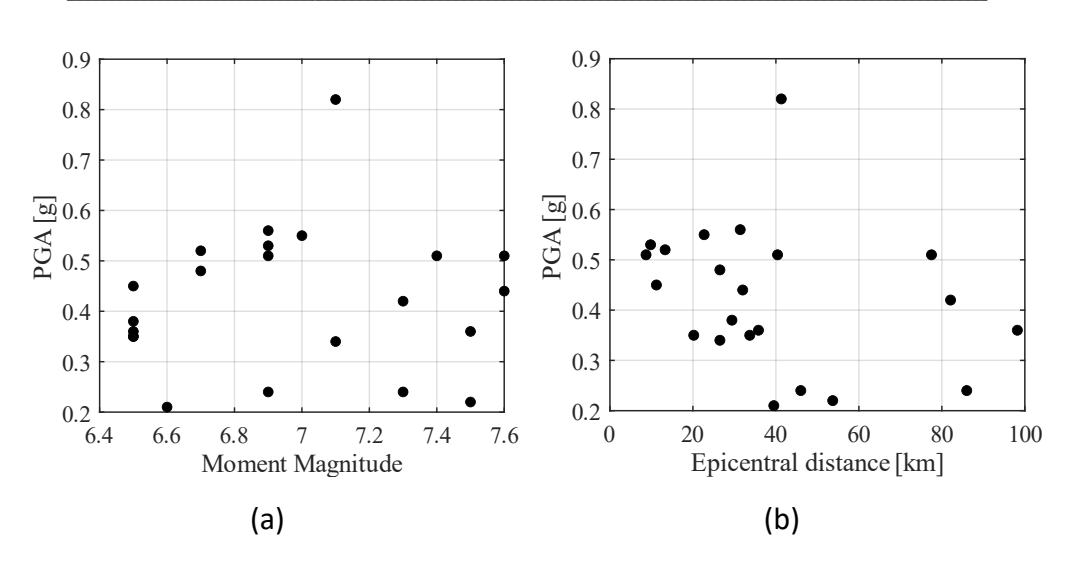


Figure 4.9 – Intensity of selected ground motion records in terms of PGA: (a) PGA versus moment magnitude; (b) PGA versus epicentral distance.

We opted for a more streamlined but rigorously validated methodology: the capacity-spectrum approach as outlined by the N2 method. This approach, incorporated within the prescriptive guidelines of Eurocode 8, presents a viable method for evaluating the seismic performance of structures. Using this method alongside the scaled FEMA P695 ground motion set enables a comprehensive analysis of the inherent variability in seismic records.

The N2 method was employed to assess demand in terms of displacement by applying an inelastic spectrum. Once the capacity curve in terms of base shear and displacement is obtained through push-over analysis, the corresponding curve for the equivalent SDOF system is defined. This involves transforming the actual MDOF structure to an equivalent SDOF system. For each building analyzed, the attainment of each damage level considered was verified.

The Figure 4.10 below shows the fragility curves for in-plane failure mechanisms.

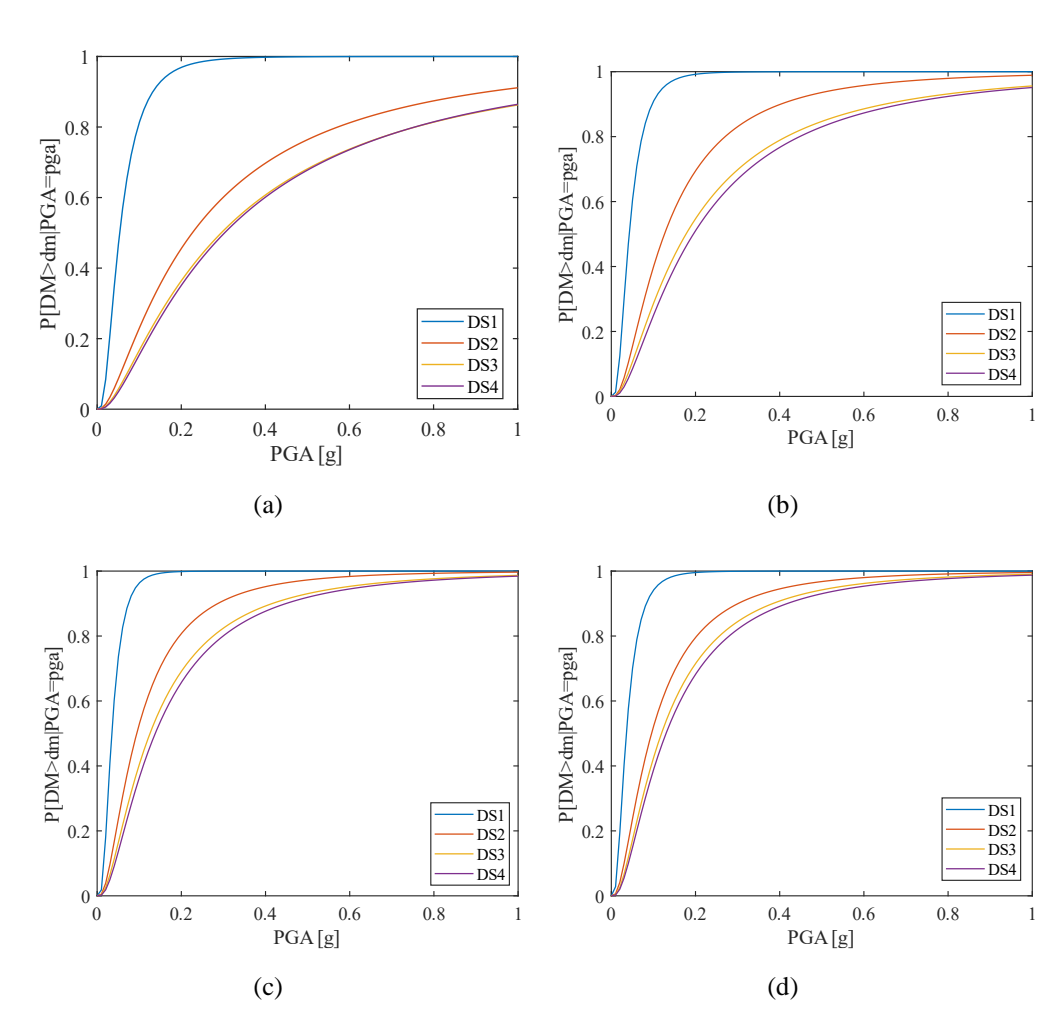


Figure 4.10 – Fragility curves for in-plane failure: (a) 1 storey; (b) 2 storeys; (c) 3 storeys; (d) 4+ storeys.

In the following Table 4.6 the parameters of the fragility curves for the various DSs and number of storeys are shown for in-plane failure.

The detailed analysis of the provided data highlights highly significant information regarding the median values of PGA associated with various DS and the influence of building height on seismic vulnerability.

Specifically, it was observed that the median PGA for DS2 is approximately 2.7 to 4.2 times greater than that for DS1.

Table 4.6 - Parameters of fragility curves for in-plane failure

Failure	No. storeys	Parameter	DS1	DS2	DS3	DS4
	1	μ [g]	0.054	0.226	0.295	0.303
	1	β	0.707	1.102	1.118	1.085
	2	μ [g]	0.043	0.126	0.178	0.195
ID	2	β	0.644	0.905	1.013	0.986
IP	3	μ [g]	0.035	0.094	0.126	0.138
	3	β	0.590	0.860	0.930	0.910
	4.	μ [g]	0.032	0.094	0.122	0.132
	4+	β	0.555	0.854	0.905	0.910

This difference underscores the significant increase in seismic demands required to reach more advanced damage states. Furthermore, there is an increase of 30–41% in the median PGA values when transitioning from DS2 to DS3, followed by an additional increment of 3-10% when advancing from DS3 to DS4. These progressive increases clearly highlight the escalating seismic demands associated with higher levels of damage. In parallel, the analyzed data reveal a gradual reduction in the median collapse capacity as the building height increases, represented by the number of storeys. Specifically, the median collapse capacity decreases by a significant 36% when transitioning from single-storey buildings to two-storey buildings, followed by a further reduction of 29% between two-storey and three-storey buildings, and a smaller decline of 4% when moving from three to four storeys. These results clearly demonstrate the heightened vulnerability of taller structures, a critical aspect in both seismic design and structural risk assessment. Another noteworthy aspect concerns the increase in the parameter β , which reflects growing variability and uncertainty in seismic performance predictions as higher damage states are considered. Porter (2020) recommends using a single β value for all fragility curves to avoid intersections between them. However, we verified that no intersections occurred within the range of 0 to 1 g, and we intentionally chose to investigate the effect of varying β to explicitly assess its influence on the fragility curves.. Specifically, the dispersion ranges between 0.56 and 1.12, indicating greater challenges in accurately predicting the seismic behavior of structures under severe damage conditions. It is observed that β tends to decrease as the number of stories increases, suggesting that height may become a dominant parameter compared to other sources of variability. Moreover, β generally decreases from DS3 to DS4—with only one limited exception—possibly indicating a clearer trend as collapse is approached, where structural behavior becomes more deterministic.

The same procedure performed to obtain the in-plane fragility curves was carried out on the non-linear capacity curves obtained for the out-of-plane failure.

Figure 4.11 shows the fragility curves for out-of-plane failure and in the Table 4.7**Errore.** L'origine riferimento non è stata trovata., the parameters of the fragility curves for the various Damage States (DS) and number of storeys are shown for out-of-plane failure.

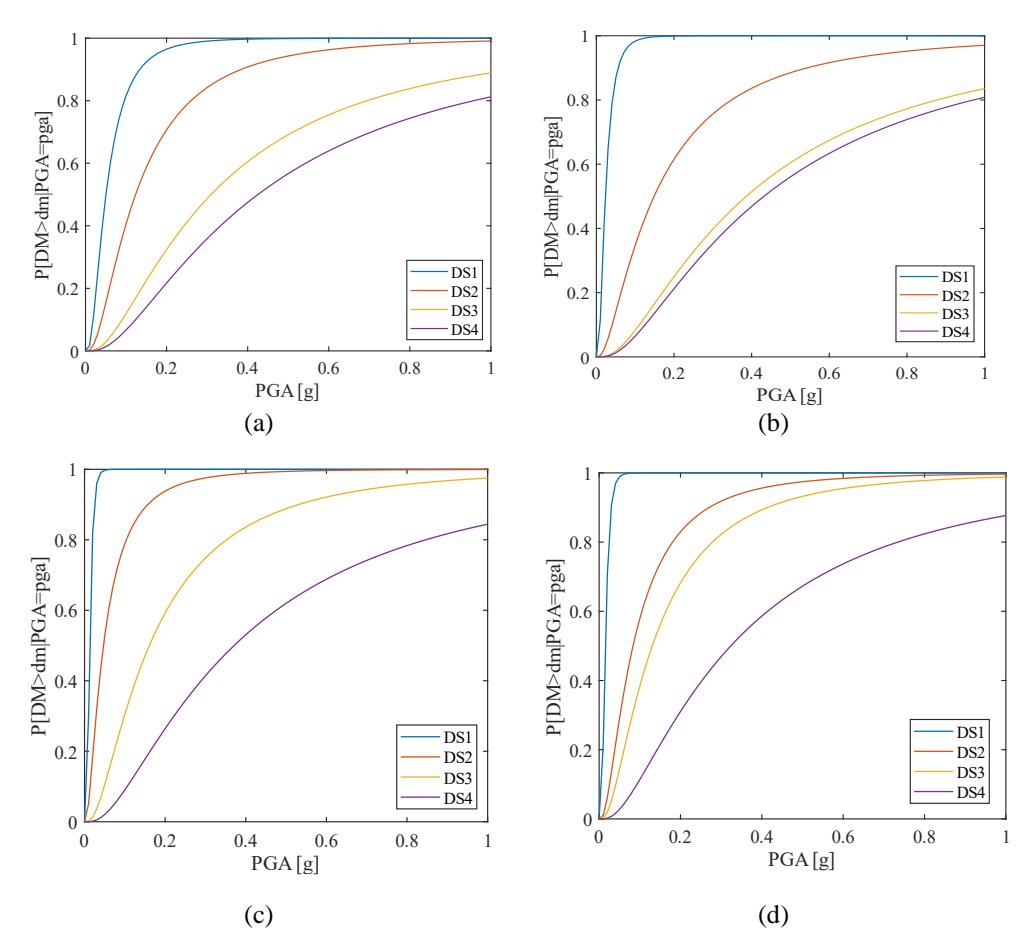


Figure 4.11 – Fragility curves for out-of-plane failure: (a) 1 storey; (b) 2 storeys; (c) 3 storeys; (d) 4+ storeys.

Table 4.7- Parameters of fragility curves for out-of-plane failure

		Parameter	•		DS3	DS4
	1	μ [g]	0.016	0.078	0.432	0.444
	1	β	0.473	0.944	0.956	0.957
0.00	2	μ [g]	0.023	0.149	0.386	0.432
		β	0.687	1.010	0.975	0.963
OOP	2	μ [g]	0.013	0.047	0.161	0.371
	3	β	0.482	0.942	0.931	0.980
		μ [g]	0.015	0.083	0.131	0.324
	4+	β	0.520	0.919	0.900	0.973

The analysis of data from the fragility curves for out-of-plane failures reveals significant insights, highlighting a marked increase in the median PGA as the damage state transitions from DS1 to DS2. For instance, in single-storey buildings, the median PGA for DS2 is approximately 4.8 times greater than that for DS1 (0.0777 g compared to 0.0161 g). For two-storey structures, this ratio increases further to about 6.5 times (0.149 g compared to 0.023 g). Meanwhile, for three-storey and four-plus-storey buildings, the ratios are approximately 3.6 times (0.047 g compared to 0.013 g) and 5.5 times (0.083 g compared to 0.015 g), respectively.

Moreover, the median PGA values for DS3 exhibit further increases compared to DS2, with particularly significant differences observed for shorter buildings. For example, in single-storey buildings, there is a striking 456% increase in the median PGA when transitioning from DS2 to DS3 (0.432 g compared to 0.077 g). Similarly, for two-storey buildings, the increase is also substantial, at approximately 159% (0.386 g compared to 0.149 g). These increases underscore the significant escalation in seismic demands as damage levels advance.

Another noteworthy aspect is the gradual reduction in the median collapse capacity as building height increases, expressed by the number of storeys. For single-storey buildings, the median PGA for DS4 is only slightly higher than that

for DS3, whereas for two, three, and four-plus-storey buildings, more substantial increases in the median PGA are observed between DS3 and DS4. However, the analysis highlights a clear trend of decreasing median collapse capacity with increasing building height: there is a 3% reduction when moving from single-storey to two-storey buildings, a 14% reduction from two to three storeys, and a 13% reduction from three to four or more storeys.

Finally, the increase in the parameter β as damage states progress indicates growing variability and uncertainty in seismic performance predictions. This dispersion, ranging between 0.47 and 1.01, reflects the increasing complexity in interpreting the seismic behavior of structures as higher damage levels are considered. These findings emphasize the importance of accounting for such variability in seismic design and risk assessment.

In this study, the process of combining fragility curves for in-plane and outof-plane failure mechanisms is performed using the maximum probability method, a rigorous and well-established technique that enables the representation of the collapse risk of the structure by considering both mechanisms. This approach is particularly useful to ensure that the combined fragility curve captures the worst-case scenario in terms of seismic vulnerability for every level of seismic intensity considered.

The maximum probability method assumes that, for a given seismic intensity level (e.g., PGA), the collapse risk of the structure is governed by the most vulnerable failure mechanism among those considered. In other words, the combined probability of collapse corresponds to the maximum probability calculated between the two failure mechanisms, ensuring that the resulting curve always represents the most critical case. This principle can be mathematically expressed as:

$$P_{combined|IM} = max(P_{in-plane|IM}; P_{out-of-plane|IM})$$
(18)

In equation (18) $P_{combined|IM}$ is the combined probability of failure at intensity level (IM), $P_{in-plane|IM}$ is the probability of failure for the in-plane mechanism, and $P_{out-of-plane|IM}$ is the probability of failure for the out-of-plane mechanism.

The procedure is implemented in the following steps:

- 1. Identification of fragility curves: The starting point is the individual fragility curves for in-plane and out-of-plane failure mechanisms. These curves are derived from detailed analyses based on numerical models or experimental data and represent the cumulative probability of collapse as a function of seismic intensity.
- 2. Selection of seismic intensity levels: A discrete set of seismic intensity values, such as PGA, is chosen for the analysis. These levels are selected to cover a wide range of seismic scenarios, from mild to extreme events.
- 3. Calculation of maximum probabilities: For each selected seismic intensity level, the collapse probabilities derived from the fragility curves of both mechanisms are compared. The maximum probability between the two is identified and recorded. This step ensures that the combination of fragility curves always represents the worst-case risk for each PGA level.
- 4. Construction of the combined fragility curve: Once the maximum probabilities are determined for each seismic intensity level, they are used to construct the combined fragility curve. This curve graphically represents the highest collapse probability considering both in-plane and out-of-plane mechanisms.

This method offers several advantages compared to other combination techniques. However, one limitation is that a very localized out-of-plane (OOP) failure mechanism can dominate the overall building performance assessment, potentially leading to an overestimation of damage in a repair-cost estimation framework. Despite this, the method provides several benefits, including:

- Conservativeness: It ensures that the global risk is not underestimated by always considering the most critical mechanism.
- Computational Simplicity: Calculating the maximum probability for each seismic intensity level is a straightforward and easily implementable operation.
- Representativeness: It provides an accurate and comprehensive assessment of the global seismic vulnerability of the structure, integrating the characteristics of both failure mechanisms into a single curve.

The combined fragility curve obtained using the maximum probability method represents the highest collapse probability of the structure for any given seismic intensity. This approach allows for identifying seismic intensity levels that pose

significant risks to the structure and developing mitigation strategies targeted at the most vulnerable failure mechanisms.

In conclusion, applying the maximum probability method enables the development of a robust, conservative, and representative combined fragility curve, providing a clear and comprehensive assessment of the seismic vulnerability of masonry historical structures.

Figure 4.12 below shows the combined fragility curves for in-plane and out-of-plane mechanisms and in the following Table 4.7 the parameters of the fragility curves for the various Damage States (DS) and number of storeys are shown for combined failures.

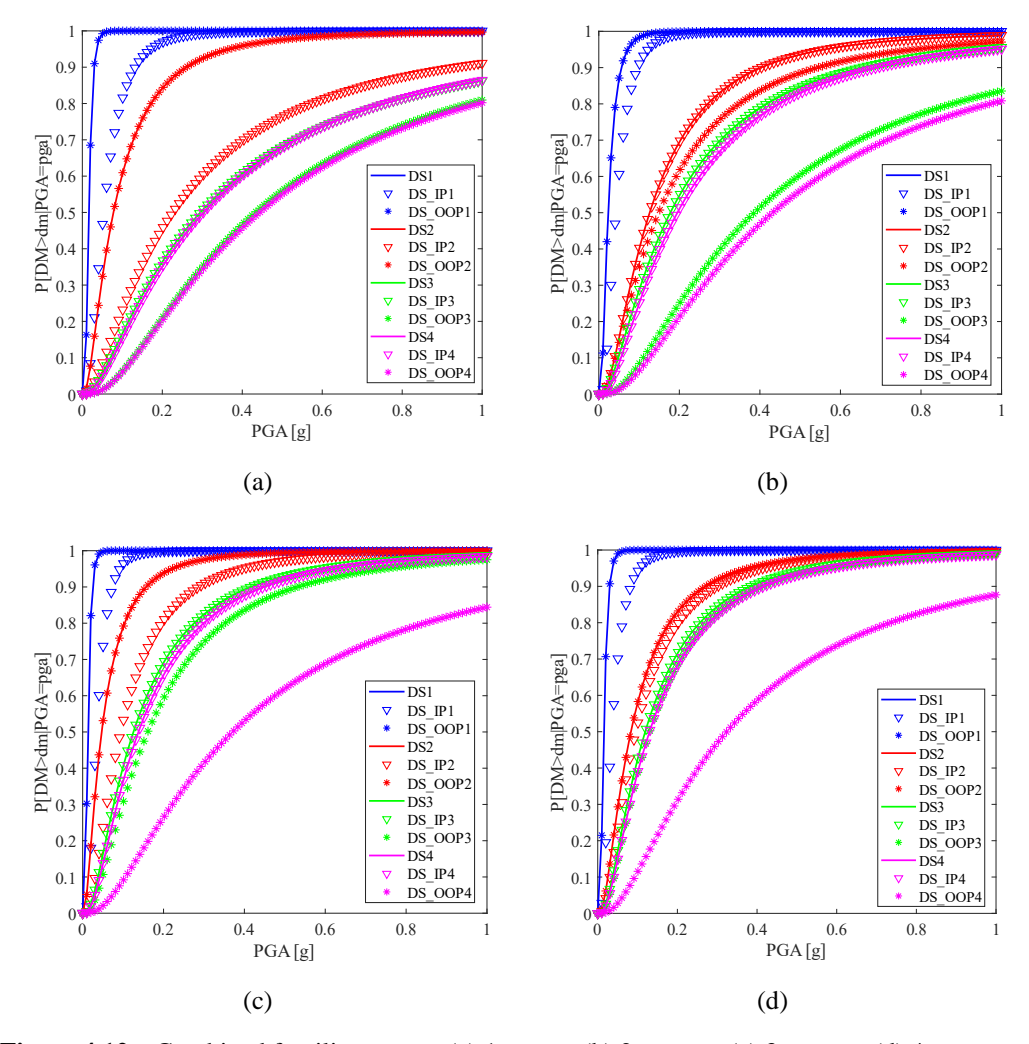


Figure 4.12 – Combined fragility curves: (a) 1 storey; (b) 2 storeys; (c) 3 storeys; (d) 4+ storeys.

Table 4.8 – Parameters of combined fragility curves

Failure	n° storeys	Parameter	DS1	DS2	DS3	DS4
	1	μ [g]	0.016	0.078	0.295	0.303
	1	β	0.473	0.944	1.118	1.085
	2	μ [g]	0.023	0.126	0.178	0.195
IP + OOP		β	0.687	0.905	1.013	0.986
	3	μ [g]	0.013	0.047	0.126	0.138
	3	β	0.482	0.942	0.930	0.910
	4	μ [g]	0.015	0.083	0.122	0.132
	4+	β	0.520	0.919	0.905	0.910

The analysis of the combined fragility curves for in-plane (IP) and out-of-plane (OOP) failure mechanisms highlights notable variations based on the number of storeys and the damage states.

For single-storey buildings, the combined median PGA shows a significant reduction of 70% compared to IP for DS1 and a reduction of 65% for DS2. For DS3 and DS4, no changes are observed, meaning that the combined values are identical to the IP values. For two-storey buildings, the combined median PGA decreases by 47% compared to IP for DS1, while no differences are noted for DS2, DS3, and DS4, indicating alignment with IP values. In the case of three-storey buildings, the combined median PGA decreases by 63% compared to IP for DS1 and by 50% for DS2. For DS3 and DS4, no changes are detected, meaning the combined values correspond to the IP ones. For buildings with four or more storeys, the combined median PGA decreases by 53% compared to IP for DS1 and by 12% for DS2, while no changes are seen for DS3 and DS4, showing alignment with IP values.

When comparing the combined curves to the OOP ones, no differences are observed for DS1 and DS2 in single-storey buildings, indicating that the combined values match the OOP ones. However, for DS3 and DS4, the combined median PGA decreases by 32% compared to OOP. In two-storey buildings, no changes are noted for DS1, showing agreement with the OOP values, while for DS2, the combined median PGA decreases by 15% compared to OOP.

Significant reductions of 54% and 55% are observed for DS3 and DS4, respectively. For three-storey buildings, no differences are noted for DS1 and DS2, indicating alignment with the OOP values. For DS3, the combined median PGA decreases by 22% compared to OOP, while a significant reduction of 63%

is observed for DS4. For buildings with four or more storeys, no differences are detected for DS1 and DS2, while the combined median PGA decreases by 7%

for DS3 and by 59% for DS4 compared to OOP.

Overall, the combined fragility curves generally show lower median PGA values compared to both the IP and OOP curves, reflecting a more conservative assessment of seismic demand. The most pronounced reductions are observed in the early damage states (DS1 and DS2) for the IP curves, while substantial decreases are noted in the higher damage states (DS3 and DS4) for the OOP curves. These findings underline the critical importance of accounting for both in-plane and out-of-plane mechanisms to provide an accurate and comprehensive evaluation of structural seismic vulnerability.

4.1.3. Strengthened intervention and impact on fragility

The first step in evaluating the necessary interventions for the selected buildings was a detailed analysis of the CARTIS database.

The CARTIS database allows for identifying the percentage of buildings that have already undergone strengthening and analyzing the types of interventions performed.

Specifically, for the Campania region, it was found that 43% of buildings constructed before 1919 have been consolidated, while the remaining 57% remain in their original condition (as-built). The 43% of consolidated buildings were further classified based on the type of intervention carried out: 52% underwent local interventions, 41% seismic improvement interventions, and only 7% were subjected to seismic retrofitting.

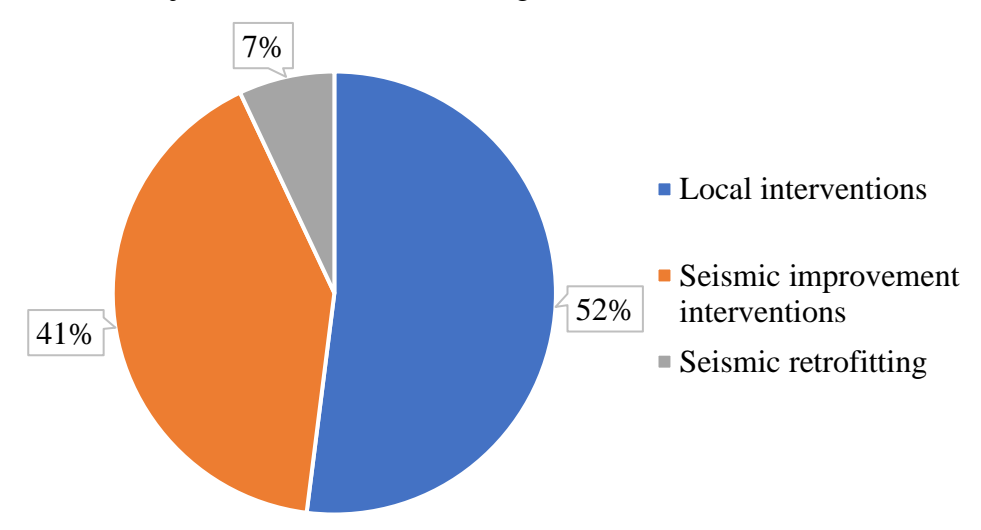


Figure 4.13 – Distribution of types of seismic intervention in buildings in Campania..

This classification provides key insights into the current state of the historical building stock in Campania, highlighting that most interventions have focused on less invasive solutions, such as local and improvement interventions, while seismic retrofitting, which is more complex and expensive, has been less commonly implemented.

The percentage of buildings consolidated through improvement or retrofitting interventions was essential for estimating the number of buildings still requiring strengthening using two specific techniques: RP, considered a traditional and well-established solution, and FRCM systems, representing an innovative approach in seismic protection. This distinction between traditional and innovative techniques allows for integrating well-tested solutions with modern technologies, optimizing both the effectiveness of the interventions and the allocation of available resources.

Once the data was organised, we proceeded with the automatic generation of buildings, through a procedure implemented in MATLAB, for the selected subtypology.

Once the i-th building was generated based on these properties, nonlinear static analyses were conducted for both the as-built buildings and those retrofitted with RP and FRCM systems.

For the traditional retrofitting using reinforced plaster, a 5% increase in mass was considered, and a factor of 1.5 was applied to the RP, as specified in Table C8.5.II of Commentary No. 7/2019 for regular tuff masonry.

For the innovative strengthening technique (FRCM), the increase in mechanical properties was taken into account through notions supported by available literature and scientific articles (Table 4.9). In particular, the enhancement factors were determined by calculating the average ratio between the unreinforced and reinforced parameters, as reported in various research articles focused on masonry strengthened with FRCM. The selected references include studies by Faella et al. (2010, 2004), Prota et al. (2006), Parisi et al. (2013), Balsamo et al. (2011), and Marcari (2004). (Table 4.7).

Table 4.9 – Coefficients to be assigned to parameters for FRCM

Parameter	Unit of measurement	Mean	Standard Dev.	CoV
$τ0$, $f_{ν}0$	[MPa]	3.53	1.49	42%
f_t	[MPa]	3.11	0.68	22%
$\mu_{\scriptscriptstyle V}$	[-]	1.48	0.58	39%

The first result obtained was the nonlinear static analyses on the set of generated buildings for the three sets of buildings: (i) as-built; (ii) RP; (iii) FRCM.

For each of these three sets, four series of capacity curves were derived for the two directions of seismic action, X direction (Figure 4.14) and Y direction (Figure 4.15), and two different horizontal force distributions (proportional to masses and proportional to the first mode). Below are the capacity curves for asbuilt buildings, RP, and FRCM for the X direction and for the Y direction, for the mass-proportional and inverted triangular distributions.

The capacity curves show: (i) an increase in maximum base shear that can be supported by strengthened structures of approximately 40-50% compared to asbuilt buildings; (ii) an increase in initial stiffness of approximately 100% for strengthened buildings compared to as-built buildings; (iii) a decrease in displacement associated with maximum base shear of approximately 30% for strengthened buildings compared to as-built buildings.

For each model analysed, the capacity was determined for the damage levels considered and compared with increasing levels of seismic demand. For each PGA level, the frequency with which each damage level is exceeded was assessed.

In this way, a series of points were derived for each damage level to represent, as the seismic intensity level changed, the probability that that damage level would be exceeded. By means of a regression analysis, the points thus identified were interpolated through a least-squares regression from a lognormal cumulative distribution function and the parameters characterising it were derived. Thus Figures 4.15 shows the fragility curve.

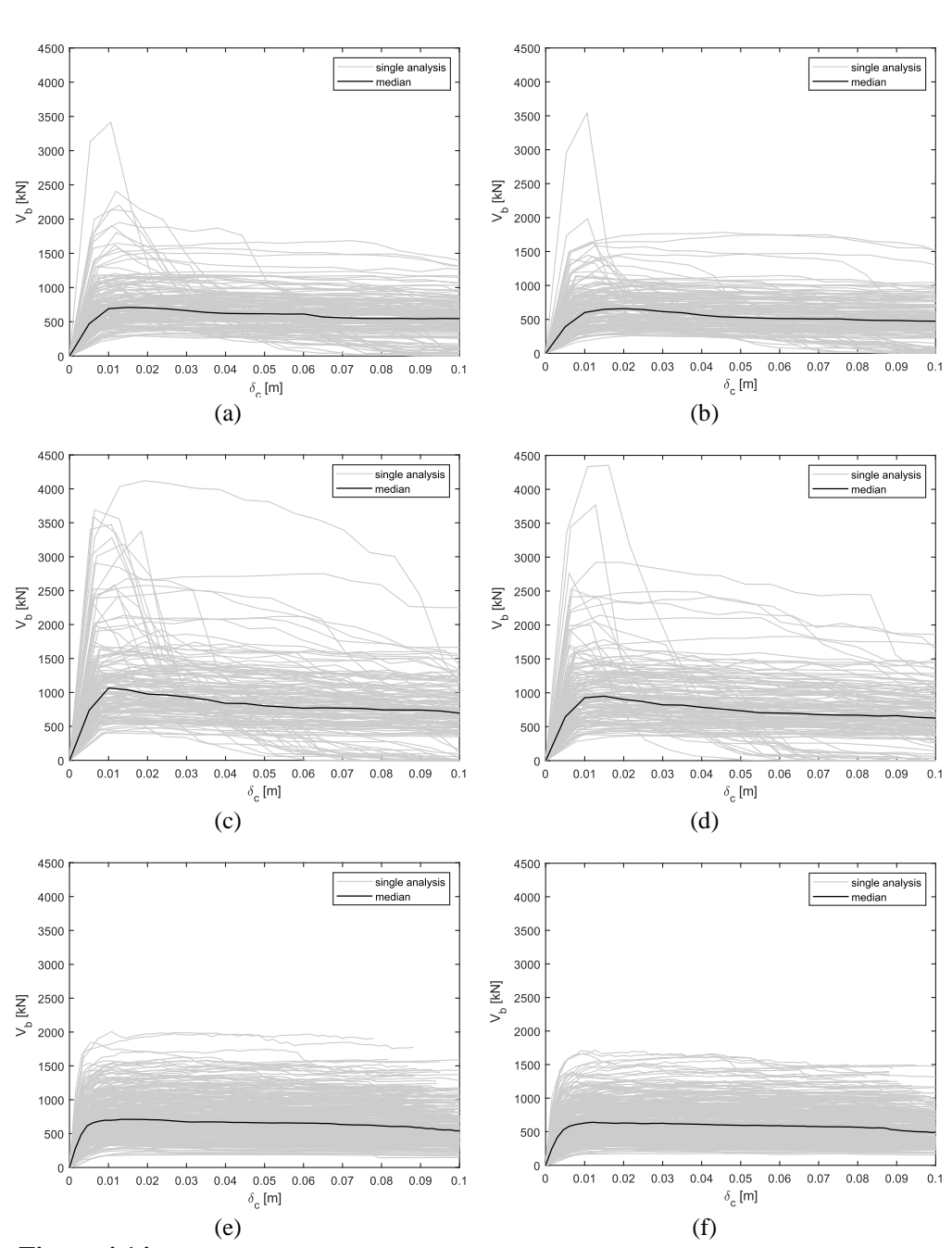


Figure 4.14 – Capacity curves in the X-direction: (a) as-built \propto masses; (b) as-built \propto 1st mode; (c) RP \propto masses; (d) RP \propto 1st mode; (e) FRCM \propto masses; (f) FRCM \propto 1st mode.

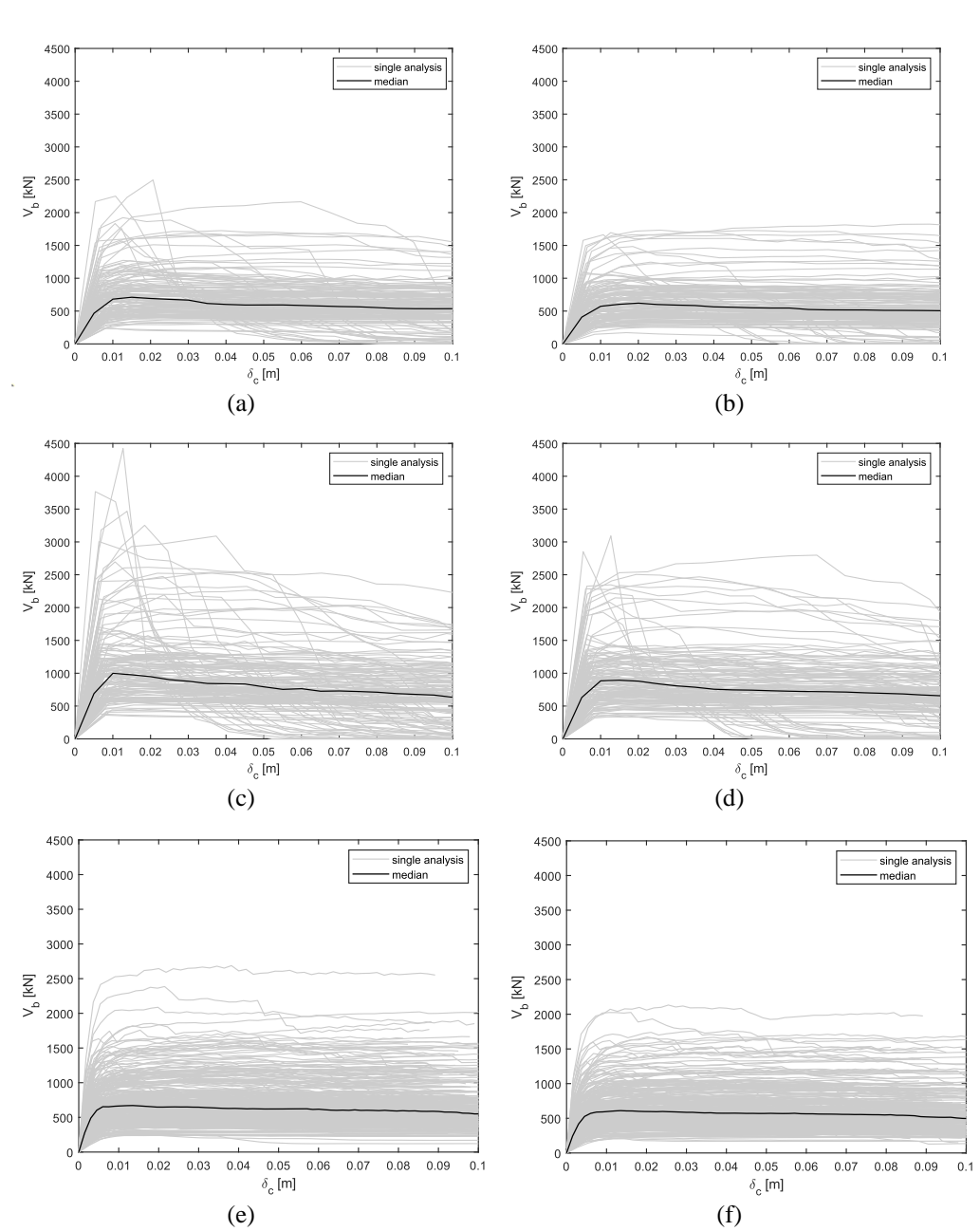


Figure 4.15 – Capacity curves in the Y-direction: (a) as-built \propto masses; (b) as-built \propto 1st mode; (c) RP \propto masses; (d) RP \propto 1st mode; (e) FRCM \propto masses; (f) FRCM \propto 1st mode.

Table 4.10 - Difference in peak displacement, peak shear and initial stiffness between strengthened and as-built buildings

Direction	Force profile	Δd_{peak}	ΔV_{peak}	ΔK_0
X	Modal	-25%	+42%	+90%
	Mass	-33%	+50%	+125%
Y	Modal	-25%	+44%	+92%
	Mass	-33%	+41%	+111%

From the fragility curves, we can deduce that for DS1 and DS2 (lower damage levels), the values are almost identical across the three configurations, suggesting that the strengthening intervention, whether with RP or FRCM, has minimal impact at lower damage levels.

Starting from DS3, a clear difference between configurations is observed. The as-built buildings show higher values compared to the reinforced buildings, indicating that reinforcement has a positive effect in reducing seismic vulnerability at higher damage levels.

For DS4 and DS5 (higher damage levels), reinforcement with both RP and FRCM leads to a reduction in vulnerability compared to the as-built state, with slightly better performance from RP compared to FRCM. This suggests that RP might provide greater protection for severe structural damage.

In summary, it can be inferred that the reinforcement intervention is particularly effective at advanced damage states (DS3, DS4, DS5), with a reduced impact at lower damage levels.

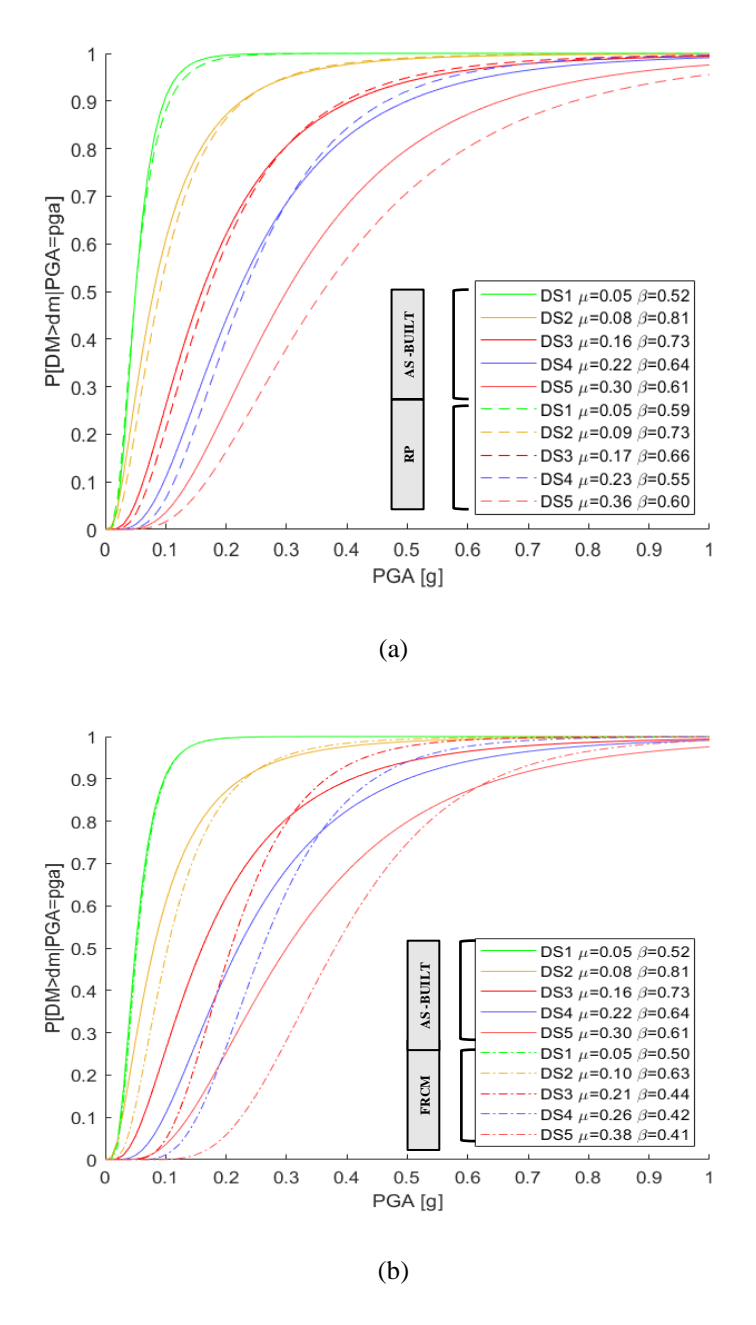


Figure 4.16 - Fragility curves: (a) as-built vs. RP; (b) as-built vs. FRCM

4.2. Risk assessment

Seismic risk is defined as a combination of three fundamental elements: **hazard, vulnerability, and exposure**. Hazard represents the probability of the occurrence of an earthquake of a certain intensity in a specific area. Vulnerability describes the expected degree of damage to a particular structure or group of structures exposed to such an event. Finally, exposure identifies the value of elements at risk (e.g., people, buildings, cultural heritage, or infrastructure) that could be affected by a seismic event.

Seismic risk assessment is based on the integration of these three factors to estimate the potential consequences of an earthquake, both in terms of physical damage and societal and economic impacts. This assessment can be carried out using different approaches, distinguishing between **conditional** and **unconditional** risk scenarios.

In the case of unconditional risk, utilized in this study, the analysis does not rely on a single seismic event with a specific return period (as in conditional risk). Instead, it considers a predefined observation time window (e.g., 10, 50, or 100 years). This approach accounts for the probability of one or more seismic events of varying intensities occurring within the selected time frame.

Mathematically, unconditional risk is obtained by integrating hazard curves with fragility and vulnerability models of the structures. The result is a probabilistic estimate of expected losses (e.g., the number of damaged buildings or the economic cost of repairs) considering all possible seismic events that might occur during the observation period.

In this study, the unconditional risk analysis was chosen for several reasons:

- 1. Holistic Approach: By considering a time window rather than a single event, the unconditional analysis allows for the evaluation of the overall risk to which historical masonry buildings are exposed. This is particularly useful for planning large-scale retrofitting interventions.
- 2. Applicability to Multiple Scenarios: This approach enables the modeling of the impact of a range of seismic intensities that could occur, rather than focusing on a single specific scenario.

3. Compatibility with Preventive Strategies: Unconditional risk assessment is particularly suited to identifying interventions that reduce long-term risk, accounting for the full range of seismic events expected over the lifespan of the structures.

Seismic risk assessment is thus a critical topic for the protection and preservation of the built environment, particularly for historical masonry buildings. These structures, characterized by greater structural vulnerability, are often exposed to seismic actions that threaten their integrity and the safety of their occupants.

The objective of this work was to analyze the seismic risk of such structures, evaluating the impact of different structural retrofitting techniques and various types of seismic actions (in-plane and out-of-plane). This approach enabled the identification of the most advantageous strategies in terms of risk reduction and resource optimization.

For data processing and analysis, the IRMA platform (Italian Risk Maps) was utilized. IRMA is an innovative tool designed to assist the scientific community in seismic risk assessment and in generating damage maps and scenarios. The platform integrates predefined databases (e.g., census data on residential buildings) with customizable exposure models and fragility curves, allowing users to simulate realistic seismic scenarios. The OpenQuake calculation engine, embedded in the platform, enables the execution of probabilistic and deterministic risk analyses based on seismic hazard models adopted by Italian regulations.

This study used IRMA to analyze unconditional damage scenarios, assessing the effectiveness of various retrofitting techniques in reducing risk. The results contribute not only to a better understanding of seismic risk but also to the development of practical strategies for protecting historical masonry buildings and mitigating seismic impacts.

4.2.1. Risk evaluation

The IRMA platform incorporates predefined damage-to-risk matrices to convert building damage levels into risk indicators, such as usability, economic losses, and human casualties.

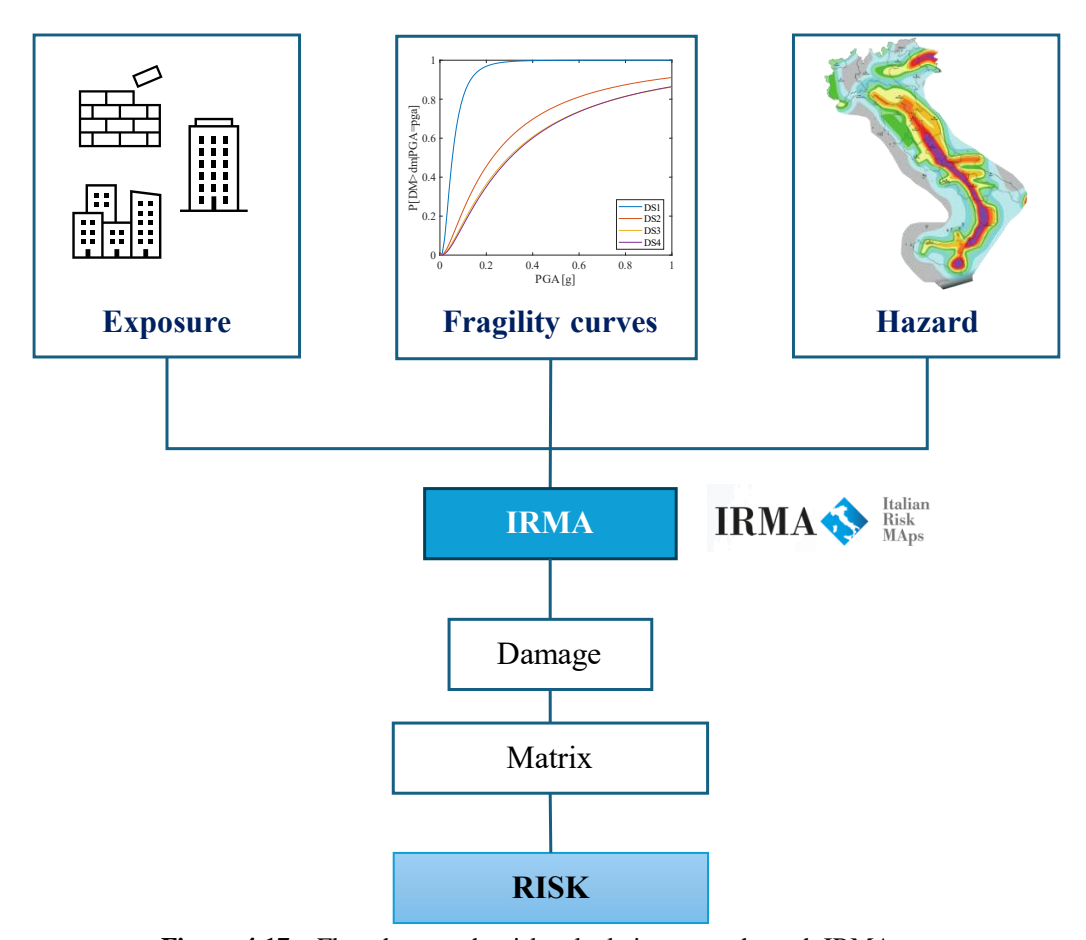


Figure 4.17 – Flowchart on the risk calculation steps through IRMA

These matrices are crucial for transforming structural damage data into actionable insights about risk. The values presented here were derived by combining in-plane and out-of-plane data from the default IRMA matrices, resulting in a customized set of matrices for my analysis (Borzi et al. 2018, 2020)

• Matrix 1: Buildings usability impact

This matrix defines the usability status of buildings at different damage levels (D1–D4).

The usability categories include: (i) Usable: Buildings that remain operational; (ii) Not Usable (Short Term): Temporarily non-operational buildings; (iii) Not Usable (Long Term): Buildings requiring significant repair to regain usability; (iv) Collapsed: Buildings that are irreparable.

Table 4.11 – Matrix 1 building usability impact (Borzi et al. 2018, 2020)

Damage level	Usable (%)	Not usable (short time span) (%)	Not usable (long time span) (%)	Collapsed (%)
D1 - operational	100	0	0	0
D2 - immediate occupancy	60	40	0	0
D3 - life safety	0	30	70	0
D4 - collapse prevention	0	0	0	100

• Matix 2: Economic losses

Matrix 2 estimates repair or reconstruction costs as percentages of the building replacement cost, depending on the damage level. The default reconstruction cost in IRMA is $\leq 135,000/\text{m}^2$.

Table 4.12 – Matrix 2 percentages used for computation of economic losses (Borzi et al. 2018, 2020)

Damage level	Cost of repair or replacement (%)
D1 - operational	2
D2 - immediate occupancy	10
D3 - life safety	50
D4 - collapse prevention	100

• Matrix 3: Human Losses

Matrix 3 provides coefficients to estimate fatalities and injured based on the severity of building damage. This is critical for assessing the societal impact of seismic events.

Table 4.13 – Matrix 3 relationship among damage level, fatalities and injuried (Borzi et al. 2018, 2020)

Damage level	Fatalities	Injured (%)
D1 - operational	0	0
D2 - immediate occupancy	0	0
D3 - life safety	1	5
D4 - collapse prevention	10	30

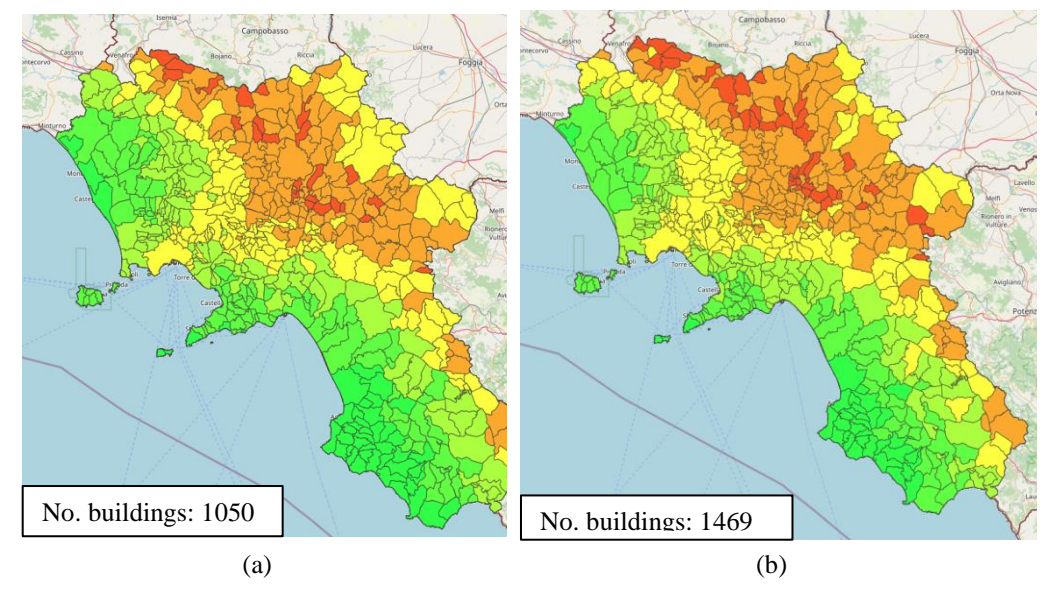
The matrices were uploaded to IRMA, replacing the default values integrated for damage states ranging from 1 to 5, as established by the European Macroseismic Scale (EMS).

These modifications enabled a more accurate risk assessment, aligned with the specific vulnerabilities of historical masonry buildings, while adhering to the damage states previously described in the analyses conducted.

4.2.2. Evaluation of the influence of soil type on seismic risk

For the risk calculation, exposure data, fragility curves, and the damage-to-risk matrices described earlier were implemented in the IRMA platform. A crucial aspect for accurate evaluation is the choice of soil type, as it significantly influences the results through seismic amplification effects.

In a preliminary phase, a parametric analysis was carried out to assess the stratigraphic effects of soil. Four soil types, classified according to standard typologies, were considered: A (rigid soil): hard rock or rock-like deposits with negligible seismic amplification effect; B (intermediate soil): deposits of dense or stiff sand, gravel, or over-consolidated clay, which exhibit moderate amplification of seismic waves; C (soft soil): deep deposits of loose-to-medium dense sand, gravel, or clay, which amplify seismic waves more significantly than Type B soils; D (deformable soil): very soft or loose soils, with high deformability and pronounced amplification effects. For each soil type, the number of buildings damaged at the DS4 level (very severe damage) was calculated.



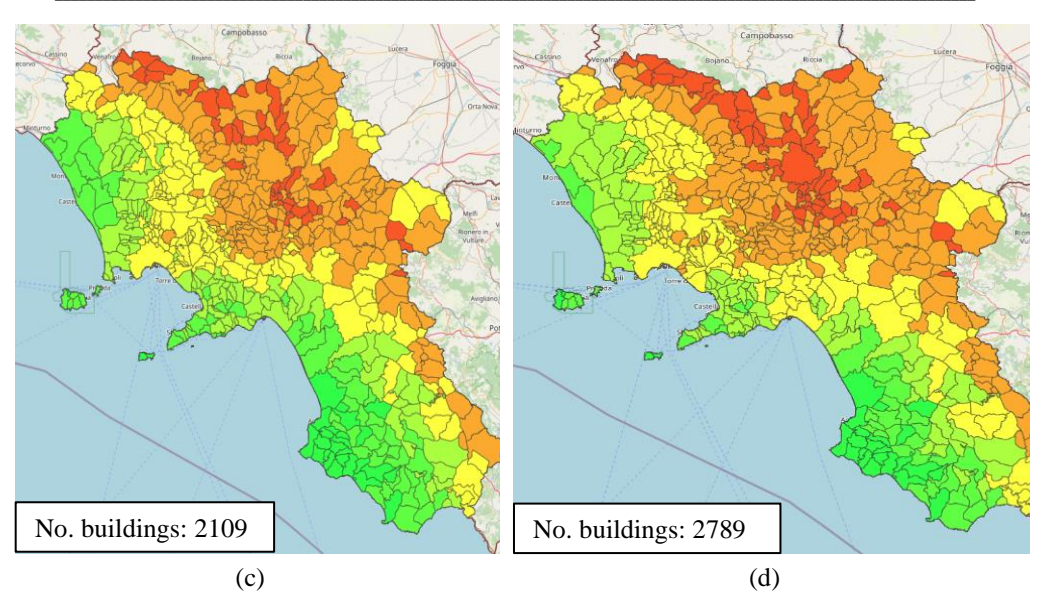


Figure 4.18 – Damage maps at DS4 as the soil type differs: (a) Soil type A; (b) Soil type B; (c) Soil type C; (d) Soil type D.

The results revealed a clear increase in the number of damaged buildings as the soil transitions from rigid to more deformable types. Specifically: an increase of +18% was observed when transitioning from soil A to soil B; an increase of +17% when transitioning from soil B to soil C; an increase of +9% when transitioning from soil C to soil D.

Based on the stratigraphic maps of the Campania Region, aggregated by Forte et al. (2019), the percentage distribution of outcropping soil types is as follows:

- Type B: 59% (the most prevalent),
- Type C: 30%,
- Type A: 9%,
- Type D: 2% (the least prevalent).

Considering this distribution and to achieve a more realistic and representative stratigraphic characterization, the soil aggregation proposed by Forte et al. (2019) and implemented in the IRMA platform was adopted.

This approach allows the analysis to account for the actual local geological conditions, thereby reducing inaccuracies.

The percentage of error introduced by assuming a homogeneous soil type across the entire region, as opposed to the real soil distribution, was calculated.

The findings showed the error increases significantly when a homogeneous soil type of A or D is assumed, as these types are less represented in the region (9%

and 2% of the territory, respectively). Conversely, the error decreases substantially when a homogeneous soil type of C is assumed, with an error of just 6.8%, as it more closely reflects the average regional conditions.

The results are summarized in the following table:

Table 4.14 – Number of buildings damaged (DS4) and percentage error for each soil type compared to the aggregation proposed by Forte et al. (2019).

Soil Type	No. building	s Error [%]	Source
A	1050	-46.8%	EC8
В	1469	-25.6%	EC8
C	2109	+6.8%	EC8
D	2786	+41.3%	EC8
Aggregated soil type(A–D)	1974	-	Forte et al. (2019)

Adopting a realistic stratigraphic distribution based on the aggregation proposed by Forte et al. (2019) allowed for more precise risk assessments. While using a homogeneous soil type simplifies the model, it can introduce significant errors, especially when the chosen soil type does not reflect the prevalent conditions in the region.

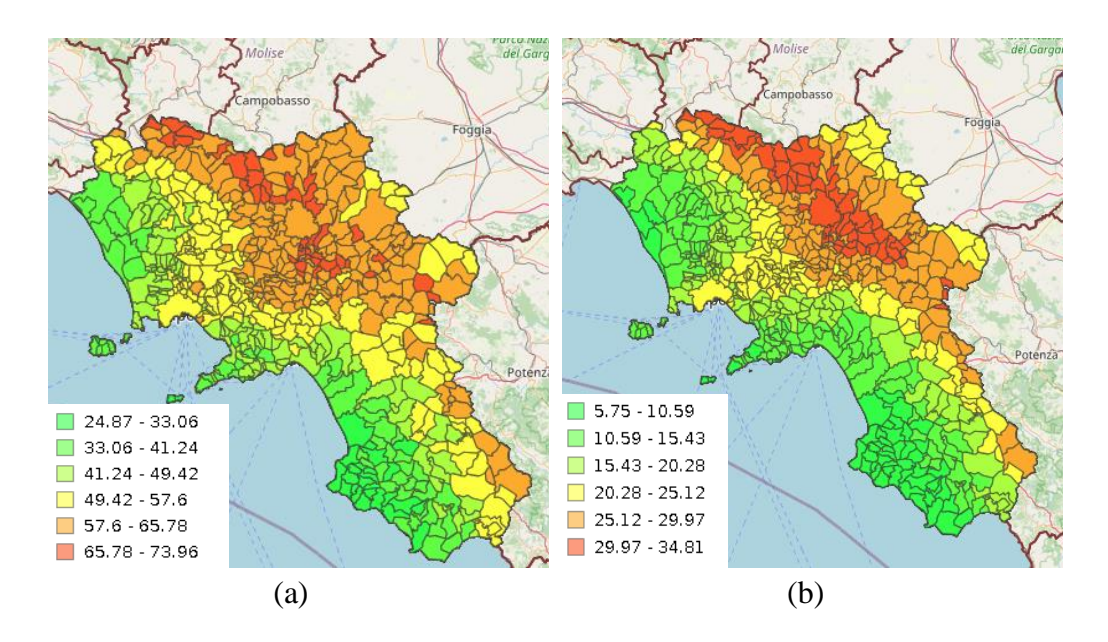
4.2.3. Risk assessment for in-plane and out-of-plane failure

Once the soil type was defined and the 50-year window selected damage maps for various damage states were calculated, the assessment of the associated risk was performed. Initially, risk was calculated separately for in-plane and out-of-plane failure, using the fragility curves described earlier for each case. Subsequently, the combined risk was evaluated by integrating the fragility curves for both in-plane and out-of-plane actions.

The generated maps revealed that the percentage of buildings reaching a state of failure due to in-plane actions is significantly higher than those affected by out-of-plane failure.

However, the combination of the two curves produced intermediate percentages, closer to those of in-plane action. These findings confirm that in-plane structural behavior is the predominant contributor to damage, although the impact of out-of-plane actions is not negligible.

In addition, specific maps were generated to represent (Figure 4.19): buildings collapsed buildings (structures that are irreparable following the seismic event).



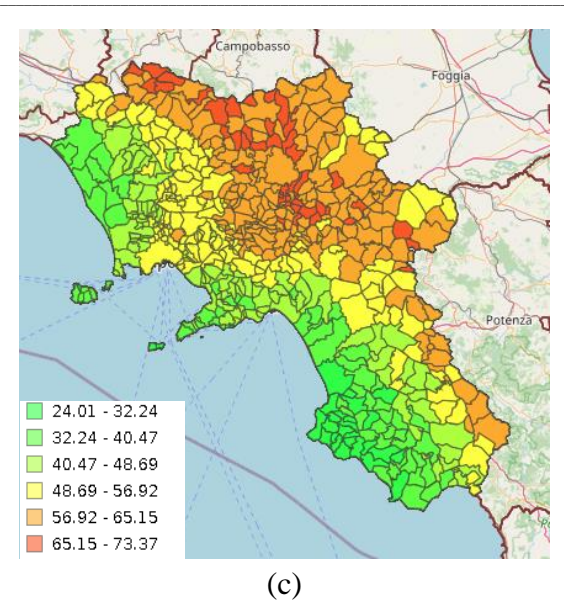


Figure 4.19 – Damage maps by percentage of buildings at collapsed: (a) in-plane failure; (b) out-of-plane failure; (c) combination in-plane and out-of-plane failure

The unconditional risk was selected for a time window of 1 year, and the analysis of the extracted data was carried out. This allowed for the quantification of: the number of buildings damaged for each damage state considered; estimated human losses (injuried and fatalities); usability, i.e., the percentage of buildings usable in the short and long term; and economic losses for the three scenarios analyzed: in-plane (IP) failure, out-of-plane (OOP) failure, and the combined in-plane and out-of-plane failure (IP+OOP).

This integrated analysis enables a more accurate identification of building vulnerabilities and the potential economic and societal impact, providing a solid foundation for planning mitigation measures and recovery strategies.

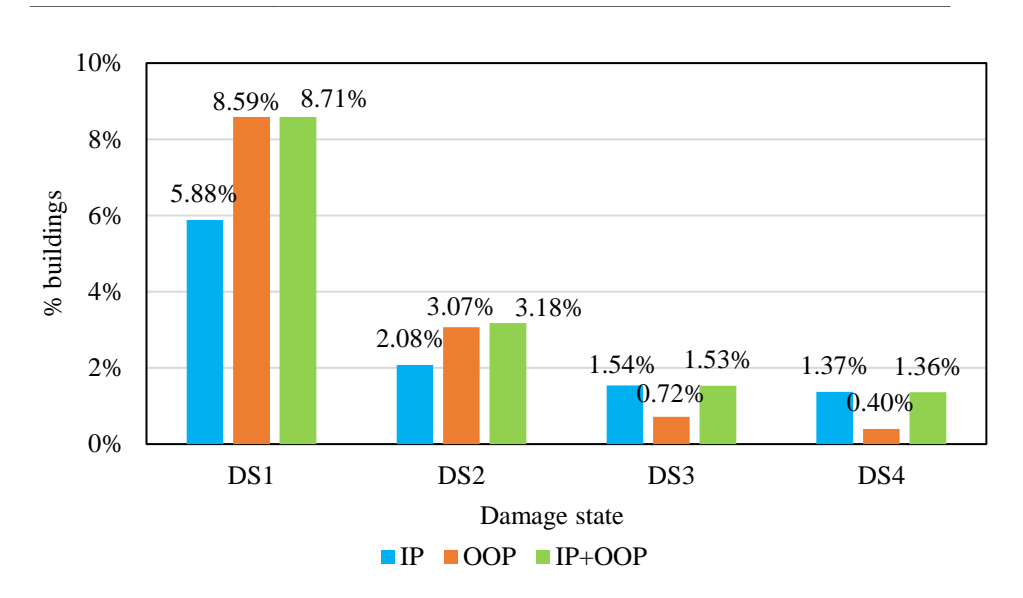


Figure 4.20 – **P**ercentage of damaged buildings for different damage states for different failure modes

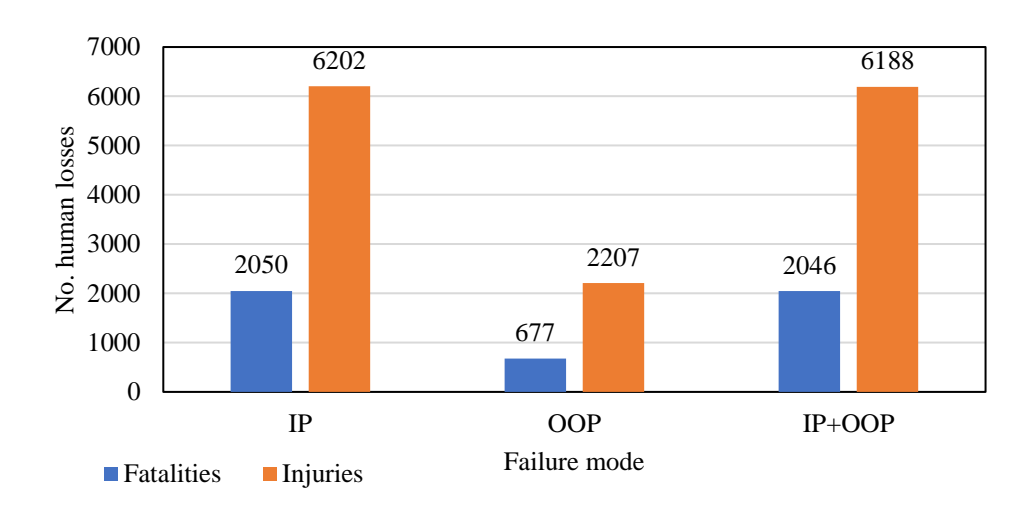


Figure 4.21 – Number of human losses (fatalities and injured) for different failure modes

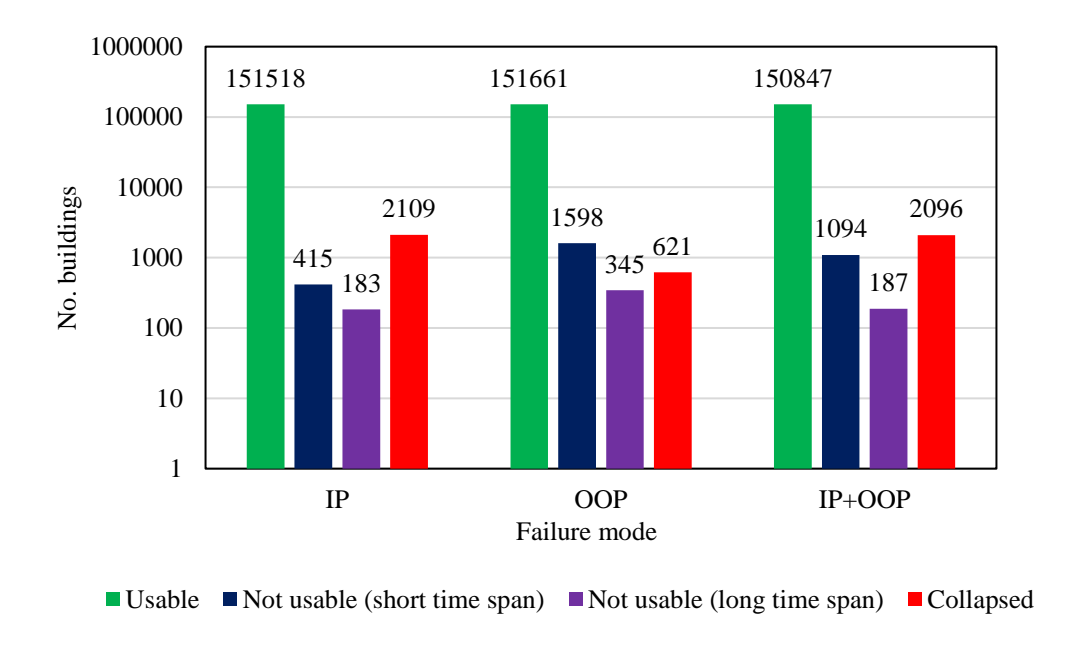


Figure 4.22 – Number of buildings' usability for different failure modes

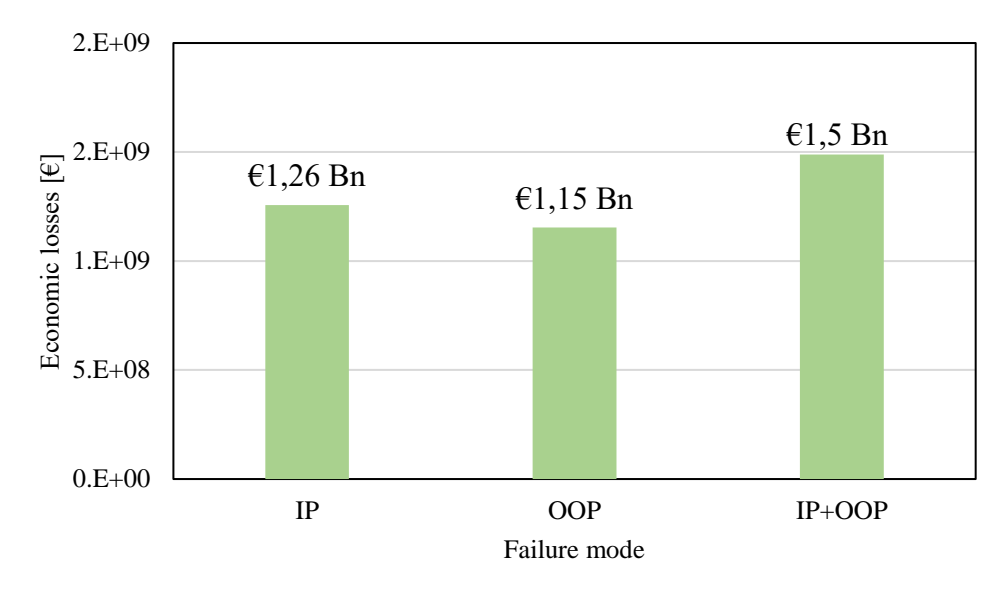


Figure 4.23 – Economic losses for different failure modes

Figure 4.22 clearly shows that the highest losses occur in the case of the combination of the two failures (in-plane and out-of-plane). This result is likely

due to the fact that a significant number of buildings sustain out-of-plane damage, rendering them unusable in the long term.

Specifically, the number of buildings classified as unusable for a long period due to this combined failure mechanism (IP+OOP) amounts to 345. This results in a higher economic loss, estimated at approximately $\[\in \]$ 1.5 billion. This explains why the greatest economic loss is observed when considering both failure mechanisms simultaneously.

This factor directly impacts the magnitude of economic losses, as buildings unusable for an extended period require more complex and costly repair interventions, as well as higher overall economic losses. Consequently, the combination of the two failures represents a critical scenario in terms of economic impact.

This analysis highlights how the integration of the two failure mechanisms leads to increased complexity in managing seismic risk, necessitating more strategic planning to address the impacts effectively, both in the short and long time span.

4.2.4. Impact of sustainable technology for risk mitigation

The same methodology used for the risk assessment of as-built buildings was applied to buildings retrofitted using two different reinforcement techniques: traditional RP and innovative FRCM. For each type of intervention, specific fragility curves, obtained in Section 4.1.3, were implemented and used for risk calculation.

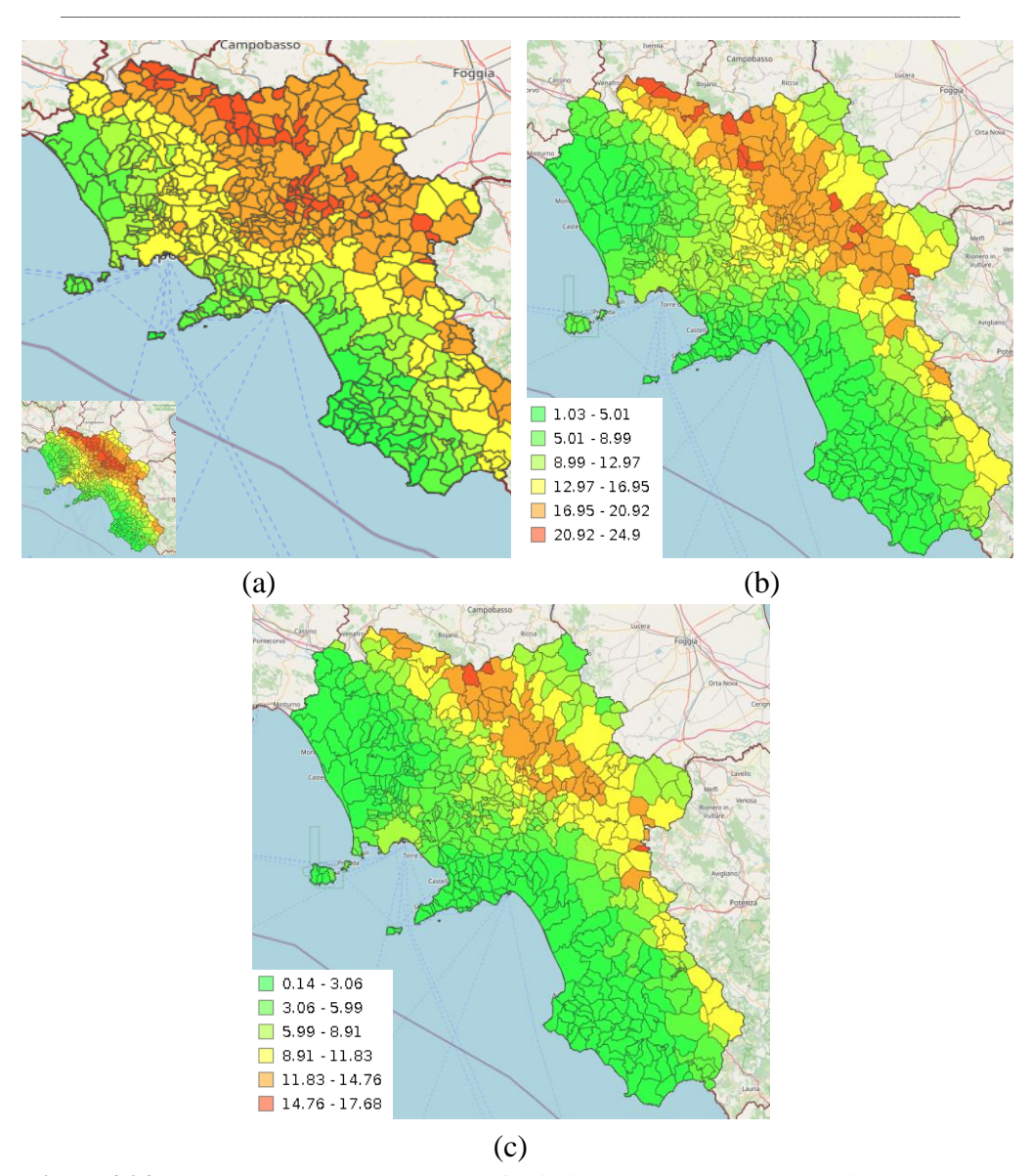
Subsequently, a comparative evaluation was conducted between the retrofitted buildings and the as-built ones to quantify the effectiveness of the reinforcement techniques in reducing seismic risk.

The produced damage maps highlighted a significant reduction in the number of damaged buildings with the adoption of the reinforcement techniques. Specifically, for DS4 shown in Figure 4.23, a reduction of approximately 68% in the number of damaged buildings was observed when transitioning from the asbuilt condition to the RP condition. An additional reduction of approximately 30% was recorded when transitioning from RP to buildings retrofitted with FRCM.

These results underline the effectiveness of both reinforcement techniques in mitigating seismic risk, with a particularly noticeable impact already achieved through the adoption of RP. However, the use of the innovative FRCM system provides further improvement, demonstrating that newer technologies can offer significant advantages not only in terms of damage reduction but also in the durability and performance of the reinforcement.

The FRCM system stands out for its intrinsic characteristics, such as lightness, chemical and mechanical compatibility with existing structures, and greater resistance to degradation compared to traditional materials.

These qualities make it particularly suitable for the reinforcement of historical and masonry buildings, where the additional weight and visual impact of interventions must be minimized.



 $\begin{tabular}{ll} \textbf{Figure 4.24}-Damage maps by percentage of buildings at collapsed: (a) as-built; (b) RP; (c) \\ FRCM \end{tabular}$

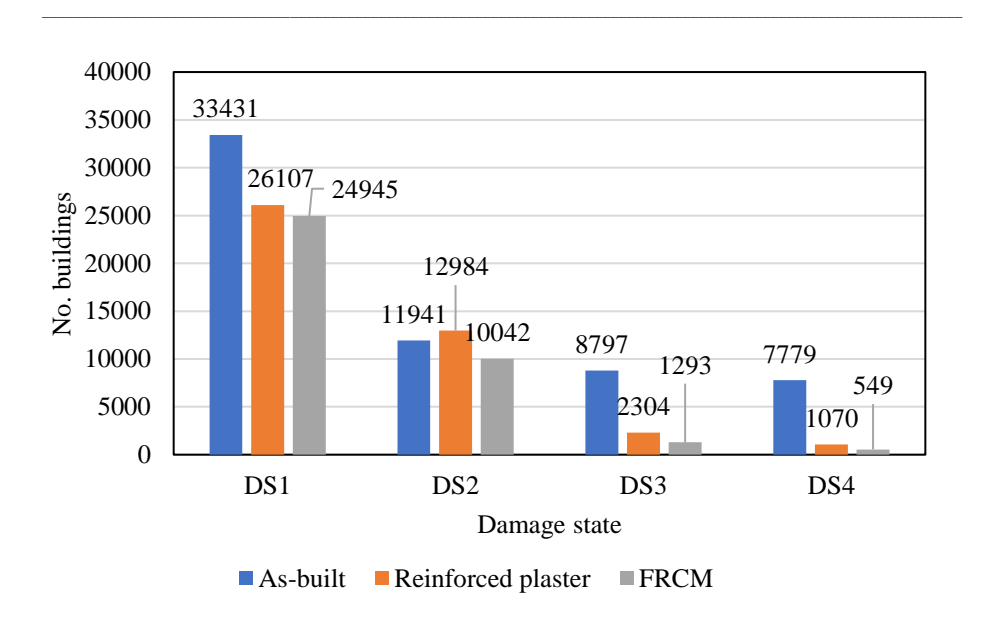


Figure 4.25 – Percentage of damaged buildings for different damage states for different retrofit technologies

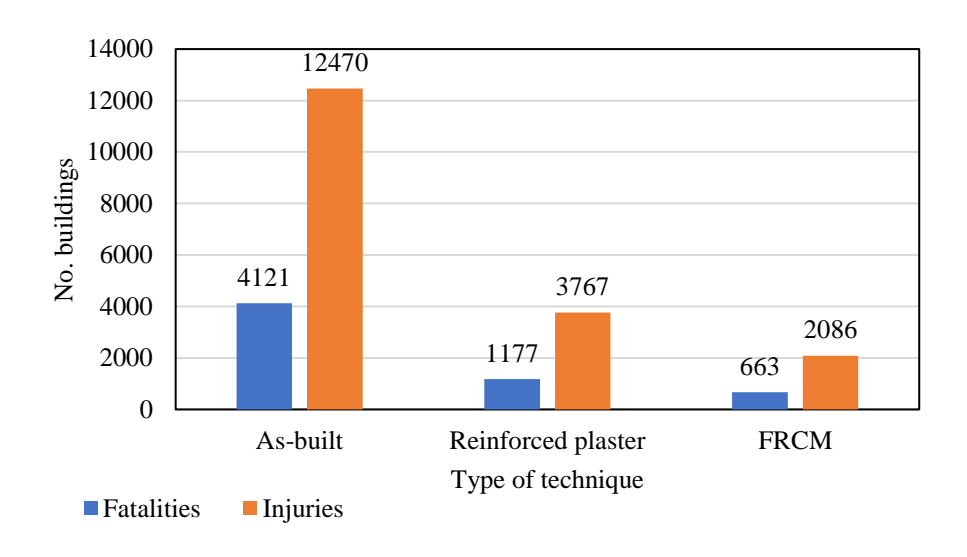


Figure 4.26 – Number of human losses (fatalities and injured) for different retrofit technologies

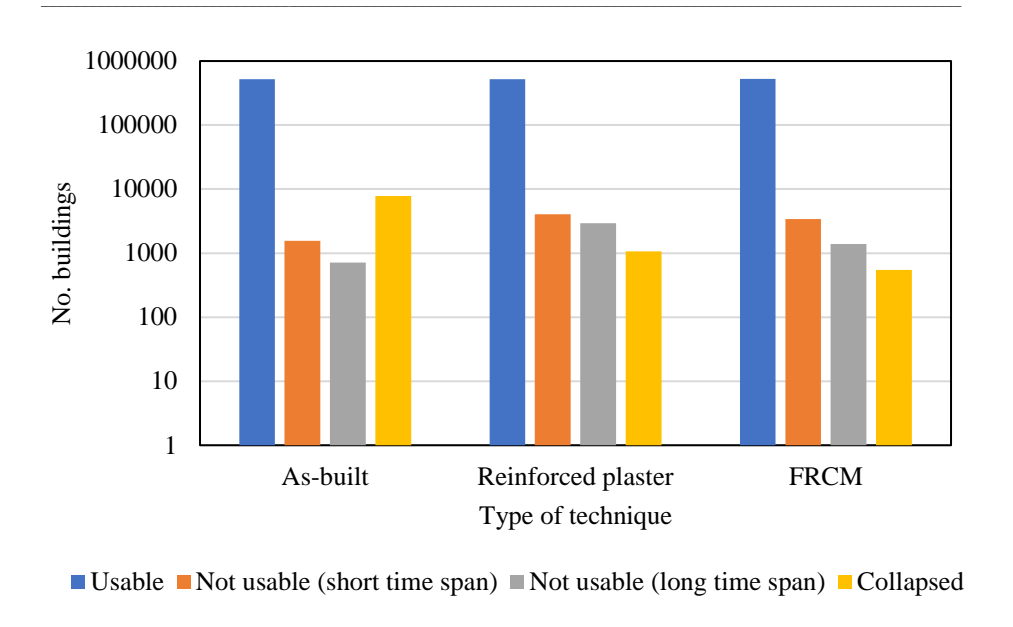


Figure 4.27 – Number of buildings' usability for different retrofit technologies

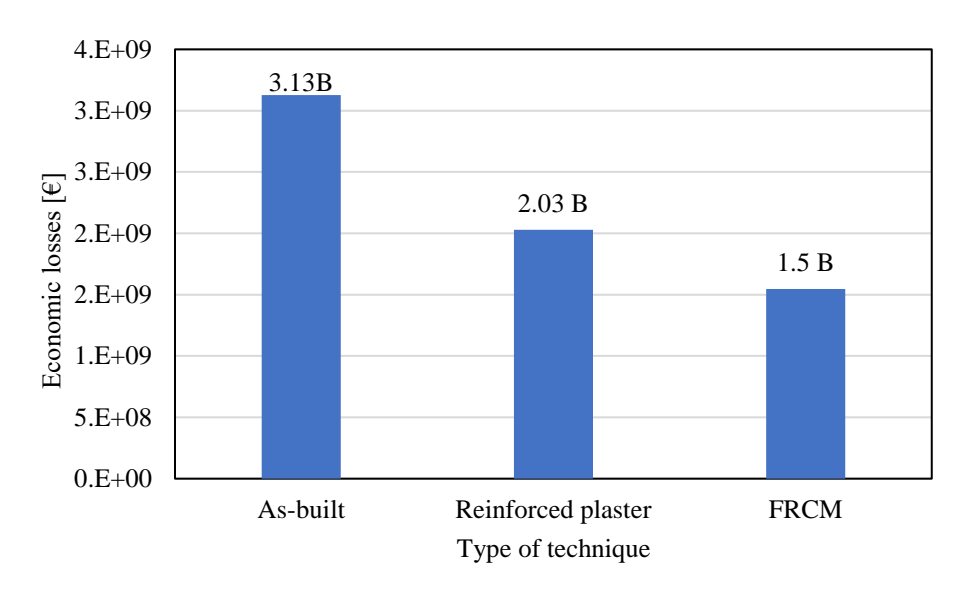


Figure 4.28 – Economic losses for different retrofit technologies

The provided bar chart (Figure 4.26) clearly illustrates a significant percentage decrease in life and limb losses when comparing as-built buildings to those retrofitted using RP or FRCM techniques. Similarly, a notable reduction is evident in the injured: their number decreases from 12,470 in as-built buildings

to 3767 for those with RP, representing a decrease of around 70%, while with the adoption of FRCM, the injured further decline to 2086, corresponding to a reduction of approximately 83% compared to as-built structures.

This data highlights the effectiveness of both reinforcement techniques in reducing human casualties during seismic events. The reduction is particularly significant with the use of FRCM, which achieves the highest percentage decrease in both fatalities and injured.

The performance of FRCM can be attributed to its superior mechanical properties, including better energy dissipation and improved structural behavior under seismic loads. Additionally, its lighter weight and compatibility with existing materials make it an ideal solution for reducing seismic risk in vulnerable buildings.

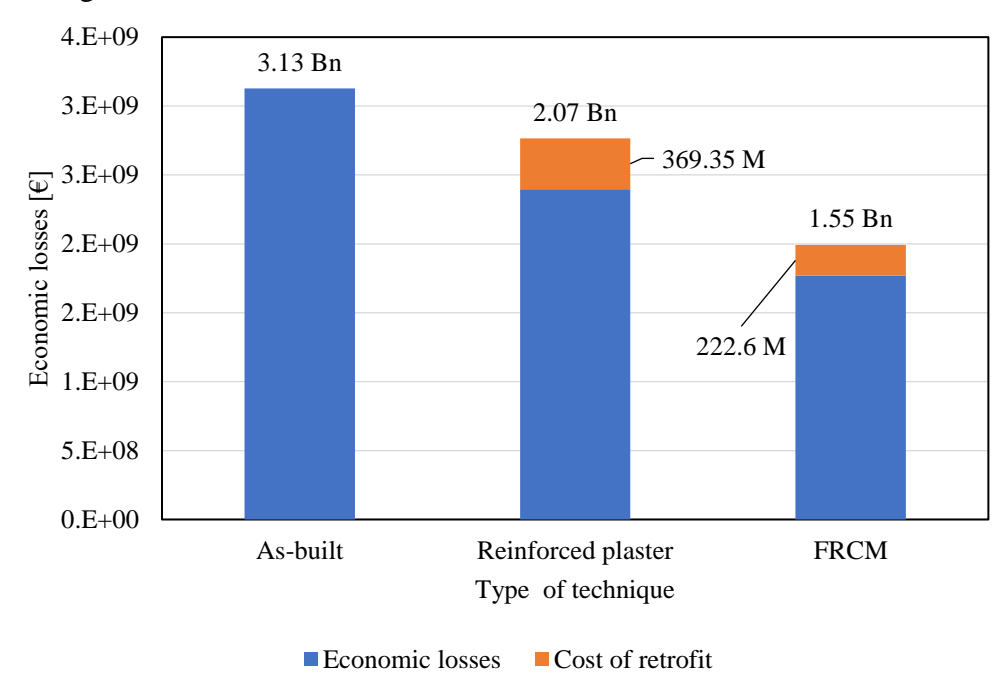


Figure 4.29 – Economic losses and cost of retrofit for different retrofit technologies

Economic losses are a key factor in assessing the effectiveness of retrofitting techniques. As shown in Figure 4.28, in addition to direct economic losses caused by structural damage, it is crucial to include intervention costs associated with the adopted retrofitting techniques.

To obtain a comprehensive evaluation, repair costs per square meter were integrated into the analysis, based on official price lists from the Campania Region for residential buildings.

Specifically, the costs considered for the two retrofitting techniques refer to the strengthened wall surface, excluding the openings of windows and doors. The calculations were performed based on the vertical wall surface area, considering this volume for the application of the reinforcement:

- 293.01 €/m² for buildings retrofitted with RP (traditional technique);
- 176.58 €/m² for buildings retrofitted with FRCM (innovative technique).

Based on these parameters and estimating the total areas of the buildings analyzed, repair costs were added for each technique, resulting in the total losses illustrated in Figure 4.29. The analysis of total losses, which include direct economic losses and intervention costs, highlighted significant reductions in overall losses with the adoption of retrofitting techniques.

The calculations show an 23% overall reduction in economic losses between asbuilt buildings and buildings retrofitted with RP, while between asbuilt buildings and buildings retrofitted with FRCM the overall reduction in economic losses increases to 43%.

These results clearly demonstrate the greater effectiveness of FRCM compared to RP in reducing total losses, both due to its lower strengthening costs and its ability to limit structural damage.

The inclusion of intervention costs in the analysis of economic losses provides a more realistic evaluation of the benefits of retrofitting techniques. While both techniques are effective in reducing losses, FRCM stands out as the most advantageous solution due to its lower cost per square meter and higher capacity to mitigate seismic risk.

This result highlights the importance of considering not only structural effectiveness but also economic efficiency when planning large-scale interventions, particularly in high seismic risk areas. The adoption of innovative technologies like FRCM represents a strategic investment to reduce future economic losses and enhance the performance of buildings.

CHAPTER 5 – APPLICATION TO A REPRESENTATIVE CASE-STUDY BUILDING IN PORTICI (PROVINCE OF NAPLES)

5.1 Selection of the case study

The case study selected for my doctoral thesis is a building located in Campania, in the municipality of Portici (province of Naples), featuring a construction type dating back to a period prior to 1919. The choice of this structure is not random but is motivated by its alignment with the most representative class of buildings in the Campania region, according to recent statistical analyses and collected data. Specifically, it is a three-story construction, a typology that accounts for a significant percentage of the historical building stock in this area.

Moreover, the building features a regular masonry structure made of soft stone, specifically tuff, units classified as Class C1. This type of masonry was the most widespread in Campania during that construction period, chosen for its mechanical properties, local availability, and relatively low cost. Tuff, being lightweight and easy to work with, was commonly used to build regular and stable structures that suited both traditional construction methods and the architectural and functional requirements of the time.

The selection of this type of building is particularly relevant for the study of seismic vulnerability within the historical building stock of Campania. Buildings constructed before 1919, with three floors and regular tuff masonry, represent an ideal sample for investigating structural weaknesses and identifying effective intervention strategies, both for preservation and for improving seismic safety.

The building's floors are composed of fired clay block-reinforced concrete slabs, a widely used to improve the structure's strength and stability while maintaining a lightweight arrangement. The building has a rooftop deck, a practical and functional solution that was common for buildings of that time, extending the living space.

The internal staircase is made of reinforced concrete, connecting the ground level to the top floor.

This building represents a significant example of the region's historical architecture, showcasing both local construction techniques and the integration of materials typical of that time. Its structural characteristics and location make it an ideal case study for analyzing structural vulnerabilities in relation to seismic actions and for evaluating the impact of intervention techniques, both traditional and innovative, on the overall structural response.

5.2 Geometrical and mechanical properties of the building

The geometry of the building is organized across three distinct levels, each with a slightly different layout but consistent with the typical functions of a historical residential structure. Notably, each room is connected to the others without the presence of corridors or partitions dividing the spaces. From the floor plans, it can be observed that there are three walls along the x-axis and four walls along the y-axis, with the addition of an oblique perimeter wall rotated 30° relative to the x-axis.

The ground floor (Figure 5.1) features a spatial distribution consisting of several rectangular rooms aligned along the building's main axis, parallel to the x-axis. The load-bearing external and internal walls, thicker than those on the upper floors, provide structural stability and are constructed with regular tuff masonry. The thickness of both the internal and external walls is 800 mm. Additionally, a centrally located internal staircase connects the ground floor to the upper levels.

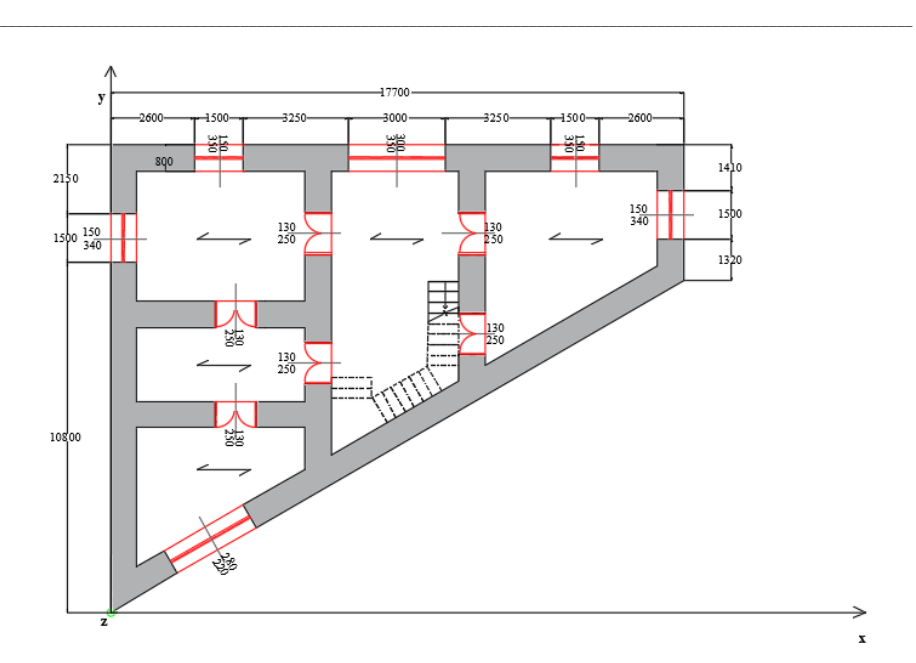


Figure 5.1 – Ground floor plan of the case study

The first floor (Figure 5.2) maintains a layout similar to the ground floor, with rooms of comparable size but minor variations in internal openings. The load-bearing walls, while slightly thinner than those on the ground floor (70 cm, thus reduced by 10 cm), continue to play a critical role in ensuring resistance to vertical loads and seismic actions. The internal staircase, still centrally positioned, remains the primary vertical connection element, providing optimized access to the main rooms. At this level, the floor plan retains the slightly irregular geometry observed on the ground floor.

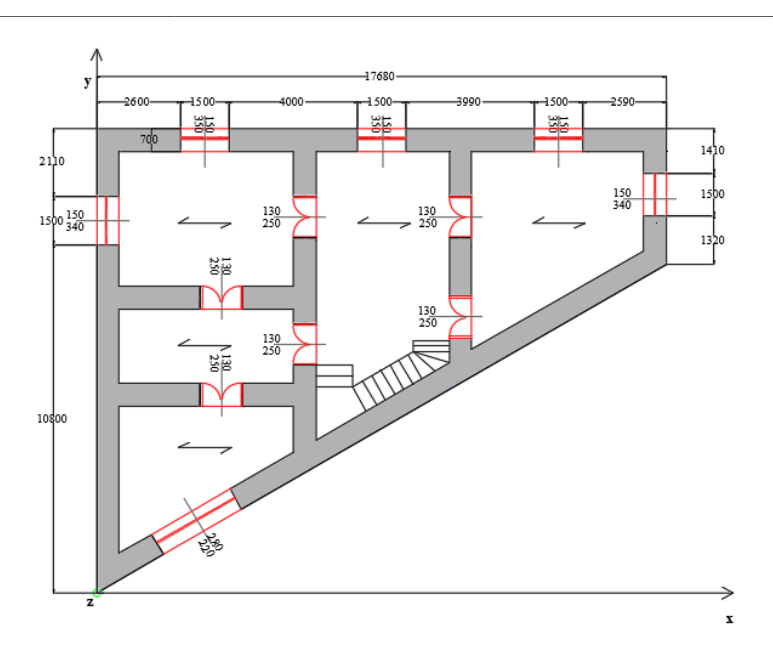


Figure 5.2 – First floor plan of the case study

The second and final floor (Figure 5.3) has a simplified layout compared to the lower floors, primarily for structural and functional reasons. The perimeter and partition walls are further reduced in thickness (60 cm), indicating a deliberate effort to reduce loads on the underlying levels. This floor, intended for lighter functions, has fewer openings while maintaining a consistent layout with the lower levels. The internal staircase reaches this second and final floor, ensuring continuity of access throughout all levels. From this floor, a door leads to a small terrace at the same level, which is connected to the rooftop deck via an external iron staircase.

The building's floor plan configuration reflects a functional and structural organization typical of historical masonry buildings in the Campania region. The spatial distribution, the central position of the staircase, and the variation in wall thickness across floors are all design choices aimed at balancing structural stability with the usability of internal spaces. The irregularity of the floor plan near the southwestern wall requires particular attention in the structural analysis, as it may introduce significant torsional effects under seismic actions. Below is the ground floor plan (Figure 5.4) with the numerical identification of the walls, allowing for the individual discretization of the walls and the schematization of the EFM, which will be implemented in the MATLAB code.

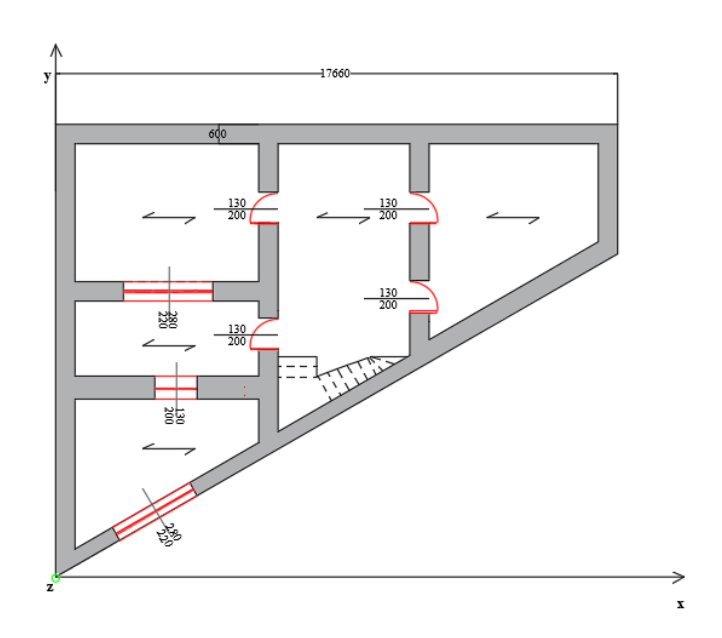


Figure 5.3 – Second floor plan of the case study

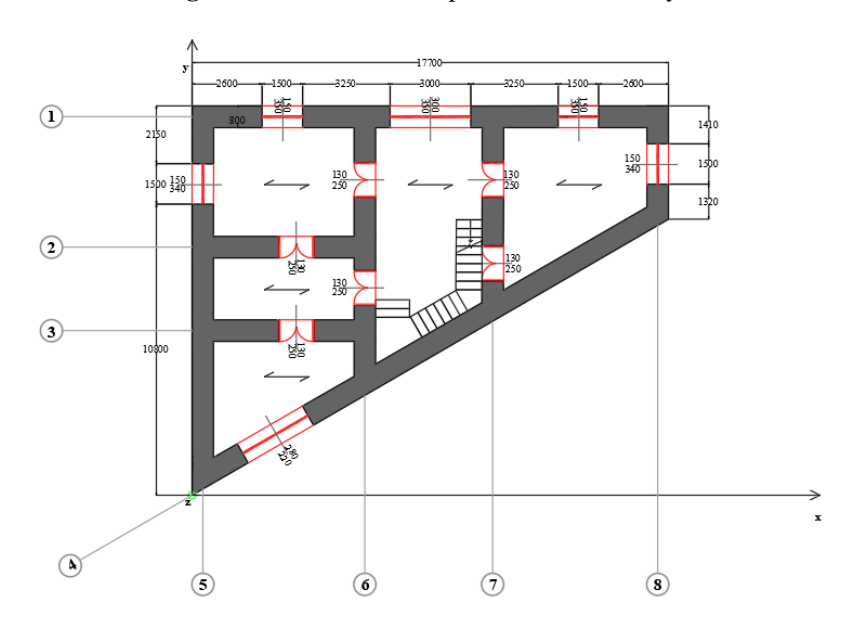


Figure 5.4 - Identification of the walls along x and y direction of the case study

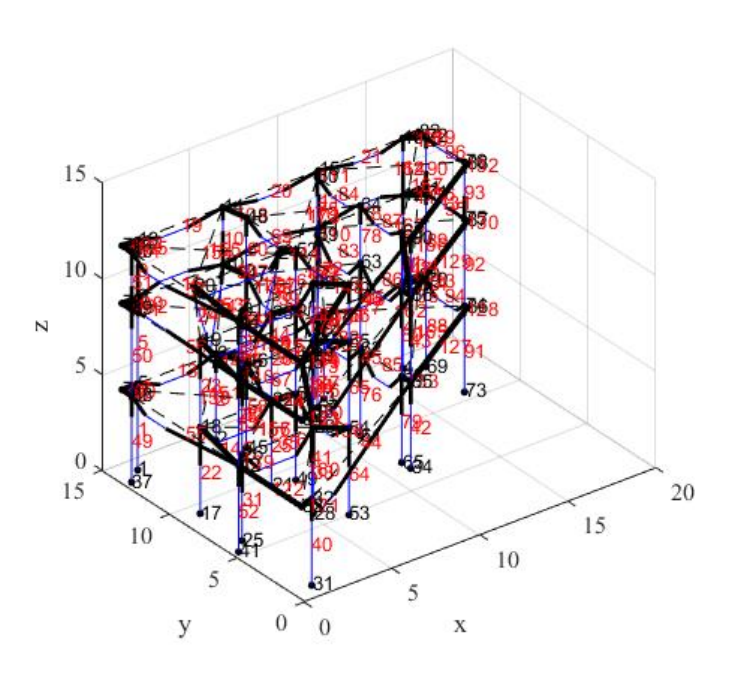


Figure 5.5 – Structural system of case study building: equivalent frame view

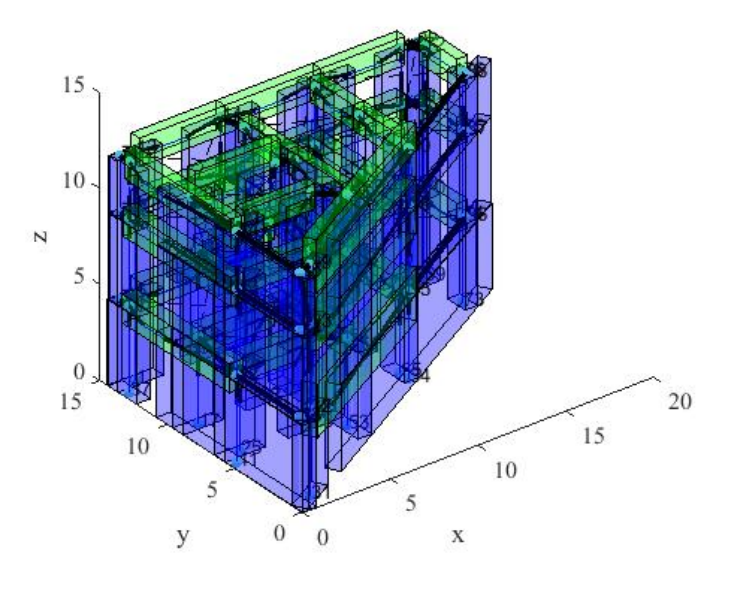


Figure 5.6 – Structural system of case study building: solid view

The mechanical properties of the masonry used are those prescribed by Commentary No. 7/2019 and summarized in Table 5.1.

Table 5.1 – Mechanical properties

Masonry	Variable	Unit of measurement	Va (Comr no. 7	Used value	
			min	max	
	f_m	MPa	2.00	3.20	2.6
	$ au_{O}$	MPa	0.04	0.08	0.06
	f_{v0}	MPa	0.10	0.19	0.145
Regular soft	E	MPa	1200	1620	1410
stone masonry	G	MPa	0.33*E		465.3
	f_t	MPa	$0.05*f_m$		0.13
	$G_{\!f\!t}$	N/mm	0.	025	0.025
	w	kN/m^3	13	16	16

5.3 Structural analysis and application of the proposed methodology

In this study, a preliminary modal analysis was first performed on the building under investigation. This analysis identified the three fundamental vibration modes, one for each direction, with corresponding periods of 0.2370 s, 0.1815 s, and 0.1609 s, respectively.

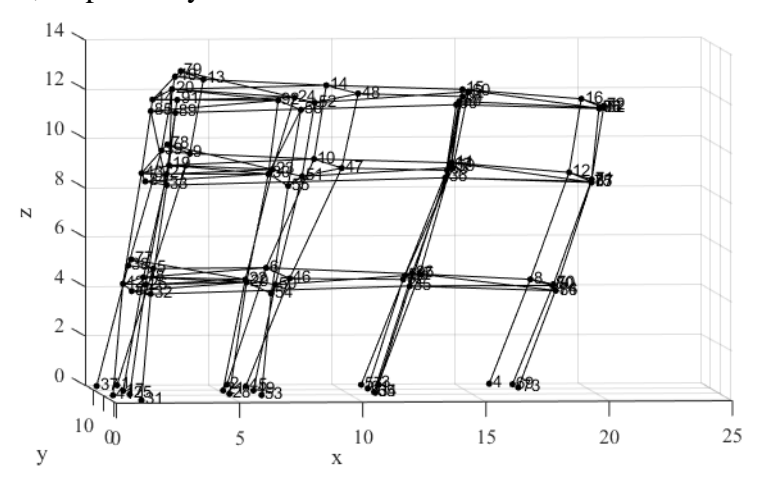


Figure 5.7 – First mode of vibration

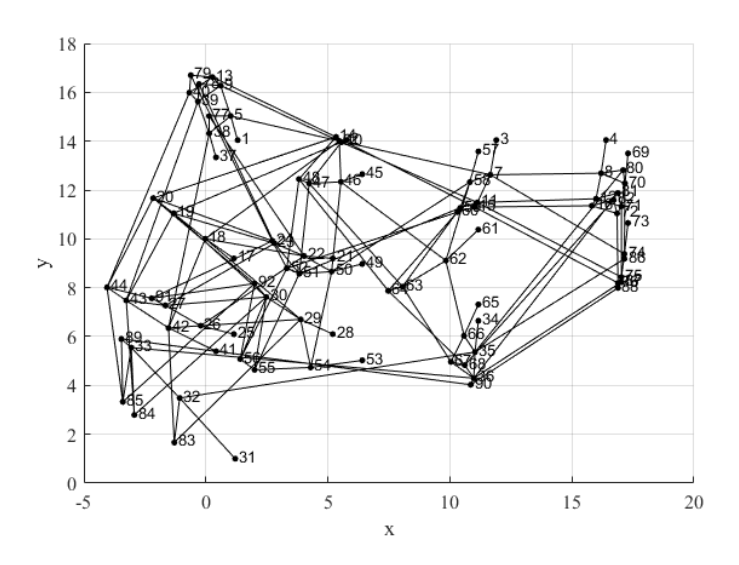


Figure 5.8 – Second mode of vibration

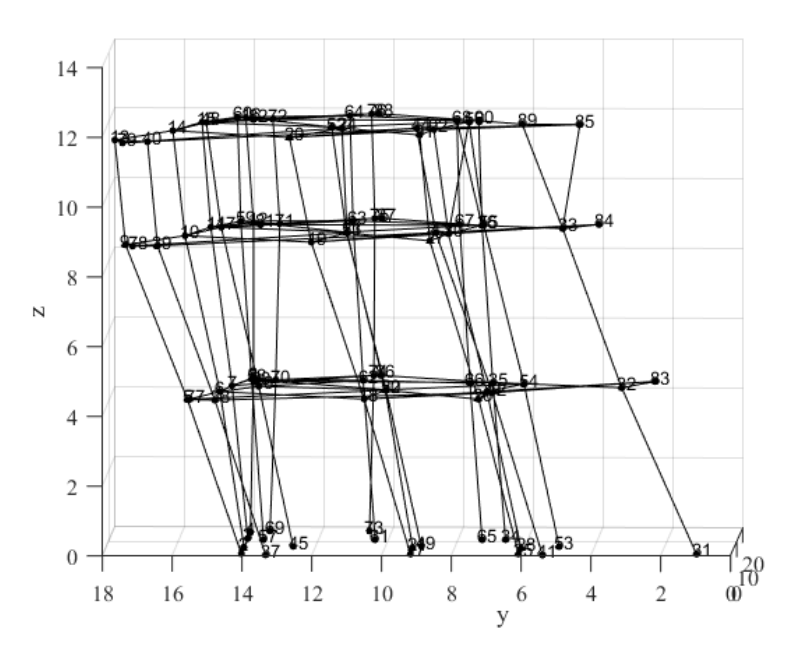


Figure 5.9 – Third mode of vibration

Notably, the second mode is torsional, an expected result given the irregular plan layout typically found in historical buildings of this type. The building has a total mass of 1517 tonnes (or Mg), with a participating mass in the fundamental modes of 1181 tonnes, corresponding to approximately 78% of the total mass.

Subsequently, nonlinear static analyses were carried out to assess the global behavior of the building in the two principal directions, X and Y, considering both positive and negative load applications. These analyses were performed using displacement control, with the control point set at the centroid of the third-floor diaphragm (roof level). The applied forces were distributed according to two primary configurations:

- Mass-proportional distribution (constant): In this case, the horizontal forces applied were directly proportional to the masses of each floor.
- Simplified-first-mode-proportional distribution (inverted triangular): The forces were distributed based on a proxy vertical modal participation, calculated as the relative height of each floor compared to the building's total height (12 meters). The modal distribution coefficients (ϕ_i) were defined as follows:
- > Third floor: 1.00 (height 12.0 m);
- Second floor: 0.75 (height 9.0 m);

First floor: 0.38 (height 4.5 m).

The nonlinear static analyses allowed for a comprehensive characterization of the building's behavior under various load configurations, highlighting the main failure mechanisms and providing a basis for subsequent structural strengthening interventions.

Table 5.2 – Parameters obtained from the case study analysis

Floor	m	Φi	φ _i x m _i	M	m*	M/m*	Γ	Γ
		1 -					(∝masses)	(∝1st mode)
[-]	[tonne]	[-]	[tonne]	[tonne]	[tonne]	[%]	[-]	[-]
1st	668.00	0.38	253.84					
2nd	519.23	0.75	389.42	1517	1181	78	1.00	1.17
3rd	329.44	1.00	329.44					

Based on the analyses conducted, the following considerations can be drawn regarding the behavior of the building. In the positive Y direction Figure 5.10 (Y+, red curve) with a distribution proportional to the first mode, the maximum base shear capacity (V_b) is approximately 3300 kN, with a corresponding control displacement (δ_c) close to 0.03 m.

In the negative Y direction (Y-, green curve), a slightly less performant behavior is observed, with a lower maximum Vb value (around 2700 kN) and a similar displacement limit as in the positive direction. This behavior reflects the influence of the torsional response and the geometric irregularities of the building, which result in a slight asymmetry between the positive and negative directions.

For the mass-proportional distribution, it is noted that in the positive Y direction (Y+, cyan curve), the base shear capacity increases significantly, exceeding 4000 kN, with displacements similar to those observed with the first-mode proportional distribution. In the negative Y direction (Y-, purple curve), the peak Vb reaches approximately 3800 kN, higher than the values obtained with the modal distribution. This result indicates that the mass distribution positively affects the overall capacity, highlighting a greater contribution of the upper-floor masses to the structural behavior.

In the X direction (Figure 5.11), considering the first-mode proportional distribution, in the positive X direction (X+, grey curve), the maximum capacity is approximately 3200 kN. In the negative X direction (X-, black curve), a

significant reduction in capacity is observed, with a V_b peak of about 2300 kN. This behavior can be attributed to lower stiffness in the negative direction, likely caused by an asymmetric distribution of mass and resistance.

For the mass-proportional distribution, in the positive X direction (X+, blue curve), the maximum capacity is higher, reaching 3800 kN. In the negative X direction (X-, yellow curve), an improvement is observed compared to the first-mode proportional distribution, with a maximum V_b again of about 3800 kN, although the behavior is less regular at large displacements.

In general, it can be said that:

- The mass-proportional force distribution generates higher global capacities compared to the first-mode proportional distribution, highlighting a greater contribution from the upper-floor masses.
- A certain asymmetry is observed between the positive and negative directions in both axes, which is more pronounced in the X direction, consistent with the building's geometric and torsional irregularities.
- ➤ The curves for the Y direction exhibit higher overall capacities compared to the X direction.

The analyses also revealed that the sudden loss of load-bearing capacity, highlighted by the drop in maximum base shear, can be attributed to the failure of several panels due to shear and flexure, primarily localized on the ground floor. This phenomenon leads to the formation of a "soft storey" in the building, compromising its overall structural behavior.

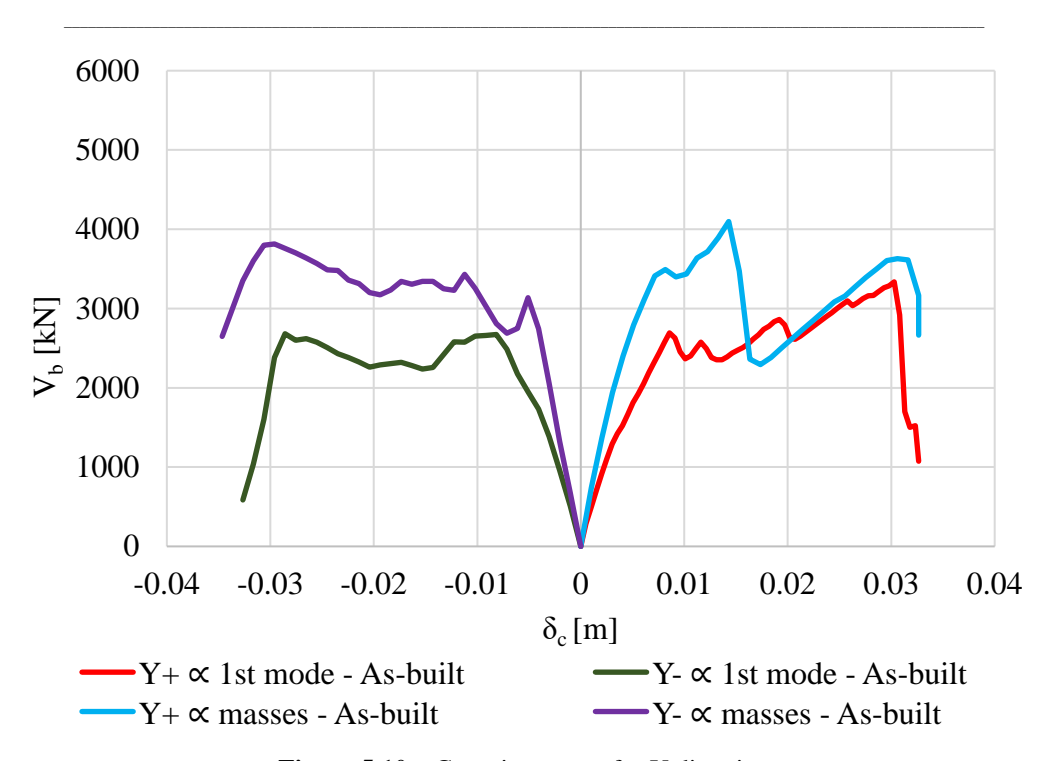


Figure 5.10 – Capacity curves for Y direction

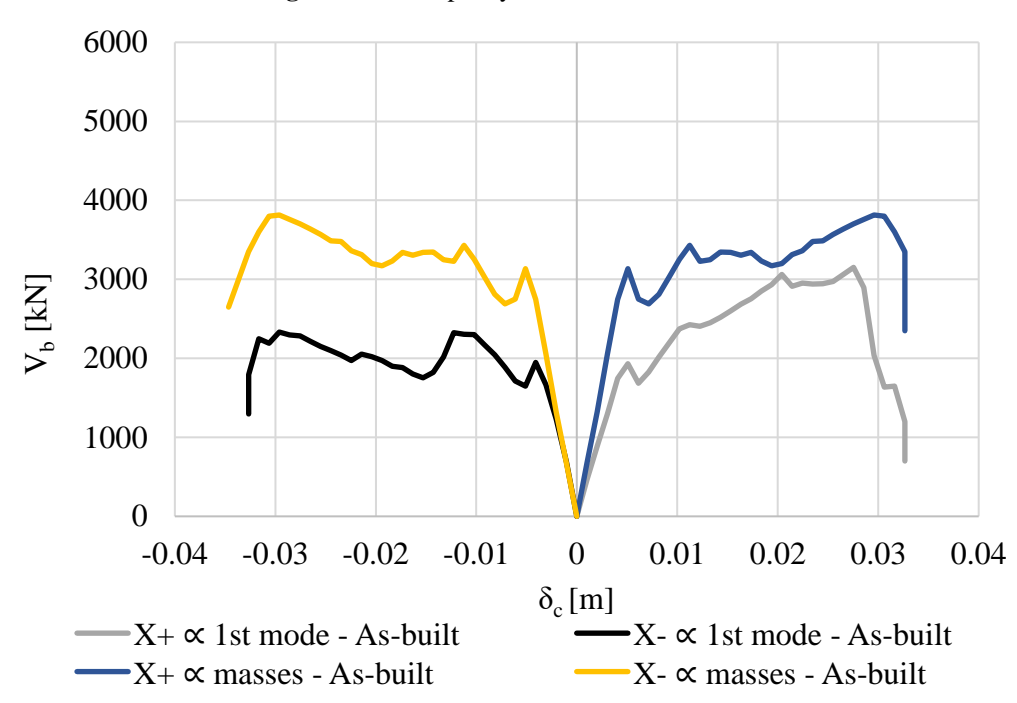


Figure 5.11 – Capacity curves for X direction

The nonlinear static analysis conducted on the as-built building revealed several critical aspects of its structural behavior, particularly the concentration of damage at the ground floor. This area emerged as the critical failure zone, with collapse mechanisms dominated by the failure of masonry panels, primarily due to high shear stresses and the geometry of the structure. These vulnerabilities highlighted the inherent limitations of unreinforced masonry historical buildings, which exhibited both low load-bearing capacity (V_b) and limited ultimate displacement (δ_c) in their as-built state. To address these deficiencies, targeted strengthening interventions were designed, focusing exclusively on the ground floor. Two techniques were applied: RP and FRCM, both implemented on the two faces of the masonry walls. The capacity curves obtained for both principal directions, X and Y, are shown in the following figures 5.12 and 5.13, and the results are analyzed in detail.

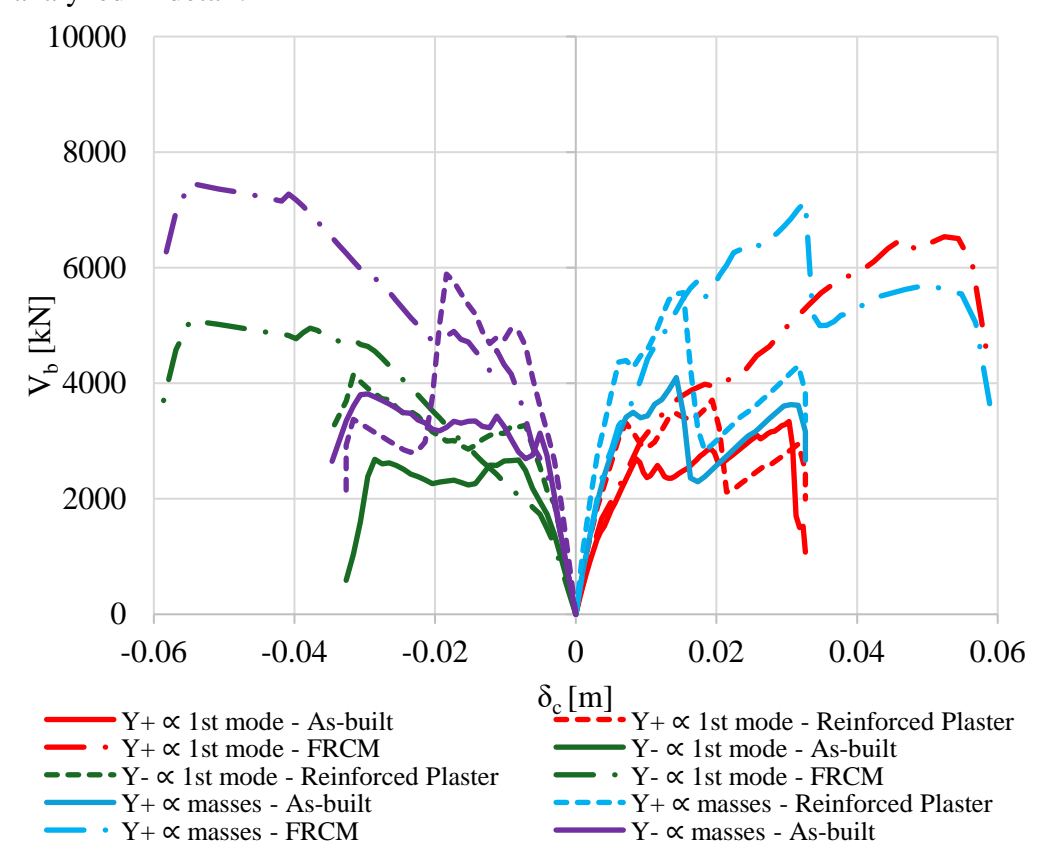


Figure 5.12 – Global capacity curves of buildings for Y direction and proportional to 1st mode of vibration and masses

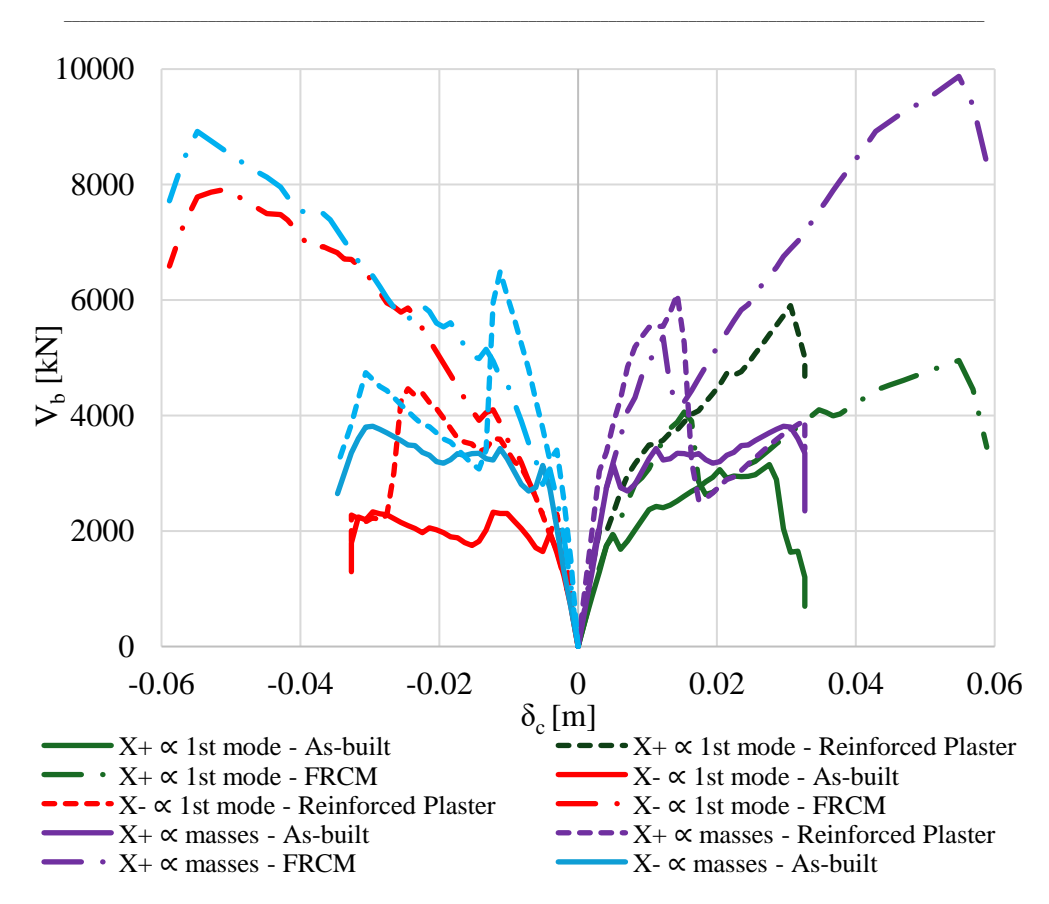


Figure 5.13 – Global capacity curves of buildings for X direction and proportional to 1st mode of vibration and masses

For RP, a strength enhancement coefficient of 1.5, as recommended by Commentary n.7/2019, was applied. The analysis revealed that this intervention produced a substantial increase in peak base shear capacity ($V_{b,\ peak}$), with improvements ranging from 36% to 87%, depending on the direction and force profile considered. Additionally, RP significantly enhanced the initial stiffness of the structure, reducing the displacement corresponding to the peak capacity (e.g., from 0.0303 m to 0.0194 m in the Y+ direction with the first-mode distribution). This increased stiffness proved effective in limiting global deformations under seismic loads. However, the ultimate displacement remained comparable to the as-built configuration, indicating that while RP is highly effective in improving strength, it has limited impact on the structure's ability to undergo deformations beyond the elastic limit.

On the other hand, FRCM, implemented with coefficients derived from scientific literature, demonstrated even greater improvements in structural behavior. FRCM significantly increased the peak base shear capacity, with improvements reaching up to 239% (e.g., in the X- direction with mass-proportional distribution). Moreover, FRCM provided a substantial increase in the displacement corresponding to the peak capacity ($\delta_{c,peak}$), reflecting a marked improvement in the building's global ductility. For instance, in the Y+ direction, the ultimate displacement increased from 0.0303 m to 0.0514 m, representing a 70% increase. Unlike RP, the initial stiffness remained virtually unchanged compared to the as-built state, but the FRCM intervention significantly enhanced the post-elastic behavior of the structure, allowing for a more ductile response and greater energy dissipation capacity.

When comparing the two interventions, their distinct advantages become evident. RP prioritizes an increase in stiffness and base shear capacity, effectively improving strength without significantly altering the ultimate displacement. Conversely, FRCM not only substantially increases base shear capacity but also enhances ultimate displacement, making the building more ductile and capable of withstanding large deformations before collapse.

The percentage increases in capacity (ΔV_{peak}) and displacement (Δd_{peak}) further illustrate these differences (Table 5.3 and 5.4). For example, in the X- direction with the first-mode force profile, FRCM achieved a 239% increase in Vb,peak, compared to 91% with RP. Similarly, in the Y+ direction with the mass-proportional distribution, FRCM increased the ultimate displacement by 70%, nearly three times the increase achieved by RP.

The behavior observed in both directions highlights key differences between the as-built and strengthened configurations. In the Y direction, the as-built building exhibited early collapse due to failure in the vertical panels on the ground floor. Strengthening interventions significantly improved the response, with FRCM providing a better balance between strength and ductility. In the X direction, the as-built configuration showed lower load-bearing capacity due to reduced lateral stiffness and the complex geometry of the structure. The strengthening interventions, particularly with FRCM, resulted in more pronounced improvements in the X direction, drastically enhancing both load-bearing capacity and deformation capacity.

In conclusion, the interventions were appropriately focused on the ground floor, the critical failure zone of the structure. Among the techniques analyzed, FRCM

proved to be the most effective intervention, achieving superior results in both load-bearing capacity and ductility, thereby reducing the risk of sudden collapse. Compared to RP, FRCM provides better performance due to its combination of tensile strength and flexibility. This study underscores the importance of targeted interventions like FRCM in improving the safety of historical masonry buildings.

Table 5.3 – Difference in peak displacement and peak shear between strengthened and as-built buildings for Y direction

Divertion	Fanas mustis	Cono	V _{b,peak}	δc,peak	Δd_{peak}	ΔV_{peak}
Direction	Force profile	Case	[kN]	[kN]	[%]	[%]
		As-built	3336.27	0.0303	-	-
	1st mode	RP	3707.06	0.0194	36	11
Y +		FRCM	6535.60	0.0514	70	96
1 +		As-built	4097.46	0.0143	-	-
	masses	RP	5568.43	0.0153	7	36
		FRCM	7147.98	0.0327	129	74
		As-built	2682.30	-0.0286	-	-
	1st mode	RP	4145.09	-0.0316	11	55
Y -		FRCM	5078.75	-0.0490	71	89
		As-built	2682.30	-0.0286	-	-
	masses	RP	4145.09	-0.0316	38	54
		FRCM	5078.75	-0.0490	66	96

Table 5.4 – Difference in peak displacement and peak shear between strengthened and as-built buildings for X direction

Direction	Eanna mustila	Cono	V _{b,peak}	δc,peak	Δd_{peak}	ΔV_{peak}
Direction	Force profile	Case	[kN]	[kN]	[%]	[%]
		As-built	3151.40	0.0276	-	-
	1st mode	RP	5903.97	0.0306	11	87
X+		FRCM	4953.71	0.0490	78	57
Λ $+$		As-built	3814.57	0.0296	-	-
	masses	RP	6104.69	0.0143	52	60
		FRCM	9874.24	0.0490	66	159
		As-built	2332.65	-0.0296	-	-
	1st mode	RP	4464.14	-0.0245	17	91
X -		FRCM	7916.14	-0.0469	59	239
		As-built	3814.57	-0.0296	-	-
	masses	RP	6495.08	-0.0112	62	70
		FRCM	8920.70	-0.0490	66	134

Subsequently the ζ_E coefficient was calculated for the analysed cases. This coefficient is a measure of the safety level against seismic actions, defined by the Italian Building Code (IMIT 2019) as the ratio between the maximum seismic action the structure can withstand and the maximum seismic action considered in the design of a new building on the same site and with the same characteristics (except for specific cases, $\zeta_E = PGA_c / PGA_d$).

If this ratio exceeds 1, the verification is satisfied. When the assessed structure shows an insufficient value of ζ_E , it becomes necessary to define the type of intervention to be carried out, taking into account various factors.

For masonry structures, the initial interventions include:

- Repair or remediation of defects, aimed at eliminating construction deficiencies:
- Local interventions, focused on resolving structural detailing deficiencies in undamaged constructions, without altering the global structural behavior.

These interventions are non-systematic and limited, ensuring reduced costs and minimal impact on the equilibrium configuration the structure has reached over its lifespan. If required, the focus shifts to structural improvement, which aims to enhance the safety level of the construction. This category includes interventions that modify the global or local structural behavior.

The ζ_E parameter can be less than 1. To achieve an adequate safety level, the Code specifies:

- For Class III buildings used as schools and Class IV (critical in an emergency) buildings:
 ζ_E ≥ 0.6;
- For other Class III (large gathering) and Class II (normal gathering) buildings: an increase of at least 0.1 in ζ_E compared to the as-built value.

If the objective is to achieve the safety level required for a new building ($\zeta_E = 1$), seismic retrofitting is necessary. However, to limit costs, retrofitting is considered achieved when 80% of the required safety level is reached ($\zeta_E \ge 0.8$) in the following cases:

- Vertical load increases exceeding 10% at the foundation level due to changes in building class or intended use;
- Voluntary retrofitting carried out by the owner due to insufficient safety levels, excluding cases such as raised sections, floor expansions, or significant structural transformations (§8.3 of the Italian Building Code (IMIT 2019)).

To calculate ζ_E , it is necessary to determine the maximum seismic action the structure can sustain (PGA_c), based on displacement capacity and demand.

The capacity represents the structural performance at each limit state, evaluated through experimental data or Code provisions.

For each limit state:

- Operational: 70% of the maximum base shear;
- Damage limitation: Maximum base shear;
- Life safety: 80% of the maximum base shear on the softening branch;
- Collapse prevention: 50% of the maximum base shear on the softening branch.

The demand depends on the structural non-linear behavior and is calculated using the N2 Method. This method transforms a MDOF system into an equivalent SDOF system using the fundamental mode participation factor (Γ_1). The capacity curve is scaled to derive a simplified model.

1. Scaling the curves:

$$\delta^* = \frac{\delta_c}{\Gamma_1} \tag{19}$$

$$V^* = \frac{V_b}{\Gamma_1} \tag{20}$$

2. Bilinear approximation:

Secant stiffness as the ratio between 70% of the maximum base shear and the corresponding displacement;

Ultimate displacement corresponding to a 20% reduction in the maximum base shear;

Ultimate shear determined by equalizing the areas under the bilinear and scaled capacity curves.

3. Initial period calculation:

$$T^* = 2\pi \cdot \sqrt{\frac{m_e^*}{k_e^*}} \tag{21}$$

4. Demand determination:

$$S_{D,e}^{*}(T^{*}) = \frac{S_{ae}^{*}(T^{*})}{\omega^{*2}} = S_{ae}^{*}(T^{*}) \cdot \left(\frac{T^{*}}{2\pi}\right)^{2}$$
(22)

• For $T^* \ge T$ C: elastic demand

$$d_{\max}^* = d_{e,\max}^* = S_{D,e}(T^*)$$
 (23)

• For $T^* \le T_C$: increased demand using the ductility factor (q^*)

$$d_{\text{max}}^* = \frac{d_{e,\text{max}}^*}{q^*} \left[1 + (q^* - 1) \frac{T_C}{T^*} \right]$$
 (24)

In equation (24) q* is:

$$q^* = \frac{S_e(T^*)}{F_v^*} \cdot m^* \tag{25}$$

If $q^* \le 1 \rightarrow d^*_{max} = d^*_{e,max}$

5. Calculation of PGA_c

The displacement capacity and demand are equated to determine PGA_c, considering the period T* and the seismic response spectrum.

For the analyzed cases, with $T_C \le T^* \le T_D$, the following relation is used:

$$S_{e}(T^{*}) = a_{g} \cdot S \cdot F_{o} \cdot \frac{T_{C}}{T^{*}}$$
(26)

From this (26), the maximum acceleration sustained by the structure is derived and compared to the PGA of the site to calculate ζ_E .

This value enables the assessment of the safety level and the planning of necessary interventions.

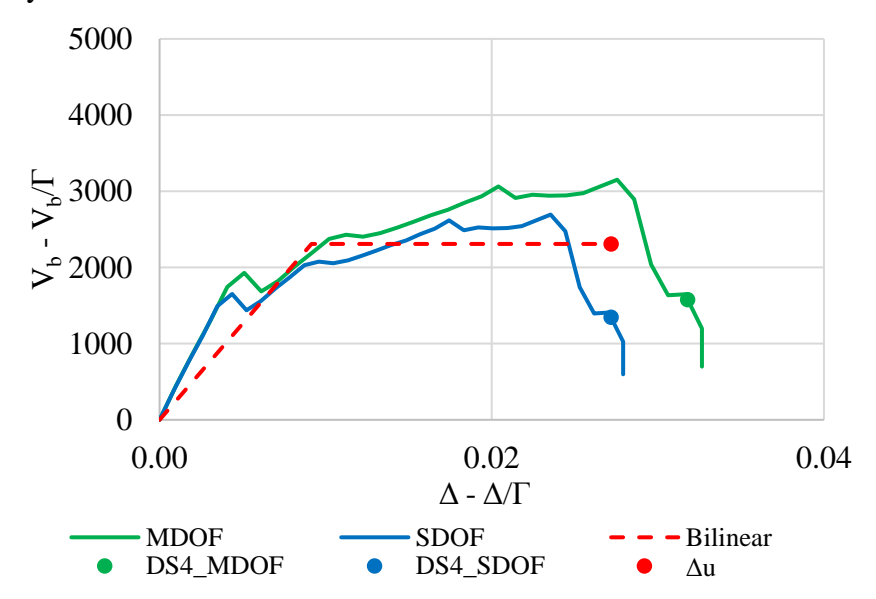


Figure 5.14 – MDOF, SDOF and bilinear curve for proportional analysis of the first mode of vibration

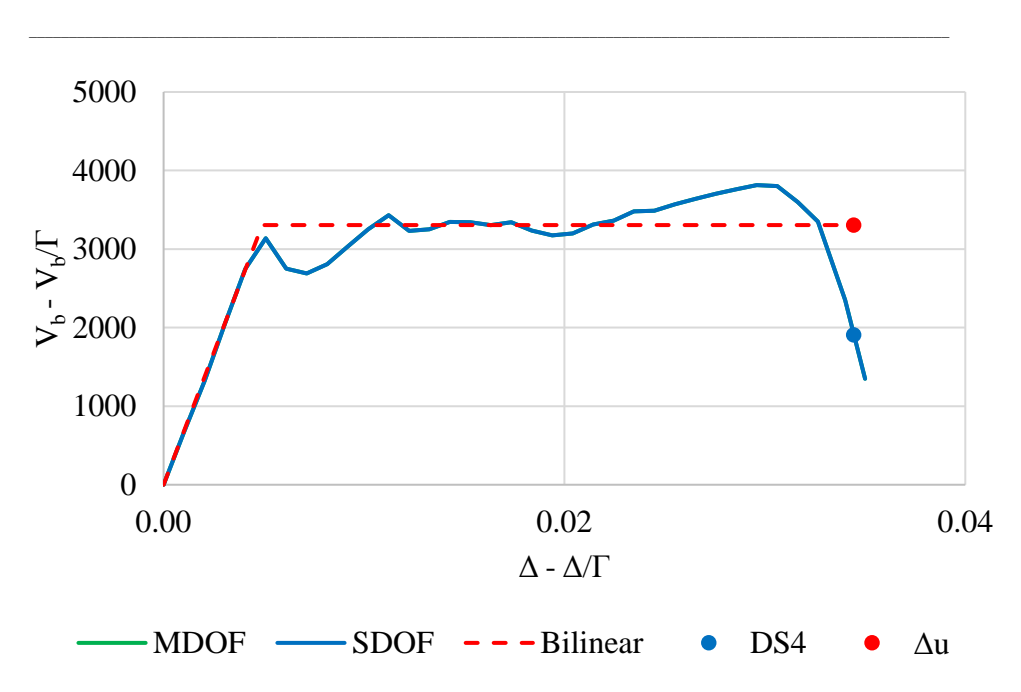


Figure 5.15 – MDOF, SDOF and bilinear curve for mass-proportional analysis

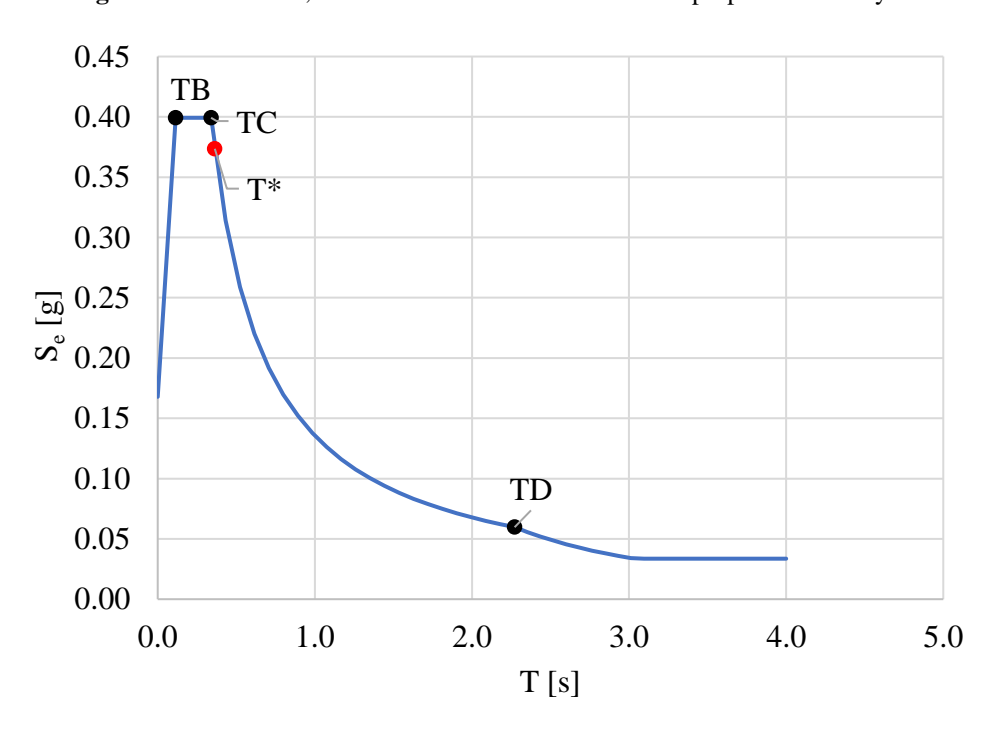


Figure 5.16 – Response spectrum of the site under examination

The analysis of the ratios between the capacity displacement ($\delta_{\rm C}$) and the demand displacement (δ_D) provides valuable insights into the structure's ability to meet seismic safety requirements in relation to its ductility. These values were

calculated for the as-built configuration, RP, and FRCM in the X direction (X+ and X-), considering both mass-proportional and modal force profiles (Figure

5.17 and Table 5.5).

For the as-built configuration in the X+ direction, the ratio for both force profiles is below 1. Specifically, for the mass-proportional profile, the ratio is 0.79, indicating that the capacity displacement is lower than the seismic demand, leaving the structure vulnerable to collapse. For the modal profile, the ratio slightly improves to 0.98, almost satisfying the demand but still insufficient to ensure structural safety. With strengthening using RP, the ratio increases to 1.04, exceeding the demand and demonstrating that RP provides sufficient capacity to resist the expected earthquake. This improvement is even greater with the modal profile, where the ratio reaches 1.44, indicating a significant enhancement over the as-built configuration, with greater ability to withstand higher seismic forces. With strengthening using FRCM, the ratio reaches 2.27 for the mass-proportional profile, demonstrating a capacity more than double the demand, with an extremely safe and ductile response. Similarly, with the modal profile, the ratio is 2.25, confirming that FRCM is the most effective intervention for improving both strength and ductility.

For the X- direction, the as-built configuration with the mass-proportional profile shows a ratio of 0.74, similar to the X+ direction and insufficient to meet the seismic demand. With the modal profile, the ratio improves to 1.06, indicating that in this configuration, the as-built state barely satisfies the seismic demand. With RP, the ratio for the mass-proportional profile increases to 1.07, providing adequate capacity to meet the seismic demand. For the modal profile, the ratio reaches 1.48, similar to the X+ direction, confirming a significant improvement in structural capacity.

Finally, with FRCM, the ratio increases to 2.26 for the mass-proportional profile, demonstrating excellent capacity to resist seismic actions with a highly ductile response. For the modal profile, the ratio reaches 1.78, highlighting that even for the more demanding profile, FRCM offers superior performance compared to both RP and the as-built configuration.

The as-built configuration exhibits evident vulnerabilities in both directions (X+ and X-), with ratios below 1 in most cases, particularly for the massproportional profile. RP significantly improves safety, bringing the ratios above 1 in all cases. However, the improvement in ductility is limited, and the post-elastic behavior remains less effective compared to FRCM. FRCM emerges as the most effective solution, with ratios that exceed 2 for the mass-proportional profile and reach high values even for the modal profile. This indicates greater ductility, strength, and energy dissipation capacity compared to the other interventions.

In conclusion, RP is a valid option for improving structural safety, but FRCM stands out for its ability to provide superior overall performance, making the building significantly more resilient to seismic actions.

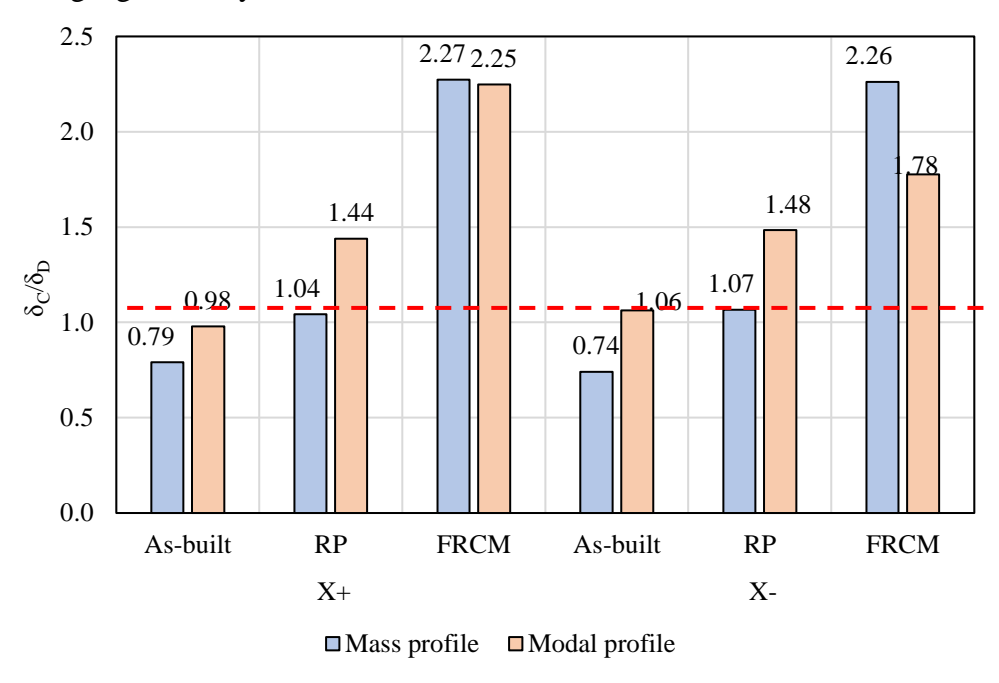


Figure 5.17 – Comparison of capacity / demand ratios for the X-direction, force profile proportional to the first mode and masses

The same analysis was conducted for the Y direction (Figure 5.18 and Table 5.6). For the Y+ direction, in the as-built configuration with the mass-proportional profile, the ratio is 0.68, indicating insufficient capacity to meet seismic demand. With the modal profile, the ratio improves slightly to 0.96, almost meeting the seismic demand but still falling short of the safety threshold. When RP is applied, the ratio increases to 1.10, exceeding the demand and providing sufficient capacity to resist the expected earthquake.

Table 5.5 – Relationships between capacity and demand in terms of displacement for the X direction

Case	Mass profile			Modal profile		
	$\delta_{\rm C}$	δ_{D}	δ_C/δ_D	$\delta_{\rm C}$	δ_{D}	$\delta_{C}\!/\delta_{D}$
As-built	0.019	0.024	0.79	0.023	0.024	0.98
RP	0.015	0.014	1.04	0.026	0.018	1.44
FRCM	0.050	0.022	2.27	0.043	0.019	2.25
As-built	0.020	0.027	0.74	0.028	0.026	1.06
RP	0.016	0.015	1.07	0.033	0.022	1.48
FRCM	0.052	0.023	2.26	0.044	0.025	1.78
	As-built RP FRCM As-built RP	Case δc As-built 0.019 RP 0.015 FRCM 0.050 As-built 0.020 RP 0.016	Case δc δb As-built 0.019 0.024 RP 0.015 0.014 FRCM 0.050 0.022 As-built 0.020 0.027 RP 0.016 0.015	Case δc δD δc/δD As-built 0.019 0.024 0.79 RP 0.015 0.014 1.04 FRCM 0.050 0.022 2.27 As-built 0.020 0.027 0.74 RP 0.016 0.015 1.07	Case δc δD δc/δD δc As-built 0.019 0.024 0.79 0.023 RP 0.015 0.014 1.04 0.026 FRCM 0.050 0.022 2.27 0.043 As-built 0.020 0.027 0.74 0.028 RP 0.016 0.015 1.07 0.033	Case δc δD δc/δD δc δD As-built 0.019 0.024 0.79 0.023 0.024 RP 0.015 0.014 1.04 0.026 0.018 FRCM 0.050 0.022 2.27 0.043 0.019 As-built 0.020 0.027 0.74 0.028 0.026 RP 0.016 0.015 1.07 0.033 0.022

For the modal profile, the ratio further increases to 1.55, demonstrating a significant improvement over the as-built configuration and greater capacity to withstand higher seismic forces. With the FRCM, the ratio reaches 2.38, showing a capacity more than double the demand, ensuring extremely safe and ductile behavior. For the modal profile, the ratio rises even further to 2.48, confirming that the FRCM is the most effective intervention for improving both strength and ductility.

For the Y- direction, in the as-built configuration, the ratio remains below unity for both the mass-proportional profile (0.72) and the modal profile (0.70), indicating that the capacity displacement is insufficient to meet seismic demand and highlighting significant vulnerability in this configuration for the Y-direction. When RP is applied, the ratio increases to 1.55, providing adequate capacity to satisfy seismic demand. However, for the modal profile, the ratio is 1.08, just enough to meet the demand, though still representing a notable improvement over the as-built configuration. With the FRCM, the ratios reach 2.38 and 1.94, demonstrating excellent capacity to resist seismic actions, with highly ductile behavior and superior performance compared to both RP and the as-built configuration.

As highlighted in the X direction, the RP intervention also proves to be a valid solution for improving structural safety in the Y direction. However, the FRCM stands out for its ability to ensure superior global performance. This makes the building significantly more resilient to seismic actions, both in terms of strength

and ductility, offering performance far superior to the as-built configuration and the RP intervention.

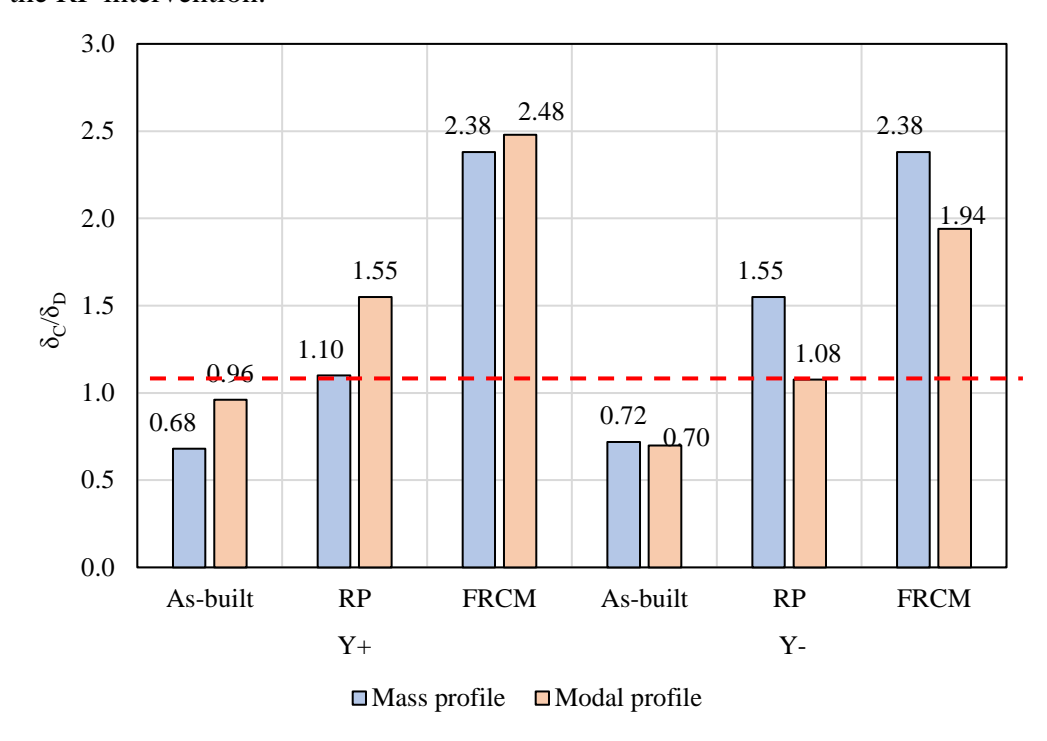


Figure 5.18 – Comparison of capacity and demand ratios for the Y-direction, force profile proportional to the first mode and masses

Table 5.6 – Relationships between capacity and demand in terms of displacement for the Y direction

DS4	Case	Mass profile			Modal profile		
		$\delta_{\rm C}$	δ_{D}	$\delta_{C}\!/\delta_{D}$	$\delta_{\rm C}$	δ_{D}	$\delta_{C}\!/\delta_{D}$
	As-built	0.017	0.025	0.68	0.024	0.025	0.96
Y+	RP	0.015	0.014	1.10	0.028	0.018	1.55
	FRCM	0.050	0.021	2.38	0.047	0.019	2.48
Y-	As-built	0.019	0.027	0.72	0.019	0.027	0.70
	RP	0.022	0.014	1.55	0.027	0.025	1.08
	FRCM	0.050	0.021	2.38	0.043	0.022	1.94

The ζ_E ratio was subsequently calculated as the ratio between the maximum peak ground acceleration (PGA) that the structure can withstand (PGA_c) and the PGA expected for the reference site (PGA_d). In this study, the PGA of demand was set at 0.168 g, a value determined based on the seismic characteristics of the site under consideration. The PGA of capacity (PGA_c) was calculated using the results of the nonlinear static analyses conducted for the as-built configuration, the configuration with RP, and the one with FRCM. This calculation was based on the capacity curves obtained while taking into account the mechanical properties of the structure and the characteristics of the site where the building is located. All calculations were carried out for the Life-safety limit state, corresponding to a DS4 damage state.

The ζ_E ratio, obtained by dividing the capacity PGA by the demand PGA, serves as a clear and concise indicator for comparing the structural capacity against the seismic demand level.

The results show that the as-built condition generally shows insufficient safety levels compared to the requirements for a new construction, with $\zeta_E < 1$ in most directions. Exceptions include the Y- direction, where $\zeta_E = 1.24$ for the mass profile, and the X- direction, where $\zeta_E = 1.00$. However, the modal profile underperforms in some cases, such as $\zeta_E = 0.74$ for X-. These results highlight the necessity of implementing strengthening measures.

The Reinforced Plaster (RP) interventions demonstrate a significant improvement in seismic safety, increasing ζ_E well above 1 in all directions, with values ranging from 1.05 to 2.00. This indicates that RP interventions are effective in meeting the minimum requirements for new constructions, providing an acceptable safety level.

The FRCM (Fibre-Reinforced Cementitious Matrix) interventions stand out for their exceptional performance, with ζ_E values consistently exceeding 2 and even reaching 3.18 in the Y- direction. This type of intervention proves to be the most effective, significantly enhancing the seismic capacity of the structure across all directions.

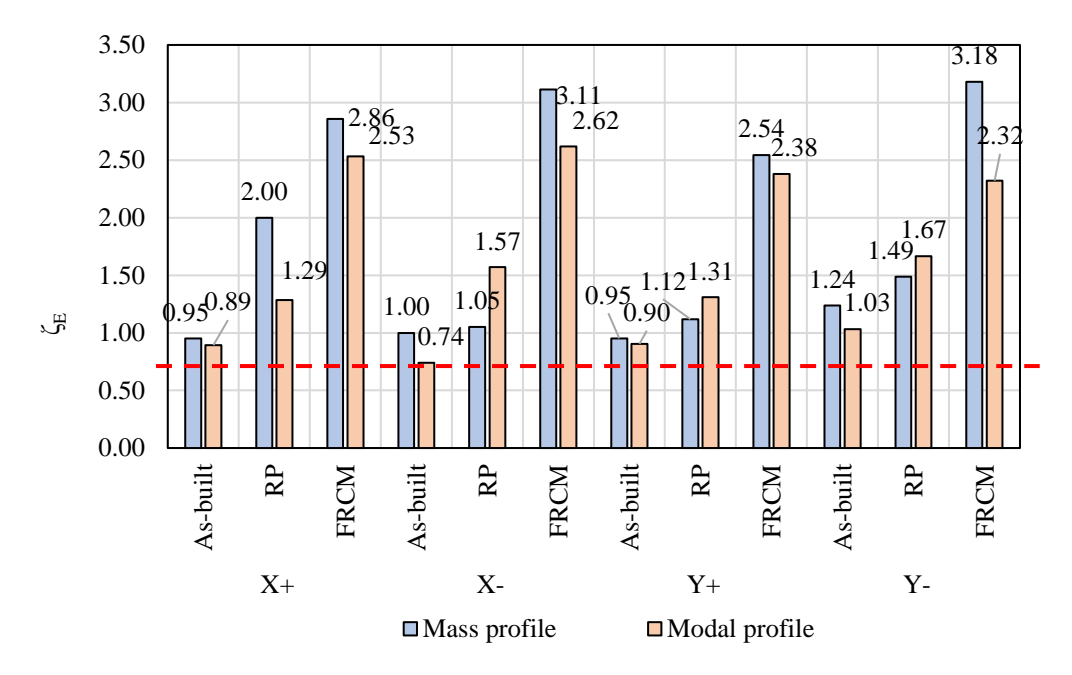


Figure 5. 19 – Comparison of ζ_E values with the application of strengthening

Table 5.7 – Values of ζ_E for the X direction and Y direction

DS4	C	Mass profile			Modal profile		
	Case	PGA c	PGA _d	$\zeta_{ m E}$	PGA _c	PGA _d	$\zeta_{ m E}$
	As-built	0.160		0.95	0.152		0.90
Y+	RP	0.188		1.12	0.220		1.31
	FRCM	0.427		2.54	0.400		2.38
	As-built	0.208		1.24	0.174		1.03
Y-	RP	0.250		1.49	0.280		1.67
	FRCM	0.534	0.168	3.18	0.390	0.168	2.32
	As-built	0.160	0.106	0.95	0.150		0.89
X+	RP	0.336		2.00	0.216		1.29
	FRCM	0.480		2.86	0.425		2.53
	As-built	0.168		1.00	0.124		0.74
X-	RP	0.177		1.05	0.264		1.57
	FRCM	0.523		3.11	0.440		2.62

In summary, while the as-built condition reveals several structural deficiencies, the RP interventions offer substantial and sufficient improvements to comply with the code requirements. FRCM interventions, on the other hand, deliver outstanding safety levels, achieving seismic capacities far beyond the minimum threshold, making them the optimal solution for maximizing structural safety.

CHAPTER 6 – CONCLUSION AND POTENTIAL FUTURE DEVELOPMENTS

The study presented in this dissertation has addressed the seismic vulnerability assessment and risk mitigation of historical masonry buildings through a multiscale methodology. By integrating advanced modeling techniques with sustainable intervention strategies, this research provides a comprehensive framework for safeguarding historical structures while enhancing their resilience to earthquakes. The following conclusions can be drawn:

- Proposed methodology: The multi-scale methodology developed in this study allows for a detailed evaluation of seismic vulnerability at various scales from territorial to site-specific scale, in this latter case encompassing both the overall structural system and individual components. This approach is particularly effective in capturing the complex behavior of masonry structures under both in-plane and out-of-plane actions, enabling the identification of failure mechanisms and critical vulnerability sources. A novel aspect of this methodology is the integration of both in-plane and out-of-plane failure mechanisms into unified fragility curves, using nonlinear static and kinematic analysis of different structural models (i.e., macro-element and rigid-multi-body models). The analysis produced then ensures a comprehensive understanding of the seismic response of historical masonry buildings, accounting for the interactions between different types of structural failures.
- Regional-scale results: The regional-scale analysis presented in Chapter 4 enabled the development of combined fragility curves for in-plane and out-of-plane failure mechanisms, providing an accurate assessment of the seismic vulnerability of historical buildings in Campania. The use of the CARTIS database highlighted the importance of accounting for the typological diversity of masonry for reliable evaluations. The results demonstrate that reinforcement interventions, including innovative techniques such as FRCM, can significantly enhance structural resilience,

offering essential tools for planning risk mitigation strategies at the territorial level.

- Application to a real case-study building: The application of the methodology to a representative building in Portici (province of Naples) demonstrated its practicality and effectiveness. Nonlinear static analyses highlighted the building's critical weaknesses in the as-built condition, particularly at the ground floor level, where the onset of soft-story mechanisms was observed. These results underscore the importance of targeted interventions.
- Effectiveness of strengthening techniques: The integration of territorial and single-building scales has demonstrated significant effectiveness in assessing seismic vulnerability and planning targeted interventions. At the territorial scale, the use of the IRMA platform highlighted substantial reductions in human and economic losses with the application of strengthening techniques. For instance, the adoption of Fiber Reinforced Cementitious Matrix (FRCM) systems reduced human casualties by approximately 84% and the injured by 83%, compared to the as-built condition, significantly improving the safety of masonry buildings in high-risk seismic zones. Economic losses were similarly reduced, with FRCM interventions achieving a 52% reduction compared to the as-built configuration, outperforming traditional RP, which achieved a 35% reducing, the analysis of a representative case study in Portici demonstrated how structural strengthening increased the ratio between the Peak Ground Acceleration (PGA) of capacity and the PGA of demand (ζ_E) . For the as-built configuration, ζ_E values remained below 1 (e.g., 0.89) in the X+ direction for first mode profiles), indicating insufficient safety. Strengthening with RP improved ζ_E to values above 1 (e.g., 1.29 in the same direction), while FRCM interventions achieved superior results, with ζ_E exceeding 2 in several cases, highlighting exceptional seismic resilience. These results confirm the complementarity of the two scales: the regional-level analysis identifies priority areas and typologies for while interventions, single-building assessments validate the effectiveness of proposed solutions, such as FRCM, in enhancing structural safety and reducing seismic risks.

Building upon the findings of this research, several avenues for future exploration are proposed:

- Integration of advanced materials: Further investigation into the application of innovative materials, such as textile-reinforced mortars or bio-based composites, could enhance the effectiveness and sustainability of strengthening techniques. Comparative studies between these materials and traditional solutions would provide valuable insights for selecting optimal interventions.
- Refinement of reinforcement modeling: A future development of this research could involve refining the modeling of reinforced plaster (RP) by replacing the amplification factors (1.5) suggested by the guidelines with experimentally derived values obtained from laboratory tests. This approach would allow for a more accurate representation of the material's actual mechanical behavior, leading to improved reliability in numerical simulations and structural assessments.
- Case studies: Expanding the application of the proposed methodology to a wider range of case studies across different regions and typologies would help refining the approach and validating its general applicability. This would also allow for creation of a robust database of fragility curves tailored to multiple building types.
- Soil-structure interaction: Investigating the influence of soil-structure interaction on the seismic response of historical masonry buildings could provide deeper insights into the role of foundation conditions. This is particularly relevant for buildings situated in areas with complex geotechnical profiles.
- *Post-intervention monitoring*: Implementing long-term monitoring systems for retrofitted buildings would provide valuable data on the performance of strengthening techniques over time. This would enable the validation and refinement of current methodologies based on real-world performance.

In conclusion, this research represents a significant step forward in the seismic assessment and retrofitting of historical masonry buildings. By addressing both theoretical and practical aspects, this study lays a solid foundation for future studies aimed at enhancing the resilience of cultural heritage structures in seismically active regions.

BIBLIOGRAPHY

- Angelillo M., Fortunato A., Gesualdo A., Iannuzzo A., Zuccaro G. (2018). Rigid Block Models for Masonry Structures. International Journal of Masonry Research and Innovation, 3, 349. DOI: 10.1504/IJMRI.2018.095701
- ATC. Earthquake damage evaluation data for California (ATC-13). Redwood City (California): Appl. Technology Council; 1985
- Augenti N., Parisi F. (2010). Constitutive Models for Tuff Masonry under Uniaxial Compression. Journal of Materials in Civil Engineering, 22(11). DOI: 10.1061/(asce)mt.1943-5533.0000119.
- Balsamo A., Prota A., Iovinella I., Morandini G. (2011). Comportamento sperimentale di muratura di tufo rinforzata con FRG a base di ecopozzolana.
- Basaglia A., Cianchino G., Cocco G., Rapone D., Terrenzi M., Spacone E., Brando G. (2021) An automatic procedure for deriving building portfolios using the Italian "CARTIS" online database. Structures 34 pp 2974-2986
- Biglari M., Formisano A. (2020) Damage Probability Matrices and Empirical Fragility Curves From Damage Data on Masonry Buildings After Sarpolezahab and Bam Earthquakes of Iran. Front Built Environ;6.
- Binda (2005). Methodologies for the vulnerability analysis of historic centres in Italy. WIT Vol. 83, Pages 279 9th International Conference on Structural Studies, Repairs and Maintenance of Heritage Architecture, STREMAH 2005
- Bisol G.D., Prajapti S., Sorrentino L. and AlShawa O. (2023). Vertical spanning wall elastically restrained at the top: validation and parametric dynamic analysis. Bulletin of Earthquake Engineering (2024) 22:3951–3978
- Block P, Ciblac T, Ochsendorf J (2006) Real-time limit analysis of vaulted masonry buildings. Comput Struct 84(29–30):1841–1852
- Borzi B., Faravelli M., Onida M., Polli D., Quaroni D., Pagano M., Di Meo A. (2018) Piattaforma IRMA (Italian Risk MAps). GNGTS, pp 382–388.
- Borzi B., Onida M., Faravelli M., Polli D., Pagano M., Quaroni D., Cantoni A. (2020) IRMA platform for the calculation of damages and risks of residential buildings, Bulletin of Earthquake Engineering 19:3033–3055.
- Braga F., Dolce M., Liberatore D. (1982) Southern Italy November 23, 1980, Earthquake: a statistical study of damaged buildings and a ensuring review of the M.S.K.-76 Scale. CNR-PFG n.503. Roma

- Brando G., Cianchino G., Rapone D., Spacone E., Biondi S. (2021) A CARTIS-based method for the rapid seismic vulnerability assessment of minor Italian historical centres. International Journal of Disaster Risk Reduction 63 102478
- Breymann G. A. (1926)Trattato generale di costruzioni civili con cenni speciali intorno alle costruzioni grandiose, Milano, Vallardi, Vol. I: Warth, Otto, Costruzioni in pietra e strutture murali
- Calvi G.M., Pinho R., Magenes G., Bommer J.J., Resrepo-Velez L.F., Crowley H. (2006) Development of seismic vulnerability assessment methodologies over the past 30 years. ISET Journal of Earthquake Technology No. 472, Vol. 43, No. 3 pp. 75-104
- Casapulla C. (1999). Resistenze Attritive in una Parete Muraria Soggetta ad Azioni Normali al suo Piano Medio, L'Ingegneria Sismica in Italia, Atti IX convegno Nazionale ANIDIS, Torino.
- Cattari S. Lagomarsino S. and Resemini S. (2008). Modeling of vaults as equivalent diaphragms in 3D seismic analysis of masonry buildings, 1st edition, pg. 8, ISBN 9780429151965
- CEN, 2005. EN 1996-1-1: Eurocode 6-Design of masonry structures-Part 1-2: General rules-Structural fire design, BrusselsD'Altri, A.M., Sarhosis, V., Milani, G. et al. (2020). Modeling Strategies for the Computational Analysis of Unreinforced Masonry Structures: Review and Classification. Arch Computat Methods Eng 27, 1153–1185 https://doi.org/10.1007/s11831-019-09351-x.
- Chiozzi A, Grillanda N, Milani G, Tralli A (2018) UB-ALMANAC: an adaptive limit analysis NURBS-based program for the automatic assessment of partial failure mechanisms in masonry churches. Eng Fail Anal 85:201–220
- Chiozzi A, Milani G, Tralli A (2017) A genetic algorithm NURBS-based new approach for fast kinematic limit analysis of masonry vaults. Comput Struct 182:187–204
- Como M., Iori I., & Ottoni F. (2019). Scientia abscondita. Arte e scienza del costruire nelle architetture del passato. Venezia: Marsilio
- D'Ayala D. (2005). Force and Displacement Based Vulnerability Assessment for Traditional Buildings. Bulletin of Earthquake Engineering, 3(3), 235-265.
- D'Ayala D., & Paganoni S. (2011). Assessment and Analysis of Damage in L'Aquila Historic City Centre after 6th April 2009. Bulletin of Earthquake Engineering, 9(1), 81-104.

- D'Ayala D., & Speranza E. (2003). Definition of Collapse Mechanisms and Seismic Vulnerability of Historic Masonry Buildings. Earthquake Spectra, 19(3), 479-509.
- D'Ayala, D. (1999). Correlation of seismic damage between classes of buildings: churches and houses. In A. Bernardini (Ed.), Seismic damage to masonry buildings: proceedings of the International Workshop on Measures of Seismic Damage to Masonry Buildings (pp. 41-58). Taylor and Francis.
- De Felice G. (1999). Le strutture murarie: dall'osservazione alla previsione del danno sismico. In: Codice di Pratica per la Sicurezza e la Conservazione del Centro Storico di Palermo, (A cura di A. Giuffrè e C. Carocci) Ed. Laterza, 1st ed., Roma-Bari, pp. 99-120.
- De Martino G, Di Ludovico M, Prota A, Moroni C, Manfredi G, Dolce M. (2018) Estimation of repair costs for RC and masonry residential buildings based on damage data collected by post-earthquake visual inspection. Bulletin of Earthquake Engineering; 15(4): 1681–706
- Del Gaudio C., De Martino G., Di Ludovico M., Manfredi G., Prota A., Ricci P., et al. (2017) Empirical fragility curves for masonry buildings after the 2009 L'Aquila, Italy, earthquake. Bulletin Earthquake Engineering; 17:6301–30
- Di Carlo F., & Coccia S. (2020). Collapse state of elliptical masonry arches after finite displacements of the supports. Engineering Failure Analysis, vol. 114, 104593, ISSN 1350-6307.
- Di Pasquale S. (1996). L'arte del costruire. Tra conoscenza e scienza. Venezia: Marsilio.
- Dolce M., Kappos A., Mase A., Penelis G., Vona M. (2006) Vulnerability assessment and earthquake damage scenarios of the building stock of Potenza (Southern Italy) using Itlian and Greek methodologies. Engineering Structures 28 pp. 357-371
- Dolce M., Speranza E., Giordano F., Borzi B., Bocchi F., Conte C., Di Meo A., Faravelli M., Pascale V. (2017) Da.D.O. A web-based tool for analyzing and comparing post-earthquake damage database relevant to national seismic events since 1976. In: Proceedings of the 17th Italian Conf on Earthq Eng ANIDIS. Pistoia, Italy
- Dolce M., Speranza E., Giordano F., Borzi B., Bocchi F., Conte C., Di Meo A., Faravelli M., Pascale V. (2019) Observed damage database of past Italian earthquakes: the Da.D.O. WebGIS. Bollettino di Geofisica Teorica ed Applicata Vol. 60, No. 2, oo. 141-164.

- Dolce M.; Masi A.; Goretti A. (1999). Damage to buildings due to 1997 Umbria-Marche earthquake. In Seismic Damage to Masonry Buildings, 1st ed.; Springer: Cham, Switzerland; pp. 71–80.
- Donà M., Carpanese P., Follador V., Sbrogio L., da Porto F. (2020) Mechanics-based fragility curves for Italian residential URM buildings. Bulletin of Earthquake Engineering 19(8): 3099- 127
- EN 1998-1: Eurocode 8 Design of structures for earthquake resistance Part 1: General rules, seismic actions and rules for buildings
- Faella C., Martinelli E., Nigro E., Paciello S., (2004). Tuff masonry walls strengthened with a new kind of cfrp sheet: experimental tests and analysis . 13th world conference on earthquake enfineering, Vancouver, B.C., Canada, Paper n. 923
- Faella C., Martinelli E., Nigro E., Paciello S., (2010) Shear capacity of masonry walls externally strengthened by a cement-based composite material: An experimental campaign. Construction and Building Materials 24 (2010) 84–93
- Faenza L., Michelini A., Crowley H., Borzi B., Faravelli M. (2021) ShakeDaDO: a data collection combining earthquake building damage and ShakeMap parameters for Italy. Artificial Intelligence in Geosciences, Volume 1, 2020, pp 36-51.
- Fajfar P. (2000). A Nonlinear Analysis Method for Performance-Based Seismic Design. Earthquake Spectra, 16(3), 573-592. Earthquake Engineering Research Institute. DOI: 10.1193/1.1586128.
- Fajfar P., Gaspersic P. (1996) The N2 method for the seismic damage analysis of RC buildings. Earthquake Engineering & Structural Dynamics Volume 25, Issue 1 p. 31-46
- FEMA (2009). FEMA P695: Quantification of Building Seismic Performance Factors, Federal Emergency Management Agency, Washington, D.C., USA
- Forte G., Chioccarelli E., De Falco M., Cito P., Santo A., Iervolino I. (2019). Seismic soil classification of Italy based on surface geology and shear-wave velocity measurements, Soil Dynamics and Earthquake Engineering, Vol. 122, p. 79-93, ISSN 0267-7261.
- Gelfi P. (2002). Role of horizontal backfill passive pressure on the stability of masonry vaults. International Journal for Restoration of Buildings and Monuments = Internationale Zeitschrift Für Bauinstandsetzen Und Baudenkmalpflege, 8(6), 573–589.

- Giuffrè A., (1989). Mechanics of Historical Masonry and Strengthening Criteria, XV Regional Seminar of Earthquake Engineering, Ravello, Ed. Kappa, pp. 60-122.
- Giuffrè A., (1999). Sicurezza e conservazione dei Centri Storici, Il caso Ortigia, (A cura di A. Giuffrè) CNR-GNDT, Ed. Laterza, 2nd ed., Bari.
- Heyman J. (1982). The masonry arch. Chichester: Ellis Horwood Series in Engineering Science.
- Hobbs B., Ting M., Gilbert M., (1994). An Analytical Approach for Walls Subjected to Static and Dynamic Out-of-plane Point Loads, Proceedings 10th International Brick/Block Masonry Conference, Calgary, pp. 329-338.
- Huerta S. (2004). Arcos, bóvedas y cupolas: Geometria y equilibrio en el cálculo traditional e estructuras de fábrica, Madrid: Instituto Juan de Herrera.
- ISTAT (2011). 15th Italian national census of population and housing. Italian National Institute of Statistics. http://dati-censimentopopolazione.istat.it/
- Italian Ministry of Infrastructures and Transportation (IMIT), (2019). Circolare 21 gennaio 2019, n. 7 C.S.LL.PP.: Istruzioni per l'applicazione dell'«Aggiornamento delle "Norme tecniche per le costruzioni"» di cui al decreto ministeriale 17 gennaio 2018. Rome.
- Kappos A.J., Panagopoulos G., Panagiotopoulos C., Penelis G. (2006) A hybrid method for the vulnerability assessment of R/C and URM buildings. Bulletin of Earthquake Engineering; 4: 391–413.
- Lagomarsino S., Cattari S., Ottonelli D. (2021) The heuristic vulnerability model: fragility curves for masonry buildings. Bulletin of Earthquake Engineering. 19(8):3129-3163. doi: 10.1007/S10518-021-01063-7.
- Lagomarsino S., Penna A., Galasco A., Cattari S. (2013). TREMURI program: An equivalent frame model for the nonlinear seismic analysis of masonry buildings. Engineering Structures, vol. 56, 1787-1799.
- Legge 1 giugno 1939, n. 1089. "Tutela delle cose d'interesse artistico o storico." Pubblicata nella Gazzetta Ufficiale n. 184 dell'8 agosto 1939.
- Lourenço PB (2002). Computations on historic masonry structures. Progress Struct Eng Mater 4(3):301–319
- Marcari G. (2004). Rinforzo sismico di murature di tufo con materiali fibrorinforzati (PhD thesis). Dottorato di Ricerca in Ingegneria delle Costruzioni, XVII Ciclo, Università degli Studi di Napoli Federico II.
- Marmo F., Rosati L. (2017) Reformulation and extension of the thrust network analysis. Comput Struct 182:104–118

- MATLAB version 9.8.0.1. Natick, Massachusetts: The MathWorks Inc., 2023.
- Milani, G. (1920). L'ossatura murale : studio statico-costruttivo ed estetico-proporzionale degli organismi architettonici, con speciale riferimento alle strutture elastiche nelle loro varie e moderne applicazioni pratiche. Torino: C. Crudo & C.
- Ministero delle Infrastrutture e dei Trasporti. (2019). Circolare 21 gennaio 2019, n. 7 C.S.LL.PP. Istruzioni per l'applicazione dell'«Aggiornamento delle "Norme tecniche per le costruzioni"» di cui al decreto ministeriale 17 gennaio 2018. Gazzetta Ufficiale della Repubblica Italiana, Serie Generale n. 35 dell'11 febbraio 2019 Supplemento Ordinario n. 5.
- National Research Council CNR (2014). Instructions for the assessment of the seismic reliability of existing buildings. CNR-DT 212/2013, Rome.
- Parisi F. and Acconcia E. (2020). Formulation and experimental validation of distributed plasticity macro-element for unreinforced masonry walls. In "Brick and Block Masonry-From Historical to Sustainable Masonry" CRC Press (Ed). Cracow, pp. 152-158.
- Parisi F., Iovinella I., Balsamo A., Augenti N. and Prota A. (2012), In-plane behaviour of tuff masonry strengthened with inorganic matrix-grid composites in diagonal compression. ECCM 2012 Compos. Venice, Proc. 15th Eur. Conf. Compos. Mater. 45, 1657.
- Parisi F., Sabella G., Augenti N. (2016). Constitutive Model Selection for Unreinforced Masonry Cross Sections Based on Best-Fit Analytical Moment-Curvature Diagrams. Engineering Structures, 111, 451-466. Elsevier Ltd. DOI: 10.1016/j.engstruct.2015.12.036.
- Parisi F. & Augenti N. (2013). Seismic capacity of irregular unreinforced masonry walls with openings. Earthquake Engineering and Structural. 42(1):101–121.
- Parisse F., Cattari S., Marques R., et al. (2021). Benchmarking the Seismic Assessment of Unreinforced Masonry Buildings from a Blind Prediction Test. Structures, 31, 982-1005. Elsevier. DOI: 10.1016/J.ISTRUC.2021.01.096.
- Penna A, Lagomarsino S., Galasco A. (2014). A Nonlinear Macroelement Model for the Seismic Analysis of Masonry Buildings. Earthquake Engineering and Structural Dynamics, 43(2), 159-179. John Wiley and Sons Ltd. DOI: 10.1002/EQE.2335.

- Porter K. (2020). A Beginner's Guide to Fragility, Vulnerability, and Risk. University of Colorado Boulder, 136 pp.,
 - https://www.sparisk.com/pubs/Porter-beginners-guide.pdf.
- Portioli F., Cascini L., Landolfo R. (2017). On the Use of Point Contact Models for Collapse Mechanism and Dynamic Analysis of Masonry Structures, 1:(2017), pp. 2470-2477, 6th International Conference on Computational Methods in Structural Dynamics and Earthquake Engineering, COMPDYN 2017.
- Prota A., Marcari G., Fabbrocino G., Manfredi G., Aldea C., (2006). Experimental In-Plane Behavior of Tuff Masonry Strengthened with Cementitious Matrix–Grid Composites. J. Compos. Constr. 10, 1081–1097. https://doi.org/10.1061/(ASCE)1090-0268(2006)10:3(223)
- Riuscetti M., Carniel R. and Cecotti C. (1997). Seismic vulnerability assessment of masonry buildings in a region of moderate seismicity. Annali di geofisica, Vol. XL, n.5.
- Rondelet J., (1827). Traité théorique et pratique de l'Art de bâtir, Paris.
- Rosti A., Rota M., Magenes G., Penna A. (2019) Derivazione di curve di fragilità empiriche per edifici residenziali in muratura. XVII Convegno ANIDIS L'ingegneria sismica in Italia Ascoli Piceno 2019 15-19 Settembre, Italy
- Rosti A., Rota M., Penna A. (2020a) Empirical fragility curves for Italian URM buildings Bulletin of Earthquake Engineering, vol. 19
- Rota M., Penna A., Magenes G. (2010) A methodology for deriving analytical fragility curves for masonry buildings based on stochastic nonlinear analyses. Engineering Structures 32 pp. 1312-1323
- Sorrentino L., Cattari S., da Porto F., Magenes G., Penna A. (2019). Seismic behaviour of ordinary masonry buildings during the 2016 central Italy earthquakes. Bull Earthquake Eng (2019) 17:5583–5607.
- Spacone E., Ciampi V., Filippou F.C. (1996). Mixed Formulation of Nonlinear Beam Finite Element. Computers and Structures, 58(1), 71-83.
- Tocchi G., Polese M., Di Ludovico M., Prota A. (2021) Regional based exposure models to account for local building typologies. Bulletin of Earthquake Engineering
- Turnsek, V., Cacovic, F. (1970). Some Experimental Results on the Strength of Brick Masonry Walls. 2nd International Brick Masonry Conference, Stoke-on-Trent.

- Valluzzi, M.R. (2007). On the vulnerability of historical masonry structures: analysis and mitigation. Mater Struct 40, 723–743.
- Whitman R.V. (1973) Damage probability matrices for prototype buildings. Structures publication, vol 380. MIT, Boston
- Zuccaro G., Dolce M., De Gregorio D., et al. (2015) La scheda CARTIS per la caratterizzazione tipologico-strutturale dei comparti urbani costituiti da edifici ordinari. Valutazione dell'esposizione in analisi di rischio sismico. In: Proceedings of the 34th National Conference of GNGTS. Trieste
- Zucconi M., Ferlito R., Sorrentino L. (2018) Simplified survey form of unreinforced masonry buildings calibrated on data from the 2009 L'Aquila earthquake. Bulletin of Earthquake Engineering. 16:2877–911
- Zucconi M., Sorrentino L. (2022) Census-Based Typological Damage Fragility Curves and Seismic Risk Scenarios for Unreinforced Masonry Buildings. Geosciences, 12, 45.

AUTHOR'S PUBLICATIONS

- Buonocunto V., Acconcia V., Parisi F. (2024). Effect of traditional strengthening interventions on seismic fragility of URM buildings. 18th World Conference on Earthquake Engineering. Milano, Italy.
- Buonocunto V., Parisi F, Serino G., D'Ayala D. (2024). Seismic vulnerability analysis of historic masonry buildings with multi-mode failure modelling. 18th World Conference on Earthquake Engineering. Milano, Italy.
- Parisse F., Buonocunto V. et al. (2024). Harmonization of the predicted post-peak seismic response of URM structures in Finite Element Models. 18th World Conference on Earthquake Engineering. Milano, Italy.
- Acconcia E., Buonocunto V., Parisi F. (2023). Numerical investigation on the flange effect in unreinforced masonry wall system through nonlinear finite element modelling, Proceedings of COMPDYN 2023 -9th International Conference on Computational Methods in Structural Dynamics and Earthquake Engineering, Athens, Greece.
- Buonocunto V., Serino G., Parisi F. (2023). Large-scale vulnerability analysis of historical masonry buildings. Proceedings of COMPDYN 2023 - 9th International Conference on Computational Methods in Structural Dynamics and Earthquake Engineering, Athens, Greece.
- Parisse F., Buonocunto V. et al. (2023) Investigating the seismic response of URM walls with irregular opening layout through different modeling approaches 9th International Conference on Computational Methods in Structural Dynamics and Earthquake Engineering, Athens, Greece.
- Buonocunto V., Acconcia E., Parisi F. (2022). Seismic fragility modelling of unreinforced masonry buildings in Campania region. XIX ANIDIS Conference, Seismic Engineering in Italy. Torino, Italy.
- Acconcia E., Buonocunto V., Parisi F. (2020). Nonlinear static Analysis
 of masonry buildings through fibre-based capacity modelling.
 Proceedings of COMPDYN 2021 8th International Conference on
 Computational Methods in Structural Dynamics and Earthquake
 Engineering, Athens, Greece.

APPENDIX A

Numerical analyses of arches with ARCO program

Table A.1 – Numerical Report of Arch 1

Table 71.1	Arch 1		
Section	σ _e [MPa]	σ _i [MPa]	% comp
1	0.276	0.276	100
2	0.257	0.282	100
3	0.244	0.283	100
4	0.236	0.28	100
5	0.231	0.274	100
6	0.229	0.267	100
7	0.229	0.257	100
8	0.231	0.247	100
9	0.235	0.235	100
10	0.239	0.224	100
11	0.244	0.213	100
12	0.249	0.203	100
13	0.253	0.193	100
14	0.258	0.185	100
15	0.262	0.178	100
16	0.265	0.172	100
17	0.267	0.168	100
18	0.269	0.166	100
19	0.269	0.165	100
20	0.269	0.166	100
21	0.267	0.168	100
22	0.265	0.172	100
23	0.262	0.178	100
24	0.258	0.185	100
25	0.253	0.193	100
26	0.249	0.203	100

max [MPa]		
σ _e [MPa]	0.276	
σ _i [MPa]	0.283	
% comp	100	

e [mm]		
Left 0		
Crown	9.6	
Right	0	

Reactions at the		
Supports		
H ₁ [kN] 52.07		
$H_{\rm r}$ [kN] 52.07		
V_1 [kN] 40.85		
$V_{r}[kN]$ 40.85		

Tie axial	
force [kN]	52.07

27	0.244	0.213	100
28	0.239	0.224	100
29	0.235	0.235	100
30	0.231	0.247	100
31	0.229	0.257	100
32	0.229	0.267	100
33	0.231	0.274	100
34	0.236	0.28	100
35	0.244	0.283	100
36	0.257	0.282	100
37	0.276	0.276	100

Table A.2 – Numerical Report of Arch 2

	•	Arch 2	
Section	σ _e [MPa]	σ _i [Mpa]	% comp
1	0.543	0.543	100
2	0.539	0.532	100
3	0.535	0.522	100
4	0.532	0.513	100
5	0.528	0.505	100
6	0.524	0.498	100
7	0.521	0.492	100
8	0.516	0.487	100
9	0.521	0.483	100
10	0.508	0.481	100
11	0.503	0.479	100
12	0.499	0.478	100
13	0.494	0.477	100
14	0.49	0.477	100
15	0.487	0.477	100
16	0.484	0.477	100
17	0.481	0.477	100
18	0.479	0.478	100
19	0.478	0.478	100
20	0.478	0.478	100
21	0.478	0.478	100
22	0.479	0.478	100

Max [MPa]		
σ	e [MPa]	0.543
σ	i [MPa]	0.543
%	6 comp	100

e [mm]		
Left	0	
Crown	0	
Right	0	

Reactions at the Supports		
H _l [kN]	114.7	
$H_r[kN]$	114.7	
$V_1[kN]$	61.81	
$V_r[kN]$	61.81	

Tie axial	
force [kN]	114.7

23	0.481	0.477	100
24	0.484	0.477	100
25	0.487	0.477	100
26	0.49	0.477	100
27	0.494	0.477	100
28	0.499	0.478	100
29	0.503	0.479	100
30	0.508	0.481	100
31	0.512	0.483	100
32	0.516	0.487	100
33	0.521	0.492	100
34	0.524	0.498	100
35	0.528	0.505	100
36	0.532	0.513	100
37	0.535	0.522	100
38	0.539	0.532	100
39	0.543	0.543	100

APPENDIX B

Fibre element formulation: Finite Element Modeling Approach

The displacement of each end of a beam in the plane can be described, in general, by two translation components and one rotation. The deformation state of the element can therefore be described by six displacement components, collected in the **vector**:

$$\mathbf{s}_{1}^{\mathrm{T}} = \{\mathbf{u}_{1}', \mathbf{v}_{1}', \mathbf{\varphi}_{1}', \mathbf{u}_{2}', \mathbf{v}_{2}', \mathbf{\varphi}_{2}'\} \tag{B.1}$$

By removing the rigid motion, it is possible to describe the deformation state of the element through the rotation of nodes and the corresponding axial displacement between them, Δ . Therefore, in general, only three components are necessary to uniquely describe the deformation state of a beam.

These three components are collected in the vector:

$$\mathbf{s}_{\mathsf{f}}^{\mathsf{T}} = \{ \boldsymbol{\varphi}_{\mathsf{1}}', \boldsymbol{\varphi}_{\mathsf{2}}', \boldsymbol{\Delta} \} \tag{B.2}$$

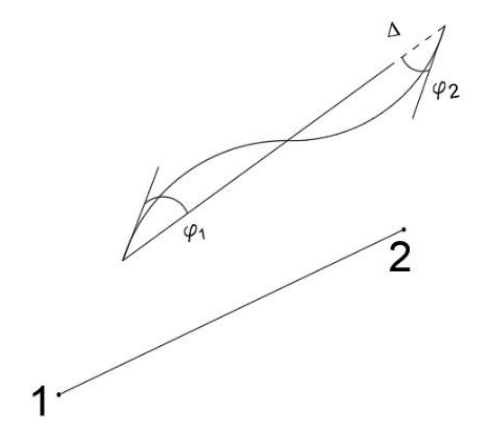


Figure B.1 – Beam elementary displacement

The relationship between the vector s_f and the vector s_l is described by equations below:

$$\varphi_1 = \varphi_1' - \frac{v_2' - v_1'}{l} = \frac{v_1'}{l} + \varphi_1' - \frac{v_2'}{l}$$
(B.3)

$$\phi_2 = \phi_2' - \frac{v_2' - v_1'}{l} = \frac{v_1'}{l} + \phi_2' - \frac{v_2'}{l}$$
(B.4)

$$\Delta_{l} = v_2' - v_1' \tag{B.5}$$

which, in matrix form, becomes:

$$\mathbf{s}_{\mathbf{f}} = \mathbf{T}^{\mathsf{T}} \mathbf{s}_{\mathbf{l}} \tag{B.6}$$

where T^T is the transpose of the transformation matrix.

At each end of the beam, a force, regardless of its orientation, and a couple can be considered as general agents.

$$\mathbf{f}_{l}^{T} = \left\{ \mathbf{F}_{x1}, \mathbf{F}_{y1}, \mathbf{M}_{z1}, \mathbf{F}_{x2}, \mathbf{F}_{y2}, \mathbf{M}_{z2}, \right\}$$
(B.7)

The terms of the vector f_l , together with the actions acting on the beams, are linked by three equilibrium relationships and are therefore dependent on each other. To fully and uniquely define the actions, only three components are sufficient, which constitute the fundamental set of end actions.

$$f_{f} = T^{T} f_{l} = \begin{cases} M_{1} \\ M_{2} \\ N_{1} \end{cases}$$
 (B.8)

The matrix T is the same as the one considered for displacements, and its expression is:

$$T = \begin{bmatrix} 0 & 0 & -1 \\ \frac{1}{l} & \frac{1}{l} & 0 \\ 1 & 0 & 0 \\ 0 & 0 & 1 \\ -\frac{1}{l} & -\frac{1}{l} & 0 \\ 0 & 1 & 0 \end{bmatrix}$$
 (B.9)

where l is the length of the frame element.

It is possible to write the equilibrium relationships:

$$f_f = K_f s_f \tag{B.10}$$

where K_f is the fundamental stiffness matrix of the element, which depends on the applied displacements.

A nonlinear pushover analysis was implemented in MATLAB® using an iterative incremental approach to numerically integrate the moment-curvature response and evaluate shear deformations and rocking-induced displacements. The wall is assumed to be fixed at the base and subjected to a shear force V and an axial load N at the top. The top displacement is determined by integrating curvatures and shear strains along the wall height, with an additional contribution from a pseudo-rigid rotation caused by progressive toe crushing, known as rocking. Following the approach proposed by Parisi (2010), the total relative displacement of the wall can be computed using Equation _:

$$\delta = \delta_F + \delta_S + \delta_r \tag{B.11}$$

where:

$$\delta_F = \int_0^H \varphi^F(x) dx \tag{B.12}$$

$$\delta_{s} = \int_{0}^{H} \gamma^{V}(x) dx \tag{B.13}$$

$$\delta_r = \theta^R H \tag{B.14}$$

and $\varphi^F(x)$ is the curvature at any height x of the wall, $\gamma^V(x)$ is the shear strain, and θ^R is the rocking rotation that is lumped at the base section.

• Flexural behaviour

The proposed approach enables a direct evaluation of flexural behavior by analyzing shear, bending moments, and extensional deformation across the entire macroelement, provided that the displacements, rotations at the end nodes, and the applied normal stress are known. To achieve this, it is first necessary to describe the distribution of elementary deformations along the macroelement. Then, with the constitutive model, it becomes possible to derive the stress state within the element, followed by the shear and normal stresses.

For a rectangular section subjected only to in-plane stress, the axial force can be determined using the following equation based on the stress distribution:

$$N = t \int_{-B/2}^{B/2} \sigma_Z(\varepsilon_Z(y)) dy$$
(B.15)

where:

t is the width of the section, $\sigma_Z(\varepsilon, y)$ represents the constitutive law and $\varepsilon_Z(y) = u + y\varphi_2$, where u is the extensional strain of the barycentric fibre of the section.

The extensional strain can be evaluated through an iterative procedure and consequently the stress diagram can be derived. The bending moment on the end sections will be provided by the equation:

$$M_{y} = t \int_{-B/2}^{B/2} \sigma_{Z}(\varepsilon_{Z}(y)) y \, dy$$
(B.16)

Using fiber discretization for the section, equations above can be approximated as:

$$N = A \sum_{j=1}^{ni} \sum_{i=1}^{ni} \sigma_Z(\varepsilon_Z(y))$$
(B.17)

$$M_{y} = A \sum_{j=1}^{ni} \sum_{i=1}^{ni} \sigma_{Z}(\varepsilon_{Z}(y)) y$$
(B.18)

where A is the area of the section.

Applying this procedure while varying the curvature enables the generation of the moment-curvature diagram for the section under a specified normal force, as described in Parisi and Acconcia (2020)

The bending moment along the macroelement height varies linearly from My(0) to My(H):

$$M_{y}(x) = M_{y}(H) - \frac{M_{y}(H) + M_{y}(0)}{H}$$
(B.19)

with the bending moment known, the curvature distribution along the height can be determined.

Notably, when the curvature in an end section surpasses the value corresponding to the maximum resisting moment, the moment in that section can no longer increase. As curvature further increases, the bending moment gradually decreases according to the post-peak softening branch of the moment-curvature diagram. This causes a reduction in bending moments in the intermediate sections as well, creating a disparity in bending between the base and the upper sections. In the post-peak phase, the major contribution to wall displacement comes from the curvature of the end sections. Figure B.2 illustrates the evolution of moment and curvature profiles along the height of the wall as lateral drift increases. The bending moment rises until $\theta = 0.40\%$, after which it begins to decrease as θ progressively approaches the ultimate value, corresponding to the masonry's ultimate compressive strain and, consequently, the ultimate curvature of the cross sections (toe crushing failure).

The curvature profile remains linear only at low drift levels, specifically up to $\theta = 0.09\%$. As drift increases, the curvature in the sections near the base grows more rapidly than in the upper sections, leading to a concentration of the displacement contribution around the base region

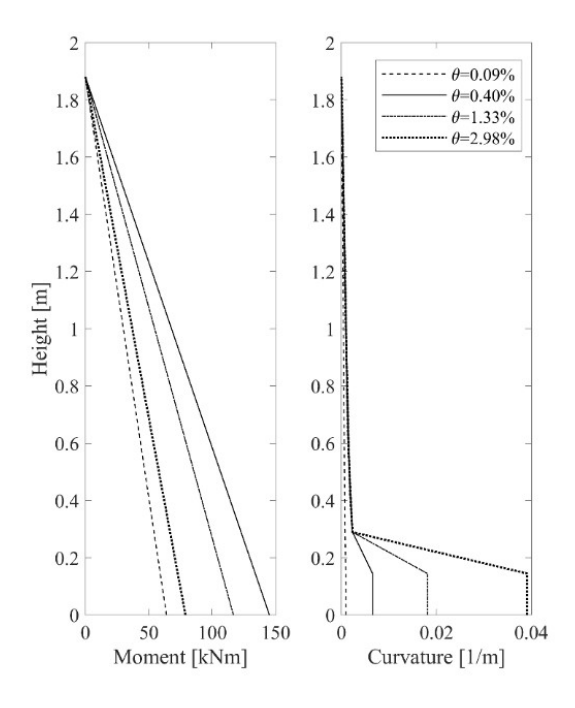


Figure B.2 – Moment and curvature profiles under increasing drift ratio (Parisi and Acconcia 2020)

To determine the rotation of each section along the element height:

$$\delta_2^F = \delta_1^F + \int_0^H \varphi^F(x) \, dx$$
 (B.20)

The integration of curvature along the element height provides the flexural contribution to rotation along the frame:

$$\varphi^F(x) = \varphi_1^F + \int_0^x \varphi(x) dx$$
 (B.21)

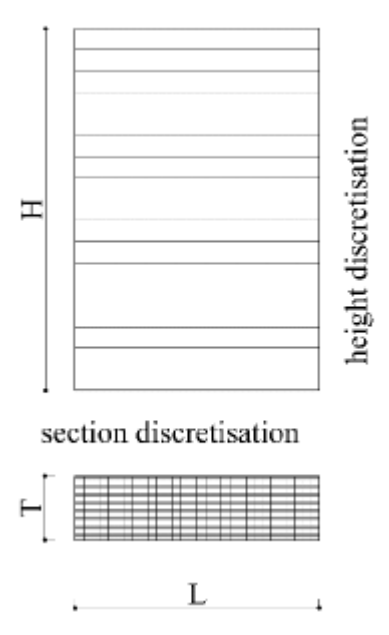


Figure B.3 – Fibres discretisation of the macroelement

The equation provides the flexural contribution to the rotation along the entire frame element obtained by integrating the curvature. The term φ_1^F represents the flexural part of the displacement of node 1.

The displacement of node 2 can be calculated through equation below, by the integration of the rotation along the element's height.

$$\delta_2^F = \delta_1^F + \int_0^H \varphi^F(x) \, dx \tag{B.22}$$

Using fiber discretization, the above equations become:

$$\delta_2^F = \delta_1^F + \int_0^H \varphi^F(x) \, dx$$
 (B.22)

$$\varphi_k^F = \varphi_{k-1}^F + H \frac{\varphi_k}{n} \tag{B.23}$$

$$\delta_n^F = \delta_1^F + H \sum_{k=1}^n \varphi_k^F \tag{B.24}$$

• Shear behaviour

Once the bending moments of the two end nodes are known, the boundary conditions allow for the determination of shear through the equation:

$$V_z = \frac{M_y(0) + M_y(H)}{H}$$
 (B.25)

where H is the height of the macroelement.

To evaluate the shear behavior of the macroelement, it was assumed that the degradation of shear stiffness is proportional to the flexural one, so that the ratio of flexural to shear modulus of elasticity remains constant. The flexural modulus of elasticity is calculated for each fiber in the section as the ratio of the normal stress to the extensional strain:

$$E_{i,j} = \frac{\sigma_{z,(i,j)}}{\varepsilon_{z,(i,j)}} \tag{B.26}$$

where: $\sigma_{z,(i,j)}$ is the normal stress of the fiber (i,j), $\varepsilon_{z,(i,j)}$ is the corresponding axial strain of the generic fibers i and j.

The tangential modulus of elasticity is assumed constant for the entire crosssection with an average value given by:

$$E_{avg} = \sum_{A} \frac{E_{i,j}}{n} \tag{B.27}$$

where n is the number of fibers a.

The proposed capacity model considers that, at each analysis step, the ratio between E_{avg} and the average shear modulus is constant according to:

$$G_{avg} = 0.3 E_{avg} \tag{B.28}$$

As lateral wall deformation increases, sections closer to the base experience more cracking, reducing the effective length (L_{eff}) of these sections. The shear deformation at a given height z is calculated as:

$$\gamma(z) = \chi \frac{V}{G_{avg} L_{eff} T}$$
(B.29)

where $\chi = 1.2$ and T is the wall thickness.

The shear contribution to wall displacement can be evaluated by integrating the shear deformation along the wall height:

$$\delta_2^V = \delta_1^V + \int_0^H \gamma(z) \, dz \tag{B.30}$$

$$\delta_n^V = \delta_1^V + H \sum_{k=1}^{n_k} \gamma_k \tag{B.31}$$

If the shear strength, determined by sliding shear or diagonal cracking, is less than the acting shear, the wall undergoes shear failure, exhibiting different postpeak behavior compared to bending (Parisi and Augenti, 2013). The model considers a horizontal plateau once shear capacity is reached.

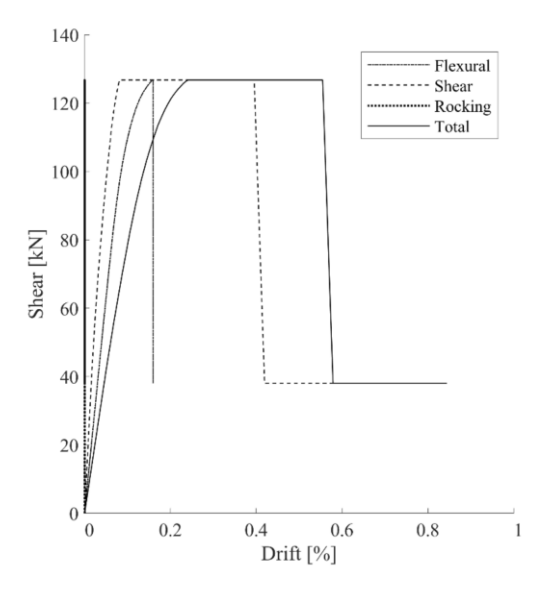


Figure B.4 – Drift-shear curve of a flexure-dominated wall, highlighting the individual contributions of flexural, shear, and rocking components. (Parisi and Acconcia 2020)

Denoting δ_e^V as the displacement associated with the shear strength, the shear strength of the wall remains constant until displacement δ_p^V , given by:

$$\delta_p^V = \mu_{V,max} \delta_e^V \tag{B.32}$$

where $\mu_{V,max}$ is a ductility factor related to peak shear force.

A residual shear force is considered with a second plateau ending at a displacement given by:

$$\delta_u^V = \mu_{Vr} \delta_e^V \tag{B.33}$$

where μ_{Vr} is a ductility factor related to residual shear strength.

The wall's shear strength is defined by local crisis criteria: diagonal tension cracking occurs when the principal tensile stress at the panel centroid reaches the masonry's tensile strength (Turnsek and Cacovic, 1970). The dimensionless lateral strength for diagonal cracking is expressed in terms of the normalized shear force V_t/N_u and axial force N/N_u , where N_u represents the ultimate axial force capacity of the panel:

$$\overline{V}_t = \beta \sqrt{1 + \frac{\overline{N}}{p\beta}} \tag{B.34}$$

where: β is the ratio between diagonal tensile strength at zero axial load (τ c0) and uniaxial compressive strength of masonry (fm); and p is a shear stress distribution factor defined as the ratio between the maximum and the average shear stresses (τ_{max} and $\tau_n = V/A$, respectively) The factor p is typically set as follows: p = 1 in the case of walls with aspect ratio $H/L \le 1$; p = 1.5 if $H/L \ge 1.5$; and p = H/L if 1 < H/L < 1.5. The sliding shear resistance is predicted using the Mohr-Coulomb failure model, assuming sliding when the maximum shear stress reaches the sliding shear strength:

$$\overline{V}_a = \frac{1}{p} \left(\gamma + \mu_a \overline{N} \right) \tag{B.35}$$

where: γ is the ratio of shear strength at zero axial load (f_{v0}) to uniaxial compressive strength of masonry (f_m); μ_a is the friction coefficient

In cases of bed joint creep, the coefficient of friction decreases with mean normal stress as:

$$\mu_a = \frac{0.17}{\sqrt[3]{\left(\frac{\sigma_n}{f_m}\right)^2}} \tag{B.36}$$

For stepped diagonal sliding, both masonry units and mortar joints contribute to friction, typically ranging from 0.3 to 0.8.

Both Eurocode 6 (CEN 2005) and the Italian Building Code (IMIT 2019) suggest $\mu_a = 0.4$.

• Rocking behaviour

After the peak compressive strain (ε_p) is reached on the end sections, it is assumed that any further increase in curvature induces a rotation of the rigid wall body. This rotation is evaluated as follows:

$$\theta_r = (\varphi_i - \varphi(\varepsilon_p))\Delta z \tag{B.37}$$

where:

- ϕ_i is the curvature of the base section at the *i-th* stage of analysis
- $\phi(\epsilon_p)$ is the curvature corresponding to the peak compressive strain of the masonry
- Δz is the distance between the section where ϵ_p is reached and the nearest internal section

The strain value at which peak strain is reached is assessed by considering that a plane section before bending remains plane after bending:

$$\varphi(\varepsilon_p) = \frac{\varepsilon_p}{\frac{L}{2} + \frac{u}{\varphi}} \tag{B.38}$$

In the above equation, the denominator represents the width of the compressed part of the section. This differs from the reacting section width (L_{eff}) because the tensile strength of masonry is assumed to be non-zero.

The displacement contribution due to rocking is given by:

$$\delta_2^R = \delta_1^R + \theta^R H \tag{B.39}$$

Figure B.5 illustrates the significant influence of rocking behavior on the postpeak segment of the capacity curve, leading to an exceptionally high displacement capacity.

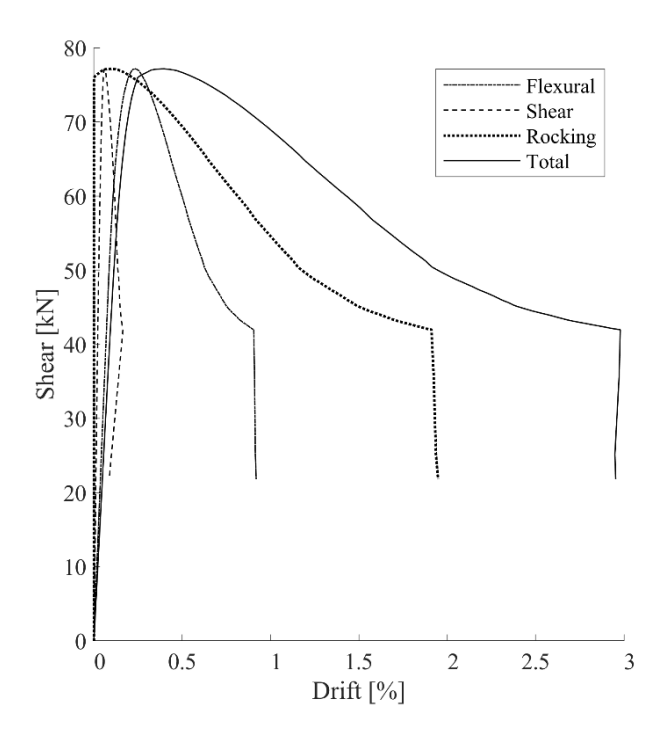


Figure B.5 – Shear-drift response of a flexure-dominated URM wall, showing the contribution of flexural, shear, and rocking components to the overall behavior. (Parisi and Acconcia 2020)

